Vol. 126 Nos. 1-6

May-June 1959

PROCEEDINGS OF THE ACADEMY OF SCIENCES

OF THE USSR

(DOKLADY AKADEMII NAUK SSSR)

Physical Chemistry Section

A publication of the Academy of Sciences of the USSR

IN ENGLISH TRANSLATION

Year and issue of first translation:
Vol. 112, Nos. 1-6 Jan.-Feb. 1957

Annual subscription	*$160.00*
Single issue	*35.00*

Printed in the United States of America

PROCEEDINGS OF THE ACADEMY OF SCIENCES OF THE USSR

Physical Chemistry Section

Volume 126, Numbers 1-6 May-June, 1959

CONTENTS

CONTENTS (continued)

CONTENTS (continued)

INJECTION AND EXTRACTION OF MINORITY CURRENT CARRIERS AT THE SURFACE OF A GERMANIUM ELECTRODE, AS THE RESULT OF ELECTROCHEMICAL PROCESSES

Yu. V. Pleskov

Institute of Electrochemistry of the Academy of Sciences of the USSR

(Presented by Academician A. N. Frumkin, February 3, 1959)

Oxidation-reduction processes at a germanium electrode show a number of special features, associated with the semiconducting properties of germanium. It has been shown [1-3], for instance, that the process of anodic dissolution of germanium differs from the dissolution of a metal in that, holes participate, i.e., the atoms going into solution give up part of their electrons, not to the free, but to the filled band of the semiconductor. The view has been expressed [1] that all reduction processes at a germanium electrode occur with the participation of only the free electrons of the semiconductor, but this view has not been confirmed by later work [4, 5], whose authors found no difference in the rate of evolution of hydrogen at cathodes of germanium of the n- and p-types. It has been suggested [5] that, in the reduction of dissolved ions at a germanium electrode, electrons are transferred to ions, not from the free, but from the filled bands of the germanium, leaving holes remaining; in this way, the reaction of electroreduction should serve as a means of injecting holes into the semiconductor. It should be noted that, in the work cited [5], two simultaneous processes were occurring on the surface of the germanium (reduction of dissolved ions and dissolution of germanium), so that it was not possible to give an unequivocal analysis of the results obtained.

Determination of the sign of the current carrier, participating in an electrochemical reaction at a semiconducting electrode, is of great interest. In this paper, we have investigated, from this point of view, the mechanisms of some processes at a germanium electrode.

The electrode was of p-type monocrystalline germanium, with a specific resistance of 2.5 ohm·cm and a diffusion length for the minority carriers of 0.7 mm, in the form of a disc of diameter 6 mm and thickness of about 0.1 mm. The crystallographic orientation of the surface was (111). An ohmic contact, in the form of a nickel ring, was soldered round the circumference of the disc with tin. The absence of any rectifying action at the contact was checked by studying the voltage current characteristics, using alternating (by means of an oscilloscope) and direct current. The electrode surface was polished, and before measurement, was treated with cleaning mixture SR-4, made up from reagents of the highest purity. The electrode was attached by silicone lacquer to the rim of the opening in the bottom of a funnel shaped polystyrene vessel, suspended inside an electrochemical cell. The ring contact and the current lead to the electrode were insulated with a layer of pure paraffin wax. Solutions to be investigated were placed inside the polystyrene vessel and inside the cell, so that the lower surface of the germanium disc was in contact with the solution in the cell, and its upper surface was in contact with the solution in the polystyrene vessel. By means of two independent electrodes, it was possible to pass current through either surface of the germanium electrode, and to measure the potential of the latter relative to the corresponding comparison electrode. Measurements were carried out in the dark in an atmosphere of purified nitrogen.

All the potential values were given relative to a normal hydrogen electrode.

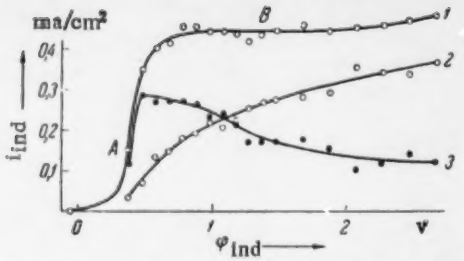

Fig. 1. Extraction of holes in the anodic dissolution of germanium in N H_2SO_4. 1) Normal polarization curve of indicator process; 2) the same with anodic dissolution on the polarization side (i_{pol} = 0.5 ma/cm²); 3) decrease in i_{ind} as the result of extraction.

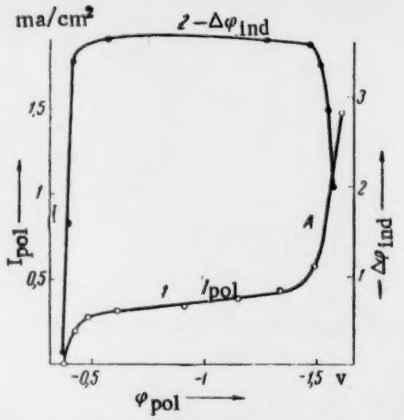

Fig. 2. Effect of the evolution of H_2 on the injection of holes into a germanium electrode by reduction of $K_3Fe(CN)_6$. 1) Cathodic polarization curve recorded with a solution of 1.3 N in KOH and 0.03 M in $K_3Fe(CN)_6$; 2) change in potential on the indicator side (at i_{ind} = 0.55 ma/cm²) when the reduction process took place on the polarization side.

Since the thickness of the germanium electrode was considerably less than the diffusion length of the holes, the injection or extraction of holes on one side of the electrode, resulting from an electrochemical reaction, would affect, by diffusion of holes, any electrochemical reaction occurring on the other side of the electrode (if the kinetics of this reaction depended on the concentration of holes). By chosing, as an indicator process, the anodic dissolution of germanium, which is very sensitive to the concentration of holes in the semiconductor [1-3], we were able to investigate whether an electrochemical reaction, occurring on the other side of the electrode, altered the concentration of holes in the sample. We called the side of the electrode, on which the indicator reaction took place, the indicator side; the other side was called the polarization side*.

To check for the absence of essentially continuous pores through the electrode, which might distort the results, we altered, over a wide range (by passage of current), the germanium potential on one side, and, at the same time, controlled the potential on the other side. The independence of the potentials on the two sides showed that the electrode was continuous enough. Separate experiments showed that the effect described below, of the interaction of two processes occurring on opposite sides of a flat germanium electrode, disappeared if the thickness of the electrode was more than 7 times the diffusion length of the holes.

We carried out the following measurements to ensure that the effects described below were not due to the existence of an electric field within the germanium or to the properties of the ring contact. Solution was removed from the polarization side, and a small area ohmic contact (a probe) was applied to the dry surface of the germanium disc. The flow of current between the probe and ring contact, regardless of its direction and value (within a few ma), had no effect on the speed of the indicator process. Thus, the indicator process was unaffected by the passage of current through the polarization side of the electrode, if there was no change in the concentration of holes.

A polarization curve of the indicator process, recorded with N H_2SO_4, is shown in Fig. 1, 1. The curve had a well defined region of "current saturation" (region B), caused by the low concentration of holes on the indicator side. When an anodic current was passed through the polarization side, the constant rate of the indicator process was reduced (Fig. 1, 2), which showed that there was a decrease in the concentration of holes in the electrode as the result of extraction.

* The method described recalls that used for investigating the effects of protons, diffusing through an electrode, on the hydrogen overvoltage [6]. But in our case, there was no transfer of material through the electrode.

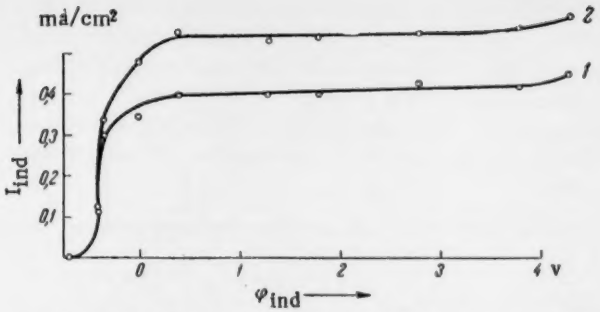

Fig. 3. Injection of holes by reduction of $K_3Fe(CN)_6$ at a germanium electrode. 1) Normal polarization curve for the indicator process in 1.3 N KOH; 2) the same when $K_3Fe(CN)_6$ was reduced on the polarization side (i_{pol} = 0.4 ma/cm²).

It was interesting that, with a constant rate of extraction, the effect of extraction on the rate of the indicator process depended on the potential on the indicator side (Fig. 1, 3). However, this dependence was not difficult to explain. At low values of the potential, the rate of anodic dissolution of germanium was determined by the speed of the electrochemical stage of the process and did not depend on the concentration of holes. Therefore, in the potential region A (Fig. 1), the anodic dissolution of germanium was unaffected by the extraction of holes, occurring as the result of other processes. On the other hand, at very positive potentials (region B), when the concentration of holes on the indicator side was reduced to the limit, the speed of the process was determined by the rate of volumetric generation of holes, and could be reduced, as the result of extraction, to less than a half. The maximum effect of extraction was observed at a potential of about 0.5 v, when the rate of anodic dissolution already depended on the concentration of holes in the sample, but this concentration was still very high.

The most interesting investigation, by the method described, was that into the mechanism of reduction processes at a germanium cathode, since opposing views have been expressed in the literature on this question. Fig. 2, 1 shows a polarization curve for the reduction of $K_3Fe(CN)_6$ in 1.3 N KOH. When $K_3Fe(CN)_6$ was reduced on the polarization side of the electrode, the rate of the indicator process (in 1.3 N KOH) was considerably increased (Fig. 3). This fact could only be explained as being due to an increase in the concentration of holes in the semiconductor as the result of injection, associated with the process of reduction of ferricyanide. Consequently, the $Fe(CN)_6^{3-}$ ions, reduced at the germanium electrode, obtained their electrons, not from the free, but from the valence band of the semiconductor.

Thus, the injection of holes into a germanium electrode, when a reduction reaction was taking place, has been demonstrated by a direct method. Similar results were obtained if the ferricyanide was replaced by potassium permangenate (in N sulfuric acid)*.

It should be noted that the effect of injection on the indicator process was markedly diminished if evolution of hydrogen commenced at the germanium electrode at the same time as the reduction of ferricyanide (Fig. 2, 1, region A). We judged whether the indicator process was retarded or facilitated by the simultaneously occurring process on the polarization side, by the shift in potential on the indicator side, $\Delta\varphi_{ind}$, in the direction of positive or negative values respectively, at constant current density, i_{ind}. The effect of injection decreased with increasing rate of evolution of H_2 (Fig. 2, 2), the phenomenon being reversible if the rate of evolution of H_2 was not high. However, if the rate of hydrogen evolution reached 10^{-2} amp/cm², then, after 2-3 minutes, the electrode completely lost its power to affect injection or extraction on the indicator side. This power of reduction to affect injection could be restored if the polarization side of the electrode was etched chemically or anodically. Similar results were obtained with the reduction of MnO_4^- ions.

*An increase in the rate of anodic dissolution on the indicator side also occurred if holes were injected into the germanium by other means, for example, by illumination of the polarization side of the electrode, or by including in the circuit a p-n junction in the forward direction, located close to the germanium-electrolyte interface [2,7].

The reason for this unexpected effect was, evidently, that the hydrogen evolved at the germanium cathode entered into the crystal lattice of the semiconductor, and reduced the lifetime of the minority current carriers [8]. The result of entry of hydrogen on the polarization side was to form a surface layer, where the rate of recombination was higher, so that any change in the concentration of holes, due to injection or extraction, was reduced as the result of recombination (or generation, respectively) in this layer. The hydrogen entering the germanium rapidly escaped from the crystal lattice, if the time and rate of evolution of H_2 were inconsiderable. It is obvious that, in this case, the depth of penetration of hydrogen into the germanium and the bonding energy of Ge-H were small.

Our sincere thanks are due to Prof. B. N. Kabanov for his help in the interpretation of the results.

LITERATURE CITED

[1] W. H. Brattain and C. G. B. Garrett, Bell Syst. Techn. J. 34, 129 (1955).

[2] A. Uhlir, Bell Syst. Techn. J. 35, 333 (1956).

[3] E. A. Efimov and I. G. Erusalimchik, J. Phys. Chem. 32, 413, 1103 (1958).

[4] E. A. Efimov and I. G. Erusalimchik, J. Phys. Chem. 32, 1967 (1958).

[5] H. Gerischer and F. Beck, Z. Phys. Chem., N. F., 13, 389 (1957).

[6] I. A. Bagotskaya, Proc. Acad. Sci. USSR 107, 843 (1956).

[7] S. G. Ellis, Phys. Rev. 100, 1140 (1955).

[8] S. G. Ellis, J. Appl. Phys. 28, 1262 (1957).

Received January 31, 1959

RING DISC ELECTRODES

Academician A. N. Frumkin and L. I. Nekrasov

The M. V. Lomonosov Moscow State University

In the last few years, increasing use has been made of the rotating disc electrode in the field of electrochemical research, which enables processes to be investigated both in the diffusion and kinetic regions. The value of this electrode is connected with the existence of the precise theory of convective diffusion at a rotating disc, developed by V. G. Levich [1].

In this paper, we describe a method of investigating the final and intermediate (stable and unstable) products of an electrochemcial reaction occurring at the surface of the disc, which enabled us to widen the sphere of application of the disc electrode and to use it for the solution of new problems.

For this purpose, we used a rotating "ring" disc electrode, consisting of a combination of two independent electrodes – a disc and a ring, located in the same plane and separated by a narrow insulating strip. Final and intermediate products, formed in the process of electrolysis at the disc electrode, could be registered by reduction or oxidation at the ring electrode, which could be used to obtain a polarization curve with limiting diffusion current of the substance to be investigated. If the shape of the polarization curve was known, then, in a number of cases, it was sufficient to confine the experiment to measurement of the value of the current through the ring electrode at a potential corresponding to the region of limiting current, for any particular value of the current through the disc. The most general form of application of the method would include the recording of a few polarograms on the ring for different values of the potential applied to the disc, which would always allow the optimum conditions to be established for the investigation of any intermediate products.

The method was only applicable to the investigation of unstable intermediate products under conditions such that the starting material, or the end product of the reaction, did not react on the ring in the range of potential, in which the product to be investigated was reduced (or oxidized).

Unstable products could disappear as the result, either of further reactions on the surface of the electrode, or of processes occurring in the body of the solution, such as interaction with solvent or other components of the solution, disproportionation, etc. In this paper, we have confined ourselves to the first case.

Since the life of the unstable intermediate products might be very short, it was desirable, in order to increase the sensitivity of the method, to obtain the maximum rate of transfer of the intermediate products from the disc to the ring. This could be achieved by reducing the thickness of the insulating strip between disc and ring, and by increasing the speed of rotation of the electrode.

Since, in a hydrodynamic sense, the proposed electrode could be considered as a rotating disc, it was permissible to use the quantitative theory of this type of electrode. Yu. B. Ivanov and V. G. Levich [2] proposed the following formula, connecting the density of the diffusion current j(r), of the intermediate product particles at the ring electrode at distance, r, from the center of the disc, with the constant rate of conversion, k, of intermediate to final product on the disc electrode:

$$j(r) = \frac{0{,}4\, j_0}{1 + \frac{k\delta_{0B}}{D_B}} \frac{r_1^2 r_2}{r^3} \frac{\left[1 - \frac{3}{4}\left(\frac{r_1}{r_2}\right)^3\right]^{1/3}}{\left[1 - \left(\frac{r_2}{r}\right)^3\right]^{1/3}\left[1 - \frac{3}{4}\left(\frac{r_1}{r}\right)^3\right]}, \qquad (1)$$

where $r_1 \leq r \leq r_3$; j_0 was the diffusion current density of the particles of starting material on the disc; r_1, r_2 and r_3 were the radii of the three electrode zones (Fig. 1); D_B was the diffusion coefficient of the intermediate product; δ_{0B} was the thickness of the diffusion restricted layer for the intermediate product.

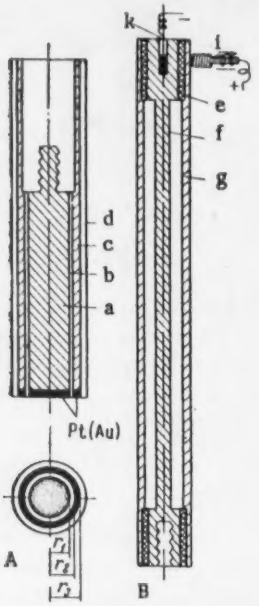

Fig. 1. Ring disc electrode (A), and spindle of device for rotation (B) (section).

To obtain the total current in a concrete example, it was necessary to substitute our values of the parameters and to integrate Equation (1) over the surface of the ring electrode, which gave

$$I_k = \frac{0{,}45 I_0}{1 + k\delta_{0B}/D_B}, \qquad (2)$$

where I_K was the value of the limiting diffusion current through the ring and $I_0 = nFj_0$. Using this equation, it was easy to find the value of k for the intermediate product.

The intermediate product formed was removed from the surface of the disc by further transformation and by diffusion into the bulk of the solution, so that, for the case of limiting diffusion current for the starting material, we could write the equation

$$j_0 = \frac{D_A c_{0A}}{\delta_{0A}} = kc_{sB} + \frac{D_B c_{sB}}{\delta_{0B}}, \qquad (3)$$

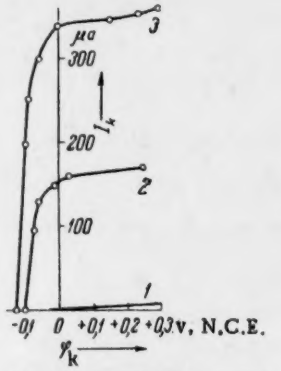

Fig. 2. Polarization curves for the oxidation of hydroquinone at a platinum ring electrode (m = 2150 rpm). 1) $I_0 = 0$; 2) $I_0 = 450$ μa; 3) $I_0 = 900$ μa.

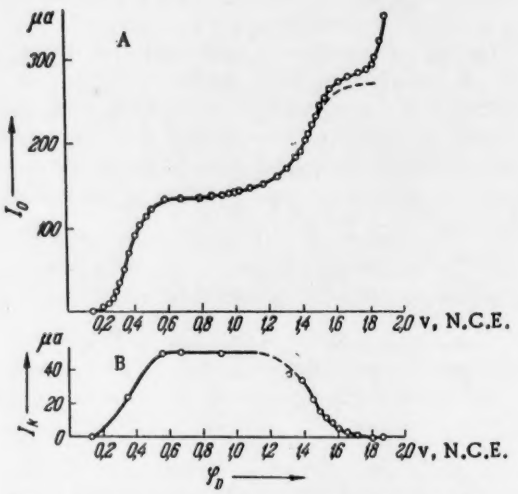

Fig. 3. A) Polarographic curve for the cathodic reduction of oxygen, at a gold amalgamated disc electrode, in 0.1 N NaOH (m = 2150 rpm) (the dotted line was corrected for background current). B) Corresponding curve for the relation between the limiting current, for the oxidation of H_2O_2 at a ring electrode, and the potential of the disc electrode.

where c_{0A} was the volume concentration of the starting material; c_{sB} was the surface concentration of the intermediate product; D_A and δ_{0A}, respectively, were the diffusion coefficient and thickness of the diffusion restricted layer for the starting material. Substituting the value of k from (3) in (2), it was not difficult to obtain the relation

$$I_k = 0{,}45 I_0 \left(\frac{D_B}{D_A}\right)^{2/3} \frac{c_{sB}}{c_{0A}}. \qquad (4)$$

Equation (4) somewhat resembled the equation for concentration polarization, but differed from the latter in that the strength of the current through the ring altered in proportion to the value of c_{sB}, and not $(c_{0B} - c_{sB})$, as would be found if polarographic curves were recorded for a solution containing intermediate product at initial concentration c_{0B}. Thus, if the rate of formation of intermediate product was constant (I_0 = constant), then the ring current should fall in proportion to the approach of the disc current to saturation, and the relation between I_k and the potential of the disc electrode should have the form of a reversed polarographic wave.

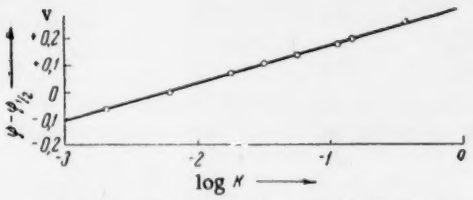

Fig. 4. Relation between the logarithm of the velocity constant, for the reaction of reduction of H_2O_2, and potential.

The electrode used is shown in Fig. 1 A: a was a brass cylinder, with a soldered disc of platinum or gold; b was a brass tube, with a soldered ring of platinum or gold; c was a thin (0.25 mm) insulating sleeve of Teflon. The external coating, d, of the electrode was also of Teflon; the metallic parts were firmly embedded in the Teflon sleeves. The dimensions of the working zones of the electrode were determined by the following parameters: r_1 = 0.25 cm; r_2 = 0.275 cm; r_3 = 0.36 cm. Fig. 1 B shows a section of the spindle of the device for rotation, into which the working electrode was screwed. Because of the insulation, e, between the inner, f, and outer parts, g, parts, it was possible to have independent current connections through the spindle, both to the disc and ring electrodes. Current connections to the spindle were provided by mercury h and sliding i contacts. For rotation, the electrode was provided with a hydraulic mercury seal, making it possible to use speeds of rotation up to 15,000 rpm, with completely effective sealing. The measuring arrangements consisted of two independent polarization and compensation systems, for measuring the potentials of both electrodes.

The reductions of quinone and of oxygen were selected as reactions for developing the use of the ring disc electrode and for checking the theoretical formulas.

Experiments on the reduction of quinone and hydroquinone were carried out at a platinum disc electrode in N KCl solution, and in a phosphate buffer at pH 7. Polarization curves for the oxidation of the hydroquinone formed, at the platinum ring, in N KCl, are shown in Fig. 2. It was found that, in the case of the formation of a stable product (k = 0), however much hydroquinone there was, with a ring of the above dimensions, it was possible to register 38 ± 1% of the product formed.

Of particular interest to us, was the reaction of reduction of oxygen, occurring at an amalgamated electrode, in alkaline solution, in the two stages:

$$O_2 + 2e^- + 2H_2O \rightarrow 2H_2O_2;$$

$$H_2O_2 + 2e^- \rightarrow 2OH^-,$$

which corresponded to the two waves on the polarogram.

In the region of the first wave, H_2O_2 was a stable product (k = 0) and could accumulate in the solution, but, in the region of the second wave, it behaved as an intermediate product (k > 0). Fig. 3, shows: A) the polarization curve for the cathodic reduction of oxygen, at a gold amalgamated disc electrode, in 0.1 N NaOH, and B) the corresponding curve for the relation between the diffusion current, for the oxidation of the hydrogen peroxide

formed, at the gold ring electrode, and the potential of the disc electrode. The yield of H_2O_2 registered, expressed as a percentage, corresponded, in the region of the first wave, to the same value as the yield of hydroquinone (37%), i.e., close to the calculated theoretical value (45%), but slightly less. The divergence was still less if allowance was made for the fact that Equation (1) gives results about 5% too high [2]. In the region of the second wave, this yield fell with rising potential in proportion to the change in the value of c_{sB}, and the graph, constructed with I_k and c_{sB} as coordinates, was found to be a straight line, thus, confirming the correctness of Equation (4).

Another indication of the correctness of the method could be obtained by checking Equation (2). Fig. 4 shows the relation between the logarithm of the velocity constant, for the reaction of reduction of H_2O_2, and potential, in which the straight line was based on direct determination of the velocity constant in H_2O_2 solution from kinetic data, according to the equation

$$i = knF\,[H_2O_2]_s = k_1 nF\left(1 - \frac{i}{i_d}\right)[H_2O_2]_0 \exp\left(-\frac{\alpha F\,(\varphi - \varphi_{1/2})}{RT}\right),$$

and points calculated from Equation (2), together with the experimental value of the numerical coefficient

$$I_k = \frac{0{,}38\, I_0}{1 + K\delta_{0B}/D_B}. \qquad (5)$$

The value of the diffusion coefficient of H_2O_2 in 0.1 N NaOH, approximately $9.3 \cdot 10^{-6}$ cm^2/second, was determined experimentally, by means of the disc electrode. Agreement with the value of the velocity constant, calculated by the second method, was satisfactory.

It should be noted, that, when measuring the oxidation current of H_2O_2 at the ring, in order to avoid passifying the gold electrode, it was necessary to work with high rates of increase of potential (2.5 v/minute). In this case, the whole polarographic curve was recorded in about 15 seconds, which was achieved by using a modernized Heyrovsky polarograph with a higher speed of rotation of the drum. The current was measured with a milliammeter, only in the region of potential corresponding to the limiting diffusion current. With slower measurements of the polarization curves, the electrode was rendered passive, and the process was limited, not by diffusion, but by kinetic factors.

LITERATURE CITED

[1] V. G. Levich, Physico-Chemical Hydrodynamics, (Acad. Sci. USSR Press, 1952) p. 50.

[2] Yu. B. Ivanov and V. G. Levich, Proc. Acad. Sci. USSR, 126, No. 5 (1959).*

Received March 3, 1959

* See C. B. Translation.

DEPENDENCE OF THE RATE OF AN ACID-CATALYZED REACTION ON THE BASICITY OF THE REAGENT IN THE CASE OF "GENERAL ACID CATALYSIS "

Yu. L. Khaldna, A. I. Tal'vik and V. A. Pal'm

Tartu State University

(Presented by Academician V. N. Kondrat'ev, December 24, 1958)

Acid-catalyzed reactions, occurring in not too strongly acid media, are usually classified as of two types: conforming to the rules of either "general acid catalysis" or "specific acid catalysis" by hydrogen ions [1]. The term "general acid catalysis" is used when the velocity constant of the reaction can be expressed as a polynomial, each term of which is proportional to the concentration of some acid present in the system:

$$k = k_{H_2O}[H_2O] + k_{H^+}[H^+] + k_{A_1H}[A_1H] + k_{A_2H}[A_2H] + \ldots \quad (1)$$

The term "specific acid catalysis" by hydrogen ions is applied when the velocity constant of the reaction is proportional only to the concentration of hydrogen ions (in water $[H_3O^+]$):

$$k = k_{H^+}[H_3O^+]. \quad (2)$$

In concentrated solutions, of acids, and with some anhydrous acids, the logarithm of the velocity constant for a series of acid catalyzed reactions is found to be directly proportional to the Hammet acidity function, H_0 [2, 3]. In this case, the mechanism of the reaction must be represented by the scheme:

$$\begin{aligned} &1.\ B + H^+ \rightleftarrows BH^+, \quad \text{rapid} \\ &2.\ BH^+ + C \xrightarrow{k_0} \text{products of reaction, slow.} \end{aligned} \quad (3)$$

Taking into account the degree of protonization of the reagent, the observed velocity constant of a reaction, occurring in accordance with Scheme (3), is given by the expression [4, 5]

$$k = k_0 h_0 / (h_0 + K_a), \quad (4)$$

where k_0 is the velocity constant of conversion of the protonized form; K_a is the basicity constant of the reagent; $-\log h_0 = H_0$. According to (4), at high acidities, when $h_0 \gg K_a$, there is an approach to complete protonization of the reagent and $k = k_0$. This was shown experimentally by A. I. Tal'vik and V. A. Pal'm, for the case of the acid hydrolysis of ethyl acetate.

At the present time, it is not clear whether all acid-catalyzed reactions have a mechanism in accordance with the Scheme (3), the special feature of which is a rapid equilibrium protonization of the reagent and a subsequent comparatively slow conversion of the protonized form. In the case of "specific acid catalysis" by hydrogen ions, a positive answer to this question does not meet with any serious objections. But, the problem is somewhat more complicated in the case of "general acid catalysis." A relation of type (1) may, at first glance, be

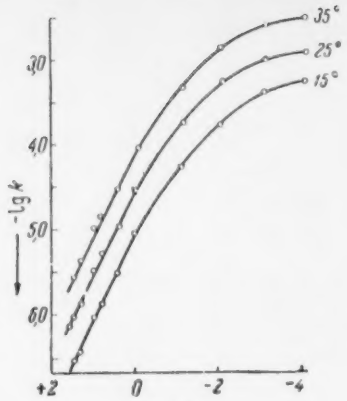

Fig. 1

TABLE 1

[HCl] mole/liter	$h_0 \cdot 10^{-3}$	$\frac{k_1^{25°}}{[Cl^-]} \cdot 10^4$	[HCl] mole/liter	$h_0 \cdot 10^{-3}$	$\frac{k_1^{25°}}{[Cl^-]} \cdot 10^4$
8,71	1,00	1,038	10,25	3,98	1,051
9,25	1,59	1,058	10,70	6,30	1,043
9,75	2,52	1,064	11,18	10,00	1,026

interpreted only in the sense that, in a given case, the slow stage of the reaction is the transfer of proton to reagent, where each acid in the system gives up protons at a different characteristic rate. Most of the cases of "general acid catalysis" which have been investigated are prototropic transformations. For this reason, theoretical views on this type of acid-catalyzed reaction are closely linked with views on the mechanisms of prototropic transformations.

The acid-catalyzed enolization of acetone proceeds according to a typical scheme of prototropic transformation:

$$CH_3-\overset{O}{\overset{\|}{C}}-CH_3 + H^+ \rightarrow CH_3-\overset{OH}{\overset{|}{C^+}}-CH_3 \rightarrow CH_3-\overset{OH}{\overset{|}{C}}=CH_2 + H^+. \qquad (5)$$

Dawson and his co-workers only considered this reaction from the point of view of agreement of the observed velocity constants wtih a type (1) relationship, and did not go into more detailed considerations of its mechanism [7, 8]. Lowry [9] and Swain [10] proposed a trimolecular mechanism for the prototropic transformation, which was written for acetone as follows:

$$AH + O=\overset{CH_3}{\overset{|}{C}}-CH_2-H + OH_2 \rightarrow A^- + HO-\overset{CH_3}{\overset{|}{C}}=CH_2 + H_3O^+. \qquad (6)$$

where AH is any acid. Dawson and Swain [11] later also adopted this point of view.

But, there are a number of results in the literature which do not agree with the hypothesis of a trimolecular mechanism. These include the results of an investigation of the halogenation of acetone in heavy water and the case of deuterated acetone [12], and also the kinetics of oxygen exchange of acetone labelled with O^{18} [13]. The hypothesis of a trimolecular reaction for the enolization of acetone has been subjected to a critical review by Bell [14].

It can be shown, that, in the case of an acid-catalyzed reaction, proceeding according to a scheme of prototropic transformation:

$$\begin{aligned} &1.\ HB: + H^+ \rightleftarrows HBH^+, \quad \text{rapid;} \\ &2.\ HBH^+ + :C \rightleftarrows BH + HC, \quad \text{slow;} \end{aligned} \qquad (7)$$

where C is any base, present in the system, an expression of type (1) for the velocity constant can be deduced from the same initial assumptions as were used in deducing Equation (4). Suppose that the reaction consists of coordination of a proton to an unshared pair of electrons in the basic center of the reagent and of subsequent loss of a proton from any other place in the reagent molecule. Present in the system are: the reagent HB, the acids H_2O, H_3O^+ and A_1H, and the bases OH^-, H_2O and A_1^-. The concentration of HBH^+ is given by

$$[HBH^+] = [HB]_0 h_0 / (h_0 + K_{aHB}).$$

The reaction velocity is limited by the rate of interaction of HBH^+ with the different bases present in the system. The observed velocity constant is therefore equal to

$$k = (k_{OH^-} h_0 [OH^-] + k_{H_2O} h_0 [H_2O] + \sum_i k_{A_i^-} h_0 [A_i^-])(h_0 + K_{a\,HB})^{-1}. \quad (8)$$

In dilute acids $h_0 = [H_3O^+]$. Under conditions such that $h_0 \ll K_{aHB}$, Expression (8) becomes the following:

$$k = \frac{k_{OH^-}}{K_{aHB}} [H_3O^+][OH^-] + \frac{k_{H_2O}}{k_{aHB}} [H_2O][H_3O^+] + \sum_i \frac{k_{A_i^-}}{K_{aHB}} [H_3O^+][A_i^-]. \quad (9)$$

Since $[H_3O^+][OH^-] = K_w$ and $[H_3O^+][A_i^-] = K_{A_iH}[A_iH]$, where K_w is the ionic product of water and K_{A_iH} is the dissociation constant of A_iH, Expression (9) can be rewritten as:

$$k = \frac{k_{OH^-}}{K_{a\,HB}} K_w + \frac{k_{H_2O}}{K_{a\,HB}} [H_3O^+] + \sum_i \frac{k_{A_i^-}}{K_{a\,HB}} [A_iH]. \quad (10)$$

It is easily seen that Formulas (10) and (1) are completely analogous. Expressions of the type (9) and (10), and a number of other possible abstract variants, have been derived by Pedersen [15] and Bell [16]. We have investigated the kinetics of the enolization of acetone in aqueous solutions of hydrochloric acid, at HCl concentrations from 0.04 to 11.2 N, at 15, 25 and 35°. Under these conditions, the value of H_0 varied from +1.5 to -4.0. The rate of reaction was measured spectrophotometrically by the disappearance of bromine consumed in the bromination of acetone, the rate of which was equal to the rate of enolization [6]. From the value of $H_0 = 0$, the relation between the logarithm of the observed unimolecular velocity constant, k_I, and the acidity function, H_0, was linear and had unit slope. At 25° our results were in satisfactory agreement with those of other investigators [8, 19]. At more negative values of H_0, the curve relating log k_I and H_0 was "bent", as in the acid hydrolysis of ethyl acetate (see Fig. 1). At higher concentrations of HCl, the velocity constant was proportional to the Cl^- concentration and did not depend on the acidity (see Table 1).

Our results suggested the following mechanism for the acid-catalyzed enolization of acetone:

$$1.\ CH_3-\overset{O}{\overset{\|}{C}}-CH_3 + H^+ \rightleftarrows CH_3-\overset{OH}{\overset{|}{\underset{+}{C}}}-CH_3, \quad \text{fast;}$$

$$2.\ (a)\ CH_3-\overset{OH}{\overset{|}{\underset{+}{C}}}-CH_3 + H_2O \xrightarrow{k_{H_2O}} CH_3-\overset{OH}{\overset{|}{C}}=CH_2 + H_3O^+, \quad \text{slow;} \quad (11)$$

$$(b)\ CH_3-\overset{OH}{\overset{|}{\underset{+}{C}}}-CH_3 + Cl^- \xrightarrow{k_{Cl^-}} CH_3-\overset{OH}{\overset{|}{C}}=CH_2 + HCl.$$

At low HCl concentrations, the rate was limited by stage 2a), and at high HCl concentrations by stage 2b).

We calculated the values of k_{H_2O}, k_{Cl^-}, and K_a, the basicity constant of acetone. The value of k_{Cl^-} was obtained from the proportionality of k_I and the Cl^- concentration at high values of h_0 and $[Cl^-]$. The values of k_{H_2O} and K_a were calculated from the slope of the curve relating log k_I and H_0, in its linear region at low acidities. The calculation was carried out over the range of values of H_0 from -0.2 to -1.0. From this we calculated the variation of H_0 with temperature [19]. The following values were obtained:

$$k_{H_2O} = 4{,}6 \cdot 10^4 e^{-13700/RT}; \quad k_{H_2O}^{25°} = 4{,}3 \cdot 10^{-6};$$

$$k_{Cl^-} = 2{,}7 \cdot 10^7 e^{-15500/RT}; \quad k_{Cl}^{25°} = 1{,}0 \cdot 10^{-4};$$

$$K_a = e^{-22/R} e^{+7800/RT}; \quad pK_a^{25°} = -091.$$

For the transfer of a proton from H_3O^+ to the carbonyl group of acetone, the energy absorbed was about 8 kcal/mole, and the increase in entropy was 22 units.

Substitution of the values obtained for k_{H_2O}, k_{Cl^-} and K_a in the formula

$$k = (k_{H_2O}\, a_{H_2O} + k_{Cl^-}\, [Cl^-])\, h_0\, (h_0 + K_a)^{-1} \qquad (12)$$

enabled us to calculate the values of k_I, which agreed well with experiment for all values of H_0 from +4 to -4, except for the range -1 to -3. Over this range, the calculated values of k_I were greater than the experimental ones, but not more than twice as much.

The activity of water was introduced into Equation (12), since the activity coefficient of H_2O altered considerably with increasing concentration of HCl. The activity coefficient of Cl^-, on the other hand, did not change significantly [17], so that it was permissible to use simply $[Cl^-]$.

From these results, it follows that, in this particular case, the so called "general acid catalysis" does not differ in principle from "specific catalysis". The reaction rate is limited by the concentration of the protonized form of the reagent. The catalytic activity of the medium is proportional to its acidity, and not to the concentration of any acid.

LITERATURE CITED

[1] R. P. Bell, Acid-Base Catalysis, Oxford, 1941.

[2] L. P. Hammett and A. J. Deyrup, J. Am. Chem. Soc. 54, 279 (1932).

[3] L. P. Hammett and M. A. Paul, J. Am. Chem. Soc. 56, 827 (1934).

[4] V. A. Pal'm, "Investigation of the Kinetics and Mechanism of Reaction of the Chlorination of p-Phenylurethylansulfonic Acid With Chlorosulfonic Acid," Dissertation, Tartu (1956).*

[5] V. A. Pal'm, J. Phys. Chem., 32, No. 3, 620 (1958).

[6] A. Lapworth, J. Chem. Soc., 1904, 30.

[7] H. M. Dawson and M. Leslie, J. Chem. Soc., 1909, 1860.

[8] H. M. Dawson and J. Powis, J. Chem. Soc., 1913, 2135.

[9] J. M. Lowry, J. Chem. Soc., 1927, 2544.

[10] C. G. Swain, J. Am. Chem. Soc. 72, 4578 (1950).

[11] H. M. Dawson, and E. Spivey, J. Chem. Soc., 1930, 2180.

[12] O. Reitz, Z. Phys. Chem. A, 179, 119 (1936).

[13] M. Cohn and H. C. Urey, J. Am. Chem. Soc. 60, 679 (1938).

[14] R. P. Bell and P. Jones, J. Chem. Soc., 1953, 88.

[15] K. J. Pedersen, J. Phys. Chem. 38, 581 (1934).

[16] R. Bell, Collection, Catalysis, Investigation of Homogeneous Processes, IL, 1957, p. 33-37.* *

[17] M. I. Vinnik, R. N. Kruglov and N. M. Chirkov, J. Phys. Chem. 30, No. 4, 827 (1956).

[18] A. I. Gel'bshtein, G. G. Sheglova and M. I. Temkin, Proc. Acad. Sci. USSR 107, No. 1, 103 (1956).

[19] D. P. N. Satchell, J. Chem. Soc., 1957, 2878.

Received December 11, 1958

* In Russian.

* * Russian translation.

AFTEREFFECTS OF THE IRRADIATION OF METHYL METHACRYLATE IN THE PRESENCE OF OXYGEN

B. L. Tsetlin, V. A. Sergeev, S. R. Rafikov, Corresponding Member Acad. Sci. USSR V. V. Korshak, P. Ya. Glazunov and L. D. Bubis

Institute of Organometallic Compounds of the Academy of Sciences of the USSR
Institute of Physical Chemistry of the Academy of Sciences of the USSR

It is known that, under definite conditions, oxygen inhibits the radical-induced polymerization of many vinyl monomers. Radiation-induced polymerization, proceeding by a radical mechanism, is also inhibited by oxygen [1]. In agreement with this, we found that methyl methacrylate did not polymerize when exposed to ionizing radiation in the presence of air; its viscosity did not alter appreciably even after prolonged irradiation. But the monomer, after irradiation in air and subsequent storage, may polymerize spontaneously, at room temperature or below, with a high degree of conversion; the necessary condition for the commencement of such polymerization is the prevention of access of atmospheric oxygen to the irradiated monomer [2]. The irradiated monomer does not polymerize in the presence of air, even after prolonged storage. This method of polymerization, based on the use of the energy of ionizing radiation, may have considerable practical interest, since radiation-induced chain processes of polymerization provide one of the most practicable means of using radiation in chemistry [3]. For this reason, we have investigated the basic principles of this process.

The monomer was irradiated with fast electrons, of energy 900 kev, the source of which was the accelerator of the Institute of Physical Chemistry of the Academy of Sciences of the USSR; the electron beam was controlled by means of an ionization chamber [4]. The cell for irradiation was an open cylindrical glass vessel, with a double wall for cooling the monomer with running water. The cell diameter was 50 mm, the thickness of the monomer layer irradiated was 25 mm. A constant concentration of atmospheric oxygen in the monomer was ensured by agitation with a magnetic stirrer. The kinetics of polymerization of the irradiated monomer was investigated dilatometrically, using a mercury dilatometer [5]. The irradiated monomer was poured into the dilatometer in the air, then frozen, evacuated to a pressure of the order of 10^{-2} mm Hg, melted, frozen again and evacuated, after which the dilatometer was filled up with mercury and placed in a thermostat for polymerization to occur.

We investigated the kinetics of the polymerization of methyl methacrylate as a function of its previous irradiation (dose R and dose intensity R') and the polymerization temperature.

Figure 1 shows characteristic kinetic curves obtained for the polymerization of irradiated methyl methacrylate, recorded at 20° as a function of the dose (in this series of tests, the dose intensity, R', was constant). To a first approximation, the general character of the kinetic curves did not differ from that of similar curves for polymerizations induced by peroxides and other radicals. They were characterized by a constant initial rate of polymerization (V_0), with subsequent autoacceleration (the "gel effect"). The rate of polymerization increased with increasing values of R, with V_0 proportional to $R^{1/2}$ (Fig. 2). These facts already showed that the observed polymerization was taking place by a radical mechanism, with the characteristic bimolecular termination of kinetic chains as the result of recombination of macroradicals, and the linear dependence of the rate of the initial reaction on the concentration of initiating radicals. It was natural to assume that the initiating

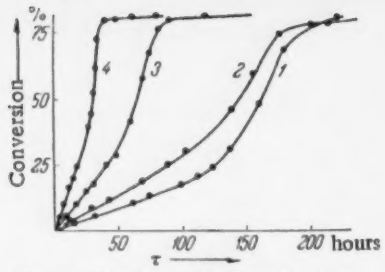

Fig. 1. Kinetics of polymerization of irradiated methyl methacrylate at 20°. The dose intensity was $2.2 \cdot 10^{17}$ ev/cm^3 · sec. The dose was: 1) $1.3 \cdot 10^{19}$ ev/cm^3; 2) $6.6 \cdot 10^{19}$ ev/cm^3; 3) $2.0 \cdot 10^{20}$ ev/cm^3; 4) $8.0 \cdot 10^{20}$ ev/cm^3.

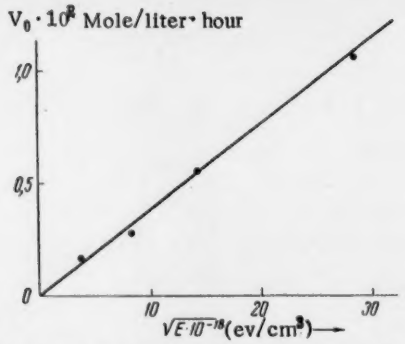

Fig. 2. Relation between initial rate of polymerization of irradiated methyl methacrylate and dose (at dose intensity of $2.2 \cdot 10^{17}$ ev/cm^3 · second).

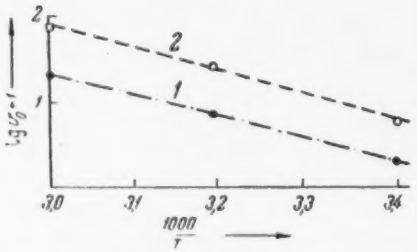

Fig. 3. Relation between initial rate of polymerization of irradiated methyl methacrylate and temperature, at doses: 1) $6.6 \cdot 10^{19}$ ev/cm^3; 2) $4.0 \cdot 10^{20}$ ev/cm^3 (dose intensity $2.2 \cdot 10^{17}$ ev/cm^3 · second).

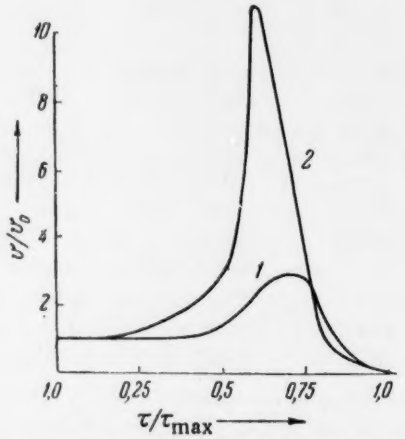

Fig. 4. Effect of method of initiation on the shape of the kinetic curves for the polymerization of methyl methacrylate (temperature 60°). 1) Polymerization of previously irradiated monomer (dose $4 \cdot 10^{20}$ ev/cm^3); 2) polymerization of methyl methacrylate in the presence of 0.01% of benzoyl peroxide.

substances were products of the radiation induced oxidation of methyl methyacrylate, i.e., peroxides, formed on irradiation of organic compounds as the result of interaction with oxygen of the first formed radicals [6]. Indeed, iodometric determination of peroxidic substances in samples of irradiated methyl methacrylate, represented in Fig. 1, showed that the number of peroxide groups formed was proportional to the dose, and, consequently, that V_0 was proportional to $C^{1/2}$, where C was the concentration of peroxide groups. This was in agreement with the assumptions made as to the character of the process.

Investigation of the effect of the intensity of the dose on V_0 showed that, over the range of values of R' from $5 \cdot 10^{16}$ to 10^{18} ev/cm^3 · second, equal doses of radiation, obtained by altering the ratio of R' to irradiation time, did not have the same effect; the greater R', the less was V_0, and it was found that V_0 was proportional to $(R')^{-1/4}$.

Figure 3 shows the effect on V_0 of the temperature at which the polymerization of irradiated methyl methacrylate was carried out. It was calculated from these results that the over-all activation energy for the process, E, was 11.2 kcal/mole, considerably less than the analogous value of 19.7 kcal/mole for the polymerization of methyl methacrylate by benzoyl peroxide [7]. Using the experimental value for the over-all

activation energy of polymerization, and the known values for chain growth (6.3 kcal/mole) and chain breaking (2.8 kcal/mole), it was calculated that the activation energy for initiation of the reaction was 13.0 kcal/mole. This was less than the value for the decomposition of methyl methacrylate peroxide, obtained by its thermal oxidation (22.0 kcal/mole) [8]. Highly active peroxide groups were obtained by the radiation oxidation of methyl methacrylate, and these were responsible for the possibility of carrying out low temperature polymerization by this means. The nature of this effect required further investigation. It was possible that the high activity of the peroxide was due to its oxidation-reduction interaction with other products of the radiation induced oxidation of the monomer (aldehydes, etc.).

A more detailed study of the kinetic curves obtained showed that they were considerably more smooth running than in the case of polymerization of methyl methacrylate by benzoyl peroxide; the "gel effect" was observed at a significantly higher degree of conversion and the ratio of the maximum speed in the autoaccelerating stage to the initial speed was less. This is shown graphically in Fig. 4, where the curves are compared for the relation between relative speed of polymerization (ratio of speed at a given moment to the initial speed) and relative duration. This special feature of the shape of the kinetic curves is evidently associated with the fact, that, in our case, termination of kinetic chains was brought about, not only by recombination of macromolecules (retardation of this process with increasing viscosity of the system is also responsible for the "gel effect" [9]), but also by interaction of the growing chains with particles of relatively low molecular weight.

The method of radiation polymerization described here retains the main advantage of the normal method of radiation polymerization – the possibility of carrying out the process at low temperature – and also enables the processes of irradiation and polymerization of the monomer to be performed separately, using continuous irradiation of a stream of monomer and subsequent polymerization of the latter outside the sphere of influence of the radiation. An important advantage of the method is also the smooth nature of the kinetic polymerization curves, which should considerably facilitate block polymerization.

LITERATURE CITED

[1] M. Magat, Coll. Czechoslov. Chem. Comm. 22, 141 (1957).

[2] V. V. Korshak, S. R. Rafikov, V. A. Sergeev and B. L. Tsetlin, Author's Certificate No. 116349 (1958).

[3] S. S. Medvedev, Collection, Isotopes and Radiation in Chemistry, (Acad. Sci. USSR Press, 1958) p. 103.*

[4] P. Ya. Glazunov and G. B. Radzievskii, Collection, Action of Ionizing Radiations on Inorganic and Organic Systems, (Acad. Sci. USSR Press, 1958) p. 395.*

[5] B. N. Moryganov, L. I. Efimov and V. V. Lyubimova, Treatise on the Chemistry and Technology of Polymers, vol. 2, Gorki (1958) p. 368.*

[6] N. A. Bakh, Collection, Radiation Chemistry, (Acad. Sci. USSR Press, 1955) p. 145.*

[7] G. V. Schulz and F. Blaschke, Z. Phys. Chem., B. 50, 305 (1941).

[8] Cheng Ping and Tien Jn-Lin, Acta chim. sinica 24, 2, 135 (1958).

[9] G. V. Schulz and G. Harborth, Makromolek. Chem. 1, 106 (1947).

Received February 25, 1959

* In Russian.

MECHANISM OF THE RADIATION-INDUCED DECOMPOSITION OF HYDROGEN PEROXIDE

B. V. Érshler, M. A. Nezhevenko and G. G. Myasishcheva

Institute of Theoretical and Experimental Physics of the Academy of Sciences of the USSR

(Presented by Academician A. I. Alikhanov, January 28, 1959)

In papers on the radiation-induced decomposition of H_2O_2 [1-9], no attempt has been made to compare the yield, $G_{H_2O_2}$, of this process with the precise data of Allen [10] on the radiolysis of water by γ-rays. This data may be represented by the equation

$$(2k + l)\, H_2O = (2m + n)\, H_2O = n\mathrm{H} + m\,\mathrm{OH} + l\, H_2O_2 + k\, H_2, \qquad (I)$$

where n = 3.64, m = 2.86, l = 0.87, k = 0.48, are Allen's coefficients giving the numbers of the corresponding particles produced by the absorption of 100 ev of radiation. We thought that such a comparison might make it possible to explain the mechanism of the process. This would be facilitated if radiolysis of aqueous solutions of H_2O_2 was carried out in the absence of H_2 and O_2, achieved, for example, by passing carefully purified N_2 through the liquid. Under these conditions, if reaction between the radicals H and OH could be disregarded, the only reactions which could occur without the liberation of oxygen would be the following

$$H_2O_2 + \mathrm{H} \rightarrow H_2O + \mathrm{OH}; \qquad (II)$$

$$H_2O_2 + \mathrm{OH} \rightarrow H_2O + HO_2; \qquad (III)$$

$$HO_2 + \mathrm{H} \rightarrow H_2O_2. \qquad (IV)$$

The occurrence of reaction (IV) has usually been disregarded, but, in its absence, the inequality $-G_{H_2O_2} > \frac{3}{2}\,m + \frac{1}{2}\,n - l = 6.02$ must be obeyed. Consequently, the inequality $-G_{H_2O_2} < 6.02$, found in our experiments, showed clearly that reaction (IV) did occur. Thus, the group of reactions (I), (II), III, and (IV) (subsequently denoted as (A) had to be considered in any mechanism for the decomposition of the peroxide.

The following reactions can occur in H_2O_2 solutions with liberation of oxygen:

$$HO_2 + \mathrm{OH} \rightarrow H_2O + O_2; \qquad (B)$$

$$H_2O_2 + HO_2 \rightarrow H_2O + \mathrm{OH} + O_2; \qquad (C)$$

$$HO_2 + HO_2 \rightarrow H_2O_2 + O_2; \qquad (D)$$

$$H_2O_2 + 2HO_2 \rightarrow 2H_2O_2 + O_2 \qquad (E)$$

S. Ya. Pshezhetskii and his co-workers [9] considered reaction (B) to be the most probable for chain breaking in the decomposition of hydrogen peroxide. Hart [4] thought that reaction (E) was the most probable, while others selected reaction (D). Identification of the main chain breaking reaction in the decomposition of H_2O_2 was made possible by comparing Allen's data with the value of $G_{H_2O_2}$, under conditions such that chains were practically

absent, i.e., when oxygen was liberated mainly by the reaction of chain breakage ($-G \lesssim 6$). The following expressions for $G_{H_2O_2}$ were derived by the stationary state method, using decomposition mechanisms involving the different reactions for the liberation of O_2:

Mechanism	Expression	
A + B	$\frac{k_{II}k_B}{k_{III}k_{IV}} = \frac{(1/2\,n - 1/2\,m + l - G)\,(1/2\,m - 1/2\,n + l - G)}{(3/2n + 1/2\,m - l + G)\,(m + n)}$;	(1)
A + C	$\frac{k_{II}k_C}{k_{IV}}[H_2O_2]^2\,(1/2\,I)^{-1} = \frac{n-m}{n+m}\,(1/2m - 1/2\,n + l - G)$;	(2)
A + D	$\frac{k_{II}k_D^{1/2}}{k_{IV}}[H_2O_2]\,(1/2\,I)^{-1/2} = \frac{(1/2n - 1/2m + l - G)\,(1/2m - 1/2n + l - G)^{1/2}}{(3/2n + 1/2m - l + G)}$;	(3)
A + E	$\frac{k_E k_{II}^2}{k_{IV}^2}[H_2O_2]^3\,(1/2\,I)^{-1} = \frac{(1/2m - 1/2n + l - G)\,(1/2n - 1/2m + l - G)^2}{(1/2m + 3/2n - l + G)^2}$,	(4)

where k_i are the velocity constants for the reactions indicated by the subscripts, $[H_2O_2]$ is the concentration of hydrogen peroxide and I is the intensity of radiation.

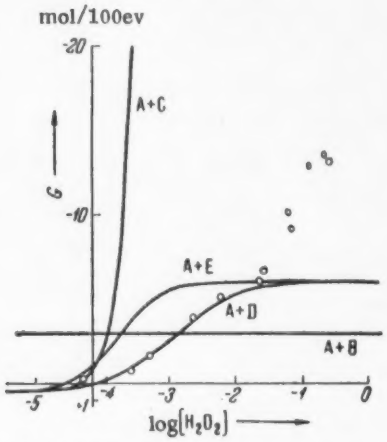

Fig. 1. Curves for G as a function of (log F^{1}/P), constructed for all mechanisms, transferred without change to the graph of G as a function of (log $[H_2O_2]$), and moved parallel to the log $[H_2O_2]$ axis until coincidence with the experimental points is recorded, in the region $-G < 6.0$; the concentrations of H_2O_2 in mole per liter.

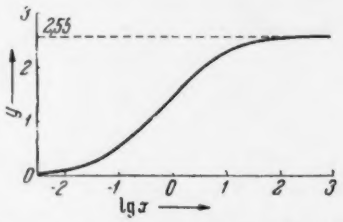

Fig. 2. Graph of y = function (log x) constructed from Equations (7) and (8).

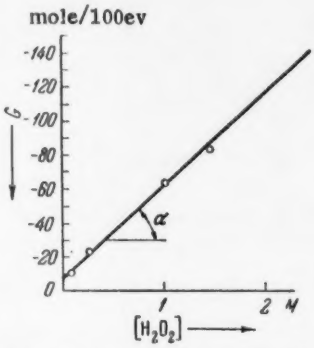

Fig. 3. Graph of G as a function of $[H_2O_2]$ in accordance with Eq. (11), at $I = 8 \cdot 10^{20}$ ev/liter·min.

It is clear that curves could be constructed for $G_{H_2O_2}$ as a function of F^{1}/P, , where F is the function of $G_{H_2O_2}$ on the right hand side of Eqs. (2), (3) or (4) and p is the power of $[H_2O_2]$ in the same equation; G is a constant in Eq. (1), so that, for $0.48 < -G < 6.02$, it was sufficient to know the Allen coefficients. It is also clear that the curves obtained in this way would coincide in shape with the curves for $G_{H_2O_2}$ as a function of (log $[H_2O_2]$), and would differ from the latter only in their position along the x axis. It followed from the equations that, with changing I and constant k_i (i.e., temperature), the curves of $G_{H_2O_2}$ as a function of (log$[H_2O_2]$) would move parallel to the x axis without

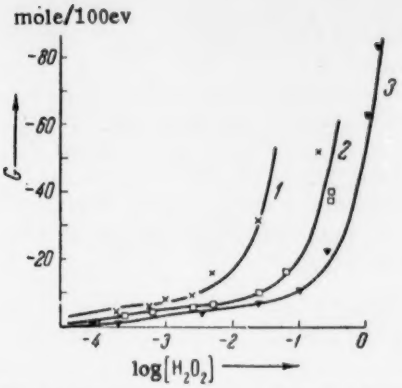

Fig. 4. Theoretical curves of G as a function of ($\log[H_2O_2]$), constructed from Eqs. (7), (8) and (10), with $M = 1.2 \cdot 10^{-2}$. 1) $I = 1.16 \cdot 10^{19}$ ev/liter · minute; 2) $I = 4.4 \cdot 10^{19}$ ev/liter · minute; 3) $I = 8 \cdot 10^{20}$ ev/liter · minute $[H_2O_2]$ in mole/liter.

changing shape. Fig. 1 shows such curves for all the mechanisms considered. It is obvious that the results obtained (the points)* for $-G_{H_2O_2} < 6$, agreed only with the curve for the mechanism A + D, and clearly differed from the others. From these results $\frac{k_{II}}{k_{IV}} k_D^{1/2} =$ $= 0.6\ \text{liter}^{1/2}\ \text{mole}^{-1/2}\ \text{second}^{-1/2}$.

For $-G_{H_2O_2} > 6$, reaction C was added to reactions A + D to maintain the chain process. For the mechanism A + D + C:

$$G_{H_2O_2} = k - \frac{2}{I}(D + C), \tag{5}$$

where D and C were the rates of the corresponding reactions

$$D = k_D [HO_2]^2, \quad C = k_C [HO_2][H_2O_2]. \tag{6}$$

For the determination of $[HO_2]$, starting from (6), we derived by the method of stationary states the expression

$$[HO_2]^2 = \left[m + n \frac{1 - k_{IV}[HO_2]/k_{II}[H_2O_2]}{1 + k_{IV}[HO_2]/k_{II}[H_2O_2]} \right] \frac{I}{2k_D}, \tag{7}$$

which gave $[HO_2]$ as a function of $[H_2O_2]$, three constants k_i and the Allen coefficients. Introducing the new terms $\underline{x}$ and $\underline{y}$, where

$$[H_2O_2] = x \frac{k_{IV}}{k_{II}} \left(\frac{I}{2k_D} \right)^{1/2}, \quad [HO_2] = y \left(\frac{I}{2k_D} \right)^{1/2}, \tag{8}$$

we obtained from (7) the curve

$$y\,(\lg x) \tag{9}$$

(Fig. 2), whose shape depended only on the Allen coefficients and not on I and k_i.

Combining (5), (6) and (8), we obtained

$$G_{H_2O_2} = k - [y^2 + Qxy], \qquad Q = k_C k_{IV} / k_D k_{II}. \tag{10}$$

It followed from Eq. (10) that the shape of the curve of $G_{H_2O_2}$ as a function of (log x) did not depend on the intensity of irradiation, and from (8) that the curves of $G_{H_2O_2}$ as functions of (log x) and ($\log[H_2O_2]$) were identical in shape, but differed in their positions along the abscissa axis. It also followed from these three equations that, with changing intensity, the curve $G_{H_2O_2}$ as a function of ($\log[H_2O_2]$) remained parallel to its original position, but moved along the abscissa axis, the movement being equal to the increase in $\log I^{1/2}$.

For the determination of Q in Eq. (10), it was noted that, for large values of $\underline{x}$ and consequently for large values of $[H_2O_2]$, $y \to 2.55$ (see Fig. 2), and for $G_{H_2O_2}$, on the basis of (10) and (6),

* The values of $G_{H_2O_2}$ shown were obtained with solutions of hydrogen peroxide which had been redistilled three times under reduced pressure without boiling (t = 35°).

$$G_{H_2O_2} = 0{,}48 - \left[2{,}55^2 + 2{,}55\,\frac{k_C}{k_D^{1/2}}\,\frac{[H_2O_2]}{(1/2\,I)^{1/2}}\right] = -6{,}02 - 3{,}6\,\frac{k_C}{k_D^{1/2}}\,I^{-1/2}[H_2O_2], \qquad (11)$$

i.e., $G_{H_2O_2}$ became a linear function of $[H_2O_2]$. The experimental values of $G_{H_2O_2}$, for large values of $[H_2O_2]$, agreed excellently with the linear equation (11) (Fig. 3). The intercept of this straight line on the ordinate axis was ~ 6. From the slope of the line, we found $k_C/k_D^{1/2} = I^{1/2} \tan\alpha/3.6 = 7.2 \cdot 10^{-3}$ liter$^{1/2}$ mole$^{-1/2}$ second$^{-1/2}$. Hence, $Q = (k_C/k_D^{1/2}) : (k_{II}k_D^{1/2}/k_{IV}) = 1.2 \cdot 10^{-2}$. The curve relating $G_{H_2O_2}$ and $(\log[H_2O_2])$, constructed on the basis of Eqs. (10) and (9), using this value of Q, agreed well with the experimental results over the whole range of $G_{H_2O_2}$. It is evident from Fig. 4, that, with changing intensity, this curve, in accordance with theory, moved parallel to itself along the $\log[H_2O_2]$ axis by an amount equal to the increase in $\log I^{1/2}$.

The above analysis showed that radiation-induced decomposition of hydrogen peroxide proceeded by the mechanism A + D + C. This type of analysis could, evidently, also be used for different radiolytic processes.

LITERATURE CITED

[1] O. Risse, Z. Phys. Chem. 140 A, 133 (1929).

[2] H. Fricke, J. Chem. Phys. 3, 364 (1935).

[3] S. R. Johnson, J. Chem. Phys. 19, 1204 (1951).

[4] E. J. Hart and M. S. Matheson, Disc. Farad. Soc. 49, 1160 (1953).

[5] F. S. Dainton and J. Rowbottom, Trans. Farad. Soc. 49, 1160 (1953).

[6] A. O. Allen, C. J. Hochanadel, J. A. Ghormley and T. W. Davis, J. Phys. Chem. 56, 575 (1952).

[7] P. I. Dolin, Collection, Reports on Radiation Chemistry, (Acad. Sci. USSR Press, 1955) p. 7.*

[8] V. I. Veselovskii and G. S. Tyurikov, Collection, Reports on Radiation Chemistry, (Acad. Sci. USSR Press, 1955) p. 61.*

[9] V. Ya. Chernykh, S. Ya. Pshezhetskii and G. S. Tyurikov, Theses of the Proceedings of the 1st All-Union Conference on Radiation Chemistry, (Acad. Sci. USSR Press, 1957) p. 18.*

[10] A. O. Allen, Rad. Res. 1, 85 (1954).

Received January 26, 1959

* In Russian.

ELECTRON DIFFRACTION STUDY OF THE STRUCTURE OF VINYL CHLORIDE AND TRICHLOROFLUOROETHYLENE

P. A. Akishin, L. V. Vilkov and Yu. I. Vesnin

M. V. Lomonosov Moscow State University

(Presented by Academician V. N. Kondrat'ev, February 5, 1959)

Vinyl chloride C_2H_3Cl and trichlorofluoroethylene C_2F_3Cl are the starting monomers in the production of several important polymers, and therefore, it is important to know their molecular structures, not only to understand the polymerization mechanism, but also to explain certain problems connected with the theory of molecular structure. By the latter we mean mainly the concepts of a partial double bond character, which are frequently invoked [1-3] to explain bond-length variations in organic halo compounds. Thus, it was assumed that the shortening of the C-Cl bond in vinyl chloride due to a partial double bond character should be accompanied by the lengthening of the C-C bond to 1.38 A as compared with r(C-C) = 1.34 A in ethylene. It should be noted that an electron diffraction study of C_2H_3Cl [4] gave a range of r(C-C) values from 1.30 to 1.38 A, the authors of that paper, however, relying primarily on resonance representation gave preference to the value of r(C-C) = 1.38 A. Later, on the basis of these same ideas, attempts were made [1, 2] to explain the difference between the C-Cl bond lengths in C_2H_3Cl and C_2Cl_4 (which were actually within the range of experimental errors) by assuming that the double bond character of the C-Cl bond decreased as the number of halogens on a carbon was increased. It is obvious that any structural arguments used for C_2H_3Cl are also valid for C_2F_3Cl, for which until now there isn't any structural data available.

The electron diffraction patterns of C_2H_3Cl and C_2F_3Cl vapors were obtained in a previously described [5] apparatus. The patterns were interpreted by estimating the intensities visually; two methods were used: radial distribution (rD(r) curves) and successive approximations [6] (I(s) curves). In the investigation of vinyl chloride we introduced a temperature factor into the interatomic C-H and Cl-H distances.

1. Investigation of vinyl chloride. We obtained and computed seven sets of electron diffraction patterns (4 patterns per set) for vinyl chloride vapor (b.p. $-13.8°$)*. From the experimental values of s and I(s) listed in Table 1, we constructed an experimental curve (Fig. 2) and then calculated the radial distribution curve (Fig. 1, I) whose principal peaks corresponded to the following interatomic distances**: 1) 1.32 A, r(C=C); 2) 1.72 A, r(C-Cl); 3) 2.71 A, r(C . . . Cl). The radial distribution curve (Fig. 1, II) was calculated from the theoretical Curve a (Fig. 2) by extrapolating the experimental intensity curve from s = 5.0 to s = 0.0. This curve had maxima at 1.35 A, and 2.72 A.

Essentially, the method of successive approximations gave a more accurate r(C=C) distance. In calculating the theoretical intensity curves (Table 2, Fig. 2) we used the r(C-Cl) and r(C . . . Cl) values from rD(r) curves, while r(C-H) = 1.07 A and $\angle HCH = 120°$ were taken from the literature [7]. Since the scattering of electrons by hydrogen atoms is rather insignificant, any errors in the selected parameters would not appreciably affect the theoretical curves. Curve a gave the best agreement with the experimental curve; a certain divergence in the

*We obtained vinyl chloride from the kinetics and catalysis laboratory in the Chemistry Department of MGU; we wish to thank the workers of that laboratory, A. M. Rambaev and S. I. Skuratov.

**Dash is used to denote distances between bound atoms and dotted line between unbound ones.

TABLE 1

Electron Diffraction Measurements on Vinyl Chloride Vapors (λ = 0.054-0.057 A; the average distance between nozzle and plate was 116 mm)

Max.	Min.	$I(s)$	s_{exp}	$\frac{s_{theor}}{s_{exp}}$, Curve g	$\frac{s_{theor}}{s_{exp}}$, Curve g
2		+20	5,96	1,018	1,038
	3	—16	6,38	1,000	1,016
3		+12	7,41	(1,029)	1,042
	4	—1	8,59	—	—
4		+3	9,64	0,997	1,027
	5	—1	10,81	—	—
5		+10	12,03	0,997	1,005
	6	—9	13,46	0,999	1,004
6		+8	14,63	1,017	1,027
	7	—6	17,75	0,994	1,002
7		+6	19,00	1,007	1,017
	8	—4	20,40	1,010	1,019
8		+2	21,58	0,996	1,019
Average value				1,003	1,020
Average deviation				±0,007	±0,010

TABLE 2

Theoretical Curve Parameters for Vinyl Chloride (r in A)*

Curves	Interatomic distances		Bond angles
	$r(C=C)$	$r(C\cdots Cl)$	∠CCCl
a	1,32	2,71	125
b	1,36	2,71	122
c	1,28	2,71	129
d	1,34	2,71	123
e	1,30	2,71	126
f**	1,32	2,71	125
g	1,32	2,68	123

*We took r(C — Cl) = 1.72 A.

**This curve was computed with the temperature factor, $a_{C\ldots Cl}$ = 0.0022, taken into account.

region of the 4th maximum, as well as in the relative intensities of the 6th and 7th maxima can be attributed to an error in the visual measurements. We obtained the following parameters for vinyl chloride: r(C — C) = = 1.32 ± 0.02 A; r(C — Cl) = 1.72 ± 0.01 A; ∠CCCl = 1.25 ± 2°; we also used r(C — H) = 1.07 A and ∠HCH = = ∠HCCl = 120°.

2. Investigation of trifluorochloroethylene. We obtained and calculated out 9 sets of electron diffraction patterns of C_2F_3Cl (b.p. = 27.9° at 760 mm)* vapors. With the obtained values of s and I(s) (Table 3), we constructed an experimental intensity curve (Fig. 4). The middle section of the diffraction pattern (from s = 8 to 13) was so diffused that although we visually detected three maxima, we were unable to determine their intensities. The radial distribution curve (Fig. 3) was calculated from an experimental intensity curve in which the middle section was traced by dots (Fig. 4). The maxima on the rD(r) curve corresponded to the following interatomic distances in the molecule.

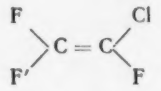

1) 1,32 A — r C — F & r(C=C);
2) 1,72 A — r (C—Cl);
3) 2,32 A — r (C..F), r = (F..F′);
4) 2,67 A — r (Cl..F); r (C···Cl), r (F′..F″);
5) 3,07 A — r (Cl..F);
6) 3,57 A — r (C..F″);
7) 3,93 A — r (Cl..F′).

Peaks 6 and 7 could only be resolved when the artificial temperature factors used in calculating rD(r) were neglected. Let us note that if we disregard the middle section of the experimental intensity curve in calculating the rD(r) curve the position of maxima still remains unchanged. Curve II in Fig. 3 was calculated from the experimental intensity curve, the middle section of which was obtained by extrapolating the best theoretical Curve e. Mean-

*We are obliged to L. S. German and B. L. Dyatkin, workers at the Laboratory of Fluoroorganic Compounds of the Institute of Heteroorganic Compounds of the Acad. Sci. USSR, for supplying us with the C_2F_3Cl.

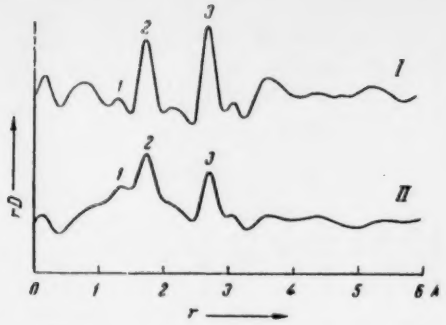

Fig. 1. Radial distribution curves for C_2H_3Cl.

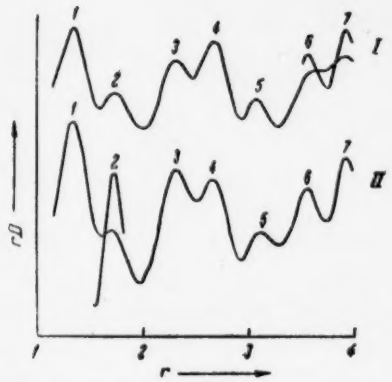

Fig. 3. Radial distribution curves for C_2F_3Cl.

TABLE 3

Electron Diffraction Measurements on Trifluorochloroethylene Vapors (λ = 0.054-0.057 Å; average distance between nozzle and plate was 116 mm)

Max.	Min.	$l(s)$	s_{exp}	$\frac{s_{theor}}{s_{exp}}$, Curve e
	2	—20	4,31	0,986
2		+20	5,33	(1,031)
3		+2	11,57	0,996
	4	—8	13,65	1,000
4		+7	14,74	1,007
	5	—1	15,74	(1,018)
5		+3	16,64	1,001
	6	—4	18,15	1,005
6		+3	19,81	1,010
Average value				1,001
Average deviation				±0,006

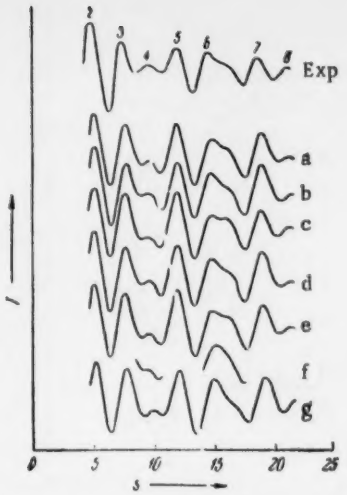

Fig. 2. Experimental and theoretical intensity curves for C_2H_3Cl.

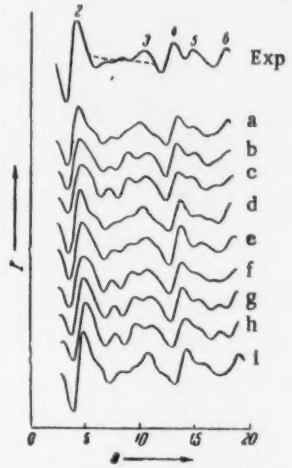

Fig. 4. Experimental and theoretical intensity curves for C_2F_3Cl.

while, r(C − Cl) changed to 1.695 A. We could also get a nicely resolved peak at 1.715 A, by neglecting the temperature factor in calculating rD(r). Thus, it became clear that small intensity variations in the middle section of the diffraction pattern ($8 < s < 13$), which could not be accurately determined, had no significant effect on the position of maxima on the rD(r) curve.

The C_2F_3Cl molecule contains 8 independent parameters. The distances r(C − F) = 1.32 A and r(C − Cl) = 1.72 Å were unequivocally determined from the rD(r) curve whose maxima were in good agreement with the planar configuration of the molecule. The

TABLE 4

Theoretical Curve Parameters for Trifluorochloroethylene* (r in A)

Curve	Interatomic distance	Bond angles, in °			Curve	Interatomic distance	Bond angles, in °		
	r(C – C)	∠FCF'	∠FCC	∠CICC		r(C – C)	∠FCF'	∠FCC	∠CICC
a	1,31	110	125	123	f	1,31	114	123	130
b	1,31	110	125	127	g	1,31	114	127	127
c	1,31	110	125	130	h	1,31	114	130	127
d	1,31	114	123	123	i	1,34	114	123	123
e	1,31	114	123	127					

We did not vary the values of r(C – F) = 1.32 A, r(C – Cl) = 1.72 A, and ∠CICF = 114° assuming a planar model.

parameters r(C – C) = 1.31 A and ∠CICF* = 114° were taken from the data given for C_2F_4, C_2Cl_4 and C_2Br_4 [8, 9]. By using the method of successive approximations we obtained more precise values for three parameters: ∠FCF', ∠CCF, and ∠CCCl (Table 4). The theoretical Curve e gave the best agreement with the experimental intensity distribution (Table 4, Fig. 4). We obtained the following parameters for C_2F_3Cl: r(C – C) = 1.31 A (assumed value); r(C – F) = 1.32 ± 0.01 A; r(C – Cl) = 1.72 ± 0.02 A; ∠CICF = 114° (assumed); ∠FCF = 114° ± 2°; ∠CCF = = 123 ± 1°; ∠CCCl = 127° ± 1.5°.

Our value of r(C=C) = 1.32 A in C_2H_3Cl agrees with the most reliable recent data for: C_2H_4 (1.334 A [10], C_2F_4 (1.31 A), 1,1-$C_2H_2F_2$ (1.32 A) [8], 1,1-$C_2H_2Cl_2$ (1.32 A) [11], and C_2Cl_4 (1.30 A). The value of r(C – Cl) = 1.72 A in C_2H_3Cl and C_2F_3Cl agrees with the data from 1,1-$C_2H_2Cl_2$ (1.727 A) [11] and C_2Cl_4 (1.72 A) [12].

The results of this work as well as our examination of the literature data indicate that no elongation of the C=C bond in halogen derivatives of ethylene is observed (one can rather note a tendency toward shortening), nor were any systematic changes observed in the C – Cl bond length with increasing number of halogen atoms.

LITERATURE CITED

[1] L. Pauling, The Nature of the Chemical Bond, 1947 [Russian translation].

[2] J. A. Ketellar, Chemical Constitution, Elsevier, Amsterdam, 1953.

[3] A. E. Chichibabin, Fundamentals of Organic Chemistry 1 (1933).*

[4] L. O. Brockway, J. V. Beach and L. Pauling, J. Am. Chem. Soc. 57, 2693 (1935).

[5] A. V. Frost and P. A. Akishin, et al., Bull. Moscow Univ. No. 12, 85 (1953).

[6] K. Hedberg and A. J. Stosik, J. Am. Chem. Soc. 74, 954 (1952).

[7] P. Allen and L. Sutton, Acta. Cryst. 3, 46 (1950).

[8] I. Karle and J. Karle, J. Chem. Phys. 18, 963 (1950); 20, 63 (1952).

[9] P. A. Akishin, L. V. Vilkov and V. M. Tatevskii, Bull. Moscow Univ. No. 1, 143 (1957).

[10] L. S. Bartell and R. A. Bonham, J. Chem. Phys. 27, No. 6, 1414 (1957).

[11] S. Sekino and T. Nishikawa, J. Phys. Soc. Japan 12, No. 1, 43 (1957).

Received February 2, 1959

*In Russian.

EQUILIBRIUM SYNTHESIS OF ETHYL ALCOHOL

Yu. M. Bakshi, A. I. Gel'bshtein and M. I. Temkin

L. Ya. Karpov Physicochemical Scientific Research Institute

(Presented by Academician, S. S. Medvedev, January 26, 1959)

The extent to which the reaction proceeds during vapor phase hydration of ethylene depends on the equilibrium

$$C_2H_4\,(g) + H_2O\,(g) = C_2H_5OH\,(g). \qquad (1)$$

The gases involved in Equilibrium (1) cannot be assumed to behave ideally under the industrial conditions used for this reaction. Therefore, it is essential to distinguish between $K_p = P_{C_2H_5OH}/P_{C_2H_4}P_{H_2O}$, where $P_{C_2H_5OH} = PN_{C_2H_5OH}$ (P = total pressure, $N_{C_2H_5OH}$ – the mole fraction of C_2H_5OH) etc., and $K_f = f_{C_2H_5OH}/f_{C_2H_4}f_{H_2O}$, where C_2H_5OH is the fugacity of C_2H_5OH etc. This complicates the study of Equilibrium (1), since the methods of calculating fugacities in gaseous mixtures have not been sufficiently well developed, particularly in mixtures of highly polar components. A series of papers [1-14] have been devoted to the study and calculation of Equilibrium (1); the results, however, were frequently conflicting. Calculations done by Vvedenskii and Fel'dman [12] are being frequently used [15-17]. A kinetic study of Reaction (1) revealed that the fractions of ethylene reacting under equilibrium conditions were much below the values calculated in [12]. And so it was this fact that prompted us to carry out an experimental study of Equilibrium (1); the results are presented below.

Investigation was carried out in a stainless steel flow reactor. Phoshoric acid on silica gel (about 40% H_3PO_4 by weight of catalyst) was used to catalyze the reaction.

Approximate values of K_p were first obtained by synthesizing the alcohol from mixtures of ethylene and water vapor with various amounts of catalyst. To get more precise values of K_p we passed different mixtures of ethylene, water vapor, and alcohol over the catalyst; in some mixtures the ratio between the partial pressures $P_{C_2H_5OH}/P_{C_2H_4}P_{H_2O}$ was greater, in others slightly smaller than K_p. In this manner though we approached the equilibrium from two sides, we obtained practically identical results.

Water or water + alcohol mixtures were transferred by means of a high pressure piston into the evaporator where the vapors were mixed with ethylene. Dehydration of ethyl alcohol yielded at least 99.5% pure C_2H_4. The temperature of the catalyst was measured with a chromel – alumel thermocouple, which was calibrated on the boiling points of pure compounds; temperature variations did not exceed ± 3°. Pressure was measured with a calibrated manometer and remained constant within ± 0.5 atm.

After leaving the reactor, the gaseous mixture passed through a water-cooled condenser, a dry ice trap, a rheometer, and a gas meter. Alcohol was determined by esterification with formic acid [18]; we also determined the yields of side reaction products such as $(C_2H_5)_2O$ and polymers of ethylene.

Experimental results are shown in Table 1. Volumetric rates were obtained from the ratio between the rate of alcohol consumption (0°, 1 atm) and the volume of the catalytic layer. The average values of K_p obtained from experiments on water + alcohol mixtures are given in Table 2.

TABLE 1

Temp. °C	p, in atm	Vol. flow rate of C_2H_4/hr	Compn. of initial mixture, in mol. fract.			Compn. of outgoing mixture, in mol. fract.				$K_p \cdot 10^3$, atm^{-1}
			C_2H_4	H_2O	C_2H_5OH	C_2H_4	H_2O	C_2H_5OH	$(C_2H_5)_2O$	
258	21	670	0,624	0,376		0,638	0,342	0,0169	0,0029	3,69
258	41	1100	0,690	0,310		0,691	0,279	0,0248	0,0052	3,14
258	41	1100	0,706	0,277	0,0170	0,718	0,252	0,0246	0,0054	3,32
258	41	1100	0,720	0,253	0,0270	0,716	0,254	0,0244	0,0056	3,27
258	41	830	0,690	0,310		0,697	0,272	0,0251	0,0058	3,23
258	81	1100	0,696	0,304		0,695	0,260	0,0316	0,0133	2,16
258	81	1100	0,721	0,257	0,0220	0,737	0,211	0,0308	0,0212	2,44
258	81	1100	0,750	0,215	0,0350	0,703	0,230	0,0340	0,0330	2,60
258	81	830	0,695	0,305		0,657	0,295	0,0395	0,0085	2,52
286	41	1370	0,628	0,372		0,653	0,328	0,0192		2,19
286	41	1370	0,651	0,334	0,0150	0,621	0,355	0,0207	0,0034	2,29
286	41	1370	0,664	0,312	0,0240	0,613	0,358	0,0207	0,0083	2,31
286	41	910	0,632	0,368		0,621	0,356	0,0203	0,0027	2,24
286	51	1370	0,632	0,368		0,628	0,346	0,0228	0,0032	2,06
286	51	1370	0,658	0,323	0,0190	0,640	0,330	0,0240	0,0060	2,23
286	51	1370	0,666	0,307	0,0269	0,638	0,333	0,0249	0,0041	2,28
286	51	910	0,634	0,366		0,602	0,368	0,0250	0,0050	2,21
286	71	1370	0,644	0,356		0,622	0,335	0,0315	0,0115	2,13
286	71	1370	0,683	0,285	0,0320	0,623	0,328	0,0318	0,0170	2,19
286	71	910	0,678	0,294	0,0280	0,617	0,337	0,0280	0,0180	1,90
286	71	910	0,682	0,286	0,0318	0,618	0,334	0,0314	0,0166	2,14
286	81	2500	0,637	0,363		0,615	0,354	0,0255	0,0055	1,44
286	81	1370	0,646	0,354		0,597	0,356	0,0333	0,0137	1,93
286	81	1370	0,671	0,309	0,0200	0,675	0,274	0,0324	0,0186	2,16
286	81	1370	0,689	0,279	0,0320	0,641	0,304	0,0340	0,021	2,16
286	81	910	0,645	0,355		0,614	0,338	0,0336	0,0144	2,00
286	81	910	0,672	0,306	0,022	0,650	0,303	0,0326	0,0144	2,04
286	81	910	0,683	0,281	0,0[illegible]	0,645	0,312	0,0308	0,0122	1,89
286	81	680	0,650	0,350		0,600	0,344	0,0340	0,0220	2,03
318	41	440	0,362	0,638		0,362	0,621	0,0148	0,0[illegible]22	1,61
318	41	440	0,367	0,625	0,0080	0,367	0,615	0,0152	0,0028	1,64
318	41	440	0,375	0,607	0,0180	0,362	0,620	0,0154	0,0036	1,67
318	81	440	0,377	0,623		0,361	0,601	0,0293	0,0088	1,67
318	81	440	0,393	0,590	0,0170	0,366	0,594	0,0286	0,0114	1,62
318	81	440	0,406	0,563	0,0310	0,367	0,593	0,0289	0,0111	1,64
345	41	440	0,260	0,740		0,253	0,736	0,0082	0,0028	1,08
345	41	440	0,264	0,730	0,0060	0,254	0,734	0,0088	0,0032	1,15
345	41	440	0,265	0,724	0,0110	0,255	0,734	0,0091	0,0020	1,20
345	81	440	0,267	0,733		0,254	0,727	0,0155	0,0035	1,04
345	81	440	0,277	0,716	0,0070	0,251	0,726	0,0158	0,0072	1,07
345	81	440	0,287	0,690	0,0230	0,256	0,715	0,0189	0,0091	1,27
365	41	440	0,252	0,748		0,240	0,750	0,0071	0,0029	0,962
365	41	440	0,261	0,735	0,0040	0,239	0,740	0,0069	0,0141	0,952
365	41	440	0,265	0,724	0,0110	0,239	0,748	0,0068	0,0062	0,928

TABLE 2

Temp. °K	Average $\frac{N_{H_2O}}{N_{C_2H_4}}$	$K_p \cdot 10^3$ 41 atm	51 atm	71 atm	81 atm	$\frac{\log K_\gamma}{P} \cdot 10^4$	$K_f \cdot 10^3$	$K_{f\,calc}$ (a)	(b)
531	0,33	3,30	—	—	2,52	29,3	4,35	5,04	7,97
559	0,51	2,30	2,25	2,08	2,03	14,2	2,64	2,99	4,74
591	1,7	1,65	—	—	1,63	1,32	1,67	1,74	2,79
618	2,9	1,18	—	—	1,17	0,90	1,19	1,16	1,86
638	3,1	0,94	—	—	—	—	—	0,88	1,43

If the gaseous mixtures deviate only slightly from ideal behavior, we can apply the following equation of state

$$V = \frac{RT}{P} + B, \tag{2}$$

where V is the molar volume of the mixture, and B the second virial coefficient, whose value depends on the composition of the mixture

$$B = \sum_i \sum_j B_{ij} N_i N_j. \tag{3}$$

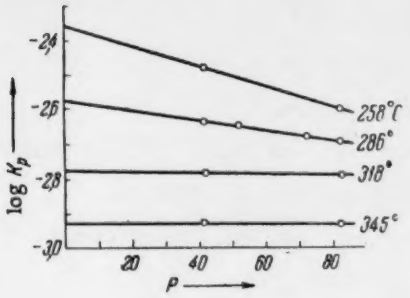

Fig. 1.

Numbers $B_{ij} = B_{ji}$ are both functions of T. With the help of equation [19]

$$RT \ln \gamma_i = \int_0^P \left(\bar{V}_i - \frac{RT}{P} \right) dP, \tag{4}$$

where $\bar{V}_i$ is the partial molar volume and $\gamma_i = \frac{f_i}{N_i P}$ the activity coefficient, we get

$$\ln \gamma_i = \frac{2B_i - B}{RT} P, \tag{5}$$

where

$$B_i = \sum_j B_{ij} N_j. \tag{6}$$

(See [20]). Since K_γ can be defined by

$$\ln K_\gamma = \sum_i \nu_i \ln \gamma_i, \tag{7}$$

where ν_i are stoichiometric activity coefficients (positive for reaction products, negative for starting materials), we will get

$$\ln K_\gamma = \frac{2 \sum_i \nu_i B_i - B \sum_i \nu_i}{RT} P. \tag{8}$$

$\frac{2 \sum_i \nu_i B_i - B \sum_i \nu_i}{RT}$ is a function of temperature and composition. Since the alcohol content in equilibrium mixtures is small, we can assume that at a given T, the above shown number depends on the ratio $N_{H_2O}/N_{C_2H_4}$. Since $K_f = K_\gamma K_p$, then at a constant $N_{H_2O}/N_{C_2H_4}$, $\ln K_p$ should be a linear function of p. In Table 2, we have listed the values of log K_f obtained by extrapolating log K_p to P = 0 at a constant $N_{H_2O}/N_{C_2H_4}$ (Fig. 1), and values of log $K\gamma/P$ determined from the slopes of these lines. For the sake of comparison, we also included in the graph of $K_{f\,calc}$: a) values interpolated from the results of spectroscopic data [13], and b) values calculated from tables of thermodynamic functions (issued by U. S. Bureau of Standards [21]) with the help of empirical equations for heat capacities [22, 23]. Calculations based on spectroscopic data were in good agreement with our experiment, particularly at high temperatures. Bureau of Standards data gave values of K_f slightly too big, evidently due to a poor choice of S°_{298} for C_2H_5OH. Our values of K_f can be expressed by equation

$$\log K_f = \frac{2093}{T} - 6{,}304, \tag{9}$$

obtained by the method of least squares. For the investigated (mixture) compositions, the values of K_γ are almost equal to 1 at temperatures close to 350°C. At lower temperatures $K_\gamma < 1$; we may assume that at more elevated temperatures $K_\gamma > 1$. In analogy with the term "Boyle's temperature" for the temperature at which B = 0, we can denote the temperature at which $K_\gamma = 1$ (for a mixture of given composition by the term "Guldberg and Waage temperature."

LITERATURE CITED

[1] F. E. Frey and H. J. Hepp, Ind. and Eng. Chem. 25, 441 (1933).

[2] N. Kozlov and P. Fedoseev, Synthetic Rubber 5, 36 (1934).

[3] F. J. Sanders and B. F. Dodge, Ind. and Eng. Chem. 26, 208 (1934).

[4] H. M. Stanley, G. J. E. Gouell and S. B. Dymock, J. Soc. Chem. Ind. Trans. 53, 205 (1934).

[5] E. R. Gilliland, R. C. Gunnes and V. O. Bowles, Ind. and Eng. Chem. 28, 370 (1936).

[6] M. P. Appleby, J. V. S. Glass and G. F. Horsely, J. Soc. Chem. Ind. Trans. 56, 279 (1937).

[7] R. H. Bliss and B. F. Dodge, Ind. and Eng. Chem. 29, 19 (1937).

[8] J. N. Pearce and J. W. Newsome, Ind. and Eng. Chem. 30, 588 (1938).

[9] W. H. Shiffler, M. M. Holm and L. F. Brooke, Ind. and Eng. Chem. 31, 1099 (1939).

[10] R. H. Ewell, Ind. and Eng. Chem. 32, 147 (1940).

[11] J. G. Aston, Ind. and Eng. Chem. 34, 514 (1942).

[12] A. A. Vvedenskii and A. F. Fel'dman, J. Gen. Chem. 15, 37 (1945).

[13] F. G. Brickwedde, M. Moskow and J. G. Aston, J. Res. Nat. Bur. Stand. 37, 263 (1946).

[14] V. V. Korobov, and A. V. Frost, Free Energies of Organic Compounds, Moscow, 1950.*

[15] M. G. Gonikberg, Chemical Equilibrium and Reaction Rates at High Pressures, Moscow, 1953.*

[16] B. A. Krentsel', Synthesis of Aliphatic Alcohols From Petroleum Hydrocarbons, Moscow, 1954.*

[17] I. I. Yukel'son, Technology of Fundamental Organic Synthesis, Moscow, 1958.*

[18] A. I. Gulyaeva, V. F. Polikarpova and Z. K. Remiz, Analysis of Products Obtained in the Manufacture of Divinyl from Ethyl Alcohol by the Method of S. V. Lebedev, Moscow, 1950.*

[19] L. J. Gillespie, J. Am. Chem. Soc. 48, 28 (1926).

[20] M. I. Temkin, J. Phys. Chem. 17, 441 (1943).

[21] Selected Values of Chemical Thermodynamic Properties, Circ. Nat. Bur. St., 500 (1952).

[22] H. M. Spencer, J. Am. Chem. Soc. 67, 1859 (1945).

[23] H. M. Spencer, Ind. and Eng. Chem. 40, 2152 (1948).

Received January 24, 1959

* In Russian.

THE STABILITY AND VISCOSITY OF CONCENTRATED SUSPENSIONS IN OLEOGELS OF METALLIC SOAPS

G. V. Belugina, S. Kh. Zakieva, Academician P. A. Rebinder and A. B. Taubman

Institute of Physical Chemistry of the Academy of Sciences, USSR

The investigation of problems connected with the stability of dispersed systems (aqueous suspensions of clays, oil suspensions of pigments in varnishes, filled polymers (rubber), et al.) has been greatly extended by the work done in our laboratory [1-3]. At the same time, it was shown that concentrated suspensions can achieve maximum stabilization only by structure formation in the solvated layers absorbed on the surface of the particles, or by developing a three-dimensional meshwork over the entire volume of the liquid dispersion medium. From the standpoint of these ideas, É. M. Natanson [4] studied the conditions for the formation and stabilization of organic sols of metals.

We used in our work the aluminum soaps of alicyclic acids to form the ordered framework, since, they give oleogels with unusual structural and mechanical properties [5, 6]. The properties of oleogels depend to a large extent on the soap composition as well as on the molecular nature of the dispersion medium and can therefore, be regulated by changing these same factors [7, 8]. With reference to this, we studied the changes in the viscosity (on standing) of aluminum salts of alicyclic acids prepared as gels in hydrocarbon media and of corresponding concentrated suspensions. The solid dispersed phase was prepared from standard industrial aluminum powder (oxidized on the surface), with the particle size ranging from 6 to 13μ. The dispersion medium consisted of a purified main paraffin cycloalkane fraction in the T-1 brand of fuel; it was prepared from the industrial product by removing polar impurities plus unsaturated and aromatic hydrocarbons until the aromatic hydrocarbon content was reduced to 1.5%*.

We used aluminum salts of alicyclic acids of the general formula $Al(OH)_n(RCOO)_m$, where $n + m = 3$, to help form the structural framework; these were prepared by a double exchange decomposition under conditions: a) where the pH of the medium was varied during precipitation and the OH content per soap molecule $n = 1.15$ (Sample a or b) where the pH was kept constant, $pH \approx 5$ for $n = 0.85$ and $pH \approx 4$ for $n = 0.9$ (Samples 2 and 3 respectively); the method was developed by one of the workers [7].

The suspensions and gels were characterized by the maximum (threshold) viscosity (η) of an almost rigid structure [8]. The viscosity of gels prepared from aluminum salts of alicyclic acids would change on standing, hence, we measured it (η) as a function of the time elapsed since the gels were formed (τ), and the first viscosity measurement was carried out two days after the gel was prepared; this time interval was essential for the "ripening", i.e., for the soap to completely dissolve and form a homogeneous gel.

We have drawn in Fig. 1 some typical curves of $\log \eta$ vs. τ for a gel prepared with 2% aluminum salt of alicyclic acids (Curve 1a) and possessing a great thickening capacity (Sample 1), and for a 50% aluminum suspension prepared on the same type of gel (1b). One can readily see that the introduction of a solid phase increases sharply the initial viscosity without, however, changing the nature of the aging process; the ($\log \eta$, τ) curves have the same shape in both cases and indicate a very rapid decline in viscosity (it dropped to $\sim 1/25$ of its initial value in one month).

*Industrial fuel T-1 was purified under the direction of S. F. Vasil'ev by means of a method developed by him.

TABLE

Solvent	Soap sample	Soap concentration	Range of maximum viscosity changes (in 4-32 days), in poises	lg K	K
Paraffin cycloalkane fraction of T-1	1	Gel conc. 2% gel (1a) suspension (2b)	8090-205 65,250-2200	0.95	8.9
	2a	Gel. conc. 2% gel (2a) suspension (2b)	3.2-~0.5 58.3-7.0	1.2	13
	2b	Gel conc. 4% gel (3a) suspension (3b)	5735-2800 55,200-36,570	1.0	10
Benzene	3	Gel conc. 4% gel (1a) suspension (1b)	256-320 1716-3100	0.90	7.9

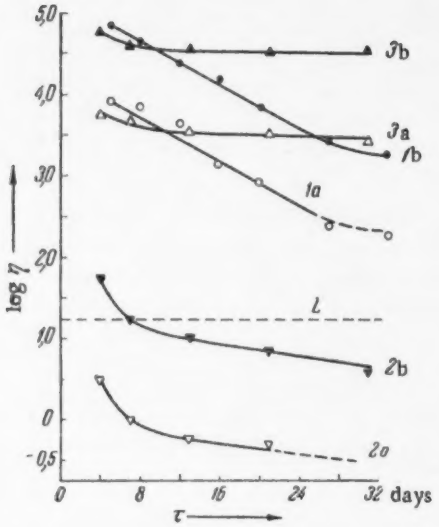

Fig. 1.

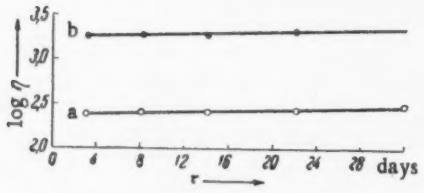

Fig. 2

Similar aging curves are also given for a 2% (Fig. 1, 2a) and 4% (Fig. 1, 3a) gels of different compositions (Sample 2) and corresponding 50% suspensions (Fig. 1, 2b, and 3b). It follows from Curves 2a and 2b that though the soap concentrations are the same as in Sample 1, the initial viscosities of both the gel and suspension are considerably lower (by 2 and more orders of magnitude). Consequently, the suspensions (below the dotted line L in Fig. 1) will separate into two layers when stored for 20-50 hours, and therefore, they have to be stirred before each viscosity determination. However, in this case as well, both curves had similar shapes, which is connected with the rapid structural thixotropic transitions occurring in gels of aluminum salts of alicyclic acids [6]. At the same time, the suspension is known to remain homogeneous for a length of time far in excess of that required for the viscosity changes.

Increase in the soap concentration to 4% (Fig. 1, 3a, b) results not only in a greatly increased initial viscosity of both systems, but also (which is particularly important) enhances the structure formation within the dispersion medium; this is why the viscosity declines more slowly with time, decreasing to only one half its value in one month.

When the paraffin cycloalkane fraction was replaced by benzene, conditions for the structure formation changed. Due to the fact that more soap can be dispersed in benzene [9] the initial viscosity of the gel should be greatly reduced, which we confirmed in the case of the 4% gel (Sample 3, Fig. 2). At the same time, the viscosities of the gel and suspension remained practically constant for one month.

We may presume that the decreased viscosities in oleogels of aluminum salts of alicyclic acids and in corresponding suspensions are caused by a latent aggregation (which sometimes becomes real when the soap precipitates*).

*This was observed when we used an industrial solvent composed of petroleum pyrolysis products with a high content of unsaturated hydrocarbons.

An examination of Table 1 and Fig. 1 and 2 reveals an interesting approximate rule which we found to be valid in all the various cases studied by us. In forming sufficiently concentrated suspensions (50% of solid phase by weight, or 25% of total volume occupied, $\varphi = v_1/(v_1 + v_2)$ regardless of the gel used or of its ageing stage and over a maximum viscosity range of 4 or more orders of magnitude we increase the viscosities by an approximately constant factor (K). Due to the wide range of viscosities it was convenient to plot these data on a semi-log paper, as $\log\eta$ vs. τ . As one can see in Fig. 1 and 2 the separation between any suspension and the corresponding gel remains constant and equal to log K. In our own cases ($100\varphi \approx 25\%$) $K \approx 10$. Curves for aging of the gel, $\eta = f(\tau)$ can be obtained by means of an affine transformation; if $\eta_0 = f_0(\tau)$ is an equation describing the ageing curve of a gel, then even allowing for some very sharp differences in the ageing process (see Fig. 1), the ageing equation for the corresponding suspension will be $\eta_\varphi = Kf_0(\tau)$.

The existence of such a simple and general rule is in itself an indication of the complete stability of suspensions stabilized with gels made of aluminum salts of alicyclic acids. The above discussed general rule would not be so unusual if it applied to dilute (unstructured) suspensions, to which we can apply Einstein's linear equation $\eta(\varphi) = \eta_0(1 + \alpha\varphi)$, where α is evidently greater than 2.5 due to the nonspherical nature of the solid particles. However, our preliminary study of the relationship between maximum viscosity and the composition of the solid dispersed phase in suspension indicates that the function is not linear when $\varphi = 0.25$ (the fraction of volume filled), but exhibits a much more rapid increase in viscosity. This follows from the discovered condition that $(\eta(\varphi)/\eta_0) - 1 = K - 1 = \text{const} \approx 9$. Usually such a rapid increase in viscosity was attributed to a coagulation-type of structure formation [10], which seems to be correct in the case of unstabilized suspensions. In our cases though, the fact that a very high value of K-1 remains constant proves that no aggregation occurs, i.e., that the dispersed phase particles are uniformly distributed over the entire dispersion medium and are only separated by very thin layers of gel. We can use the equation

$$h = \frac{\delta}{3}\left(\frac{1}{\varphi} - 1\right).$$

to estimate the approximate layer thickness h for uniformly distributed spherical particles of diameter δ. For a common case where $\varphi = 0.25$, $h \approx \delta$, and for the average dimensions of our particles $h \approx 10\,\mu$. The fact that the viscosity increment (K) (produced by dispersing a solid phase) remains constant when the fraction of volume filled is sufficiently great, indicates that concentrated suspensions are almost entirely resistant to aggregation; actually, under these conditions the suspensions will not separate into two layers even after prolonged standing. The main cause of stability here is the structured nature of the dispersion medium, i.e., the oleogel itself. It is becoming apparent that the best way (from a practical standpoint) of stabilizing suspensions which are only moderately concentrated and in which the difference between the densities of the dispersed phase and the dispersion medium is rather large is the formation of a three-dimensional ordered framework covering the entire liquid medium, i.e., a spatial jellying which will hinder any large aggregation or separation into layers, even after prolonged standing (over a month) of the suspension.

However, such a three-dimensional framework will interfere with the preparation of stable suspensions with maximum concentration. Therefore, in order to prepare these we will require some structure produced by the adsorption of surface active agents, which, it seems, will enable us to solve the very important practical problem of how to achieve the minimum "liquid (oil) density" and a uniform distribution of the solid dispersed phase and at the same time retain the desired suspension mobility.

LITERATURE CITED

[1] P. A. Rebinder, Colloid, J. 20, 527 (1958).*

[2] P. A. Rebinder, Bull. Acad. Sci. USSR, Chem. Ser. No. 5, 639 (1936); Coll. Research on the Physical Chemistry of Industrial Suspensions, (1933);** Disc. Farad. Soc. 18, 151 (1954).

[3] E. K. Venstrem, J. Phys. Chem. 2, 293 (1931); Trans. Phys. Inst. 1, 4 (1938); R. B. Ginzburg and P. A. Rebinder, J. Phys. Chem. 3, 193 (1932).

[4] E. M. Natanson, Colloid, J. 20, 556 (1958).*

[5] A. A. Trapeznikov, G. V. Belugina, Proc. Acad. Sci. USSR 87, 635, 825 (1952); 94, 97 (1954).

*Original Russian pagination. See C. B. Translation.

**In Russian.

[6] A. A. Trapeznikov, V. A. Fedotova, Proc. Acad. Sci., USSR 81, 1101 (1951); 82, 97 (1952); 95, 595 (1954); 120, 130, 811 (1954).*

[7] G. V. Belugina and A. A. Trapeznikov, Colloid, J. 20, 3 (1958).*

[8] G. V. Belugina, Dissertation, Inst. Phys. Chem. Acad. Sci. USSR (1955).**

[9] A. Alexander and V. R. Gray, J. Phys. Coll. Chem. 53, 9, 23 (1949); Proc. Roy. Soc. 200 A, 162, (1950).

[10] S. Ya. Shalyt, N. V. Mikhailov, and P. A. Rebinder, Colloid J. 19, 244 (1957).*

Received February 26, 1959

* Original Russian pagination. See C. B. Translation.
** In Russian.

A POSSIBLE MECHANISM FOR THE INITIATION OF EXPLOSIONS IN LIQUIDS

L. G. Bolkhovitinov

Institute of Chemical Physics of the Academy of Sciences, USSR

(Presented by Academician V. N. Kondrat'ev, February 6, 1959)

Bowden and co-workers [1] have experimentally demonstrated that when a certain quantity of explosive is subjected to impact an explosive decomposition begins to propagate from a rather small (in size) hot spot, which may attain a temperature of 400-450°C. It is believed that when the liquid is subjected to impact the most probable cause of hot spots is the sudden heating of minute gas spaces ($l \sim 10^{-3} - 10^{-5}$ cm), which become adiabatically compressed by the impact; as was already demonstrated by Yu. B. Khariton [2], neither the adiabatic compression of the liquid itself, nor the viscous friction caused by liquid flow between the hammer and anvil could produce any appreciable temperature rise in the liquid explosive. However, when the compression period under impact (of the order of 10^{-4} sec) is compared with the thermal relaxation time of an air bubble, it turns out that air spaces of the size $10^{-3} - 10^{-5}$ cm would be compressed isothermally by a drop hammer.

It seems to us that when a liquid is suddenly compressed an ignition mechanism is possible which would be independent of air spaces and also result in the formation of small hot spots; the whole concept can be reduced to the following.

The liquid state of matter is not stable under all temperatures and pressures. If at a given temperature the pressure should exceed a certain value the liquid state will become metastable, and the liquid will crystallize. If the specific volume of the liquid should exceed that of the solid, crystallization will be accompanied by evolution of heat and, consequently, should produce a temperature rise. The relationship between the phase transition temperature and the pressure is given by the well known Clausius-Clapeyron equation. A rapid compression of the liquid during impact can produce a noticeable temperature elevation even if only a portion of the liquid should crystallize, and the slower the crystallization velocity of a liquid under ordinary pressures the more it will tend to "supercool" under a rapid pressure increase, and the higher will its temperature rise when transition to the solid state occurs.

There are two ways of finding out under what pressure a liquid will (normal m.p. near room temperature) crystallize at 400°C.

First, since the heat of fusion of nitroglycerin (m.p. = 13.3°C) is known, and we also know the difference between the specific volumes of the solid and liquid phases [3], by writing the Clausius-Clapeyron equation in the form

$$\Delta p = \frac{\Delta T}{T} \frac{q}{(v_1 - v_s)}$$

and substituting in it T = 286°K, ΔT = 400°, q = 33.2 cal/g, $v_s = 0.57$ cm³/g, and $v_l = 0.62$ cm³/g we find that the necessary pressure is approximately equal to 3×10^4 kg/cm².

Second, from experiments done by Bridgman [4], Dow [5], and others who studied the relationship between melting point and applied pressure we can deduce that the melting point of high molecular organic compounds

increases by about 0.02° for each atmosphere of pressure. If we assume that this also holds for liquid explosives then the pressure required to produce crystallization at 400°C is 2×10^4 kg/cm^2.

Two more conditions have to be fulfilled to make the proposed initiation mechanism feasible – the region within which the process may be considered to be in a state of equilibrium must exceed considerably the critical nucleus size, and the crystallization velocity has to be such as to permit the formation of a crystal 10^{-3} –10^{-5} cm in size during the period of impact.

The region d in which we can assume the free energies of both phases to be equal will depend on the distance over which a large temperature gradient has been established during the period of impact, and it can be defined by $d \cong (\kappa t/c\rho)^{\frac{1}{2}}$. For a liquid $\kappa \cong 3.10^{-4}$ cal/cm·sec·deg, $c \cong 0.3$ cal/g·deg, $\rho \cong 1.6$ g/cm^3, and for an impact period $t \cong 10^{-4}$ sec, we get $d \cong 10^{-4}$ cm. The critical nucleus size is of the order of magnitude of[6],

$$R_k \sim \frac{\alpha v_s}{(v_1 - v_s)(p - p_s)}.$$

When $p\text{-}p_s = 10^4$ kg/cm^2 and $\alpha \cong 10^{-2}$ dynes/cm, $R_k \cong 10^{-7}$ cm, and consequently the conditions that $R_k \ll d$ is satisfied.

In order to form a crystal 10^{-5} –10^{-3} cm large during the impact it is necessary that the crystallization velocity (i.e., the increase in the crystal size in any one direction per unit time) be equal to 0.1-10 cm/sec. This value is about $10 - 10^{-3}$ times larger than the crystallization velocity of nitroglycerin under atmospheric pressure at about 0°C [3]. We can safely allow for such an increase in crystallization velocity since under 10^4 kg/cm^2 pressure and close to room temperature the state of the system is far from equilibrium. On the other hand, the effects of viscosity which would limit the crystallization rate in supercooled liquids will be negligibly small under the examined conditions, since the pressure, which accelerates crystallization, is far in excess of the viscous forces.

With standard drop hammer experiments the impact produced by dropping a 10 kg weight from a height of 30-40 cm will produce pressures of the order of $2 \times 10^4 - 3 \times 10^4$ kg/cm^2. Thus, liquid explosives which are relatively free of large gas spaces (0.1-0.01 cm in size) should be rather insensitive to impact under a drop hammer.

Earlier in the paper we proposed that even before the impact the liquid may already contain some nuclei necessary for the growth of crystals. Therefore if the liquid should be carefully purified so as to remove all foreign matter then it would become less sensitive. On the other hand introduction of even very small solid particles should render the liquid more sensitive.

A preliminary isothermal compression and a decompression of the liquid explosive right before shock should also result in increased explosion probability in the drop hammer experiment, since a precompression would leave a greater number of nuclei in the liquid. The effect of such a statistical compression was observed by S. Ljunberg [7] and has not so far received any other explanation. The presence of numerous nuclei would provide a similar straightforward explanation for the well known fact that nitroglycerin becomes more sensitive to impact when partly frozen.

Thus, the proposed hypothetical initiation mechanism not only does not contradict the facts known from practical handling of liquid explosives, but also enables us, in several cases, to provide a simple physical explanation for the observed phenomena.

LITERATURE CITED

[1] F. P. Bowden and A. D. Yoffe, Initiation and Growth of Explosion in Liquids and Solids [Russian translation] (IL, 1955).

[2] Yu. B. Khariton, Coll. The Theory of Explosives (1940) [in Russian].

[3] Naoûm, Nitroglycerin [Russian translation] (1934).

[4] P. W. Bridgman, Phys. Rev , 3, 126, 153 (1914); 6, 1, 94 (1915).

[5] R. B. Dow and H. B. Hibshman, J. Chem. Phys. 5, 960 (1937).

[6] M. A. Leontovich, Introduction to Thermodynamics (1952)[in Russian].

[7] S. Ljunberg, Arkiv fys. 11, 118 (1956).

Received January 21, 1959

FREE ENERGY CHANGE UNDER STANDARD CONDITIONS IN THE POLYMERIZATION OF ε-CAPROLACTAM*

I. E. Paukov, V. P. Kolesov, and S. M. Skuratov

M. V. Lomonosov Moscow State University

(Presented by Academician P. A. Rebinder, February 6, 1959)

The polymerization of heterocyclic compounds, particularly lactams, has intrigued many workers for quite a while. It seems that the varying readiness with which lactams (as well as other heterocyclic compounds) undergo polymerization, depending on the size of the ring, must be due to variations in the free energies of these reactions [1-3]. However, so far we know of no case where this function could be accurately calculated, mainly due to a lack of entropy data. Attempts to calculate theoretically the entropy changes in polymerization reactions [3] can result in appreciable errors.

In this paper we are presenting the results obtained from our determination of the specific heats of ε-caprolactam and poly-ε-caprolactam in the 60-373°K temperature range. From this data we calculated ΔS and ΔF for the polymerization of ε-caprolactam under standard conditions. (Values of ΔH have already been determined [4].) Measurements were carried out in a previously described [5] adiabatic vacuum calorimeter. (A new calorimetric ampule with thinner walls and consequently smaller heat capacity was designed for this work). The calorimeter and the measuring technique were tested by determining the specific heat of potassium chloride in the 60-373°K temperature range. Out data was in good agreement with the results of other workers.

The ε-caprolactam was distilled five times under dry nitrogen and dried for a long time over phosphorus pentoxide. The water content of the investigated sample was known to be less than 0.1%. The amount of impurities found during the specific heat determination was 0.05 mole%.

The poly-ε-caprolactam was prepared by dissolving a commercial sample in formic acid and slowly precipitating it by the addition of water. The sample was dried for 4 days at 130-140° in vacuo (10^{-3} mm of Hg), then cooled to room temperature at a rate of ~ 1° per 5 min. Before each measurement the sample was cooled for 24 hrs to the liquid nitrogen temperature. Once the calorimeter was filled, all the manipulations were done in a dry box. The calorimeter with the sample inside was weighed in an air-tight device which was outfitted with a soldering bit so that the calorimeter could be soldered shut after being filled with helium.

The heat capacities of ε-caprolactam and poly-ε-caprolactam, obtained by drawing a smooth curve through the experimental points, are summarized in Table 1.

In general the deviations of certain points from the smooth curve of c_p vs. T for ε-caprolactam did not exceed 0.1%, and only rarely amounted to 0.2%; for poly-ε-caprolactam they approached 0.4%. The lower accuracy in the latter case can be attributed to a small weight by volume (wt. per 1 m^3 of granular material) of the polymer. (Only 5.2 g of polymer could be placed in the calorimetric ampule.) While measuring the heat capacities we also determined the heat of fusion of ε-caprolactam, 3847 ± 8 cal/mole, and the m.p. of pure ε-caprolactam, 342.305°K. It was established that the specific heat curves of both the monomer and the polymer exhibited no anomalies in the 60-373°K temperature range. Our research failed to confirm the great anomaly observed

* Fung Shih-yen and É. A. Seregin took part in the experimental part of this work.

TABLE 1

Temp., °K	c_p of ε-caprolactam	c_p of poly-ε caprolactam	Temp., °K	c_p of ε-caprolactam	c_p of poly-ε-caprolactam
60	10,73	9,98	298,16	37,47	40,55
80	13,36	13,53	320	40,83	44,58
100	15,55	16,25	335	44,82	48,12
150	20,52	22,10	350	58,43	51,81
200	25,50	28,10	360	59,66	54,40
250	31,27	34,12	373	61,26	57,89

in the 20-48°C region and reported in [7] by workers who studied the heat capacities of various poly-ε-caprolactam samples in the −20 to + 280°C temperature range.

Standard absolute entropies ($S^0_{298.16}$) were calculated by numerically integrating a plot of the (c_p, ln T)-function. To get the entropies at 60°K we extrapolated the (c_p, T) curves to 0°K by a proper choice of Debye-Einstein functions. The equations

$$c = D\left(\frac{110}{T}\right) + E_1\left(\frac{140}{T}\right) + E_2\left(\frac{244}{T}\right) + E_3\left(\frac{560}{T}\right) + \\ + E_4\left(\frac{654}{T}\right) + E_5\left(\frac{845}{T}\right) + 20\,E_6\left(\frac{1785}{T}\right) \qquad (1)$$

for ε-caprolactam, and

$$c = D\left(\frac{130}{T}\right) + 2E_1\left(\frac{210}{T}\right) + E_2\left(\frac{361}{T}\right) + 2E_3\left(\frac{900}{T}\right) + 10E_4\left(\frac{1160}{T}\right) \qquad (2)$$

for poly-ε-caprolactam (calculated for one chain) cover the experimental data in the 60-170°K temperature range with an accuracy of ± 0.2%.

In calculating $S^0_{298.16}$ for the polymer we took S^0_0 to be equal to zero. This does not seem to introduce any grave errors, since very many, even amorphous, polymers have a very small residual entropy at 0°K. (For example, it is equal to 0.28 e.u. in amorphous rubber [6].) At the same time our polymeric sample was highly ordered (X-ray diffraction gave its degree of "crystallinity" as ~ 70%). Our calculated values of $S^0_{298.16}$ are 40.26 e.u. for ε-caprolactam and 41.36 e.u. for poly-ε-caprolactam; consequently the polymerization of ε-caprolactam at 298.16°K is accompanied by an entropy change of + 1.1 e.u. The value of ΔH, obtained earlier [4] in the Thermochemical Laboratory of MGU, was −3.7 kcal/mole in this reaction. Whence, the free energy change in the polymerization of ε-caprolactam, ΔF = − 4.0 kcal/mole at 298.16°K. Thus under standard conditions the value of free energy change in the polymerization of ε-caprolactam is mainly determined by the change in enthalpy.

LITERATURE CITED

[1] S. M. Skuratov, A. A. Strepikheev, S. M. Shtekher, and A. V. Volokhina, Proc. Acad. Sci. USSR 117, 263 (1957).*

[2] S. M. Skuratov, A. A. Strepikheev, and M. P. Kozina, Proc. Acad. Sci. USSR 117, 452 (1957).*

[3] F. S. Dainton and K. I. Ivin, Quart. Rev. 12, No. 1, 61 (1958).

[4] S. M. Skuratov, Doctoral Dissertation, MGU, (1954);** O. N. Kachinskaya, Bull. Moscow Univ., No. 2, 232 (1957).

[5] M. M. Popov and V. P. Kolesov, J. Gen. Chem. 26, 2385 (1956).*

[6] Bekkedahl, Matheson, J. Res. Nat. Bur. Stand. 15, 503 (1935).

[7] P. Marx and C. N. Smith et al., J. phys. Chem. 59, 1015 (1955).

*Original Russian pagination. See C. B. Translation.

**In Russian.

Received February 4, 1959.

ELECTRICAL CONDUCTANCE OF AQUEOUS SODIUM HYDROXIDE AT ELEVATED TEMPERATURES

I. M. Rodnyanskii, I. S. Galinker, and V. I. Korobkov

V. V. Dokuchaev Khar'kov Agricultural Institute

(Presented by Academician A. N. Frumkin, March 3, 1959)

A large number of papers have been devoted to the experimental and theoretical investigation of conductance in electrolytic solutions. Yet, almost all of them were limited to a narrow range of room temperatures, and only one set of experiments were conducted at elevated temperatures.

Noyes and co-workers were the first to measure the electrical conductance of dilute (up to 0.08 M) electrolytic solutions at elevated temperatures (306°C); they did their work as early as 1903-1910. Since then the experimental material in that field has been accumulating at a very slow rate [1-4].

Rodnyanskii and Galinker measured the electrical conductance of LiCl, NaCl, and KCl solutions [5], extending the range of temperatures and concentrations to 340° and 3 N. They showed that the equivalent conductances of alkali metal chlorides in solution pass through a maximum in the vicinity of 280-300°C. In more dilute solutions studied by Noyes, the bend in the curve of electrical conductance vs. temperature was hardly detectable. Later on, other investigators [4] also observed such conductance maxima at elevated temperatures. Moreover, depending on the nature of the electrolyte and its concentration the conductance maxima were detected at varying temperatures – around 60°C in solutions of tetravalent metal salts, around 100-115° with divalent ones, and around 280-300° with monovalent salts.

It was quite interesting to follow the changes in electrical conductance above 340°C. The solution of this problem was accompanied by certain experimental difficulties involving the choice of electrical insulators for the construction of an electrolytic cell with tightly sealed electrical leads. At elevated temperatures aqueous solutions will readily attack glass, porcelain, quartz, and similar materials. Acidic oxides in particular are very rapidly leached out of the cell material.

At the same time there is a need to work out some methods of determining electrical conductance at more elevated temperatures (~ 360°C), even under conditions involving very corrosive media, such as alkaline solutions, to satisfy the demands of chemical industry.

An instrument with a unique construction was designed for our work. Figure 1 gives a schematic representation of the electrolytic cell used and the electrical leads built into the steel plug of the autoclave.

Components 1 and 2 were made of Teflon and were designed to seal off and insulate the central core of the electrical lead 10 from the bulk of the steel plug 7. The complex design of component 1 was dictated by the fact that under pressures of 20-30 kg/cm^2, Teflon (either cold or warm) can be easily squeezed through even very narrow gaps [6].

The electrolytic cell 3 was also made of Teflon and had a capacitance of approximately 4-5 cm^{-1}. Component 4 was made of marble. This was designed to reinforce the Teflon and prevent it from being squeezed out of the constructed maze. The cell electrodes 5 and 6 were platinized. The core of the lead was insulated from the plug by a porcelain tube 11 and a mica washer 12. The steel rings 8 and 9 braced the Teflon and marble components. The steel plug 7 stoppered the autoclave, whose internal cavity had a capacity of ~ 100 ml.

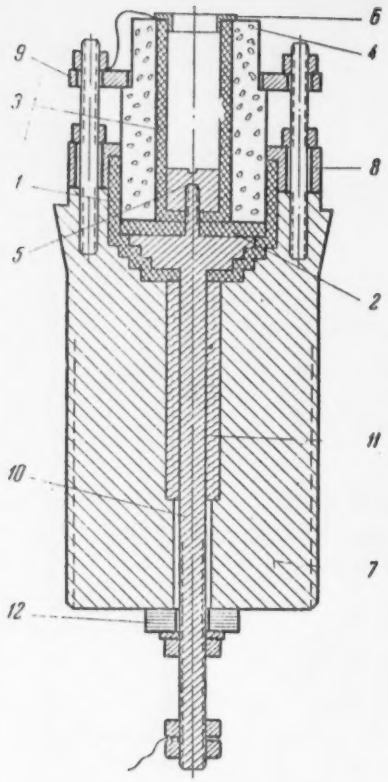

Fig. 1

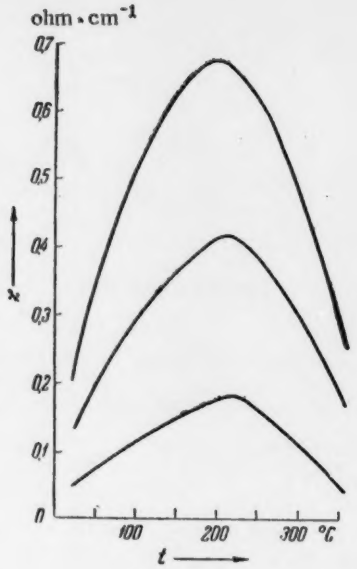

Fig. 2

The electrical conductance was measured in the following manner. An accurately determined amount of solution was placed in the steel autoclave, which was then stoppered with the steel plug and sealed off by means of the sealing ring and a tightened female screw. The autoclave was then placed into a pivoted cylindrical electric furnace.

The electrolytic cell sealed into the plug was located at the top of the autoclave and had no contact with solution. When the electrical conductance was being measured, the furnace together with the autoclave was tilted on the pivots through 180°, and the cell would then be fully submerged in the investigated solution. In this position we measured the resistance of the solution, the temperature, and the vapor pressure of water. After this we would return the furnace to its original position and take the conductance cell out of solution.

Before each experiment we determined the electrolytic capacitance of the cell by measuring the electrical conductance of three standard sodium hydroxide solutions (1, 3, and 5%) at room temperature. The electric circuits used for measuring the electrical conductance have been previously described in detail. We did our measurements with the help of a MVL-47 bridge. An audio-frequency (2000 hertz) tube generator supplied the current to the bridge, and an electronic oscillograph EO-7 was used as balance indicator.

In Fig. 2 we plotted curves showing changes in the specific conductance κ of aqueous NaOH solutions at several concentrations (1, 3, and 5%) and up to 360°.

We have to make one reservation, only two temperatures (25 and 360°) were ever maintained constant in our experiments and at these temperatures accurate electrical conductances of alkaline solutions were measured. For the sake of orientation we also carried out several measurements at intermediate temperatures. We also estimated the correction required for the change in concentration caused by evaporation.

	18°	100°	156°	218°
λ_∞	216,5	594	835	1060
$\lambda_{0,1N}$	200,6	540	738	873

One can see in Fig. 2 that all the curves had a maximum around 200-220°. With increasing concentrations the maximum

was displaced toward lower temperatures. One can also see that the specific conductance at the maximum is 2.5-3 times larger than at 360°C.

Unfortunately we are unable to describe the temperature variations of equivalent conductance with any greater degree of accuracy, since the densities of solutions at the experimental temperatures were not determined. We may assume though that the density of a 1% NaOH solution (.25 mole/liter) changes in the same way as that of pure water. This assumption is confirmed by Noyes' experiments. He found out that in 0.1 N (0.4%) NaOH the volume of solution increased by 1.180 times in going from room temperature to 218°C, while water at the same time increased by 1.186 times.

In passing, we have also shown above the equivalent conductances λ in ohm^{-1} of two NaOH solutions (infinitely dilute and 0.1 N) at various temperatures; these were based on Noyes' data.

In very dilute solutions we can correct for the volume increase by using the corresponding coefficients of water. In this way we get for a 1% (0.25 mole/liter) NaOH solution:

$$\lambda_{218^\circ} = 760 \text{ ohm}^{-1} \text{ and } \lambda_{360^\circ} = 284 \text{ ohm}^{-1}.$$

It is the first time that such an abrupt drop has been observed in the equivalent conductance of strong monovalent electrolytes after passing through a maximum. Let us note that at 340° the equivalent conductance in NaCl and KCl solutions decreased by only 5-6% relative to the maximum value [5].

Comparing the conductance curve of sodium hydroxide solutions with that of alkali metal chlorides we see that the maximum conductance of sodium hydroxide occurs at lower temperatures than that of NaCl.

At moderate temperatures both NaCl and NaOH are equally strong electrolytes in aqueous solutions, but on the basis of electrical conductance data at higher temperatures NaOH becomes a weaker electrolyte than NaCl. It seems that this may be connected with a greater percent covalent bond character in sodium hydroxide, which is also reflected in its low melting point.

A more detailed explanation of the phenomena has to be postponed till a greater amount of experimental data have been accumulated.

LITERATURE CITED

[1] M. A. Klochko, and I. G. Grigor'ev, Bull. Phys. Chem. Anal. Sec. of the Inst. Gen. Inorg. Chem., Acad. Sci. USSR, 21, 303 (1950).

[2] A. N. Campbell, E. M. Kartzmark, M. E. Bednas, and J. T. Herron, Canad. J. Chem. 32, 1051 (1954).

[3] G. L. Kobus, Trans. of the Odessa Hydrometeorological Inst., No. 7, 113 (1955).

[4] V. A. Mil'chev and S. V. Gorbachev, Sci. Proc. of the Chem. and Chem. Technology Institute, No. 2, 238 (1958).

[5] I. M. Rodnyanskii and I. S. Galinker, Proc. Acad. Sci. USSR 105, 115 (1955).

[6] D. D. Chegodaev, Fluorocarbon Polymers, Leningrad (1956).*

Received February 9, 1959

* In Russian.

THE COORDINATION NUMBER AND THE TRANSLATIONAL MOTION OF MOLECULES IN AQUEOUS SOLUTIONS OF ELECTROLYTES

O. Ya. Samoilov

N. S. Kurnakov Institute of General and Inorganic Chemistry of the Academy of Sciences, USSR

(Presented by Academician I. I. Chernyaev, January 29, 1959)

The relationship between the coordination number and the translational motion of molecules in solution has already been noted several times [1-3] before. We will try to find a quantitative relationship for the case of greatest interest to us – aqueous solutions of electrolytes. The concepts developed below will probably be equally valid for several other liquid solutions, such as fused salt systems.

Let us examine the translational motion of water molecules in dilute aqueous solutions of electrolytes containing relatively weakly hydrated ions (ions close to the boundary between positive and negative hydration [2]). Let us imagine a simplified case where the water molecules in the examined solutions may exist in two states – (i), closely surrounding the ions, and (0) in "free" water. By free water we mean all of the water molecules which are not at that particular moment in the immediate vicinity of the ions, but have as neighbors other water molecules. Among the latter some may be in the immediate vicinity of ions. On top of that let us distinguish such "free" water molecules $(H_2O)^0$ as are surrounded by only other "free" water molecules at that particular moment. Let us analyze the transitions (activated jumps) of water molecules from the immediate vicinity of the ions to the immediate vicinity of $(H_2O)^0$, and vice versa. These will very obviously be activated jumps of water molecules between states i and 0.

Let the total number of jumps (per second) between states i and 0, and in the reverse direction be $I_{i\to 0}$, $I_{0\to i}$ respectively. The exchange equilibrium between neighboring particles in solution is characterized by the fact that the average number of molecules in states i and 0 remains constant in time. Therefore the equilibrium condition may be described by the equation

$$I_{i\to 0} = I_{0\to i}. \tag{1}$$

Water molecules in solution also undergo transitions of type $i\to i$ and $0\to 0$, i.e., transitions which produce no exchange between molecules in states i and 0. Let us determine $I_{i\to 0}$ and $I_{0\to i}$.

The total number (per second) of water molecules jumping from the immediate vicinity of particles i into any of the adjacent equilibrium positions is

$$I_{i\to 0,\,i} = m_i n_i j_i,$$

where m_i is the number of particles of type i (ions) in solution, n_i the coordination number of particle i (the average number of nearest water molecules surrounding particle i), and j the average (per second) number of activated jumps involving water molecules in the immediate vicinity of the ions. The unknown $I_{i\to 0}$ is only a fraction of the number $I_{i\to 0,\,i}$. In order to find $I_{i\to 0}$ we have to multiply $I_{i\to 0,\,i}$ by ω, the probability of having a water molecule leave its equilibrium position near i and fall into a new equilibrium position closer to a $(H_2O)^0$ molecule.

By the fall of one molecule into the immediate surrounding of any other molecule in solution we simply mean that the molecule falls on a sphere of radius r_1 surrounding the other molecule, and where r_1 is the radius of the first coordination sphere (we should consider the molecule as falling into a certain diffuse spherical layer surrounding the other molecule and bounded by spheres of radius $r_1 + \delta r$ and $r_1 - \delta r$). For the molecule $(H_2O)^0$ $r_1 = R_0 \simeq 2.9$A, and for ions $r_1 = R_i \simeq r_i + r_{H_2O}$ [2]. The total surface area of all the first coordination spheres of molecules $(H_2O)^0$ is

$$S = 4\pi m R_0^2,$$

where m is the number of molecules of type $(H_2O)^0$ in solution. Let S_i be the total surface area of the first coordination spheres of particles i. Its value will be

$$S_i = 4\pi m_i R_i^2.$$

We can obviously assume in this case (the ions being close to the boundary between negative and positive hydration) that

$$w = \frac{S}{S + S_i}.$$

In order to go over from $I_{i\to 0,\,i}$ to $I_{i\to 0}$ we also have to take into account the fact that in general the probability of having the closest coordination zones [4] (first coordination spheres) of like molecules (0 – 0 or i – i)* adjoin each other is not the same as the probability of having adjacent corresponding zones of unlike molecules (i – 0 or 0 – i). This can be accomplished by introducing a corresponding coefficient k_{i0}. We can obviously assume that $k_{0i} = k_{i0}$. Thus we get

$$I_{i\to 0} = I_{i\to 0,\,i}\frac{S}{S + S_i}k_{i0} = m_i n_i j_i \frac{S}{S + S_i}k_{i0}.$$

In the same way we get

$$I_{0\to i} = I_{0\to i,\,0}\frac{S_i}{S + S_i}k_{0i} = mnj\,\frac{S_i}{S + S_i}k_{0i},$$

where n is the coordination number of $(H_2O)^0$ molecules, m their quantity in solution, and j the average (per second) number of water molecules undergoing activated jumps away from the immediate vicinity of $(H_2O)^0$ molecules.

At equilibrium Equation (1) will hold. And accordingly we will get

$$\frac{n_i}{4\pi R_i^2}j_i = \frac{n}{4\pi R_0^2}j. \qquad (2)$$

Previously in place of Equation (2) we had quoted Equation (1) from [3], but it was only valid when the ionic dimensions did not differ from those of water molecules.

Noting that $n_i/4\pi R_i^2 = \rho_i'$ and $n/4\pi R_0^2 = \rho'$ (ρ_i' and ρ' are the previously [2] introduced surface distribution densities of water molecules in the immediate vicinities of ions and water molecules respectively), we can write

$$\rho_i' j_i = \rho' j.$$

Applying the same considerations to molecules i = 1,2,3 etc., we will get

$$\rho_1' j_1 = \rho_2' j_2 = \ldots = \rho' j.$$

* For example, the designation 0 – 0 will in this case denote that the adjoining water molecules are in the immediate vicinity of two $(H_2O)^0$ molecules.

As we demonstrated in [2], one may assume

$$j = j_0 e^{-E/RT} \qquad \text{and} \qquad j_i = j_{0i} e^{-(E+\Delta E_i)/RT}. \tag{3}$$

Besides this, for ions with small ΔE_i (close to the boundary between positive and negative hydration) we can take $j_{0i} = j_0$ [2], and therefore for such ions

$$\rho_i' = \rho' e^{\Delta E_i/RT}. \tag{4}$$

Equation (4) gives the relationship between the coordiantion number of ions and water molecules and the translational motion of water molecules (ΔE_i). From this equation it follows that

$$\rho_i' > \rho', \text{when} \quad \Delta E_i > 0, \qquad \text{and} \qquad \rho_i' < \rho', \text{when} \quad \Delta E_i < 0.$$

In deriving Equation (4) we examined only the transfer of individual molecules in solution. In this case collective migration is definitely of little significance – when "blocks" of molecules undergo a relative displacement the coordination number changes only on the surface of such "blocks". It should be noted that the translational motion of water molecules in water as well as in dilute aqueous solutions of electrolytes occurs mainly inside structural vacancies [1, 2]. This fact however has no bearing on the ideas presented, since the number of molecules leaving equilibrium positions depends on the total number of activated jumps, while the probability of falling into any particular equilibrium position depends on the total area of its first coordination sphere. Let us note that Equation (4) was derived for comparatively weakly hydrolyzed ions.

Equations (2) and (3) can be used to determine the temperature dependence of coordination numbers of ions in aqueous solutions. Actually it follows from these equations that

$$\frac{n_i}{n} = \frac{R_i^2}{R_0^2} \frac{j_0}{j_{0i}} e^{\Delta E_i/RT},$$

whence

$$\frac{d}{dT}\left(\frac{n_i}{n}\right) = \left[\frac{d}{dT}\left(\frac{R_i^2}{R_0^2}\right) + \frac{R_i^2}{R_0^2}\frac{j_{0i}}{j_0}\frac{d}{dT}\left(\frac{j_0}{j_{0i}}\right) - \frac{\Delta E_i}{RT^2}\frac{R_i^2}{R_0^2}\right]\frac{j_0}{j_{0i}} e^{\Delta E_i/RT}.$$

Assuming that near the boundary between positive and negative hydration $d/dT\ (R_i^2/R_0^2) = 0$ and $d/dT\ (j_0/j_{0i}) = 0$, we will get

$$\frac{d}{dT}\left(\frac{n_i}{n}\right) = -\frac{\Delta E_i}{RT^2}\frac{n_i}{n}, \tag{5}$$

which agree with Equation (3) obtained from [3] and naturally leads to similar conclusions about the ratio of temperature changes in n_i and n.

From Eq. (5) we get the equation

$$\frac{dn_i}{dT} = \frac{n_i}{n}\left(\frac{dn}{dT} - n\frac{\Delta E_i}{RT^2}\right).$$

It is more convenient to work with the numbers Δn_i and Δn, changes in the coordination number for a 10° temperature increase (changes in n_i and n for a 1° interval are very small). For Δn_i we get

$$\Delta n_i = \frac{n_i}{n}\left(\Delta n - 10n\,\frac{\Delta E_i}{RT^2}\right), \qquad (6)$$

and since on the basis of X-ray diffraction data [2] for water at 25° n = 4.6 and $\Delta n = +0.07$,

$$\Delta n_i = n_i\,(0{,}015 - 0{,}057\Delta E_i).$$

Using the values of ΔE_i and n_i given in [2] for Na^+ and K^+ cations (these are relatively near the boundary line between positive and negative hydration) we find that

$$\Delta n_{Na^+} = +0{,}004 \quad \text{and} \quad \Delta n_{K^+} = +0{,}10$$

LITERATURE CITED

[1] O. Ya. Samoilov, J. Phys. Chem. 20, No. 12, 1411 (1946).

[2] O. Ya. Samoilov, Structure in Aqueous Solutions of Electrolytes and Hydration of Ions, Izd. AN SSSR, (1957).*

[3] O. Ya. Samoilov, Proc. Acad. Sci. USSR 121, No. 6, 1043 (1958).**

[4] O. Ya. Samoilov, Proc. Acad. Sci. USSR 58, No. 6, 1073 (1947).

Received January 16, 1959

* In Russian.

** Original Russian pagination. See C. B. Translation.

ELECTROCHEMICAL INVESTIGATION OF A PLATINUM OXIDE CATALYST

Academician Acad. Sci. Kazak SSR D. V. Sokol'skii and Yu A. Skopin

S. M. Kirov Kazak State University. Kazak Agricultural Institute

Platinum black, which is prepared from platinum oxide by reduction, has been widely applied in liquid-phase hydrations. So for the main emphasis has been on the methods of making platinum oxide [1], while the problem of its reduction in various solvents has not received enough attention. In the present communication we are presenting some data on the reduction of platinum oxide in acidic and alkaline solutions, together with the experimental potential measured on the powder and a subsequently recorded charge curve of platinum black.

The brown, powdered platinum oxide was prepared by a method described in [2]; it was thoroughly washed with distilled water to remove excess sodium nitrate and dried at 98°C. The apparatus used for the reduction of platinum oxide as well as the method of recording charge curves of powdered catalysts have been described elsewhere [3]. Preliminary experiments have shown that in acidic and alkaline solutions platinum oxide can be reduced quantitatively.

After saturating 35 ml of the solvent with hydrogen, to establish a reversible hydrogen potential on the platinum wire, we swept the hydrogen out of the gas phase with nitrogen and introduced a weighed (0.234 g) sample of PtO_2 into the apparatus. After the platinum oxide had all precipitated we blew hydrogen through the apparatus and stirred the solution to determine how much hydrogen was used up in reducing the platinum oxide.

Reduction of platinum oxide in 0.1 N, 1 N, and 5 N sulfuric acid. In Figure 1 we have plotted the amount of hydrogen absorbed as a function of time, and the potential changes on a platinum wire during the reduction of platinum oxide. During the first few minutes of stirring the potential was displaced in the negative direction by 100-120 mv, and at that particular moment the maximum reduction rate was observed. After that the potential rapidly increased to 20 mv below the reversible hydrogen value and continued to change very gradually, attaining zero toward the end of reduction. When the experiment was started, platinum oxide vigorously absorbed not only the hydrogen from the gas phase but also that adsorbed on the wire. After the theoretical amount of hydrogen required to reduce PtO_2 had been absorbed, the hydrogen potential attained its reversible value in the particular solution. The reduction rate of platinum oxide decreased with increasing acid concentration. One can see in Fig. 1 that the absorption of hydrogen continued even after the theoretical amount needed for the reduction had been absorbed. It seems that the excess hydrogen was adsorbed on the platinum black which was formed in the reduction of platinum oxide. Thus we were able to determine the quantity of hydrogen adsorbed on platinum black. In 0.1 N sulfuric acid 1 g of platinum black adsorbed 12.8 ml of hydrogen. As the acid concentration was increased the amount of hydrogen adsorbed decreased, and in a 5 N solution only 10.2 ml were adsorbed on 1 g of platinum black.

There is a way [4] by which the amount of hydrogen adsorbed on an electrode can be determined from the charge curve. In Fig. 2 we have plotted charge curves obtained on platinum black, which was prepared by the reduction of platinum oxide in 0.1 N, 1 N, and 5 N sulfuric acid, and recorded by the method described in [3]. The quantity of hydrogen adsorbed was determined from the amount of current used up in pushing the potential of the powdered platinum black to 0.36 v. The value thus obtained agreed quite well with the excess hydrogen taken up during the reduction of platinum oxide.

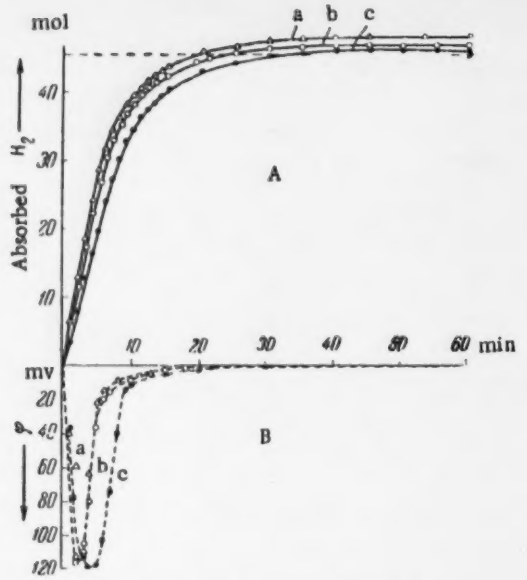

Fig. 1. A) Reduction of platinum oxide in: 0.1 N (a), 1 N (b), and 5 N (c) H_2SO_4; B) change of potential on platinum wire.

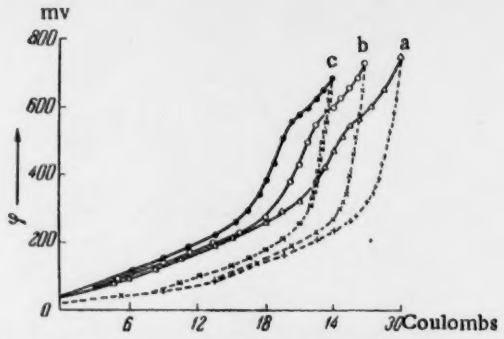

Fig. 2. Anodic and cathodic charge curves on platinum black in : 0.1 N (a), 1 N (b), 5 N (c) H_2SO_4.

We estimated the surface area of the platinum black from the capacitance of the double layer on the cathode branch of the charge curve (the capacitance of a 1 cm^2 "smooth" platinum electrode in sulfuric acid was taken to be 70 μf); we obtained the following values: 50 m^2/g in 0.1 N, 39 in 1N, and 36 in 5 Nsurfuric acid. If we assume that the percent of the platinum black surface covered with hydrogen is close to 100% (70-100%) and estimate the area from the amount of adsorbed hydrogen, we will get results which are in full accord with the area calculated from the double layer capacitance.

Reduction of platinum oxide in 0.1N, 1N, and 5 N KOH solutions. Fig. 3 shows that at all the alkali concentrations the reduction of platinum oxide was preceded by an induction period, the length of which varied with the alkali concentration. The induction period increased at higher concentrations

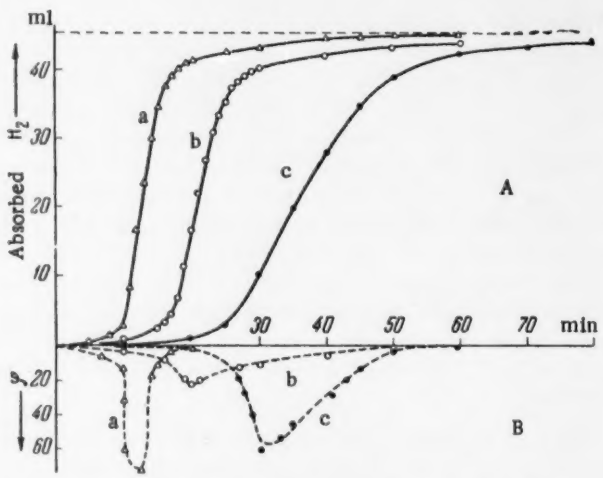

Fig. 3. A) Reduction of platinum oxide in: 0.1 N (a), 1 N (b), and 5 N (c) KOH; B) change of potential on platinum wire.

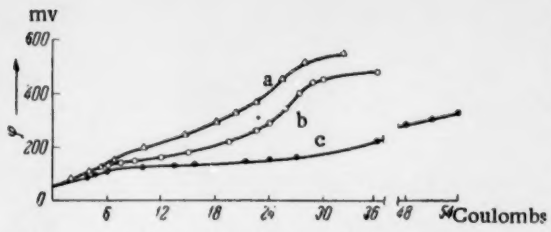

Fig. 4. Anodic charge curves on platinum black in: 0.1 N (a), 1 N (b), 5 N (c) KOH.

attaining 20 min in the 5 N solution. After the induction period was over, the reduction rate proper decreased in the order: 0.1N > 1 N > 5 N KOH. Just as in the case of sulfuric acid solutions, the maximum reduction rate was observed when the platinum wire potential was furthest displaced toward negative potentials, but the displacement itself was smaller (30-60 mv). When the amount of hydrogen absorbed approached the figure required theoretically for the reduction, the potential attained zero.

The anodic charge curves of platinum black (Fig. 4) recorded in alkaline solutions did not exhibit any well defined transitions in the double layer region. The amount of hydrogen adsorbed on platinum black was computed from the region "a", up to a potential of 0.38 v.

We obtained the following results: in 0.1 N KOH 1 g of platinum black adsorbed 12 ml of hydrogen, in 1 N 15.4 ml, and in 5 N 23 ml, i.e., with increasing alkali concentration the adsorption of hydrogen increased. By reducing the platinum oxide in alkaline solutions at 20, 40, and 60°C we found that at higher temperatures the reduction rate increased while the induction period decreased, disappearing in 0.1 N KOH at 60°.

Reduction of platinum oxide in water, ethyl alcohol, n-hexane, and benzene. The reduction rate of platinum oxide in twice-distilled water was decreased to one half its value in 0.1 N H_2SO_4, and the induction period was absent. The reduction curves of platinum oxide in ethyl alcohol and n-hexane were similar to those obtained in 0.1 N sulfuric acid. The amount of hydrogen adsorbed, determined from the excess taken up during reduction, was 12 ml per 1 g of platinum black. In benzene a 20-25 min induction period was observed after which PtO_2 was reduced at the rate of 1.5-2 ml/min.

LITERATURE CITED

[1] Coll. 1, Synthesis of Organic Reagents, p. 357 [Russian translation] (IL, 1949); R. Adams, and R. L. Shriner, J. Am. Chem. Soc., 45, 2171 (1923).

[2] V. L. Frampton, J. D. Edwards, Jr., and H. R. I. Henze, J. Am, Chem. Soc. 73, 4432 (1951).

[3] Yu. A. Skopin and D. V. Sokol'skii, Bull Acad. Sci. Kazak SSR, No. 6, 89 (1956).

[4] A. Frumkin and A. Shlygin, Bull. Acad. Sci. USSR, Chem. Ser., No. 5, 773 (1936).

Received February 10, 1959

THE ACTION OF Co^{60} γ-RAYS ON THE CRYSTAL HYDRATES OF NITRATE SALTS

A. S. Baberkin

L. Ya. Karpov Physicochemical Scientific Research Institute

(Presented by Academician S. S. Medvedev, February 4, 1959)

When irradiated, solid nitrates decompose to give nitrites and oxygen. The decomposition rate, which determines the yield of nitrite and oxygen, is specific for each form of salt and depends on its physicochemical properties. Among all the numerous papers on the action of radiation on solid nitrates there are hardly any on the chemical stability of irradiated crystal hydrates of nitrate salts. In papers [1, 2] it was only noted that the crystal hydrate of lanthanum decomposes faster than the anhydrous salt. In an earlier paper [3] we showed the effects of aggregation in irradiated calcium nitrate on the yield of nitrite.

In the present work we investigated the effect of dose intensity on the radiochemical yield of products obtained from the irradiation of crystal hydrates of divalent nitrate salts. We picked for our study the nitrates of calcium, cadmium, zinc, and magnesium. Chemically pure and analytically pure salts were sealed in glass ampules in air before irradiation. The temperature was kept at about 22° in all cases except when irradiation was done inside the K-18000 source, where it was lowered to 8-10°. The source of γ-rays was Co^{60} with a dose intensity from 0.2×10^{16} to 4.1×10^{16} ev/ml·sec. Nitrite was determined colorimetrically [4]. In Fig. 1 and 2 we have plotted the yield of nitrite obtained at various dose intensities from calcium and magnesium crystal hydrates as a function of radiation dosage.

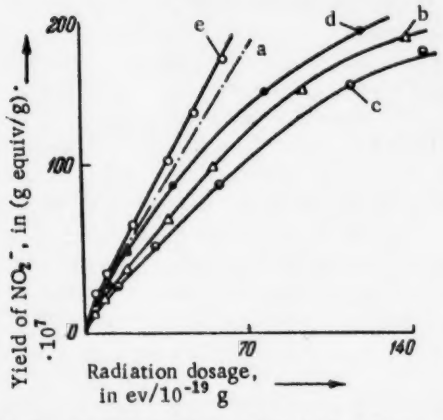

Fig. 1. $Mg(NO_3)_2 \cdot 6H_2O$. The yield of nitrite as a function of radiation dosage at various dose intensities. a) 0.2×10^{16} ev/ml · sec; b) 0.8×10^{16} ev/ml · sec; c) 1.24×10^{16} ev/ml · sec; d) 1.7×10^{16} ev/ml · sec; e) 4.1×10^{16} ev/ml · sec.

It is evident from the pictures that the initial yield of nitrite is independent of dose intensity. With increasing integral radiation dosage one can see a well defined, and specific for each salt, dependence of nitrite yield on dose intensity.

The exact initial yield of nitrite for various dose strengths at a dosage of 7×10^{19} ev/g are given in Table 1. All the investigated crystal hydrates can be subdivided into two groups, depending on the way in which the nitrite yield changes when dose intensity is varied. The first group contains calcium and cadmium nitrates, each associated with four molecules of water. The second group includes zinc and magnesium nitrates. The first group has a characteristic minimum $G_{NO_2^-}$ at a dose intensity of 0.8×10^{16} ev/ml·sec. The salts in this group behave differently at different dose intensities. While the yield of nitrite from calcium nitrate was a linear function of radiation dosage over the entire range of

TABLE 1

Yield of Nitrite in Moles/100 ev at a Dosage of 7×10^{19} ev/g

Salt	Dose intensity, in ev/ml · sec					
	$0.2 \cdot 10^{16}$	$0.48 \cdot 10^{16}$	$0.8 \cdot 10^{16}$	$1.24 \cdot 10^{16}$	$1.7 \cdot 10^{16}$	$4.1 \cdot 10^{16}$
$Ca(NO_3)_2 \cdot 4H_2O$	1,10	0,90	0,51	0,60	1,10	1,10
$Cd(NO_3)_2 \cdot 4H_2O$	0,93	—	0,67	0,86	0,86	0,95
$Zn(NO_3)_2 \cdot 6H_2O$	0,64	—	0,50	0,40	0,60	0,64
$Mg(NO_3)_2 \cdot 6H_2O$	0,80	—	0,65	0,57	0,80	0,84

dose intensities, in the case of cadmium nitrate the reverse reaction was found to predominate at certain dose intensities over the direct one.

The second group salts exhibit a minimum $G_{NO_2^-}$ at a dose intensity of 1.24×10^{16} ev/ml·sec. With zinc nitrate only over the initial portion of the curve does the reverse reaction predominate. At dosages above 35×10^{19} ev/g the rates of the reverse and direct reactions become equal. The shapes of the magnesium nitrate curves indicate that (within the range of investigated dose intensities) the reverse reaction predominates over the decomposition of nitrate ions.

The water molecules associated with the different crystal hydrates are not all equivalent as regards their chemical function and location in the salts. On the basis of thermal decomposition data [5, 6], when dehydrated, calcium nitrate loses all its water of crystallization immediately. Cadmium nitrate readily loses two water molecules upon dehydration, but the remaining two are held more tightly. It is very difficult to dehydrate the crystal hydrates of zinc and magnesium. It is not possible at the present time to estimate the function of water in the transformations of crystal hydrates caused by radiation; however, the introduction of water molecules into the crystal lattice should somehow be reflected in the free space per unit cell, the crystal lattice energy, and other factors influencing the decomposition rate of the salt. Actually, by comparing the yield of nitrite from anhydrous and hydrated salts we can see that the latter are more sensitive to γ-radiation than the anhydrous. Due to the lack of data on the structure of crystal hydrates and the number of molecules per unit cell we were unable to correlate changes in nitrite yield with the changes in the free space per unit cell or other factors and thus determine the sensitivity (towards γ-radiation) order among crystal hydrates. However, as one can see in Table 1, a sensitivity order similar to that observed [7] among anhydrous salts seems to be preserved among the crystal hydrates. As was already noted, as dose intensity was varied from 0.2×10^{16} to 4.1×10^{16} ev/ml·sec the nitrite yield passed through a minimum. The position of the minimum was specific for salts containing four or six water molecules in their structure. The formation of a minimum, in our opinion, can be explained in the following manner. Irradiation converts the solid nitrates to nitrites as shown below,

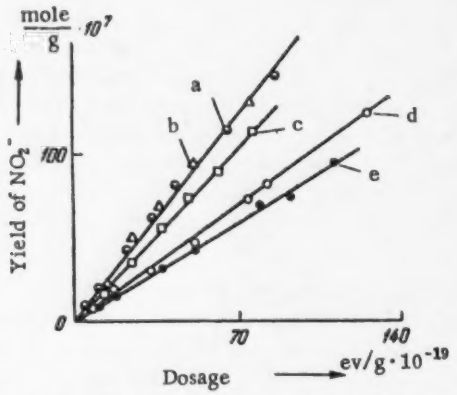

Fig. 2. $Ca(NO_3)_2 \cdot 4H_2O$. The yield of nitrite as a function of radiation dosage at different dose intensities. a) 4.1×10^{16} ev/ml·sec; b) 1.7×10^{16} ev/ml·sec; c) 0.48×10^{16} ev/ml·sec; d) 1.24×10^{16} ev/ml·sec; e) 0.8×10^{16} ev/ml·sec.

$$NO_3^- \rightarrow NO_2^- + {}^1/_2O_2. \quad (1)$$

It was assumed that the energy of the ionizing particle was used up almost evenly for the ionization and excitation of NO_3^- ions,

$$NO_3^- \rightsquigarrow NO_3 + \bar{e}, \quad (2)$$

$$NO_3^- \rightsquigarrow NO_3^{-*} \rightarrow NO_2^- + O. \quad (3)$$

In a case where the final product (nitrite) resulted from the neutralization (or recombination) of radicals (Reaction 2) the yield would be independent of the ionization density. If, on the other hand, the NO_2^- ion also formed by some other independent route, for example, through a reaction between the intermediate products and the starting material,

$$NO_3^- + O \rightarrow NO_2^- + O_2, \quad (4)$$

then the yield of nitrite would depend on the ionization density. Reaction (4) would compete with the recombinations of intermediate products

$$NO_2^- + O \rightarrow NO_3^-, \quad (5)$$

$$O + O \rightarrow O_2. \quad (6)$$

The ratio between Reactions (4) and (5, 6) will depend on the ionization density, while the ionization density for a given ionizing particle with a given energy will in turn depend on the density of the irradiated material and the dose intensity. It seems that the minimum through which the nitrite yield passes represents the appearance of numerous closely spaced dislocations in the original crystal or the formation of individual elements of a new crystal lattice, all of which would lower the effectiveness of the reverse (5) reaction in comparison with Reactions (4) and (6).

LITERATURE CITED

[1] P. Doigan and T. W. Davis, J. Phys. Chem., 56, 764 (1952).

[2] C. J. Hochanadel and T. W. Davis, J. Chem. Phys. 27, 333 (1957).

[3] A. S. Baberkin and M. A. Proskurnin, Proc. Acad. Sci., USSR 121, No. 3, 492 (1958).*

[4] B. V. Mikhal'chuk and R. E. Osherovich, Factory Labs. 9, 836 (1940).

[5] S. D. Shargorodskii and O. I. Shor, Ukr. Chem. J. 16, No. 4, 426 (1950).

[6] S. D. Shargorodskii and O. I. Shor, Ukr. Chem. J. 20, No. 4 (1954).

[7] A. S. Baberkin, Problems in Phys. Sci., No. 3 (1959).

Received January 31, 1959

*Original Russian pagination. See C. B. translation.

THE SEQUENCE OF PRODUCTS FORMED DURING THE LIQUID PHASE OXIDATION OF CYCLOHEXANE IN A STEEL VESSEL

I. V. Berezin and N. F. Kazanskaya

M. V. Lomonosov Moscow State University

(Presented by Academician N. N. Semenov, January 29, 1959)

The abundant experimental data on the liquid phase oxidation of hydrocarbons indicate that the bulk of oxidation products are formed by the decomposition of corresponding hydroperoxides. This was proven for the oxidation of cyclohexane in glass containers [1]. Certain kinetic regularities (such as the lag of the cyclohexyl hydroperoxide accumulation maximum on the kinetic curve behind the cyclohexanone and cyclohexanol reaction rate maxima, have led to the hypothesis that when cyclohexanone and cyclohexanol are formed by the oxidation of cyclohexane in a steel vessel the hydroperoxide decomposition step may be bypassed [2]. The problem can be solved kinetically by using labeled atoms, as was done in this work.

The following sequence is possible in the liquid phase oxidation of cyclohexane:

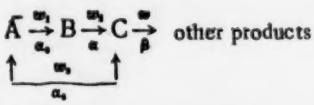

Where A is cyclohexane, B cyclohexyl hydroperoxide, C cyclohexanol or cyclohexanone; α_0, α and β are the respective specific molar radioactivities of these compounds. We were interested in the rate of direct (bypassing B) formation of C, i.e., in ω_3.

Due to the difficulties connected with the synthesis of radioactive cyclohexyl hydroperoxide we adopted the following procedure. If at a fixed time t_0, after a sufficient amount of intermediate products had accumulated in the system, we added to the reaction mixture a small quantity of the reactant A containing a radioactive carbon isotope, and from that time on any compounds formed directly from A would all be radioactive. Their specific molar radioactivity would be equal to that of the A after the introduction of the extra quantity. Since the compounds B and C present at time t_0 will slowly be used up, their specific molar radioactivities α and β will begin to increase. Knowing α_0 and the rates of growth α and β we can determine ω_3 [3].

The total radioactivity of C will be

$$I = [C]\beta; \tag{1}$$

on the other hand, the time rate of change of I can be represented by the equation

$$\frac{dI}{dt} = w_3\alpha_0 + w_2\alpha - w_4\beta. \tag{2}$$

Differentiating Equation (1), substituting into Equation (2) the value of ω_4 obtained from the equation $\omega_2 + \omega_3 = \omega_4 + d[C]/dt$, and then combining Eq. (1) and (2) we will get

$$w_3 = \frac{[C]}{\alpha_0 - \beta}\frac{d\beta}{dt} - \frac{\alpha - \beta}{\alpha_0 - \beta}w_2. \quad (3)$$

At zero time the second term of Equation (3) is zero, and $\omega_3 = ([C]/\alpha_0)(d\beta/dt_0)$. When $d\beta/dt = 0$, then $\omega_3 = 0$; when $d\beta/dt$ is different from zero there should be a route by which C may be formed directly from A.

The rate of formation of C from B (ω_2) can be calculated from the following equation proposed by M. B. Neiman [3]:

$$w_1 = \frac{[B]}{\alpha_0 - \alpha}\frac{d\alpha}{dt} \quad (4)$$

If the concentration of B can be assumed to be constant over a fixed time interval, then $\omega_1 = \omega_2$. Assuming that B undergoes a monomolecular decomposition we can integrate Eq. (4) and get

$$\alpha = \alpha_0(1 - e^{-kt}) \quad (5)$$

where t is the time since the addition of radioactive A, and k the rate constant for the decomposition of B.

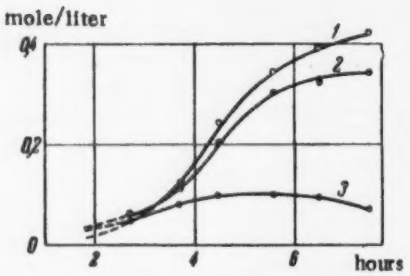

Fig. 1. Typical kinetic curves for the various products formed by the oxidation of cyclohexane in a steel container. 1) Cyclohexanone; 2) cyclohexanol; 3) cyclohexyl hydroperoxide.

Experiments on cyclohexane oxidation were performed in a steel vessel at 140 ± 0.5° at air pressure of 10 ± 0.1 atm at a rate of 80 ± 5 ml/min. Samples were collected in the course of oxidation. The cyclohexane labeled with C^{14} was prepared by reducing radioactive cyclohexanone by Hyang-Minlon's [5] method. The cyclohexane used in the oxidation was purified very thoroughly (b.p. 80-80.5°, n_D^{20} 1.4264). To improve the reproducibility of our experiments we mixed several samples of partially (to a known extent) oxidized cyclohexane (4 hours after the reaction was started, after the hydroperoxide concentration had remained approximately constant for 1.5 hours). To the oxidized sample we added about 3-5% of radioactive cyclohexane and used the resulting mixture in our experiments. We used 25 ml of mixture for each experiment. The hydroperoxide [6], cyclohexanol, and cyclohexanone [7] were analyzed quantitatively. The specific radioactivity was determined by isolating cyclohexanol as the 3,5-dinitrobenzoate, and cyclohexanone as 2,4-dinitrophenylhydrazone. The derivatives were purified by recrystallization and pyrolyzed; CO_2 was collected in a liquid oxygen trap and its radioactivity determined in a counter which could be filled with the gas. We isolated the cyclohyxyl hydroperoxide by converting it to the sodium salt [8]. After purification the hydroperoxide was decomposed with a 3% H_2SO_4 solution in acetic acid [9] to give cyclohexanone whose radioactivity was determined as described above. By means of special experiments (addition of radioactive cyclohexanone to nonradioactive oxidized samples) we showed that the ketone obtained from the decomposition of the peroxide could not contain any ketone carried over from the oxidation. In calculating the specific molar activity we introduced a correction for the number of carbon atoms in the pyrolyzed derivative.

In Fig. 1 we have drawn some typical kinetic curves for the oxidation of cyclohexane in a steel vessel, and in Fig. 2 curves for the growth of specific molar activities of cyclohexyl hydroperoxide cyclohexanol, and cyclohexanone. One can see in Fig. 2 that for cyclohexanone $(d\beta/dt)_{t=0} = 0$. This means that $\omega_3 = 0$, and consequently ther is no direct route for the formation of a ketone from cyclohexane. For cyclohexanol $(d\beta/dt)_{t=0} \neq 0$, and hence it can be prepared directly from cyclohexane.

To estimate the magnitude of ω_3 we have to know ω_2, i.e., the rate at which the hydroperoxide decomposed to cyclohexanol. As is well known, cyclohexyl hydroperoxide gives on decomposition almost equal amounts of cyclohexanol and cyclohexanone [1]. By using Equation (5) we can find both decomposition rate constants of cyclohexyl hydroperoxide. Figure 2A represents a semilogarithmic plot of this equation. The slope of this line gives a rate constant equal to $4.9 \pm 0.5 \times 10^{-2}$ min^{-1}. At zero time $\omega_3 = (d\beta/dt)([C]/\alpha_0) = 0.83 \cdot 10^{-3}$ moles/liter·min.

TABLE 1

Time after addition, min	$\frac{d\beta}{dt}$ counts/min² · · mmole	$w_3 \cdot 10^3$, moles/liter · · min	$w_2 \cdot 10^3$, moles/liter · · min	Total rate of alcohol formation $(w_3 + w_2) \cdot 10^3$	% Alcohol formed independent of hydroperoxide
0	15,2	0,83	2,65	3,48	~24
20	32	0,83	2,65	3,48	~24
30	31,5	1,26	2,83	4,09	~31
45	28	1,72	2,94	4,60	~37
60	21,6	2,14	2,94	5,08	~42

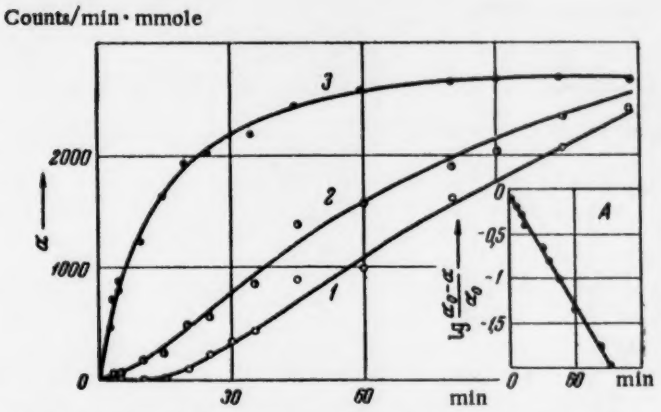

Fig. 2. Change in the specific molar activity with time. 1) Cyclohexanone; 2) cyclohexanol; 3) cyclohexyl hydroperoxide.

From Equation (3) we can calculate ω_2 at any time, for example, after 20 min, by assuming that ω_3 has not changed a lot during this time. We get $\omega_2 = 2{,}65 \times 10^{-3}$ moles/liter·min, which at that point represents 58% of the overall decomposition rate of cyclohexyl hydroperoxide. Let us also note that 60% of hydroperoxide decomposes to cyclohexanol.

In Table 1 we have compiled some rate data for the formation of alcohol at various times. Taking into account computational errors we may assume that about 30% of cyclohexanol is formed directly, bypassing the cyclohexyl hydroperoxide. Thus, when oxidation is carried out in a steel vessel, the bulk of the reaction products are still formed through the decomposition of cyclohexyl hydroperoxide.

The cyclohexanol which was formed independently of cyclohexyl hydroperoxide could in this reaction be only produced from the ROO radical. The first possible route is through a biradical cleavage. However, in the first place, biradical cleavage of such radicals (as Russell has demonstrated [10]) yields ketones and alcohols in equal amounts (in our case only the alcohol was formed directly), and in the second, if we start from this assumption and estimate the cyclohexane oxidation chain length we will find it to be less than the one experimentally observed. It seems that besides the reaction

$$ROO\cdot + RH \rightarrow ROOH + R\cdot,$$

another type of reaction is also possible involving the peroxyl radical

$$ROO\cdot + HR \rightarrow ROH + RO\cdot,$$

$$RO\cdot + HR \rightarrow ROH + R\cdot,$$

which will give exclusively cyclohexanol.

LITERATURE CITED

[1] I. V. Berezin and B. G. Dzantiev, et al., J. Phys. Chem. 31, 554 (1957).

[2] I. V. Berezin, E. T. Denisov, and N. M. Émanuél', Coll. Problems in Chemical Kinetics, Catalysis and Reactivity, Izd AN SSSR, 273 (1955).*

[3] M. B. Neiman, J. Phys. Chem. 28, 1235 (1954).

[4] I. V. Berezin, L. S. Vartanyan, and N. F. Kazanskaya, Bull. Moscow Univ., Chem. Sci. Ser., No. 2, 61 (1956).

[5] Hyang-Minlon, J. Am. Chem. Soc. 68, 2487 (1946).

[6] R. Weller, Oil and Soap 9, 89 (1932).

[7] I. V. Berezin, N. F. Kazanskaya, and G. B. Melusova, J. Phys. Chem., 32, 1218 (1958).

[8] A. Farkas and E. Passaglia, J. Am. Chem. Soc. 72, 3333 (1950).

[9] E. J. du Pont de Nemours and Co., Brit. Pat. 716820, Oct. 13, 1954; Chem. Abstr. 49, 14027g.

[10] J. Russel, Chem. Ind. 49, 1483 (1956).

Received January 27, 1959

* In Russian.

A GENERAL EQUATION FOR OSCILLOGRAPHIC POLAROGRAPHY REVERSIBLE PROCESSES IN ANODIC AND CATHODIC POLARIZATION

Ya. P. Gokhshtein

V. I. Vernadskii Institute of Geochemistry and Analytical Chemistry of the Academy of Sciences, USSR

(Presented by Academician A. N. Frumkin, January 28, 1959)

To derive a relationship between the reversible reaction current and the potential of the electrode on which the reaction occurs we have to solve a boundary problem for a system of two parabolic equations:

$$\frac{\partial c_1}{\partial t} = D_1 \frac{\partial^2 c_1}{\partial x^2}, \quad \frac{\partial c_2}{\partial t} = D_2 \frac{\partial^2 c_2}{\partial x^2}, \quad c_1(x, 0) = \psi_1(x), \quad c_2(x, 0) = \psi_2(x); \tag{1}$$

$$\frac{c_1(0, t)}{c_2(0, t)} = \frac{f_2}{f_1} \exp\left[-\frac{nF}{RT}(E_0 - E(t))\right] \equiv \omega(t); \tag{2}$$

$$D_1 \frac{\partial c_1}{\partial x}(0, t) + D_2 \frac{\partial c_2}{\partial x}(0, t) = 0; \tag{3}$$

f_1 and f_2 are the activity coefficients, c_1 and c_2 are the concentrations of the starting material and of the electrochemical reaction product respectively, at a distance x from the electrode surface and at time t, $\psi_1(x)$ and $\psi_2(x)$ are the initial distributions of the reactants in the solution and in the amalgam respectively, E_0 is the standard electrode potential of the system, $E(t) = (RT/nF)p(t) + \bar{E}$ is the function which gives the change in the electrode potential with time, $\bar{E} = E(0)$. The main purpose of solving this problem in oscillographic polarography is not the determination of concentration $c_1(x,t)$ and $c_2(x,t)$, but of the electrochemical current which is proportional to $\partial c_1/\partial x\,(0, t)$. It is obvious that having found the latter we can readily calculate the concentrations.

The problem (1)-(3) has been solved for several cases by Sevcik [1] and Randles [2]. The analytical solution used by Sevcik involves the following steps. At first we assume that $\psi_1(x) = c = \text{const}$ and $\psi_2(x) = 0$. Then by means of a Laplace transformation we determine $c_1(x, t)$, $c_2(x,t)$, and $\partial c_1/\partial x\,(0,t)$.

Below we are describing a direct method of determining $\partial c_1/\partial x\,(0, t)$. The method is quite simple, even in cases where we have not imposed any special limitations on the functions $\psi_1(x)$, $\psi_2(x)$, and $E(t)$, and it leads to general solution.

Let us assume that the problem has been solved, i.e., that we can write the actual concentration gradient at the surface as a function of time, $\varphi_1(t)$. Then the Problem (1) can be separated into two independent boundary problems:

$$\frac{\partial c_i}{\partial t} = D_i \frac{\partial^2 c_i}{\partial x^2}, \quad c_i(x, 0) = \psi_i(x), \quad \frac{\partial c_i}{\partial x}(0, t) = \varphi_i(t) \quad (i = 1, 2),$$

each of these is known as a boundary problem of the second type and yields the solution

$$c_i(x,t)=\frac{1}{2\sqrt{\pi D_i t}}\int_0^\infty \psi_i(\zeta)\left\{\exp\left[-\frac{(x-\zeta)^2}{4D_i t}\right]+\exp\left[-\frac{(x+\zeta)^2}{4D_i t}\right]\right\}d\zeta-$$

$$-\sqrt{\frac{D_i}{\pi}}\int_0^t \frac{\varphi(\tau)}{\sqrt{t-\tau}}\exp\left[-\frac{x^2}{4D_i(t-\tau)}\right]d\tau. \tag{4}$$

In order to solve Equation (2), given for the boundary between the electrode and solution, we will transform Eq. (4) to the limit $x \to 0$, which is permissible inside both integrals,

$$c_i(0,t)=\frac{1}{\sqrt{\pi D_i t}}\int_0^\infty \psi_i(\zeta)\exp\left[-\frac{\zeta^2}{4D_i t}\right]d\zeta-\sqrt{\frac{D_i}{\pi}}\int_0^t \frac{\varphi_i(\tau)}{\sqrt{t-\tau}}d\tau. \tag{5}$$

Substituting $\partial c_i/\partial x\,(0,t)=\varphi_i(t)$, in Eq. (3), multiplying by $\frac{1}{\sqrt{t-\tau}}$ and integrating we will get

$$D_1\int_0^t \frac{\varphi_1(\tau)}{\sqrt{t-\tau}}d\tau+D_2\int_0^t \frac{\varphi_2(\tau)}{\sqrt{t-\tau}}d\tau=0. \tag{6}$$

Substituting $c_1(0,t)$ and $c_2(0,t)$ from Equation (5) into Eq. (2) and solving Eq. (6) we get an equation with respect to $\varphi_1(t)$,

$$\int_0^t \frac{\varphi_1(\tau)}{\sqrt{t-\tau}}d\tau=f(t), \tag{7}$$

where the right hand of Equation (7) is denoted by $f(t)$.

$$f(t)=\frac{1}{\sqrt{D_1 t}\,[1+\omega(t)\sqrt{D_1/D_2}]}\int_0^\infty\left\{\frac{\psi_1(\zeta)}{\sqrt{D_1}}\exp\left[-\frac{\zeta^2}{4D_1 t}\right]-\right.$$

$$\left.-\omega(t)\frac{\psi_2(\zeta)}{\sqrt{D_2}}\exp\left[-\frac{\zeta^2}{4D_2 t}\right]\right\}d\zeta. \tag{8}$$

The resulting equation, containing the desired fraction $\varphi_1(t)$ inside the integral, is known as Abel's equation. Its solution,

$$\frac{\partial c_1}{\partial x}(0,t)=\varphi_1(t)=\frac{1}{\pi}\left\{\frac{f(+0)}{\sqrt{t}}+\int_0^t \frac{f'(\tau)}{\sqrt{t-\tau}}d\tau\right\} \tag{9}$$

includes the derived general equation for reversible processes. The current can be obtained by multiplying Eq. (9) by n, the number of electrons involved in the reaction, the electrode area S, Faraday's number F, and the diffusion coefficient D_1:

$$i(t)=\frac{SnFD_1}{\pi}\left\{\frac{f(+0)}{\sqrt{t}}+\int_0^t \frac{f'(\tau)}{\sqrt{t-\tau}}d\tau\right\}. \tag{10}$$

Let us take some examples to confirm the general nature of this equation. Usually $\psi_1(x)\equiv c$ and $\varphi_2(x)\equiv 0$. Then

$$f(t) = \frac{c\sqrt{\pi}}{\sqrt{D_1}\,[1 + \omega(t)\sqrt{D_1/D_2}]} \tag{11}$$

When $\omega(t) = (f_2/f_1)\exp[nF/RT\,(E(t) - E_0)] = be^{p(t)}$, then if we take a solution of type $e^{-z} + me^{z} = 2\sqrt{m}\,\mathrm{ch}\,(z + \frac{1}{2}\ln m)$, we will get

$$f'(t) = -c\sqrt{\frac{\pi}{D_1}}\,\frac{p'(t)}{4\,\mathrm{ch}^2 1/2\,[p(t) + \ln(b\sqrt{D_1/D_2})]}. \tag{12}$$

A constant potential. $\omega(t) = b = \mathrm{const}$;

$$f(t) = \frac{c\sqrt{\pi}}{\sqrt{D_1}(1 + b\sqrt{D_1/D_2})} = f(0); \quad f'(\tau) = 0;$$
$$i(t) = SnF\sqrt{D_1}c\,\frac{1}{\sqrt{\pi t}\,(1 + b\sqrt{D_1/D_2})}, \tag{13}$$

which agrees with a well known polarographic equation [3].

A linearly changing potential. Cathodic polarization $\omega(t) = be^{-at}$; $a = vnF/RT$; $v \geq 0$ is rate at which the potential changes(v/sec);

$$f(t) = \frac{c\sqrt{\pi}}{\sqrt{D_1}(1 + b\sqrt{D_1/D_2}\,e^{-at})}, \quad f'(t) = c\sqrt{\frac{\pi}{D_1}}\,\frac{a}{4\,\mathrm{ch}^2 1/2\,[at - \ln(b\sqrt{D_1/D_2})]}.$$

Substituting these functions into Eq. (10) we will get an equation for the desired current,

$$i(t) = SnF\sqrt{D_1}\,c\,\frac{1}{\sqrt{\pi}}\left\{\frac{1}{\sqrt{t}\,(1 + b\sqrt{D_1/D_2})} + \frac{a}{4}\int_0^t \frac{d\tau}{\sqrt{t-\tau}\,\mathrm{ch}^2 1/2\,a(\tau - t_{1/2})}\right\}, \tag{14}$$

where the time $t_{1/2} = \frac{\overline{E} - E_0}{v} + \frac{1}{a}\ln\frac{f_2}{f_1}\sqrt{\frac{D_1}{D_2}}$ refers to half wave potential. For the sake of comparison we are also showing Sevcik's equation derived for the same case:

$$i(t) = SnF\sqrt{D_1}\,c\,\frac{1}{\sqrt{\pi}}\left[1 + \frac{1}{b}\sqrt{\frac{D_2}{D_1}}\right]\frac{a}{4}\int_0^t \frac{d\tau}{\sqrt{t-\tau}\,\mathrm{ch}^2 1/2\,a(\tau - t_{1/2})}.$$

For large b and a (large positive initial potential relative to the equilibrium value, high rate of change of potential) Equation (14) is almost identical with Sevcik's. If, however, even one of these conditions were not fulfilled the discrepancy between the two equations would be great, and Eq. (14) would be the more accurate one. This becomes apparent, for example, when we try to convert both equations to a stationary potential case and have to take the rate of change of potential as equal to zero ($a = 0$). In such a case Equation (14) results in Eq. (13). But Sevcik's equation yields $I(t) \equiv 0$.

The equations differ considerably not only in the region of ($a = 0$) but also for small values of A. Similar discrepancy occurs also at large negative initial potentials, even when a is large, since under these conditions the first term in Equation (14) increases in importance.

Despite the great differences between Sevcik's equation and Equation (14) both equations are fundamentally correct, differing only in their range of applicability. Equation (14) is applicable over a wider range, since in deriving it we used more general assumptions concerning the time interval.

A linearly changing Potential. Anodic polarization. The potential according to law [4]

$$E(t) = \begin{cases} \overline{E} & (0 < t \leqslant t_0), \\ \overline{E} + v(t - t_0) & (t_0 < t < \infty); \end{cases}$$

$$\omega(t) = \exp\left[-\frac{nF}{RT}(E_0 - E(t))\right] = \begin{cases} b & (0 < t \leqslant t_0), \\ be^{a(t-t_0)} & (t_0 < t < \infty). \end{cases}$$

This is one of the cases where we have a large negative potential and small b. Accordingly we get from Eq. (11)

$$f(t) = \begin{cases} \dfrac{c\sqrt{\pi}}{\sqrt{D_1}(1 + b\sqrt{D_1/D_2})} & (0 < t \leqslant t_0), \\ \dfrac{c\sqrt{\pi}}{\sqrt{D_1}(1 + be^{a(t-t_0)}\sqrt{D_1/D_2})} & (t_0 < t < \infty). \end{cases}$$

Then for $t > t_0$ the general Equation (10) will give

$$i(t) = SnF\sqrt{D_1}\,c\,\frac{1}{\sqrt{\pi}}\left\{\frac{1}{\sqrt{t}(1 + b\sqrt{D_1/D_2})} - \frac{a}{4}\int_{t_0}^{t}\frac{d\tau}{\sqrt{t-\tau}\,\mathrm{ch}^2\,1/2\,a(\tau - t_{1/2})}\right\}. \tag{15}$$

The first term inside the braces will be large, since $\bar{E} < E_0 < 0$ and $b < 1$. Particularly at $t_0 = 0$,

$$i(t) = SnF\sqrt{D_1}\,c\,\frac{1}{\sqrt{\pi}}\left\{\frac{1}{\sqrt{t}(1 + b\sqrt{D_1/D_2})} - \frac{a}{4}\int_{0}^{t}\frac{d\tau}{\sqrt{t-\tau}\,\mathrm{ch}^2\,1/2\,a(\tau - t_{1/2})}\right\},$$

which agrees with Eq. (14), for the latter was derived for any positive or negative values of a.

A periodically changing potential. A saw-tooth voltage and an(isosceles) triangle-shaped voltage can be readily represented by trigonometric series, and both are given in that form in Eq. (11). Intermediate cases may be studied in a similar manner [5].

The integral $\int_0^t \frac{f'(\tau)}{\sqrt{t-\tau}}\,d\tau$, encountered in Equation (10) and in all its applications, is not always integrable.

Therefore in practice this integral has to be calculated by approximate methods. However, the form which it has in Equation (10) is unsuitable for calculation since $\tau \to t\ \frac{1}{\sqrt{t-\tau}} \to \infty$, while $f'(\tau)$ is finite. After integrating by parts

$$\int_0^t \frac{f'(\tau)}{\sqrt{t-\tau}}\,d\tau = 2\left[f'(0)\sqrt{t} + \int_0^t \sqrt{t-\tau}\,df'(\tau)\right]$$

we get a form which can be more suitably represented as a sum. In order to avoid redividing the interval (0, t) at each t we will divide the entire range of time measurements $t(0, \theta)$ into N equal parts, where θ is the time at the end of each observation. Then by taking θ/N as a unit of time, for a time $t = k$ we will get

$$\int_0^k \frac{f'(\tau)}{\sqrt{k-\tau}}\,d\tau \doteq 2\left\{f'(1)\sqrt{k} + \sum_{i=1}^{k-1}\sqrt{k-i}\,[f'(i+1) - f'(i)]\right\}. \tag{16}$$

Let us note that since $\omega(t)$ also has a meaning in nonreversible processes, then in these processes too the time variation of current can be written in the form of Eq. (10).

LITERATURE CITED

[1] A. Sevcik, Coll. Czechoslov. Chem. Comm. 13, 349 (1948).

[2] J. E. B. Randles, Trans. Farad. Soc. 44, 322 (1948).

[3] P. Delahay, New Instrumental Methods in Electrochemistry [Russian translation] (IL, 1957).

[4] Ya. P. Gokhshtein, S. V. Kuz'min, A. F. Volkov, and V. A. Yanchevskii, Bull. Branch All-Union Inst. of Sci. and Tech. Information, Subject No. 39, No. P-58-172/15 (1958).

[5] Ya. P. Gokhshtein, J. Phys. Chem. 32, 1481 (1958).

Received January 27, 1959

THE EFFECTS OF SURFACE ACTIVE MEDIA ON THE DEFORMATION AND DISINTEGRATION STUDIED BY THE METHOD OF INTERNAL FRICTION

N. V. Dekartova and V. N. Rozhanskii

M. V. Lomonosov Moscow State University

(Presented by Academician P. A. Rebinder, February 23, 1959)

The measurements of damping of free torsional vibrations have recently found many applications; in several cases the method made it possible to penetrate deeply into the mechanism of processes connected with the displacement of atoms inside solids. However, the method has not yet been applied to the study of mechanism by which the surrounding medium influences the properties of metals.

V. I. Likhtman and V. S. Ostrovskii [1, 2], who were the first to measure the dependence of plastic viscosity under steady creep on the surrounding medium, found that the viscosities greatly decreased in organic surface active media especially under stresses close to the yield point, where the effect of eased deformation (discovered by P. A. Rebinder [3]) has the most pronounced effect [4].

In the present work, by using the method of monotonic twisting we studied the effects of surface active agents on plastic deformation, and the effects on atomic relaxation by measuring the damping of free torsional vibrations (at a frequency of 7 hertz). Measurements were carried out on mono- and polycrystalline zinc, cadmium, copper, and lead wires 0.8 mm in diameter. The surface active medium consisted of a 0.2% solution of oleic acid in vaseline oil, or of mercury films (0.5, 2, and 5 μ thick) deposited by submerging the samples into mercuric salts or pure mercury. The behavior of amalgamated mono- and polycrystalline zinc was investigated most thoroughly, since some previous work [5] already established the high surface activity of mercury on zinc.

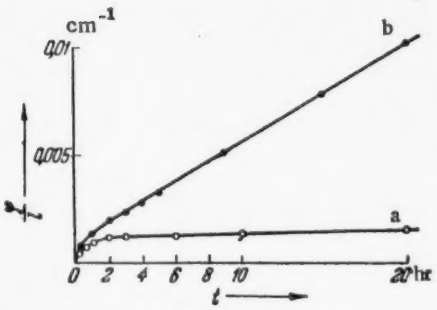

Fig. 1. Creep curves for a single zinc crystal (d = 1.0 mm, l = 20 mm) at a constant torsional moment (M = 3914 dyne·cm).
a) In air; b) in a 0.2% solution of oleic acid in vaseline oil.

When samples coated with the oleic acid solution were subjected to monotonic twisting, just as in the experiments of V. I. Likhtman and V. S. Ostrovskii, a decline was observed in the plastic viscosity (Fig. 1). It seems that increased plasticity is primarily due to a decreased surface tension at the boundary between the metal and the medium, which consequently decreases the potential barrier against the outcropping of dislocations.

Similar phenomena should also be observed in the presence of such a strong surface active agent as mercury. However, in this case the diffusion of mercury into the sample, by creating additional potential barriers against the spread of dislocation, may have a strengthening effect and consequently entail an increase in plastic viscosity. This effect will be particularly well pronounced at high deformation rates. Actually, as is shown in Fig. 2, depending on the conditions of deformation the mercury

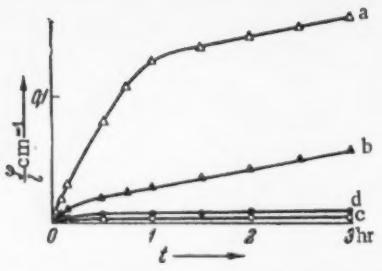

Fig. 2. Creeps curves for a single zinc crystal (d = 0.8 mm, l = 20 mm) at a constant torsional moment, t = 100°C. a) Unamalgamated sample, M = 3190 dyne·cm; b) amalgamated sample, M = 3190 dyne·cm; c) unamalgamated sample, M = 1280 dyne·cm; d) amalgamated sample, M = 1280 dyne·cm.

coating (thick enough to ensure a phase boundary on the external surface) can either result in greater plasticity or strengthening of single zinc crystals. Only the strengthening effect was observed with metals on which mercury did not exhibit high surface activity (lead, cadmium, copper) and with polycrystals, where the role of surface barriers was reduced while the intergranular boundaries became the most important potential barriers.

When single zinc crystals were coated with the oleic acid solution there was only an insignificant increase in the damping of free vibrations. The method of monotonic twisting is somewhat more sensitive, because it is connected with the substantial forces which come into play when dislocations overcome the surface barrier. Nevertheless, mercury coatings (especially on polycrystals) display very large effects over the whole experimental temperature range (from 20 to 250°C). The internal friction in amalgamated single zinc crystals is reduced to one half its normal value in the investigated temperature range. The effect increases with increasing deformation amplitude and slightly decreases with increasing thickness of the mercury film. This seems to be connected with the usual effects of alloying, while the plasticizing action of adsorbed mercury on the outer surface accounts for the decreasing effect with increasing coat thickness.

Polycrystalline samples behaved entirely different when coated with a mercury film. At low amplitudes the same type of internal friction lowering was observed. With increasing amplitude the damping at first slightly declined, but, after a certain limiting amplitude, abruptly increased (Fig. 3). This effect was only observed whenever a large amount of mercury was deposited and increased with decreasing grain size.

In Fig. 4 we have plotted the damping of torsional vibrations Q^{-1} at large amplitudes, $\varphi_0/l = 8 \times 10^{-5}\text{cm}^{-1}$, as a function of grain size for uncoated samples (dotted line) and samples with various depths of mercury film. Damping was found to increase linearly with the grain surface ρ, which was calculated from the formula

$$\rho = \frac{V_{\text{sample}}\bar{S}_{\text{grain}}}{\bar{V}_{\text{grain}}},$$

The damping of torsional vibrations in unamalgamated samples was independent of grain size and was related to damping in single crystals. This indicated that in the absence of mercury the grain boundaries did not participate in the inelastic deformation. After amalgamation the inelastic deformation was primarily localized at the grain boundaries, for the absorption of mercury lowered the free energy (at the boundaries) and entailed the possibility of inelastic deformation at the grain boundaries. The latter fact is very important for the explanation of the mechanism by which metals lose their strength when fused with surface active metals. In trying to explain why copper containing small amounts of bismuth became brittle at elevated temperatures, KêTing Sui [6] arrived at the idea of bismuth adsorption along grain boundaries. However, one can hardly attribute the loss of strength to the dissolution of intercrystalline layers, for the increase in Q^{-1} is only observed at relatively high stresses (amplitudes). It seems that the mechanism of polycrystalline deformation in surface active fused metals is similar to the deformation in single crystals and involves the lowering of surface tension at the origins of minute cracks formed through accumulated dislocations [7]. The localized deformation along grain boundaries is connected with the fact that in polycrystals the grain boundaries form the most serious barriers against the propagation of dislocation and at the same time constitute places with a maximum concentration of surface active metal.

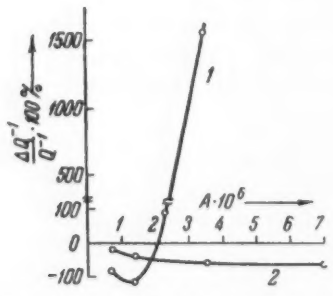

Fig. 3. Change in the internal friction as a function of the torsional vibration amplitude ($A = \varphi_0 \cdot r/l$); thickness of mercury film is 5 μ in Curve 1 and 0.5 μ in Curve 2.

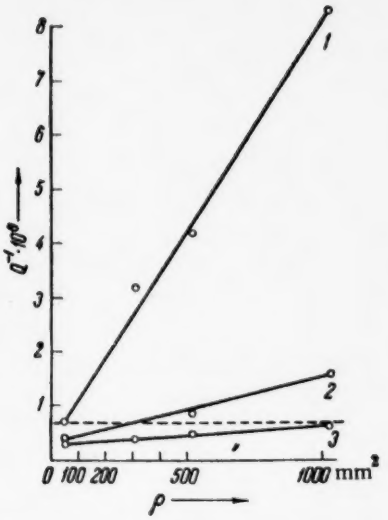

Fig. 4. Internal friction, $Q^{-1} = \delta/\pi$ (δ is the logarithmic decrement) as a function of the internal surface of samples with varying amounts of mercury coating. Curves 1, 2, and 3 are for mercury films 5, 2, and 0.5 μ thick respectively.

It should be noted that with metals on which the mercury does not exhibit high surface activity (cadmium, lead), no matter how thick the mercury coating, only a decreased internal friction is observed, which in the monotonic twisting experiments corresponds to strengthening.

The authors wish to express their deep gratitude to Acad. P. A. Rebinder, Prof. V. I. Likhtman, and E. D. Shchukin for discussion of results and valuable advice.

LITERATURE CITED

[1] V. I. Likhtman, and V. S. Ostrovskii, Proc. Acad. Sci., USSR 19, 484 (1958)*.

[2] V. S. Ostrovskii, and V. I. Likhtman, Colloid. J. 20, 640 (1958).*

[3] P. A. Rebinder, Report at the 6th Conference of Russian Physicists, (Moscow, 1928).

[4] V. N. Rozhanskii, and P. A. Rebinder, Proc. Acad. Sci., USSR 91, 129 (1953).

[5] V. N. Rozhanskii, N. V. Pertsov, E. D. Shchukin, and P. A. Rebinder, Proc. Acad. Sci. USSR 116, 769 (1957).*

[6] T. S. Kê, J. Appl. Phys., 20, 1226 (1949).

[7] V. N. Rozhanskii, Progr. Phys. Sci. 65, 387 (1958).

Received February 10, 1959

*Original Russian pagination. See C. B. translation.

ELECTRICAL CONDUCTANCE AND CATHODIC POLARIZATION OF CHROMIUM-CONTAINING SLAGS

I. N. Zakharov and O. A. Esin

Metallurgical Institute of the Ural Branch of the Academy of Sciences, USSR

(Presented by Academician I. P. Bardin, February 20, 1959)

Several authors [1-3] have admitted the possibility of forming divalent chromium (Cr^{II}) in molten slags in contact with liquid steel. We confirmed its existence [4] while measuring the solubilities of chromium oxides by the emf method. Several workers [5, 6] have expressed the opinion that divalent and trivalent chromium should differ greatly in their mobilities. Thus Kiryushkin [5] concluded that Cr^{III} must decrease and Cr^{II} somewhat increase the electrical conductance (κ) of fused $CaO + SiO_2$. Unfortunately the use of graphite crucibles, which partially reduce chromium oxides, as well as the inaccuracy of amperometric and potentiometric techniques prevents us from considering these results as reliable.

By using the same method to measure the conductance and by determining the viscosity (η), Pastukhov [6] discovered that the divalent chromium ions in slags rich in iron increased κ, while the trivalent ones increased η. Such melts however, are usually semiconductors and their electrical conductance is larger by about one order of magnitude [7] than the value found in [6].

With reference to what was just discussed it was of some interest to investigate the effects of Cr^{II} and Cr^{III} on the conductances and limiting currents in molten slags. We used tungsten or platinum electrodes and an alternating current bridge [8] to measure κ in nonferrous slags. Experiments were conducted in a carbon resistance furnace with the heater insulated by magnesite. Slags containing 40-55% CaO, 45-30% SiO_2, 8% Al_2O_3, 7% MgO and various amounts of chromic oxide were placed in corundum crucibles which usually contained a liquid copper + 10% Cr alloy. The latter by partially reducing Cr_2O_3 insured the formation of Cr^{II} in the melts.

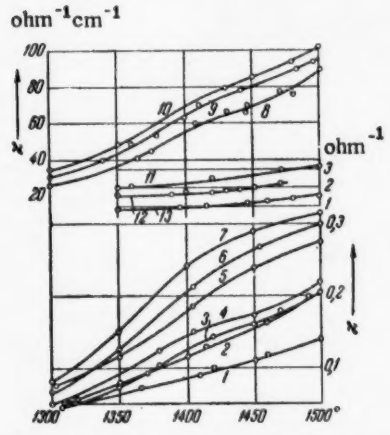

Fig. 1. Limiting conductance of chromium slags as a function of the temperature and composition. Curves 4, 7, 8, and 11 are for 0% Cr_2O_3; 3, 6, 9, and 12 for 5% Cr_2O_3; 1, 2, 5, 10, and 13 for 10% Cr_2O_3.

As may be seen in Fig. 1 the electrical conductance of a slag containing 40% CaO + 10% Cr_2O_3 (Curve 1) is appreciably higher when Cr^{II} is present (Curve 2). On the other hand κ in that same melt increases as the total concentration of chromic oxide is decreased from 10% (Curve 2) to 5% (Curve 3) and 0% (Curve 4). A similar pattern is observed in the slag with 45% CaO (Curves 5, 6, and 7 are for 10, 5, and 0% of Cr_2O_3 respectively).

Hence, when trivalent chromium is dissolved in fused CaO + MgO + Al_2O_3 + SiO_2 it greatly reduces the limiting electrical conductance, while small amounts of Cr^{II} have very little effect. Since the ionic radius of Cr^{+++} (0.63 A) is smaller than that of Cr^{++} (0.82 A) the solvation energy of the first should be smaller, and consequently one would expect the effects of these ions on the conductance of the slag to be reversed. The observed trend seems to be due to greater strength and homopolarity of the bond between Cr^{III} and the melt. In fact, according to Pauling's data [9], the percent ionic character (x) is 0.82 for Cr^{++} and 0.65 for Cr^{+++}.

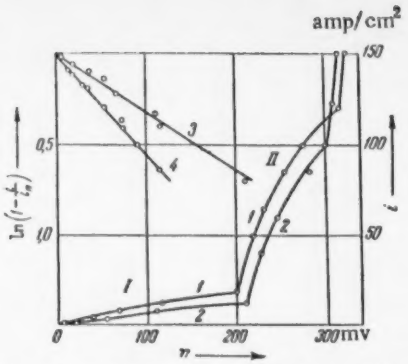

Fig. 2. Cathodic polarization on a solid tungsten cathode at 1450°C.

Due to the high conductance of ferrous slags the measurements were carried out potentiometrically [10]. Of the four tightly soldered tungsten (or platinum) electrodes the two end-ones served as current outlets while the middle ones were connected to a potentiometer. The cell was calibrated with molten ferrosilicate ($N_{FeO} = 0.67$, and $N_{SiO_2} = 0.33$) whose electrical conductance was 3.3-4 $ohm^{-1}cm^{-1}$ at 1400-1450°C [7]. The investigated slags were fused in crucibles made of Armco iron and contained 91% FeO + Fe_2O_3 + 3% SiO_2 + 3% CaO + 3% MgO. As one can see in Fig. 1 the value of κ increased with increasing Cr_2O_3 content (Curves 8, 9, and 10 refer to 0, 5, and 10% Cr_2O_3). Since molten FeO is a defect P-type (semiconductor [7, 11-13], it seems that the increased conductance in our slags must be connected with increased concentration of holes. The energy levels involved in the reactions $Fe^{++} \rightarrow Fe^{+++}$ and $Cr^{++} \rightarrow Cr^{+++}$ are very similar and the increase of the (Fe_2O_3 + Cr_2O_3%) sum increases the probability of electronic transitions.

In order to explain the effect of chromium oxides on the ionic conductance of ferrous slags we carried out some measurements in fused 65% FeO+ 35% SiO_2 in which the transference number of Fe^{++} ion is almost zero [11]. Curves 11, 12, and 13 correspond to 0, 5, and 10% Cr_2O_3 added, and their distribution indicates that electrical conductance declines with increasing content of chromic oxide. Just as in the case of nonferrous slags, this effect was explained by increased homopolarity and strength of the bond between trivalent chromium and the melt.

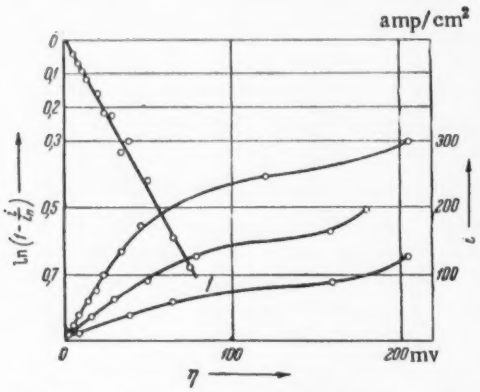

Fig. 3. Cathodic polarization on a liquid copper cathode with 2% Cr at 1450°.

To confirm the great difference between the ionic mobilities of Cr^{++} and Cr^{+++} by an independent method, we investigated the cathodic polarization (η) in nonferrous slags (with 1% of Cr_2O_3 added). The measurements were done at 1450° with the help of a commutator and in cells made of fused magnesium oxide; the method was described in [14]. Liquid alloys of copper + 2% Cr served as the anode and reference electrode. To separate the processes of overcharging and plating of chromium we used a solid tungsten cathode. Curves 1 and 2 in Fig. 2 represent the results obtained in molten 49% CaO+ 35% SiO_2 + 8% Al_2O_3 + 7% MgO + 1% Cr_2O_3. It seems that the initial portions of these curves correspond to the overcharging of

$$Cr^{3+} + e = Cr^{2+}. \qquad (a)$$

The fact that the simplest equation for the concentration polarization

$$\eta = \frac{RT}{nF} \ln\left(1 - \frac{i}{i_n}\right) \qquad (b)$$

fits well these segments (see Curve 3) when the coefficient $n \cong 1$ tends to support this contention. By contrast $n \cong 2$ for the second segment (line 4), and it corresponds to the cathodic plating of divalent chromium,

$$Cr^{2+} + 2e = Cr. \qquad (c)$$

Comparing the limiting currents in Reactions (a) and (c), which are 15-20 and 125-130 $mamp/cm^2$ respectively, we can see that the diffusion coefficient of Cr^{++} is about 6 times larger than that of Cr^{+++}. Similar results were obtained in the investigation of polarization by overcharging and plating Fe^{+++} and Fe^{++} from molten slags [15, 16]. The same applies to cathodic plating of Si^{++++}. Thus, polyvalent ions, for example, Fe^{+++}, Cr^{+++},

and Si^{++++}, which form more stable and homopolar bonds with the slag, have a much lower mobility than do other ions.

In cases where a liquid copper + 2% Cr alloy was used as a cathode the polarization curve had only one branch (Fig. 3, 2) in any one slag. Its limiting current (160 mamp/cm^2) was close to the sum of currents measured on both branches of the curve in Fig. 2 (20 + 130 = 150 mamp/cm^2). When the basicity of the slag was decreased (Curves 1, 2, and 3 correspond to 55, 50 and 45% CaO respectively) the limiting current increased from 80 to 160 and 250 mamp/cm^2; the change seems to be due to decreased viscosity of the electrolyte. All the curves in Fig. 3 obey Equation (b) with a coefficient n $\cong$ 3 (see line 4). Evidently due to the great depolarization caused by dissolving chromium in copper, Reactions (a), (c), and (d),

$$Cr^{3+} + 3e = Cr \qquad (d)$$

cannot under these conditions be separated from each other.

Thus the limiting current and electrical conductance measurements support the previously made assumptions that the ionic mobility of trivalent chromium is much lower than that of divalent chromium.

LITERATURE CITED

[1] D. C. Hilti, W. D. Torgeng, and R. L. Folkman, J. of Metals 7, No. 2, 253 (1955).

[2] S. I. Khitrik, Sci. Rep. Dnepropetrovsk Inst., No. 28, 3 (1953).

[3] P. V. Gel'd and O. A. Esin, High-temperature Reduction Processes (1958). *

[4] O. A. Esin and I. N. Zakharov, Bull. Instit. of Higher Learning, Ministry of Higher Educ., USSR, Ferrous Metallurgy 1, No. 11 (1958).

[5] Yu. P. Kiryushkin, Coll. Works, Zhdanov Metallurg. Inst., No. 4, 88 (1957).

[6] A. N. Pastukhov, Trans. 3rd Conf. on Phys-Chem. Foundations of Steel Production, Izd AN SSSR, 15 (1957).

[7] H. Inoye, I. W. Tomlinson, and L. Chipman, Trans. Farad. Soc. 49, No. 7, 796 (1953).

[8] O. A. Esin, and B. L. Zyazev, J. Inorg. Chem. 2, No. 9, 1998 (1957).

[9] L. Pauling, The Nature of the Chemical Bond [Russian translation] (1947).

[10] D. I. G. Ives and S. Swaropa, Trans. Farad. Soc. 49, No. 7, 788 (1953).

[11] O. A. Esin and A. K. Kiryanov, Bull. Acad. Sci. USSR, Div. Tech. Sci., No. 12, 28 (1955); No. 8, 20 (1956).

[12] A. F. Ioffe, Semiconductor Physics, Izd AN SSSR (1957).*

[13] E. Verway, Semiconductors [Russian translation] p. 201 (IL 1954).

[14] V. I. Musikhin and O. A. Esin, J. Phys. Chem. 32, No. 10, 2410 (1958).

[15] O. A. Esin and G. A. Torporishchev, J. Phys. Chem. 31, No. 2, 474 (1957).

[16] O. A. Esin and V. A. Chechulin, J. Phys. Chem. 32, No. 2, 355 (1958).

Received February 19, 1959

* In Russian.

THERMAL CRACKING KINETICS OF HYDROCARBONS

G. A. Panchenkov and V. Ya. Baranov

I. M. Gubkin Moscow Institute of Petrochemical and Gas Industry

(Presented by Academician A. V. Topchiev, February 19, 1959).

To find a kinetic equation for the thermal cracking we can either start from a known exact reaction mechanism, i.e., from the knowledge of all the elementary processes which enter into the complete reaction, or from certain general qualitative ideas which agree with the experiment. The first method is almost out of the question, since with the exception of certain reactions in flames, at low pressures for the great majority of chemical reactions a detailed mechanism remains still unknown. Therefore only the second method is of any real significance.

If we judge the kinetics by the general reaction of the starting material, then the thermal cracking can be written down in the following manner:

$$A \rightarrow \nu_1 A_1 + \nu_2 A_2 + \ldots + \nu_n A_n, \qquad (I)$$

where A is the starting material (it may be a mixture of hydrocarbons), A_i the reaction products, and ν_i the stoichoimetric coefficients. We can assume that the slowest step in the cracking will be the reaction between the lightweight radicals formed during the reaction from the starting materials and the original reactant molecules, i.e.,

$$W_1 = k\,[R]\,[A], \qquad (1)$$

Where W_1 is the rate of cracking, $\underline{k}$ the rate constant, [R] and [A] the concentrations of radicals and original molecules respectively. But it is possible that the rate of hydrocarbon cracking is determined by the rates of two processes – the dissociation of the starting molecules into free radicals and the subsequent reaction of these radicals with the initial molecules, i.e.,

$$W_1 = k_1\,[A] + k_2\,[R]\,[A]. \qquad (2)$$

It follows from Reactions (1) and (2) that to find out the cracking rate it is essential to know the concentrations of the radicals. For this it is necessary to determine which processes are responsible for the formation and destruction of radicals. Usually the radicals may be formed as a result of bimolecular collisions among the starting molecules, or through monomolecular dissociation of the starting molecules when excess energy becomes concentrated in certain bonds. The radicals will be destroyed by either reacting with the starting molecules or by recombination. The first reaction should yield radicals with a higher molecular weight, which will then be converted to the end products (for example, into isoalkanes or alkenes if the original molecules are alkanes). The second reaction is not highly probable due to the excess concentration of the starting material. Therefore the rate of radical formation will be

$$W_2 = k_3\,[A]^2 + k_1\,[A] - k_4\,[A]\,[R]. \qquad (3)$$

Applying to this reaction the steady-state approximation we will get

$$[R] = \frac{k_2}{k_4}[A] + \frac{k_1}{k_4}. \tag{4}$$

The third item in Equation (3) can also account for the regeneration of radicals after collision and reaction with the starting molecules; in that case k_4 will not be equal to k or k_2, but will represent the difference between the rate constants for the destruction (k_4) and regeneration (k_5) of radicals. If the formation of radicals through bimolecular collisions between the initial molecules is not very important, then by using the steady-state approximation we can get from Equation (3) $[R] = k_1/k_4$, while for a case where the monomolecular dissociation by initial molecules into radicals can be neglected we will find that $[R] = k_2[A]/k_4$. Substituting (4) into Equation (1) or (2) we will get

$$W_1 = k'\{1 + k_3'[A]\}[A], \tag{5}$$

where $k' = kk_1/k_4$; and $k_3 = k_3/k_1$ if (4) is substituted into (1), while $k' = k_2k_1/k_4$ and $k'_3 = k_2k_3/(k_1k_4 + k_2k_1)$ if (4) is substituted into (2).

The problem as to which equation, (1) or (2), should be given preference can only be resolved after the mechanism of the thermal cracking has been worked out in detail. Equation (5) is entirely adequate for the solution of practical problems. From Equations (5) and $[R] = k_1/k_4$ it is evident that if the bimolecular collisions between initial molecules do not play any important part in the formation of radicals then Equation (5) will correspond to a first order reaction. This may happen when cracking occurs at low pressures. If, however, the dissociation of initial molecules into free radicals makes no significant contribution to the total formation of radicals, then the thermal cracking will proceed as a bimolecular reaction. It seems that we should encounter this situation at moderate temperatures.

In cases where the thermal cracking is carried out as a flow process (it is important to note that in practice this reaction is always carried out in a stream of hydrocarbon) its rate equation will include Eq. (5) and, according to paper [1], will have the form

$$n_0 \frac{dx}{p\,dl} = k'\{1 + k_3'C_A\}C_A. \tag{6}$$

When the thermal cracking is carried out in the gas phase at low pressure, we may assume that the ideal gas laws apply to both the reactants and the products; then

$$C_A = \frac{(1-x)P}{(1+\beta x)RT}, \tag{7}$$

where x is the amount of reactant A decomposed over a given distance from the start of the reaction zone, $\beta = \nu_1 + \nu_2 = \ldots - 1$, P the total pressure, R the universal gas constant, and T the absolute temperature. In cases of high-pressure cracking it is important to take into consideration the deviation of gases from ideality.

Substituting Eq. (7) into (6), separating the variables, and integrating we will get

$$n_0 x = -\frac{A}{B} n_0 \ln(1-x) - \frac{k'PV_p}{BR^2T^2}, \tag{8}$$

where $A = \frac{(1+\beta)^2}{m+n}$; $B = \frac{\beta^2}{n} + \frac{\beta}{m}\left(2 + \beta - \frac{m}{n}\beta\right) - \frac{(1+\beta)^2 n}{m(m+n)}$; $m = RT + k_3'P$; $n = \beta RT - k_3'P$;

and V_p is the volume of the reaction space. At the same time it should be remembered that $\ln(m + nx) \approx \ln n + nx/m$. Plotting n_0x against $-n_0\ln(1-x)$ in Equation (8) we will get a straight line with a slope equal to A/B and an intercept on the ordinate equal to $k'PV_p/BR^2T^2$. Both members are functions of pressure and temperature.

When the cracking of petroleum products is carried out at a fixed flow rate of the crude oil the yield of gasoline fractions goes through a maximum; therefore, strictly speaking, thermal cracking should be regarded as a series reaction of the type

$$A \rightarrow \nu_1 A_1 + \nu_2 A_2 + \nu_3 A_3 \rightarrow \nu_4 A_1 + \nu_5 A_2. \quad (II)$$

In addition to all this the products are formally treated as individual molecules with the molecular weights equal to the average values of the corresponding fractions. In Equation (II) A is the starting material, A_1, A_2, and A_3 are the gas, "coke", and gasoline respectively. The second reaction stage is a decomposition of gasoline to gas and "coke", i.e., to the thermodynamically most stable products.

Any calculations involving this type of reaction are very complicated, since we do not know the exact mechanism of thermal cracking. We may suppose that the free radicals which propagate the cracking reaction are formed not only from the initial molecules of reactant A, but also from molecules composing the gasoline fraction. Such an approach leads to a very complicated differential equation which can only be solved by using computers.

We may also start from cruder but, on the other hand, simpler assumptions. It is a known fact that the higher the molecular weight of a hydrocarbon the less stable it is under thermal cracking. Hence we may suppose that molecules A will constitute the main source of free radicals. These radicals will react both with the starting molecules A and with the intermediate molecules A_3. Assuming that the rate of cracking can be described by Equation (1) we can write the following equation for the thermal cracking rate of starting molecules:

$$W_1 = k_1 [A] [R], \quad (9)$$

while for the thermal cracking rate of the intermediate (gasoline),

$$W_2 = k_2 [A_3] [R], \quad (10)$$

and for the formation rate of free radicals

$$W_3 = k_3 [A]^2 + k_4 [A] - k_5 [A] [R], \quad (11)$$

where the constants in these equations are different from the preceding ones, despite the fact that they have similar subscripts.

In flow reactions Equations (9) and (10) (according to [1]) after being substituted into (11) will acquire the forms

$$n_0 \frac{dx}{\rho\, dl} = k' C_A (1 + k_3' C_A); \quad (12)$$

$$n_0 \frac{\nu_4}{\nu_3} \frac{dy}{\rho\, dl} = k'' C_{A_3} (1 + k_3' C_{A_3}). \quad (13)$$

Solving these by a method similar to that given in [1] for successive reactions we will get an equation for the yield of the intermediate (A_3) as a function of the fraction of starting material used up

$$y = \nu_3 x + \frac{\nu_3}{1 - K} [(1 - x) - (1 - x)^K], \quad (14)$$

where K is the ratio between the rate constants of the 2nd and 1st reaction steps. The method of determining K is well known [1]. Substituting (14) into (12) and integrating the resulting equation with the help of certain simplifying approximations we will get an equation similar in form to Eq. (8) (the difference will reside in the physical significance of the constants).

Knowing k' and K we can readily calculate the rate constant for the 2nd stage of cracking. By starting with equations of type (2) for the 1st and 2nd stages we can get equations similar in form to Eq. (12) and (13).

While studying the kinetics of cracking of petroleum products we found out that in the majority of cases studied the slope of the line obtained by plotting $n_0 x$ against $-n_0 \ln(1 - x$ varied with the temperature and

pressure. If the thermal cracking had obeyed strictly a first order equation this phenomena should not have been observed. The lines exhibited a particularly large and characteristic slope change at temperatures above 570-580°C (at atmospheric pressure). At temperatures below 570° this phenomenon is less pronounced. These facts are in agreement with the above derived equation for the kinetics of thermal cracking.

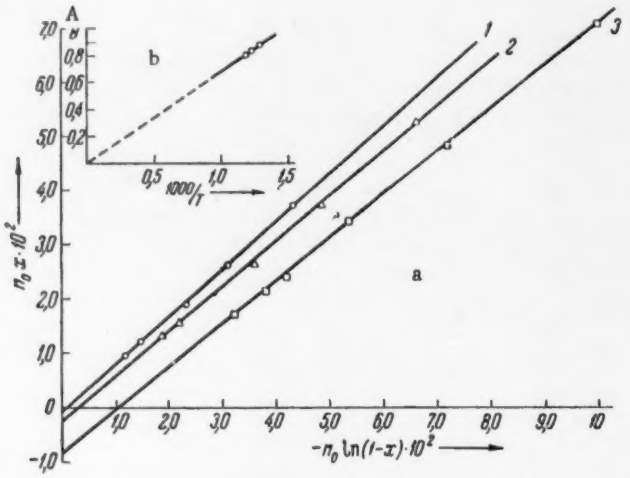

Fig. 1. a) Thermal cracking kinetics of the 320-450°C fraction of Romashkino oil. 1) 510°C; 2) 540°C; 3) 570°C. b) A/B as a function of 1/T.

As a special case to illustrate what was said above we can see the results we obtained during thermal cracking of the 320-450°C fraction of Romashkino oil. The technique and the experiment set up were described in paper [2]. The experiments were carried out at 510, 540, and 570° at atmospheric pressure. The results obtained were interpreted by means of Equations (8). As may be seen in Fig. 1 the experimental points fall quite well on the lines calculated by method of least squares. The slopes decrease with increasing experimental temperatures. The intercepts with the ordinate give the values of apparent rate constants. By using thus obtained apparent rate constants at 510, 540, and 570° C we found the activation energy for the thermal cracking of the investigated fraction to be equal to 55 kcal/mole.

Analysis of the angular coefficient in Equation (8) reveals that A is highly dependent on temperature whereas B only slightly. Therefore if we apply Equation (8) to the thermal cracking of the 320-450°C fraction Romashkino oil and plot A/B against φ (1/T) we should get a straight line passing through the origin. As may be seen in the small graph located in the upper left corner of Fig. 1 the above made assumption is borne out.

LITERATURE CITED

[1] G. M. Panchenkov, J. Phys. Chem. 22, 203 (1948); 26, 454 (1952); Sci. Rep. MGU, No. 174, Inorganic and Physical Chemistry 53 (1955); Heterogeneous Catalysis in Chemical Industry, p. 291 (Moscow, 1955); J. Chem. Phys. 51, 740 (1954).

[2] G. M. Panchenkov, and V. Ya. Baranov, Bull of the Institution of Higher Education, Petroleum and Gas, No. 1, 103 (1958).

Received February 18, 1959

IONIZATION AND DISSOCIATION OF n-OCTANE AND n-NONANE BY MONOENERGETIC ELECTRONS

V. K. Potapov, V. G. Vasil'ev, and N. N. Tunitskii

L. Ya Karpov Physicochemical Scientific Research Institute

(Presented by Academician S. S. Medvedev, February 27, 1959)

The little work that has been done on the use of monoenergetic electrons for the study of ionization curves and appearance potentials [1-3] was mainly limited to the investigation of molecule ions. V. L. Tal'roze and E. L. Frankevich also applied the method to the determination of proton affinities of certain molecules [4].

In order to explain certain problems connected with the formation of fragment ions and the excitation molecule ions under electron impact we used in this work monoenergetic electrons to study the curves for the appearance of fragment and molecule ions from n-octane, n-octane-$2D_1$, and n-nonane-$5C^{13}$ (for synthesis see [5, 9]).

Measurements were carried out in a specially designed mass spectrometer. Monoenergetic electrons were produced at the ion source by a method developed by Fox [6]. Small electric currents of the order of 10^{-17} amp were measured with a secondary emission electron-multiplier.

These were the operational conditions of the ion source: variable filament voltage on the cathode was 1.50 v, the grid voltage 0.50 v, 12% modulation at 0.1 ev electron scattering, the expanding contracting frequency 100 khertz.

TABLE 1

Appearance Potentials of n-Octane Ions

Ion	A_{exp}, ev	D_{ev}	A_{lit}, ev	Ion	A_{exp}, ev	A, calc. from Eq. (4)
$n\text{-}C_8H_{18}^+$	10,3	—	10,26 (7)	$C_6H_{12}^+$	10,6	
$C_6H_{13}^+$	10,6	0,3		$C_5H_{10}^+$	10,7	
$C_5H_{11}^+$	10,8	0,5	10,3 (8)	$C_4H_8^+$	10,85	10,6
$C_4H_9^+$	11,0	0,7	10,64 (8)	$C_3H_6^+$	10,8	10,7
$C_3H_7^+$	11,15	0,8	11,1 (8)	$C_2H_4^+$	11,7	11,5
$C_2H_5^+$	12,5	2,25				

We calibrated the energy scale of the electrons by using the appearance potential curve of Xe^+. The ionization gauge indicated that the n-octane pressure was 10^{-16} mm at the ion source and 3×10^{-7} mm in the analyzer.

In Tables 1 and 2 we have compiled the appearance potentials for the molecule ions and fragments of type $C_nH_{2n+1}^+$ and $C_nH_2^+n$ obtained from n-octane, n-octane-$2D_1$, and n-nonane-$5C^{13}$ and determined on our mass spectrometer.

TABLE 2

Appearance Potentials of Fragment Ions From n-Octane-$2D_1$ and n-Nonane-$5C^{13}$

m/e	Ion	A, ev	Molecule
44	$C_3H_6D^+$	11,1	
43	$C_3H_5D^+$	11,0	
42	$C_3H_6^+$	10,85	
57	$C_4H_7D^+$	10,95	n-Octane-$2D_1$
56	$C_4H_8^+$	10,80	
43	$C_2C^{13}H_6^+$	10,9	50% n-Nonane-$5C^{13}$
42	$C_3H_6^+$	10,9	and 50% n-nonane

The appearance potential of the molecule ion n-$C_8H_{18}^+$ is 10.3 ev and is in good agreement with the calculated [7] value, 10.26 ev. The initial portion of the appearance curve of n-$C_8H_{18}^+$ ion remains nonlinear up to 11.6 ev. The lines show bends at electron energies of 12.5 and 14.7 ev. These pecularities on the appearance curve probably correspond to various excited states of the molecule ion of n-octane.

Fragment ions of the type $C_nH_{2n+1}^+$ can be formed under electron impact from normal paraffins by a direct rupture of C – C bonds or by some other means. It was shown in paper [9] that at 70 ev (electron energies) $C_nH_{2n+1}^+$ ions are formed from n-nonane-$5C^{13}$ by the rupture of two C – bonds.

The appearance potentials listed in Table 1 correspond to the formation of a radical and an ion. As the appearance potentials calculated from the heats of formation of the fragments indicate [10], we would need higher electron energies to form a large number of neutral fragments.

On the other hand, for example, the potential for the appearance of a $C_3H_7^+$ ion from n-octane and of $C_3H_6D^+$ from labeled n-octane-$2D_1$ are identical (Tables 1 and 2). Therefore the first appearance potentials of $C_nH_{2n+1}^+$ ions correspond to the rupture of one C – C bond. However, we should not exclude the possibility that the ion may be formed by a more complex route though with the same appearance potential.

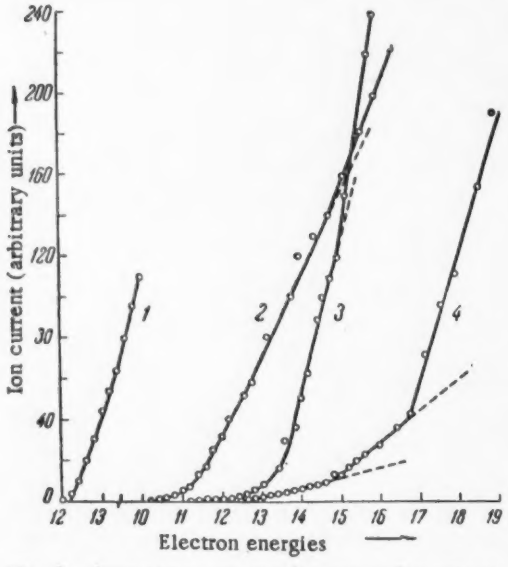

Fig. 1. Appearance curves of xenon and n-octane. 1) Xe^+; 2) n-C_8H_{18}; 3) $C_3H_7^+$; 4) $C_2H_5^+$.

Knowing the appearance potentials of the molecule ion and the fragment ions $C_nH_{2n+1}^+$ we can calculate the C – C bond energies in the n-$C_8H_{18}^+$ ion. The C – C bond energy in an n-octane ion, i.e., the excess energy which has to be supplied to the molecule ion to dissociate it according to equation

$$\text{n-}C_8H_{18} \rightarrow \text{n-}C_8H_{18}^+ \rightarrow C_nH_{2n+1}^+ + C_{8-n}H_{17-2n} \quad (1)$$

is equal to

$$D\,(C_nH_{2n+1}^+ - C_{8-n}H_{17-2n}) = A\,(C_nH_{2n+1}^+) - A\,(\text{n-}C_8H_{18}^+), \quad (2)$$

where A is the appearance potential of the ion (in electron volts).

As may be seen in Table 1 (Column 3) the energy required to rupture a specified C – C bond in a molecule ion of n-octane increases with decreasing number of carbon atoms in the $C_nH_{2n+1}^+$ ion. Thus, for example, the

energy of the second C – C bond in the n-$C_8H_{18}^+$ ion equals 0.5 ev, when the dissociation of the ion gives a C_2H_5 radical and a $C_6H_{13}^+$ ion, but 2.25 ev when a C_6H_{13} radical and a $C_2H_5^+$ ion are formed. Hence the energy of a C – C bond in an n-octane ion depends on the position of the positive charge. It seems that ion fragments of type $C_nH_{2n}^+$ cannot be obtained from normal paraffins by the rupture of a single C – C bond, but are formed by a more complicated route. The observed potentials for the appearance of these ions can be explained if we assume that at low electron energies these ions are formed simultaneously with a new molecule, in the following fashion:

$$n\text{-}C_8H_{18} \rightarrow n\text{-}C_8H_{81}^+ \rightarrow C_nH_{2n}^+ + C_{8-n}H_{81-2n}. \qquad (3)$$

Potentials for the appearance of $C_nH_{2n}^+$ ions formed according to Eq. (3) from n-octane can also be calculated from the equation [10].

$$A(C_nH_{2n}^+) = \Delta H(C_nH_{2n}^+) + \Delta H(C_{8-n}H_{18-2n}) - \Delta H(n\text{-}C_8H_{18}), \qquad (4)$$

where ΔH is the heat of formation of the ion or molecule. The calculated values of A (see Table 1) are close to the experimental ones. Hence, it follows that the activation barrier for reactions of type (3) is low and equal to 0.1-0.2 ev.

More detailed information about the mechanism of Reaction (3) can be obtained with the help of measured appearance potentials of ion fragments from n-octane-$2D_1$ and n-nonane-$5C^{13}$. It can be seen in Table 2 that $C_3H_5D^+$ ions, which are formed from the terminals of the molecule, do not appear below 11.0 ev, while $C_3H_6^+$ ions appear at 10.85 ev. Consequently at electron energies between 10.85 and 11.0 ev the $C_3H_6^+$ ions must be formed from the central portion of the molecule*. Hence Reaction (3) can proceed by the rupture of two C–C bonds and the linkage of two terminal chain portions, all in one step. The configuration of a n-octane chain with its 108°28' bond angles and free rotation about C–C bonds enables the two linking carbon atoms to approach within the distance of a chemical bond (~ 1.5 A); when a $C_3H_6^+$ or larger ion is ejected this would occur freely, without strain, while with a $C_2H_5^+$ ion ejected the approach would be somewhat strained, although the bond angles in a molecule ion are probably more easily deformed.

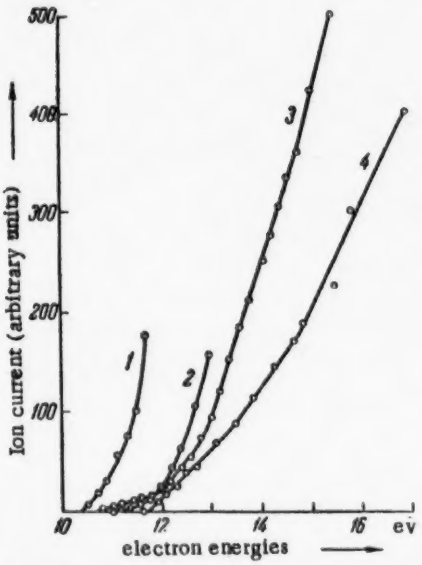

Fig. 2. Appearance curves of fragment ions from n-octane. 1) $C_6H_{13}^+$; 2) $C_3H_7^+$; 3) $C_3H_6^+$; 4) $C_2H_4^+$.

The formation of $C_nH_{2n}^+$ ions and two radicals without recombination according to equation

$$n\text{-}C_8H_{18} \rightarrow C_nH_{2n}^+ + C_iH_{2i+1} + C_kH_{2k+1}, \qquad (5)$$

where n + i + k = 8, proceeds at higher electron energies, as the calculated appearance potential of $C_nH_{2n}^+$ indicates. Thus, for example, a $C_2H_4^+$ ion formed according to Equation (5) should have an appearance potential of 14.8 ev. The bend on the appearance curve of $C_2H_4^+$ (Fig. 2) detected at 14.9 ev evidently corresponds to the formation of the $C_2H_4^+$ ion according to Equation (5).

The bends on the appearance curve of the $C_3H_6^+$ ion (Fig. 2) at electron energies of 11.9, 13, and 14.8 ev probably correspond to various processes by which the $C_3H_6^+$ ion and neutral fragments (molecules and radicals) are formed. When the ion is formed by the rupture of two or more bonds the fragments formed may be in an excited state. The bends on the appearance curves of $C_2H_5^+$ and $C_3H_7^+$ ions evidently correspond to the formation of ions and various neutral fragments, one of which may be excited.

* On the other hand, the appearance potentials of ions with masses of 42 and 43 formed from n-nonane are identical and equal to 10.9 ev (see Table 2).

It is interesting to compare the initial portions of the appearance curves for $C_nH_{2n}^+$ and $C_nH_{2n+1}^+$. Unlike the ions $C_3H_7^+$ and $C_6H_{13}^+$ the $C_2H_4^+$ and $C_3H_6^+$ ions have appearance curves with linear initial portions.

The authors wish to express their deep gratitude to M. V. Tikhomirov for the help rendered in the course of this work and discussion of results, and to M. V. Gur'ev for supplying us with the synthetic n-octane-$2D_1$, and n-nonane-$5C^{13}$.

LITERATURE CITED

[1] R. E. Fox and W. M. Hickam, J. Chem. Phys. 22, 2059 (1954).

[2] J. D. Morrison, J. Chem. Phys. 22, 1219 (1954).

[3] D. C. Frost and C. A. McDowell, Proc. Roy. Soc. A232, 227 (1955).

[4] V. L. Tal'roze and E. L. Frankevich, Proc. Acad. Sci.USSR 111, 376 (1956).

[5] M. V. Gur'ev and M. V. Tikhomirov, J. Phys. Chem. 32, 12, 2731 (1958).

[6] R. E. Fox, W. M. Hickam, D. J. Grove, and T. Kjeldaas, jr., Rev. Sci. Instr. 26, 1101 (1955).

[7] J. Lenard-Jones, Hall, Disc. Faraday Soc., 10, 18 (1951).

[8] D. P. Stevenson, Trans. Farad. Soc., 49, 867 (1953).

[9] M. V. Gur'ev, M. V. Tikhomirov, and N. N. Tunitskii, Proc. Acad. Sci. USSR 123, 120 (1958).*

[10] F. H. Field and J. L. Franklin, Electron Impact Phenomena, N. Y., (1957).

Received February 18, 1959

* Original Russian pagination. See C. B. translation.

CRYSTALLIZATION OF HILLEBRANDITE UNDER HYDROTHERMAL CONDITIONS

G. P. Stavitskaya, Yu. I. Smolin, N. A. Toropov, and E. A. Porai-Koshits

Institute of Silicate Chemistry of the Academy of Sciences, USSR

(Presented by Academician P. A. Rebinder, October 16, 1958)

In order to determine the laws governing the growth of hydrated structures, which are important in the setting of cements, we decided to investigate the crystallization of one of many hydrated calcium silicates – hillebrandite ($2\,CaO \cdot SiO_2 \cdot H_2O$), under hydrothermal conditions. In addition to this we also noted that hillebrandite dissolves at points of crystal fusion then recrystallizes somewhere else from the solution; a similar phenomenon was previously detected in the laboratories of Academician P. A. Rebinder [1] during the setting of gypsum.

The samples, synthesized from a stoichiometric mixture of amorphous silicic acid (6% water) and finely dispersed calcium oxide by being kept for varying lengths of time in the autoclave (at 180°), were studied by means of an electron microscope to permit a characterization of the outer form of the forming crystals; the crystals themselves were identified by means of an x-ray phase analysis with the help of Debye plots and ionization curves.

The initial mixture (Figs. 1a and 2a) contained silica gel (more transparent zones of the microphotograph) and fine crystals of CaO and $Ca(OH)_2$ (denser zones).

The microphotograph of a 3 hour sample (Fig. 1, b) shows amorphous aggregates of gel and crystalline calcium hydroxide, as well as individual flat, needle-shaped hillebrandite crystals; due to the small amount of crystallized material, even the most intense line of hillebrandite (shown by an arrow in Fig. 2, b) was hardly visible on a Debye plot – it was masked by the lines of calcium hydroxide and carbonate.

After a 6-hour synthesis, a great number of needle-shaped crystals grew side by side in parallel and divergent bundles (Fig. 1, c); a small amount of free gel and some large hexagonal hydroxide crystals could also be seen. The Debye plot revealed perfectly distinct narrow hillebrandite lines with the most intense calcium hydroxide lines also preserved (Fig. 2, c).

A next sample, synthesized during 12 hours, gave a Debye plot identical with the preceding one (Fig. 2, d). Yet the microphotograph of this sample (Fig. 1, d) differed considerably from the preceding whereas Fig. 1, c showed large needle-shaped crystals, formed by a common growth in a mesh-like fashion, Fig. 1, d clearly indicated that as a result of dissolution, which had begun at places of coalescence, the meshwork had broken down into individual crystals with corroded ends and surfaces, which were being further dissolved. A photograph of the next sample (Fig. 1, e), synthesized in 24 hours, revealed an almost complete destruction of all the original hillebrandite crystals; it showed a small number of large brick-shaped crystals and some large amorphous solids formed after the destruction of original crystals. This phenomenon was accompanied by reduced intensities of the hillebrandite and slightly increased intensities of calcium hydroxide lines (Fig. 2, e) in the Debye plot.

After a more prolonged synthesis, one obtains a sample which yields a beutiful Debye plot of hillebrandite with the calcium hydroxide lines entirely absent (the ionization curve is shown in Fig. 2, f). The photographs

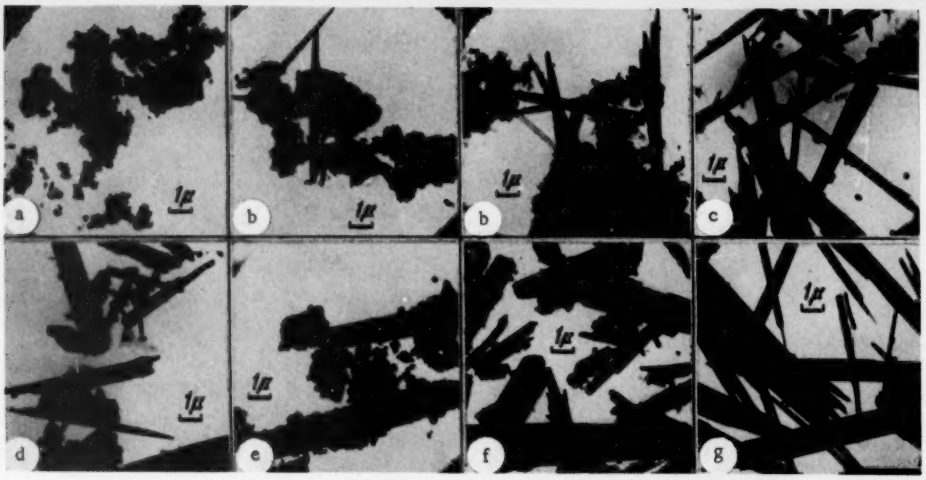

Fig. 1. Electron microphotographs of a) the initial mixture; products synthesized hydrothermally in: b) 3 hr; c) 6 hr; d) 12 hr; e) 24 hr; f) 4 days; g) 13 days.

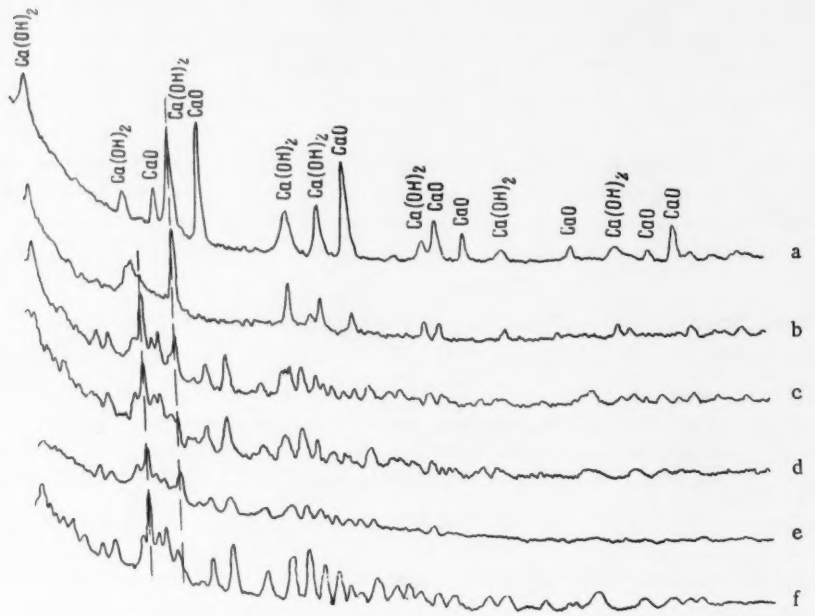

Fig. 2. Ionization curves of a) the initial mixture; products synthesized isothermally in: b) 3 hr; c) 6 hr; d) 12 hr; e) 24 hr; f) 4 days.

show very many new hillebrandite crystals in the form of large and small rods and bricks. After a 4-day synthesis one can detect the incipient splitting of crystal ends into fine threads (Fig. 1,f), while after 13 days the characteristic extended, fibrous crystals of hillebrandite are formed (Fig. 1,g).

A repeated synthesis and investigation confirmed the destruction of the original needle-shaped hillebrandite structure and the subsequent recrystallization into brick-shaped crystals, although with the processes slightly displaced in time; the latter can be attributed to the use of different starting materials and slightly different conditions in the repeated synthesis.

By comparing the intensities of the principal maxima on the ionization curves of compounds obtained during the second synthesis we could follow the change in the hillebrandite and calcium hydroxide concentrations as a function of the duration of synthesis. This change (Fig. 3) was in full accord with the previously described crystallization and recrystallization of hillebrandite from the solution (with the above noted displacement in time), while at the same time a better quantitative agreement was found between the total hillebrandite and calcium hydroxide concentrations in each solution, particularly if we consider that the operation of the ionization apparatus was not completely reliable and that small amounts of xonotlite and calcium carbonate were formed in the solution; the latter also explains the fact why after four and even more days (during the repeated synthesis) there still remained a small quantity of free calcium hydroxide.

The results obtained make it possible to divide the entire hillebrandite crystallization process under hydrothermal conditions into three stages:

1. A rapid precipitation of the bulk of coalescent needle-shaped hillebrandite crystals from the saturated silicic acid and lime solution. The segments of crystals adhering to each other should have a distorted crystal lattice.

2. As the solution becomes impoverished with respect to the starting materials, the distorted, thermodynamically unstable, segments of hillebrandite crystals begin to dissolve, i.e., the points at which crystals are joined go first. The crystal aggregates break up into individual, still continuing to dissolve, crystals.

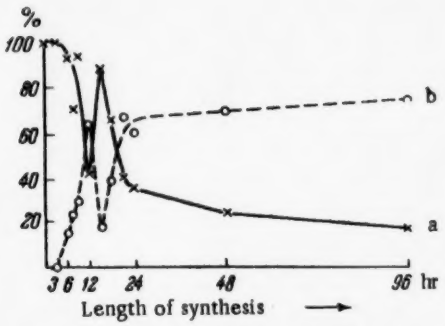

Fig. 3. Curves showing the change in the amount of free calcium hydroxide a) and hillebrandite b) in the samples as a function of length of synthesis.

3. New hillebrandite crystals grow with the correct lattice, i.e., the hillebrandite is being recrystallized through the solution. This recrystallization takes place even before all the original crystals had completely dissolved; nevertheless the solution proceeds much faster than the growth of new crystals, which only assume the almost final brick-shaped form after a 1 to 4-day synthesis, after which a mass conversion into the fibrous form ensues.

Our observations concerning the rapid growth and solution of hillebrandite with a thermodynamically unstable structure and the subsequent crystallization of correct crystals is in complete agreement with the results obtained by P. A. Rebinder and co-workers [1], who observed a similar recrystallization of anhydrous calcium sulfate through the solution which fills up the pores of plaster stone during humid storage. The possibility of recrystallization in hydrated calcium silicates, which constitute the bulk of portland cement pastes (among them also hillebrandite), was also pointed out by Bernal [2], who attached a great importance to the study of these processes as a means of explaining the solidification and setting of cement.

LITERATURE CITED

[1] E. E. Segalova, V. N. Izmailova, and P. A. Rebinder, Proc. Acad. Aci., USSR 110, 5, 808 (1956); 114, 3, 593 (1957)*; P. A. Rebinder, Bull. Acad. Sci. USSR, Div. Chem. Sci., No. 11, 1284 (1957).*

[2] J. D. Bernal, Proc. 3-d Internat. Symposium on the Chemistry of Cement, No. 9, 216 (London, 1952).

Received August 21, 1958

* Original Russian pagination. See C. B. translation.

THE STABILITY OF THE PASSIVE STATE IN METALS UNDER MECHANICAL STRESS

N. D. Tomashov and N. I. Isaev

Institute of Physical Chemistry of the Academy of Sciences, USSR

(Presented by Academician P. A. Rebinder, February 11, 1959)

Although the fact that deformation will change the electrode potential of a metal has been known for a long time [1, 2], until very recently the problems associated with the effects of mechanical stress on electrode potential have received very little attention. According to the information found in the literature, mechanical stresses usually displace the electrode potentials of metals in the negative direction [3-6]. It is evident that the principal factors responsible for the change in potential under tensile stress may be either the increased internal energy of the metal, or the disturbed continuity in the oxide film on the metal. The amount of displacement in the electrode potential of the metal (ΔE, in volts) caused by increased internal energy resulting from the deformation work can in a general case be determined from the equation

$$\Delta E = \Delta F/n \cdot 23066, \tag{1}$$

where ΔF is the free energy change in the metal (in cal/g-atom), $\underline{n}$ the valence of the metal. In a special case where the heat of deformation is small compared to the total deformation work the change in electrode potential can be calculated from the equation [3]

$$\Delta E = -1{,}1\sigma^2 v/2n\varepsilon\Phi, \tag{2}$$

where σ is the mechanical stress (kg/mm^2), $\underline{v}$ the atomic volume of the metal (cm^3), ϵ Young's modulus (kg/mm^2), Φ Faraday's constant (coulombs).

As a rule the changes in the electrode potential of a metal caused by increased internal energy are small and do not exceed 3-5 mv [7, 8]. Thus, for example, according to thermal analysis data [9, 10] the free energy in highly pure copper strongly deformed by rolling (80% reduction in area) increased by only 0.007-0.01 cal/g, which according to Formula (1) is equivalent to a 0.01 mv shift in the negative direction. For stainless steel of grade 1kh18N9T the change in potential (calculated) from Formula (2) under a tensile stress σ = 65 kg/mm^2 constitutes only 0.035 mv [6].

Experimentally determined changes in the electrode potential under mechanical stress are much larger, and depending on the medium and the processing of metal surface may constitute tens or even hundreds of millivolts. This provides a reason for maintaining that the decreased electrode potential in metals under mechanical stress is due mainly to the deformation which disrupts the oxide coating.

The state of the oxide film (its chemical composition, structure, compactness, etc.) constitutes frequently the main factor responsible for the active and passive states of metals. In this connection it was interesting to study the effects of mechanical stresses on the passive state of metals. What made it even more important was the fact the literature contains no information with regard to this problem.

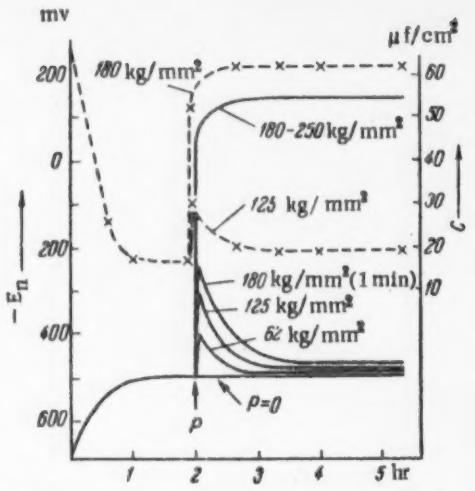

Fig. 1. Time change of the potential (solid lines) and capacitance (dotted line) of prepassivated carbon steel in N $NaNO_3$. At point P we applied the indicated stress to the samples.

The experiments were carried out on wire samples made of either carbon steel (0.75% carbon considerably strengthened by cold working), or of stainless steel of type 3Kh13 (0.25% carbon, 12.8% chromium). The mechanical characteristics of our carbon steel were: tensile strength σ_B = 260 kg/mm², the proportionality limit σ_s = 190 kg/mm². For stainless steel we had σ_B = 70 kg/mm², σ_s = 42 kg/mm². We used 1 N $NaNO_3$ and 0.01 N $K_2Cr_2O_7$ as corrosive media. These solutions have the specific property that in them previously passivated steels do not become reactivated while unpassivated ones remain active. The necessary stresses were produced by means of a swing-type tearing machine. The stress was increased at the rate of 20 kg/sec.

Carbon steel which was rendered passive by being kept for 4 days in 0.1 N $KMnO_4$ nad a +500 mv equilibrium potential in 1 N $NaNO_3$, the same potential on unpassivated steel was -120mv*. The effects of a steady tensile stress on the passive state of prepassivated steel will depend on the magnitude of the stress. The results shown in Fig. 1 indicate that stresses which produce elastic deformation in the metal (in our case up to 125 kg/mm²) induce a partial and temporary activation followed by a gradual passivation until the initial state is attained. At the same time, the greater the stress the more pronounced the activation and the longer it takes for a return to the passive state.

Stresses which caused plastic deformation and those which were close to the proportionality limit resulted in a complete reactivation of the metal. The potential in this case was displaced 600 mv in the negative direction. The passive state did not return and the potential leveled off at the equilibrium value for nonpassive steel.

The above noted phenomena can be explained by the fact that under the action of tensile stress cracks appear in the oxide film exposing portions of the activated (anodic) metal surface; this is confirmed by the greatly increased capacitance of the electrical double layer (see Fig. 1). Under stresses which produce elastic deformation in the metal the area of these newly formed anodic zones is small. With a 125 kg/mm² stress the capacitance increased by 12 μ f/cm², which corresponds to a 60% increase (over the initial value) in the activated metal surface. The pores are rapidly rendered passive on account of microcouples such as film-pore. This returns the metal to the state of passivity. Under stresses producing plastic deformation in the metal the area of anodic zones increases abruptly, which is attested by the much larger increase in the electric double layer at the electrode. For example, under a 180 kg/mm² stress ΔC = 42 μ f/cm² (Fig. 1), which corresponds to a 200% increase in the activated surface. Evidently the current densities established under these conditions are inadequate to render the pores passive, and the metal remains entirely in the activated state.

An oscillographic record showed that most of the gradual debasement of the potential occurred not at the time when the stress was being applied (8-10 sec), but after the metal was already under a static load. Evidently the debasement of the potential during this time is due to the fact that the oxide film, which is under a simultaneous action of high mechanical stress and of a corrosive medium, undergoes intensive cracking.

It has been experimentally demonstrated that the time for a complete debasement of a metal potential depends on the magnitude of the mechanical stress and lies in the range from 1.5-3 min. In connection with this, it was interesting to examine the changes in the potential of prepassivated carbon steel under brief (1 minute) stresses. In this series of experiments the sample was dynamically strained to the desired stress, kept under this (already static) stress for 1 minute, and then relieved of the stress.

The results obtained indicate that a temporary stress close to the proportionality limit has a somewhat different effect on the subsequent changes in the potential. Whereas a steady 180 kg/mm² stress removes the

* Potentials are given with reference to a standard hydrogen electrode.

passivity from the metal irreversibly, the same stress applied for just 1 minute only partially displaces the potential in the negative direction (ΔE = 200 mv), after which the metal becomes spontaneously passive and its potential acquires a value close to the initial. But if the magnitude of the brief stress is such as to produce plastic deformation in the metal, the potential becomes irreversibly displaced into the activated state. No return to passivity is observed in this case.

The above noted phenomena can be explained by the fact that when elastic stress is relieved, the deformed metal returns to its initial state, and consequently most of the cracks formed in the oxide film under tension become sealed (close up). The total area of anodic zones sharply decreases, creating conditions favorable for passivation. When the stress is removed from a plastically deformed sample, the fraction of the active metal closing up will be less, due to some residual deformation in the metal. Consequently the probability of a spontaneous return to passivity will also be reduced.

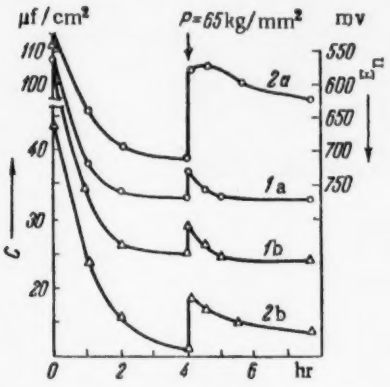

Fig. 2. Change of the electrode potential a) and capacitance b) with time on prepassivated steel. 1) In 1 N $NaNO_3$; 2) in 0.1 N Na_2SO_4. The load was applied at point P.

If, however, the duration of static stress should exceed 1.5 min, the effect observed will be similar to that taking place under a constant stress.

The increased tendency of stainless steel toward passivity changes radically (in comparison with carbon steel) its behavior in the extended state. Whereas prepassivated carbon steel becomes quickly reactivated under stresses resulting in plastic deformation, prepassivated stainless steel will remain passive under any tensile stress.

The equilibrium potential of air-oxidized steel of type 3Kh13 in 1 N $NaNO_3$ is +225 mv. A preliminary passivation shifts the equilibrium potential of this steel to +760 mv. However, as one can see in Fig. 2, even very large mechanical stresses (close to the tensile strength) fail to reactivate the steel to any significant extent (30 mv only), and the potential soon spontaneously reverts to the initial passive equilibrium value. The capacitance also changes only very slightly under the stress (ΔC = 4.5 $\mu f/cm^2$).

It has been shown that in more corrosive media the effects of mechanical stresses on stainless steel are more pronounced. Yet even under these conditions and the maximum permissible stresses the steel could not be reactivated to the original level of the unpassivated metal. Thus, for example, the equilibrium potential on unpassivated steel of type 3Kh13 in 0.1 Na_2SO_4 was +200 mv while on passivated steel it was +700 mv (see Fig. 2). Though under these conditions the effects of tensile stress were more noticeable (under a 65 kg/mm² stress ΔE = 120 mv, ΔC = 6.5 $\mu f/cm^2$), the metal did not revert to the fully unpassivated state of steel.

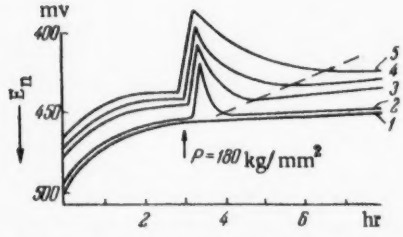

Fig. 3. The effect of mechanical stress (P) on the time change of the electrode potential of carbon steel in $K_2Cr_2O_7$ solutions. 1) P = 0.1 N solution; 2) P = 125 kg/mm² 1 N solution; 3) P = 125 kg/mm², 0.1 N solution; 4) P = 125 kg/mm², 0.01 N solution; 5) P = 125 kg/mm², 0.00 N solution.

Since in oxidizing solutions ($K_2Cr_2O_7$, $KMnO_4$, et al.,) unprepassivated stainless and carbon steels are both in a stable passive state, they display fundamentally the same properties. In the beginning there is a slight activation which is soon followed by a spontaneous return to the initial (or close to the initial) passive state. In Fig. 3 we have plotted a series of typical curves which show that as the concentration of the oxidizing agent decreases the displacement of the potential in the negative direction increases, although the stress is kept constant. Besides this, with decreasing concentration of the oxidizing agent the time needed for the return to the passive state appreciably increases.

All this can be explained in the following manner. At first, after the stress had just been applied, there are two factors exerting their influence simultaneously on the metal – the mechanical stress, which deforms the metal and creates favorable conditions for reactivation, and the oxidizing agent, which hinders the reactivation of

the metal. Consequently, at this stage under a similar stress the higher the concentration of the oxidizing agent the more intense will its passivating action be and therefore the less will the potential be displaced in the negative direction. In the second stage the deformation of the oxide film ceases and the passivating strength of the solution will be the principal factor determining the subsequent variations in the potential. Hence, the greater the passivating strength of the solution the faster will the potential be displaced back in the positive direction. And essentially such correlations were also found in other oxidizing media (for example, in $KMnO_4$ solutions).

LITERATURE CITED

[1] Wiedeman, Lehre von Electrizitat 9, 723 (1893).

[2] T. W. Richards and G. E. Behr, Zs. f. phys. Chem. 58, 301 (1907).

[3] M. E. Zaretskii, J. Appl. Chem. 24, No. 6 (1951).*

[4] A. V. Ryabchenkov, The Resistance of Steel to Corrosion Fatigue (Moscow, 1953).**

[5] H. L. Logan, J. Res. Nat. Bur. Stand. 48, 2, 99 (1952).

[6] A. V. Ryabchenkov and V. M. Nikiforova, Metallography and Processing of Metals, 8, 2 (1956).

[7] L. V. Nikitin, Proc. Acad. Sci. USSR 17, 3 (1937).

[8] L. V. Nikitin, J. Gen. Chem., 9, 9 (1939).

[9] R. Jouty, C. r. 237, No. 9, 488 (1953).

[10] G. V. Akimov and N. D. Tomashov, J. Tech. Phys. 6, No. 1, 115 (1936).

Received January 29, 1959

* See C. B. Translation.

** In Russian

THE MECHANISM OF DEGENERATE BRANCHING IN THE VAPOR-PHASE OXIDATION OF CYCLOHEXANE IN A STEEL VESSEL

I. V. Berezin, N. F. Kazanskaya and V. F. Privalov

M. V. Lomonosov State University, Moscow

(Presented by Academician N. N. Semenov, January 29, 1959)

The oxidation of cyclohexane in the liquid phase belongs to the class of chain reactions with degenerate branching [1]. Up to the present time, however, it has not been shown sufficiently clearly which of the intermediate products of the oxidation of the cyclohexane takes part in the degenerate branching reaction; the mechanism of the process is also not clear. By analogy with the liquid-phase oxidation of other hydrocarbons it might be suggested that the intermediate product in question is cyclohexyl hydroperoxide. This suggestion is supported by the fact that the addition of cyclohexyl hydroperoxide accelerates the oxidation of cyclohexane. It is still not clear whether the acceleration is caused by the radical breakdown of the cyclohexyl hydroperoxide itself or whether it is related to the formation of cyclohexanone hydroperoxide in the decomposition process, since the latter compound also exhibits a powerful accelerating effect [1].

In the present work this question was examined by studying the process of cyclohexanone oxidation in a medium of cyclohexane also undergoing oxidation. Since cyclohexanone is continuously produced and used up during the reaction, a labeled atom method was used, as in earlier experiments [2].

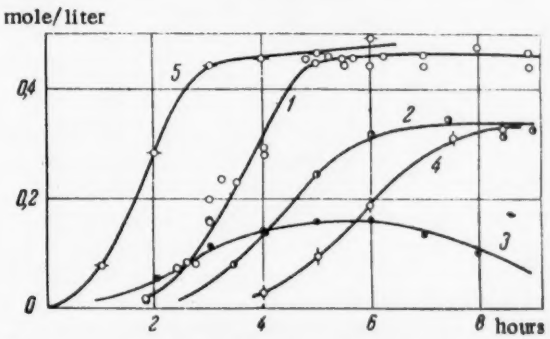

Fig. 1. Kinetic curves for the products of the oxidation of cyclohexane in a steel vessel: 1) at 150°, cyclohexanone; 2) at 150°, cyclohexanol; 3) at 150°, cyclohexyl hydroperoxide; 4) at 142°, cyclohexanone; 5) at 157°, cyclohexanone.

The oxidation of the cyclohexane, purified from aromatic hydrocarbons [3] and methylcyclopentane [4], was carried out using air at a pressure of 10 atmospheres and temperatures of 142, 150 and 157° in a steel vessel.

TABLE 1

Values of $k = W_{labeled}/C_{labeled}C_t$ at Various Temperatures and Degrees of Oxidation

Temp. °C	Time after addition, min													Mean value of k
	0	7,5	15	30	45	60	90	120	150	180	240	240	270	
142	1,42	—	—	1,29	—	1,21	—	1,47	1,33	1,12	1,10	1,21	1,20	1,22±0,2
150	1,80	—	1,70	1,66	—	1,79	1,93	1,89	1,54	—	—	—	—	1,72±0,2
157	3,79	3,83	3,48	3,45	2,76	3,14	3,09	3,13	0,77	—	—	—	—	3,34±0,28*

* The mean value of k was calculated from the oxidation data up to 90 minutes, since beyond this time at 157° tar formation takes place and the reaction kinetics are distorted.

The systems were analyzed quantitatively for cyclohexyl hydroperoxide, cyclohexanone and cyclohexanol [2]. The kinetic curves for the oxidation products at 150° and for cyclohexanone at various temperatures are given in Fig. 1. The rate of oxidation of these samples of cyclohexane was found to be slightly lower than that of the specimens used earlier [6], apparently as a result of more efficient purification in the present instance.

After a certain time interval had elapsed (5 hours at 142°, 2.5 hours at 150° and 1.5 hours at 157°), cyclohexanone labeled with radiocarbon in the carbonyl group [5] was introduced into the cyclohexane undergoing oxidation. The quantity of labeled cyclohexanone added amounted to 5% of the cyclohexanone content of the oxidation products at that moment of time. As in previous experiments, the technique of "averaging" the oxidation mixture was adopted in order to increase the reproducibility of the experiments [6]. After the addition of the radioactive cyclohexanone, samples of oxidized cyclohexane were removed; the cyclohexanone in the samples was isolated as the 2,4-dinitrophenylhydrazone and its specific activity α_t determined. The results of the radiochemical analyses were used to calculate the concentration of labeled cyclohexanone [7].

$$C_{labeled} = C_t \alpha_t/\alpha_0,$$

where α_0 is the specific activity of the cyclohexanone at the initial moment of time after introduction of the radioactive sample, α_t is the specific activity of the cyclohexanone at time t and C_t is the concentration of cyclohexanone at time t.

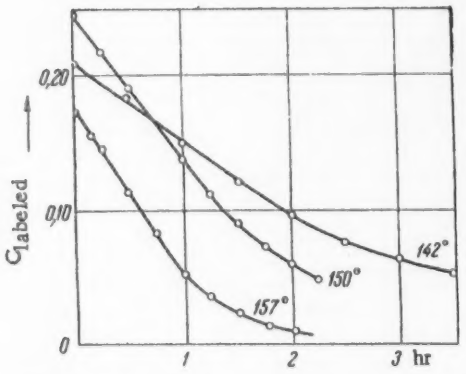

Fig. 2. Fall in concentration of "labeled" cyclohexanone during oxidation at various temperatures.

Figure 2 gives the kinetic curves for the oxidation of labeled cyclohexanone. When the curves are examined, attention is drawn to the fact that the rate of oxidation of the labeled cyclohexanone remains constant over an appreciable time interval. This may be due to the accelerating influence of the cyclohexanone, whose total concentration increases as the reaction proceeds (Fig. 1), on the oxidation process. In this case the rate of oxidation of the labeled cyclohexanone should be proportional not only to its concentration ($C_{labeled}$) but also to the total ketone concentration. If the relationship to the total concentration of cyclohexanone is of the first order, then the rate of oxidation of the labeled cyclohexanone is equal to

$$W_{labeled} = k C_{labeled} C_t, \qquad (1)$$

and k should be constant throughout the reaction. The values of k at different moments of time for various temperatures are given in Table 1.

Since $W_{labeled}/C_{labeled} = W_t/C_t$, i.e., the rate of oxidation of all the cyclohexanone is proportional to its concentration irrespective of the order of the reaction, then, taking Equation (1) into account, we have:

$$W_i = kC_i^2, \qquad (2)$$

i.e., the oxidation of cyclohexanone in a medium of cyclohexane undergoing oxidation is formally described by the equation for a reaction of the second order.

Let us examine how this kinetic relationship can be explained on the assumption that the major fraction of the degenerate branching in the oxidation of cyclohexane involves cyclohexanone.

In a medium of cyclohexane undergoing oxidation, cyclohexanone molecules are attacked by the free cyclohexyl peroxide radicals carrying the oxidation chain. This leads to removal of the hydrogen atoms in the α-position relative to the ketone group:

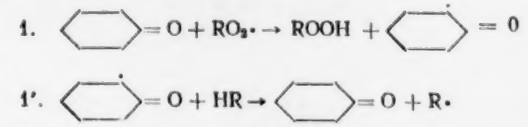

The ketoradical produced undergoes a number of rapid changes to form the α-ketohydroperoxide, which decomposes readily, as Pritzkow [8] has shown, to form the hemialdehyde of adipic acid:

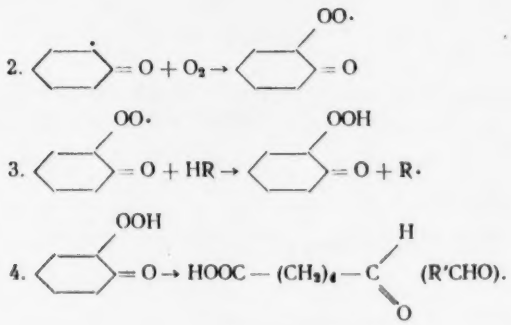

The hemialdehyde of adipic acid, like all aldehydes, is extremely readily oxidized to form the acyl hydroperoxide, which decomposes rapidly with the formation of two new radicals:

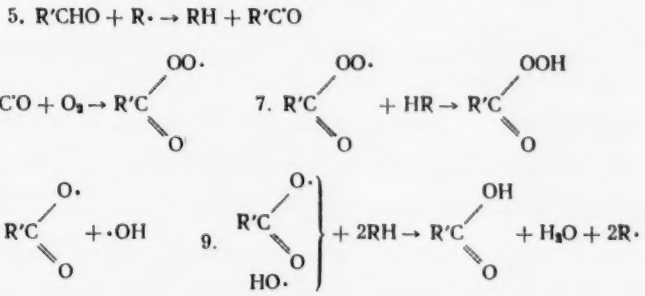

The sequence of reactions 1-9 takes place so rapidly that no measurable quantities of cyclohexanone hydroperoxide, hemidaldehyde orperoxyadipic acid can be detected [9]. On the other hand it can be seen that as a result of these reactions we obtain, in place of the one ROO· radical used up, three new radicals R·, which combine with oxygen:

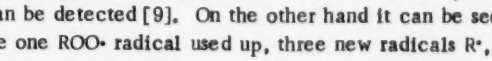

11. $2RO_2 \rightarrow$ breakage of the chain.

Since the rate of initial production of free radicals once the reaction has developed may be neglected by comparison with the rate of production as a result of branching, the latter may be taken as equal to the rate of chain breakage. If there are no side reactions leading to the consumption of ketohydroperoxide and peroxyadipic acid molecules, then the rate of branching should be equal to the rate of oxidation of the cyclohexanone and is determined by the rate of Reaction (2), which is practically irreversible:

$$W_{branching} = W_t = k_2 [C_6H_9O] [O_2]. \quad (3)$$

In the general case, as a result of side reactions, the rate of branching is less than the rate of oxidation of the cyclohexanone. Assuming that $W_{branching} = \delta W_t$, where $\delta < 1$, and using the method of stationary concentrations, we obtain the following expression for the rate of oxidation of cyclohexanone:

$$W_t = \frac{\delta k_1^2 k_2^2}{k_{11}} \cdot \frac{[C_6H_{10}O]^2 [O_2]^2}{(k_1' [RH] + k_2 [O_2])^2}. \quad (4)$$

It can be seen that the scheme outlined gives a second order expression for the rate of oxidation of cyclohexanone, which is in accrodance with the experimental data. The Expression (4) also gives the relationship between the rate and the oxygen concentration. It is known that this relationship is limiting in character [10] and the limit lies at approximately 1 atmosphere. At low partial pressures of oxygen $k_2 [O_2] \ll k_1 [HR]$ and W_t will be proportional to $[O_2]^2$. At high oxygen concentrations we have

$$W_{Ok} \approx \frac{\delta k_1^2}{k_{11}} [C_6H_{10}O]^2. \quad (5)$$

In our experiments the partial pressure of oxygen is equal to approximately 4 atmospheres and we apparently have a case where the rate of oxidation is independent of the oxygen concentration.

If considerations similar to the above are applied to the rate of oxidation of the labeled cyclohexanone, then for high oxygen pressures we have:

$$W_{labeled} = (\delta k_1^2 / k_{11}) [C_6H_{10}O]_{labeled} \cdot [C_6H_{10}O] = (\delta k_1^2 / k_{11}) C_{labeled} C_t,$$

which is the same as (1).

From this we have $k = \delta k_1^2 / k_{11}$. Since the constant for recombination of the radicals, as a rule, is independent of temperature ($E_{11} \approx 0$), the change of k with change in temperature is almost completely determined by the activation energy of Reaction (1), while $E = 2E_1$. According to our data $E = 24$ kcal/mole, from which $E_1 = 12$ kcal/mole. The low value for this activation energy is in complete accordance with the nature of the elementary reaction (1).

LITERATURE CITED

[1] I. V. Berezin, E. T. Denisov, and N. M. Émanuél', Coll. Problems of Chemical Kinetics, Catalysis and Reactivity, Izd. AN SSSR, 273 (1955).*

[2] I. V. Berezin and B. G. Dzantiev et al., Zhur. Fiz. Khim. 31, 554 (1957).

[3] Yu. K. Yur'ev, Practical Organic Chemistry, vol. 2, Izd. MGU (1957).*

[4] Leithe, Anal. Chem. 23, 423 (1951).

[5] I. V. Berezin, L. S. Vartanyan, and N. F. Kazanskaya, Vestn. MGU, ser. khim. nauk, No. 2, 61 (1956).

[6] I. V. Berezin and N. F. Kazanskaya, Doklady Akad. Nauk SSSR 126, No. 3 (1959).**

[7] I. V. Berezin, L. S. Vartanyan, B. G. Dzantiev, N. F. Kazanskaya, and N. M. Émanuél', Zhur. Fiz. Khim. 31, 340 (1957).

[8] W. Pritzkow, Chem. Ber. 87, 1668 (1954).

* In Russian.

** See C. B. translation.

[9] I. V. Berezin and E. T. Denisov, Doklady Akad. Nauk 565 R 97, No. 2, 273 (1954).

[10] D. G. Knorre, Z. K. Maizus et al., Usp. Khim. 26, No. 4, 416 (1957).

Received January 27, 1959

THE THERMAL DECOMPOSITION OF EXPLOSIVES BELOW THE MELTING POINT

G. B. Manelis and F. I. Dubovitskii

Institute of Chemical Physics, Academy of Sciences, USSR

(Presented by Academician V. N. Kondrat'ev, January 16, 1959)

Farmer [1] has shown, in a study of the thermal decomposition of tetryl below the melting point, that the condensed products of the decomposition dissolve the tetryl. Later on, Hinshelwood [2] carried out a mathematical analysis of the decomposition reaction, taking into account the formation of the liquid phase in the process. In the derivation of the equation, however, Hinshelwood made two contradictory assumptions. Thus in the calculation of the ratio of solid to liquid phase in the decomposition process, he assumed (in accordance with Raoult's law) that at constant temperature the quantity of substances in the liquid phase, in equilibrium with the solid, was constant. At the same time, in the calculation of the concentration of catalyst in the liquid phase, Hinshelwood assumed it to be proportional to the degree of conversion.

Much later, Bawn [3] examined the decomposition of organic explosives involving "partial liquefaction" during the reaction for the simplest case of two monomolecular reactions.

In the present work we examine various examples of the decomposition of solid explosives, taking account of the formation of the liquid phase. It is subsequently assumed throughout that the original explosive substance dissolves in the reaction products and that thermodynamic equilibrium between the solid and liquid phases has time to become established. The ratio of the concentrations of the original substance C_{B_l} (l = liquid) and reaction products C_{A_l} in the liquid phase $\alpha = C_{B_l}/C_{A_l} = B_l/A_l$ is constant at constant temperature and is independent of the degree of conversion up to the moment when the solid phase disappears.

The degree of conversion η is equal to $(B_0 - B)/B_0 = A/A_0$.

If the density of the reaction products differs little from that of the original substances, we may write $A_0 = B_0(1 - \mu)$, where $\mu = v_{\text{init}} - v_{\text{final}}/v_{\text{init}}$ (the extent of the volume change after complete decomposition); B_0 is the original quantity of explosive, A_0 the total quantity of condensed reaction products. The quantity of substance B in the solid phase $B_s = B - B_l$.

Up to the moment of complete dissolution, $A = B_0(1 - \mu)\eta$; $B_l = B_0 a (1 - \mu)\eta$.

If the decomposition takes place according to an equation of the 1st order in the solid and liquid phases, then the over-all rate is given by the expression where v_s and v_l are the volumes of the solid and liquid phases respectively.

$$-\frac{dB}{dt} = \frac{1}{1-\mu}\frac{dA}{dt} = k_1 C_{B_s} v_s + k_2 C_{B_l} v_l = k_1 B_s + k_2 B_l$$

The relationship between the rate of reaction and the degree of conversion is given by the expression:

$$\frac{d\eta}{dt} = k_1(1-\eta) - k_1 a(1-\mu)\eta + k_2 a(1-\mu)\eta =$$

$$= k_1 + [a(1-\mu)(k_2 - k_1) - k_1]\eta. \qquad (1)$$

Putting $a(1-\mu)(k_2 - k_1) - k_1 = k_m$, we have

$$\frac{d\eta}{dt} = k_1 + k_m \eta. \qquad (1a)$$

When $a(1-\mu)(k_2-k_1) > k_1$ and $k_2 > k_1$, the over-all rate of reaction will increase with increase in the degree of conversion up to the moment when the original substance has dissolved completely in the reaction products. After the moment at which dissolution is complete, the reaction will proceed in accordance with the usual first order equation

$$\frac{d\eta_1}{dt} = k_2(1-\eta_1).$$

The solid phase disappears at a degree of conversion η'

$$B_s = 0 = B_0(1-\eta_1') - B_0 a(1-\mu)\eta_1', \quad \eta_1' = \frac{1}{a(1-\mu)+1}. \tag{2}$$

At this moment $k_1 + k_m\eta_1' = k_2(1-\eta_1')$.

Equation (1a) gives on integration

$$k_m t = \ln\frac{k_1 + k_m\eta}{k_1}. \tag{3}$$

The kinetic curves calculated from Equation (3) are clearly S-shaped (for values of $a(1-\mu)(k_2-k_1) > k_1$).

The curve showing the relationship between the rate of reaction and the degree of conversion, calculated from Equation (1) and the classical equation for a reaction of the first order, has a characteristic appearance (Fig. 1). The maximum rate is reached in this case at the point where dissolution is complete, at $\eta = \eta'$.

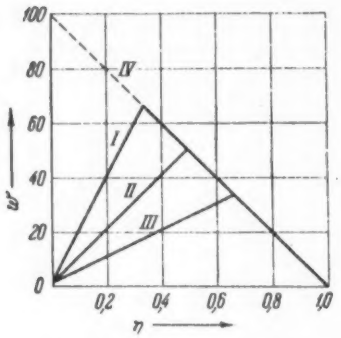

Fig. 1. The relationship between the rate of reaction and the degree of conversion, calculated from Equation (1) for $k_1 = 1$, $k_2 = 100$ and $\mu = 0.9$. The parameter a is equal to 20 for I, 10 for II and 5 for III. The straight line IV is drawn from the equation for a first order reaction.

In the case where the condensed reaction products can act as catalysts, the expression for the over-all rate of reaction must be written in the following form:

$$-\frac{dB}{dt} = \frac{1}{1-\mu}\frac{dA}{dt} =$$
$$= k_1 C_{B_s} v_s + k_2 C_{B1} v_1 + k_3 C_{B1} C_{A1} v_1 =$$
$$= k_1 B_1 + k_2 B_1 + k_3 B_1 C_{A_1};$$

where C_{A_1} is the concentration of catalyst in the liquid phase; $C_{A_1} = \alpha A/v_1$; and α is the fraction of catalyst in the condensed reaction products;

$$v_1 = B_1 + A = A(1+a), \quad C_{A_1} = \frac{\alpha}{1+a}.$$

The rate of reaction up to the point of complete dissolution in the case of catalysis by the condensed reaction products will be determined by the expression

$$\frac{d\eta}{dt} = k_1 + \left[k_2 a(1-\mu) + \frac{k_3\alpha(1-\mu)a}{1+a} - k_1 a(1-\mu) - k_1\right]\eta,$$
$$k_2 a(1-\mu) + \frac{k_3\alpha(1-\mu)a}{1+a} - k_1 a(1-\mu) - k_1 = k_m'; \tag{4}$$

where k_m' is a quantity dependent only on the temperature and is constant when the decomposition takes place with t = const. In the case of catalysis by the condensed reaction products, therefore, we again obtain an expression analogous to Equation (1) for reactions taking place according to the law of the first order:

$$\frac{d\eta_1}{dt} = k_1 + k_m'\eta. \tag{4a}$$

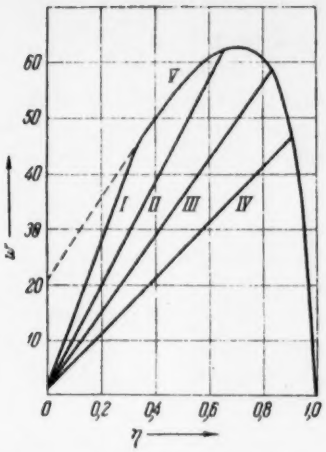

Fig. 2. Relationship between the rate of reaction and the degree of conversion, calculated from Equation (4) for $k_1 = 1$, $k_2 = 20$, $k_3 = 100$ and $\mu = 0.9$. The parameter a is equal to 20 for I, 5 for II, 2 for III and 1 for IV. The curve V is drawn from Equation (5) for reaction in the liquid phase.

Equation (4a) differs from (1a) only in the value of k_m.

After the moment of complete dissolution, which also takes place at $\eta' = 1/a(1-\mu) + 1$, the decomposition process is governed by the equation obtained earlier [4] for the autocatalytic decomposition of liquid explosives when the volume of the condensed phase is variable:

$$\frac{d\eta}{dt} = k_2(1-\eta) + k_3\alpha(1-\mu)\frac{\eta(1-\eta)}{1-\mu\eta}. \qquad (5)$$

The relationship between the rate of reaction and the degree of conversion, calculated from the Equations (4) and (5), is given in Fig. 2. The Figure shows that the maximum rate of reaction may lie at the point of complete dissolution of the original substance or later, when the reaction is taking place in the absence of any solid phase.

A feature of considerable interest is the effect of additives, including chemically inert materials, which are able to increase the rate of decomposition of the explosive by converting part of it to the liquid phase (in the case where the eutectic temperature of the system formed by the original explosive and the inert additive lies below the temperature of the experiment). The rate of decomposition in this case also will be equal to the sum of the rates in the solid and liquid phases (monomolecular reactions take place in the solid and liquid phases)

$$W = k_1 C_{B_s} v_s + k_2 C_{B_l} v_l = k_1 B_s + k_2 B_s,$$

where T is the inert additive;

$$v_l = A + B_l + T, \quad A = B_0(1-\mu)\eta,$$

$$B_l = B_0(1-\mu)a\eta + Ta, \quad B_s = B_0 - B_0\eta - B_0(1-\mu)a\eta - Ta,$$

where $a = B_l/A + T$ (the solubility of the substance B in T and in mixtures A + T is constant).

The relationship between the rate of reaction and the degree of conversion may be written:

$$\frac{d\eta}{dt} = k_1 + (k_2 - k_1)\frac{T}{B_0}a + \underbrace{[(1-\mu)a(k_2-k_1) - k_1]}_{k_m}\eta. \qquad (6)$$

In this case also, therefore, the rate of decomposition is directly proportional to the degree of conversion up to the moment of complete dissolution, after which it decreases according to the first order law, while the initial rate is directly proportional to the amount of additive or impurity and the solubility of original explosive in it (Fig. 3).

In the case where the solubility of the explosive in the inert additive differs from its solubility in the reaction products, the appropriate expression for the relationship between the solubility and the composition of the system can be readily obtained and used in the derivation of Equation (6).

At the point where the original substance dissolves completely in the reaction products, the solid phase disappears and the law governing the course of the reaction changes. For ideal systems

$$\ln N = -\frac{\lambda(T_m - T)}{RT_m T},$$

where N is the mole fraction of the dissolved substance; λ is the heat of fusion; T_m is the melting point and T is the temperature of the experiment. From Equation (2), therefore, the degree of conversion at which complete dissolution takes place decreases with increase in the temperature according to the law

$$\eta' = \frac{1-N}{1-\mu N} = \frac{1-\exp\left(-\frac{\lambda(T_m - T)}{RT_m T}\right)}{1-\mu\exp\left(-\frac{\lambda(T_m - T)}{RT_m T}\right)}$$

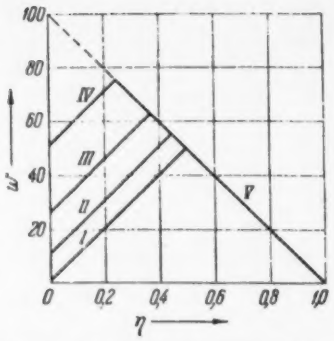

Fig. 3. Relationship between the rate of reaction and the degree of conversion, calculated from Equation (6) for $k_1 = 1$, $k_2 = 100$, $\mu = 0.9$ and $a = 10$. The ratio T/B_0 is equal to 0, 0.01, 0.025 and 0.050 for the straight lines I, II, III, and IV respectively. The straight line V is drawn from the equation for a first order reaction.

Assuming that thermodynamic equilibrium is established between the solid and liquid phases in the system formed by a decomposing explosive and its reaction products, therefore, we may obtain equations describing most of the phenomena observed in the thermal decomposition of an explosive at a temperature t below the melting point.

It should be noted that in real systems more complex cases may be observed, as a result of the complexity of the mechanism by which the chemical reaction of decomposition takes place. It is however, always necessary to take into consideration the possibility of progressive dissolution of the original explosive in the reaction products, with a corresponding change in the kinetic laws governing the reaction.

LITERATURE CITED

[1] J. Farmer, J. Chem. Soc. 117, 1603 (1920).

[2] C. N. Hinshelwood, J. Chem. Soc. 119, 721 (1921).

[3] C. E. Bawn, Chemistry of the Solid State, London, p. 254 (1955).

[4] F. I. Dubovitskii, G. B. Manelis, and A. G. Merzhanov, Doklady Akad. Nauk. SSSR 121, 668 (1958).

Received December 29, 1958

KINETICS OF SEMICONDUCTOR CATALYSTS UNDER CHEMISORPTION CONTROL

Corresponding Member Acad. Sci. USSR, S. Z. Roginskii

Many experiments done in recent years have confirmed the important role played by electronic factors in catalysis and the existence of some rather unusual electronic mechanisms in oxidation-reduction reactions on semiconductors. However, within the framework of current ideas it was impossible to explain several phenomena observed in the kinetics of these reactions without running into some serious contradictions. This made it desirable to examine the latter without the arbitrary assumption that there is some extrinsic conductance in all these catalysts, and that the holes and electrons are the only free charge carriers in chemisorption and catalysis.

We will further assume that:

1) Semiconductors used as catalysts can exhibit during the reaction intrinsic, degenerate, and extrinsic conductance of both the excess, N-type, and defect, P-type [1, 2] conductance.

2) The elementary process in the catalysis will mainly involve normal sections of the lattice, impurities in it, structural defects, and charge carriers. In a zone model this would correspond to a participation (in the catalysis) of the following: a) bound electrons in higher levels of the valence zone (Val); b) holes ; c) unbound levels (L) at the bottom of the conductance zone and d) its free electrons ; e) donor d) and acceptor (a) impurity levels in the lattice, as well as d^+ and a^-; f) surface Tamm levels (tm); g) levels of compounds dissolved in the layer adjacent to the surface or absorbed on the surface and having either acceptor or donor properties [1].

3) The bond between the adsorbed molecules and the surface has a partial covalent character and the differences in the energies of levels between which the electron transitions occur during chemisorption constitute only a portion of the total heat of adsorption.

According to the rules of series kinetics the unusual mechanism of semiconductor catalysis could not show up if the kinetics were controlled by diffusion or heat transfer. In the subsequent discussion we will assume kinetic conditions under which these manifestations would be particularly characteristic. The specificity of semiconductor catalysis can manifest itself in the participation of definite structural elements and characteristic semiconductor electron levels and in the localization of the electrons or holes on the adsorbed molecules (A^-, AB^+, etc.) [3]. In order to derive the starting kinetic equations it is necessary to set up expressions for the equilibrium concentration $C^\#$ of the intermediate complex (I_c) in terms of the concentrations of activated centers and of free and adsorbed molecules, as well as to take into account the possibility that the energy of formation of I_c may vary with the fraction of the surface covered due to nonhomogeneity and interactions [4]. At the same time we have to consider additional electron distribution equilibria between various levels and the surface charge which results in the appearance of an additional "diffusion" potential V_D; this potential can be determined from the change of the work function $\Delta\varphi$ and should include a correction for the dipole moment. To preserve the usual form of the law of mass action and other thermodynamic relationships for chemical equilibria, in cases where the reactions are accompanied by electron transitions inside the lattice and on the surface, one simply has to substitute the Gibb's chemical potentials, μ in the starting equations by the electrochemical potential $\eta = \mu + V$ (V is the electric potential) [5]. The equilibrium involving I_c differs from ordinary chemical equilibria in that one of the statistical summations in the entropy coefficient is replaced by integration over the transition path. This makes it possible to extend Schottky's derivation to the equilibrium formation of I_c in the heterogeneous catalysis. Let us examine an irreversible reaction $A + B \rightarrow AB$, which proceeds according to the scheme

$$A \xrightarrow[1]{} A_{chem} \xrightarrow[2]{+B_{gas}} AB_{chem} \xrightarrow[3]{} AB, \tag{I}$$

where anyone of these stages may control the reaction.

Several peculiarities of semiconductor catalysis can already by detected even in the simplest case where the reaction kinetics are controlled by the chemisorption of one of the starting materials, for example A. The composition of I_c will depend on the end product of this step and on the kind of activated centers which participate in the adsorption. Thus, if the end product is A^-_{chem} then A + tm, A + tm^-, A + d, and A + Val are not all equivalent with respect to the kinetic route which leads to this product. For a group of identical i-th zones the rate can be written in the form

$$w_i = -dn_{A_i}/dt = -bd[A]_i/dt = bd[AB]/dt = \nu s K_i^{\#}[X_i][A], \tag{1}$$

where n_A is the number of molecules A inside the solid phase, [A] their concentration, [AB] same for reaction products. The coefficient b includes the surface (s) to volume ratio of the reactor; the frequency ν at which I_c is transformed into completely chemisorbed molecules; $[X_i]$, the concentration of i-th centers contained in I_c; $K_i^{\#}$ the equilibrium constant for I_c obtained from Equation (2a),

$$\begin{aligned} K_i^{\#} &= \exp\left[(RT)^{-1}\left(-F^{\#}_{i(\Delta V=0)} - e\Delta V_i^{\#} \pm e\sum\Delta V\right)\right] = \\ &= \exp\left[(RT)^{-1}(-F_i^{\#})\right] = K_{0i}^{\#} M_v, \end{aligned} \tag{2a}$$

where

$$M_v = \exp\left[(RT)^{-1}\left(e\Delta V_i^{\#} \pm e\sum\Delta V\right)\right]. \tag{2b}$$

Here F^i ($\Delta V = 0$) is the free energy of formation of I_c at $\Delta V = 0$, $\Delta V_i^{\#}$ the electrical surface potential caused by I_c, while $\Sigma\Delta V$ is the same potential but resulting from the complete adsorption of all molecules. The sign of $\Sigma\Delta V$ may be identical or opposite to that of $\Delta V_i^{\#}$. As long as I_c is the only source of the charge $e\Sigma\Delta V = Q$, $e\Delta V_i^{\#}$ will be very small when $\Delta F^{\#} \gg RT$, and hence M_V in Equation (2), which gives the effects of charge on the rate, will be close to one. The charge produced by total chemisorption is one of the factors responsible for the observed self-retardation and the increased activation energy (E). According to our data, cumulative chemisorption is characterized by a linear relationship between $\Delta\varphi$ and Θ, i. e.,

$$e\Delta\varphi \cong \lambda\theta, \tag{3a}$$

while for depletion adsorption, except right at the beginning, we get a logarithmic function [6],

$$e\Delta\varphi \cong \lambda \ln\theta. \tag{3b}$$

Taking $\Delta V = \Delta\varphi$ and substituting the $\Delta\varphi$ obtained in (3a) and (3b) into Eq. (2) we will get:

$$M_v^{\#} \cong e^{-\alpha'\theta} = e^{-\alpha q}; \tag{4a}$$

$$M_v^{\#} \cong 0^{-\alpha'} = \beta q^{-\alpha'}, \tag{4b}$$

where $\alpha' = \lambda/RT$, $\alpha/\alpha' = q_{\sim}$, and $\beta = q^{\alpha'}_{\sim}$. Equation (1) can be rewritten into

$$w_i = \nu s K_{0i}^{\#}[X_i][A]M_v. \tag{1a}$$

When all the coefficients except M_V are constant, Equations (4a) and (4b) correspond to differential equations for the chemisorption and poisoning kinetics on nonhomogeneous surfaces with a uniform and exponential distribution ρ (E) with respect to E [7]. When the reaction is controlled by the chemisorption step, the reactants (B and

AB) and foreign materials (Y and Z) (provided they give the surface the same charge as that of I_c) should influence w_i through M_v according to the same law but with different λ. For all compounds except A, Θ can be the equilibrium as well as nonequilibrium value. In the latter case, if E is a linear function of Q the increase in E (ΔE, dependent on adsorption) can be expressed as a function of P_{eq} [7],

$$\Delta E = -\gamma Q = \gamma RT \ln (P/\pi_0);$$
$$M_v^{\#} = \exp(-eV/RT) = (P/\pi_0)^{-\gamma} = (P/\pi_0)^{-1/n}. \tag{5}$$

When the charges $\Delta\varphi$ induced by A, B, and AB are all of the same sign, terms $[B]^{-1/n_1}$ and $[AB]^{-1/n_2}$ appear in Eq. (1a), while with diverse signs we get $[B]^{1/n_1}$ and $[AB]^{1/n_2}$, despite the absence of B and AB in the intermediate complex. We can similarly get $[Y]^{-1/n_3}$ and Y^{-1/n_4}, etc. This is a specific type of adsorption with positive and negative modifications [7, 8]. It is also possible to get the negative power of the concentration term in Eq. (1a) or uncharged nonhomogeneous surfaces on account of blocking however, positive powers are more specific for compounds not involved in I_c but having accelerating effects on w_1 through ΔV. Equally specific is the mutual compensation of accelerating and retarding actions of compounds with opposite charges. Electronic transitions and boundary charging can also occur between two solid phases, therefore in places where there is adsorption modification one can also expect some microheterogeneous modifications caused by impurities which change the electric surface potential. If the impurities are highly enough dispersed the equations should resemble Eq. (4a) and (4b). With impurities which dissolve in the lattice and change φ (as, for example Me^+ and Me^{+++} introduced into ZnO and NiO [9]) one would normally expect a three dimensional modification, uniform in nature and sign. Some of the facts deduced from surface charging are also applicable to metals.

Let us briefly analyze the kinetic relationships connected with other coefficients of Eq. (1a). $K_{0i}^{\#}$ is a product of the entropy exp ($+ S^{\#}/R$) and enthalpy exp ($-E_0^{\#}/RT$) terms. $S_0^{\#}$ is not very sensitive to the surface change, or to changes in the energy (D) and polarity of bonds. $E_0^{\#}$ is the heat of formation of I_c at 0°K. For a fixed value of D of bonds being broken and formed during the reaction, the more polar the bonds (polarity will depend on the partition of energy between coulombic and exchange integrals) the lower will the equilibrium constant be. Therefore, besides the direct effect of ΔV on $F_i^{\#}$ there should also be some changes in $F_i^{\#}$ caused by the effects of charge on the potential energy surface, since the height of its pass will determine $E_0^{\#}$. Surface charge has an effect on the polarity. When I_c is neutral these effects may be of fundamental importance. Due to tunnel transitions the frequency ν of charged I_c may be different from kT/h and may vary with changes in D. However, in an approximate analysis of fundamental laws we can neglect this effect. $\Delta V = V_D$ represents the potential difference between the surface and the interior of the semiconductor. When the number of tm and other levels created by adsorption is small, the concentrations of charged particles $\oplus$, $\ominus$, d^+, etc., are related to their surface concentrations by ($\pm$ leV_D/RT), where l is the number of charges, and hence we can directly introduce into the kinetic equations the corresponding solid phase concentrations. The latter are connected with each other and with the concentrations of uncharged particles Val, D, A, etc. by a series of dynamic equilibria, which are maintained all the time. Therefore from any one $[X_i]$ we can calculate all the others. By contrast, at high concentrations of tm and with extensively covered surfaces $[X_i]$ becomes insensitive to the conditions inside the semiconductor, and hence one has to analyze directly the surface values of $[X_{i1}]$, $[X_{i2}]$, $X_{i3}]$, which are also interconnected by dynamic equilibria. Quite often all the particles and defects, except $\bigcirc$ and $\oplus$, can be considered stationary, in which case V_D would not have any direct effects on their concentration. Even in the simplest case considered here, where the kinetics are controlled by the chemisorption of A, the insertion of the concentration $[X_i]$ introduces curious corrections into the temperature dependence of w_i. Thus, for $X_i = \ominus$, at relatively low temperatures $[X_i] \simeq [d_0]^{1/2} \cdot \exp(-\Delta U_d/2RT)$, where ΔU_d is the difference between levels L and d. When $\underline{d}$ is excessively ionized the simple exponential relation will be disturbed, and above certain T due to complete ionization we will approach saturation up to $\underline{d}$ with $[X_i] = [d_0] = \text{const}$. Above or before attaining this T, the electrons will begin to be generated according to the scheme $Val \rightarrow Val^+ + \ominus$. This may lead to $[X_i] = [X_i]_{\text{intrinsic}} + d = [X_i]_{\text{intrinsic}} \simeq [Val] \cdot \exp(-\Delta U/2RT)$, where ΔU is the width of the forbidden bond.

On the exponential portions we will have to add $[X_i] = f(T)\Delta U_d/2$ and $\Delta U/2$ to E_{true}, which depends on $E_{0i}^{\#}$ and $\Sigma\Delta V$, while with increasing T we will observe the following sequence: $E_{obs} = E_{true} + \Delta U_d/2$, E_{obs}, $E_{true} + \Delta U/2$, and E_{true} again. Depending on the magnitude of E_{true} and the experimental conditions we will only observe a portion of this general curve. When $\underline{d}$, $\underline{a}$, tm, etc., participate directly in the formation of A_{chem}, $[X_i]$ may decrease the effect of T on $\underline{w}$. The participation of d^-, a^-, tm^-, etc., leads to some very unusual effects

of T on E_{obs}. It can be demonstrated that the above made deductions concerning the effects of surface charge and type of active centers are also applicable to highly nonhomogeneous surfaces, with their fundamental theoretical equations preserved.

LITERATURE CITED

[1] S. Z. Roginskii, Chem. and Chem. Ind. 2, 138 (1957).

[2] O. V. Krylov and S. Z. Roginskii, Proc. Acad. Sci. USSR 118, 526 (1958)*.

[3] F. F. Volkenshtein, J. Phys. Chem. 26, 1463 (1952).

[4] S. Z. Roginskii, J. Phys. Chem. 31, 2381 (1957); 32, 737 (1958).

[5] W. Schottky, Zs. f. phys. 118, 539 (1942); Halbleiter Problem, 1, Braunschweig, S. 139 (1954).

[6] É. Kh. Enikeev, L. Ya. Margolis, and S. Z. Roginskii, Proc. Acad. Sci. USSR 124, 606 (1959).*

[7] S. Z. Roginskii, Adsorption and Catalysis on Nonhomogeneous Surfaces, Izd AN SSSR (1948)**

[8] S. Z. Roginskii, J. Phys. Chem. 21, 1143 (1947); Proc. Acad. Sci. USSR 87, 1013 (1952).

[9] N. P. Keier, S. Z. Roginskii, and I. S. Sazanova, Proc. Acad. Sci. USSR 106, 859 (1956); Bull Acad Sci USSR, Phys. Ser. 21, 183 (1957).

[10] Bardeen, Phys. Rev. 7, 717 (1947).

Received February 4, 1959

* Original Russian pagination. See C. B. translation.

** In Russian.

A METHOD FOR MEASURING THE STATIONARY SURFACE CONCENTRATIONS OF THE COMPONENTS OF A CATALYTIC REACTION

G. D. Sakharov

(Presented by Academician A. D. Sakharov, February 16, 1959)

A method is proposed for the determination of the quantities of the components of a reaction, adsorbed on a catalyst (under stationary reaction conditions); the method is based on measurement of the time necessary for the substances to appear in the outlet from the reaction vessel.

Let us assume that the reaction $A \rightarrow B + C$ takes place in a flow-through apparatus under constant conditions (temperature and molar rate of supply V_0 mole/second) and that at a certain moment of time (taken as the initial moment) we interrupt the supply of substance A and, at the same moment and with the same rate of supply V_0, start the passage of the same starting substance in labeled form (A^*). The reaction $A^* \rightarrow B^* + C$ will then proceed at the same rate through all the separate stages as the reaction $A \rightarrow B + C$. It is evident that as a result of adsorption on the catalyst surface the molecules A^* and B^* will appear in the outlet from the reaction vessel slightly later than if they were not adsorbed, so that the time for which they were retained by the catalyst τ_c depended only on V_0 and the change in volume of the reactants. The rate at which the reaction components appear in the outlet from the reaction vessel can therefore be used to estimate the concentration of these components on the catalyst surface*.

Figure 1 shows the time τ plotted on the x-axis against the quantity of substance A^* leaving the reaction vessel in unit time ($dA^*/d\tau$) plotted on the y-axis. If the process is stationary and if it is possible to neglect the isotopic effect, then it is obvious that the sum of the substances A^* and A leaving the reaction vessel in unit time should be equal to $V_0(1 - y)$, (where y is the fraction of original substance converted to the final products). The quantity $dA^*/d\tau$ evidently becomes equal to $V_0(1 - y)$ only after a certain time interval has elapsed. At first, while the quantity of substance A already adsorbed on the catalyst surface is being desorbed, the amount of A^* leaving the reaction vessel in unit time will be smaller than $V_0(1 - y)$ by a corresponding amount. The shaded area S_1 is numerically equal to the quantity of substance A desorbed unchanged (after time τ). This quantity, however, is still not equal to the stationary quantity of A present on the catalyst at the initial moment, since part of the absorbed substance A is converted on the catalyst to B and C.

The rate of reaction is equal to $V_0 y$ The rate of desorption of unchanged substance A in the outlet from the reaction vessel is equal to the section ab in Fig. 1.

We know that (after a certain fairly large time interval has elapsed) all the molecules of A are removed from the surface. If, however, it is possible to neglect the isotopic effect, then the rate of all the separate stages of the catalytic process, and consequently the ratio of these rates, will remain unchanged as the substance A is gradually replaced on the surface by the substance A^*. The ratio of the number of molecules of A desorbed (and reaching the outlet from the reaction vessel) to the number of molecules of A which have reacted, will therefore be equal to the ratio of the rate of desorption to the rate of reaction at the moment τ_c.

* The time of contact τ_c may be determined experimentally. For this purpose it is necessary to introduce into the reaction mixture traces of some stable substance which is not adsorbed under the reaction conditions and measure the time required for it to appear in the outlet from the reaction vessel.

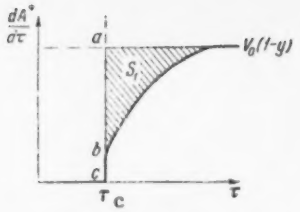

Fig. 1.

We may therefore say that the ratio of the quantity of substance A present on the catalyst at the initial moment (M_A) to S_1 is equal to the ratio of [(ab) + V_0y] to the rate of desorption of A (in the outlet from the reaction vessel).

The quantity of substance A present in the adsorbed state under stationary reaction conditions is therefore equal to

$$M_A = \frac{(ab) + V_0 y}{(ab)} S_1 = \frac{V_0 - (bc)}{(ab)} S_1.$$

The quantity of the product B on the reaction surface may be determined in analogous fashion (Fig. 2).

The sum of substances B + B* leaving the reaction vessel in unit time remains constant and equal to V_0y (under the same conditions as in the first case), but the substance B* appears in the outlet from the reaction vessel after a time lag. This delay results from the fact that time is required for the conversion of A* to B* and for the desorption of B*.

The region S_2 in Fig. 2 is numerically equal to the sum of the amount of substance B present in the adsorbed condition at the initial moment (M_B) and the amount of substance A present in the adsorbed condition at the original moment and afterwards converted to B. The second term in this sum is still unknown. It is equal to $[V_0y/(ab)]S_1$. The proposed method is therefore also applicable to the determination of the surface concentrations of the reaction products

$$M_B = S_2 - (M_A - S_1) = S_2 - \frac{V_0 y}{(ab)} S_1.$$

The quantities M_A and M_B relate to the total weight of catalyst. It is therefore necessary that the conditions (volume concentrations) at the beginning and end of the reaction vessel do not differ greatly. When y is small this follows naturally. If it is necessary to study a process for which y has some larger value, then it is possible to pass through the reaction vessel a mixture of composition corresponding to y and carry the reaction to a degree of conversion equal to $y + \Delta y$.

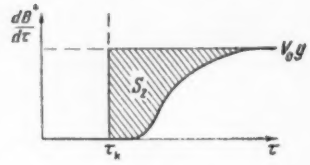

Fig. 2.

We have assumed that the influence of the isotopic effect may be neglected. In order to confirm this assumption it is necessary to make two measurements: one while the unlabeled substance is being displaced by the labeled substance and another under the reverse conditions. If the results obtained coincide, it means that the isotopic effect can be neglected.

Received February 16, 1959

QUANTUM MECHANICAL FOUNDATIONS OF THE FORMULA FOR THE ENERGY OF FORMATION OF ALKANES

V. M. Tatevskii and Yu. G. Papulov

M. V. Lomonosov Moscow State University

(Presented by Academician V. I. Spitsyn, February 14, 1959)

Parks and Parr [1] derived an equation for the total electronic energy of a molecule by representing the electronic part of the wave function as a linear combination of antisymmetrical two-electron wave functions:

$$E_e = \sum_I I_I + \sum_J \sum_{I \neq J} (J_{IJ} - K_{IJ}), \tag{1}$$

where

$$I_I = \iint \Lambda_I^* (1, 2)\, H^0 (1, 2)\, \Lambda_I (1, 2)\, d\tau_1 d\tau_2, \tag{2}$$

$$J_{IJ} = \iiiint \Lambda_I^* (1, 2)\, \Lambda_J^* (3, 4) \left[\frac{e^2}{r_{13}} + \frac{e^2}{r_{14}} + \frac{e^2}{r_{23}} + \frac{e^2}{r_{24}}\right] \times \times \Lambda_I (1, 2)\, \Lambda_J (3, 4)\, d\tau_1 d\tau_2 d\tau_3 d\tau_4, \tag{3}$$

$$K_{IJ} = \iiiint \Lambda_I^* (1,2)\, \Lambda_J^* (3,4) \left[\left(\frac{e^2}{r_{13}}\right)\Lambda_I (3, 2)\, \Lambda_J (1,4) + \left(\frac{e^2}{r_{14}}\right)\Lambda_I (4, 2)\, \Lambda_J (3, 1) + + \left(\frac{e^2}{r_{23}}\right)\Lambda_I (1, 3)\, \Lambda_J (2, 4) + \left(\frac{e^2}{r_{24}}\right)\Lambda_I (1, 4)\, \Lambda_J (3, 2)\right] d\tau_1 d\tau_2 d\tau_3 d\tau_4. \tag{4}$$

In this case $\Lambda_I (1, 2)$, etc. is the complete antisymmetric function corresponding to the electron pair (1, 2) which forms the I-th bond,

$$H^0 (1, 2) = H_N (1) + H_N (2) + \frac{e^2}{r_{12}}, \quad H_N (\zeta) = T (\zeta) - \sum_\alpha \frac{Z_\alpha e^2}{r_{\alpha\zeta}}; \tag{5}$$

numbers 1, 2 etc. denote electrons; subscripts α refer to the nuclei; T (ζ) is the kinetic energy operator for the ζ-th electron; r_{ij} and $r_{\alpha\zeta}$ are the distances between the respective particles, and e is the charge of the electron. It is evident that

$$\sum_\alpha \frac{Z_\alpha e^2}{r_{\alpha\zeta}} = \frac{Z_{I_\alpha} e^2}{r_{I_{\alpha\zeta}}} + \frac{Z_{I_\beta} e^2}{r_{I_{\beta\zeta}}} + \sum_{J,\, J \neq I} \frac{Z_{J_\gamma} e^2}{r_{J_{\gamma\zeta}}},$$

where α and β are subscripts for the nuclei in the I-th bond, while γ for the remaining nuclei. We can write

$$I_I = I_I^0 + \sum_{J,\, J \neq I} \Delta_{JI}, \tag{6}$$

where

$$I_I^0 = \iint \Lambda_I^*(1,2)\, H_I^0(!,2)\, \Lambda_I(1,2)\, d\tau_1 d\tau_2,$$

$$\Delta_{JI} = \iint \Lambda_I^*(1,2) \left[\frac{Z_{J_\gamma} e^2}{r_{J_{\gamma_1}}} + \frac{Z_{J_\gamma} e^2}{r_{J_{\gamma_2}}} \right] \Lambda_I(1,2)\, d\tau_1 d\tau_2,$$

$$-H_1^0(1,2) = T(1) + T(2) + \frac{e^2}{r_{12}} - \frac{Z_{I_\alpha} e^2}{r_{I_{\alpha_1}}} - \frac{Z_{I_\alpha} e^2}{r_{I_{\alpha_2}}} - \frac{Z_{I_\beta} e^2}{r_{I_{\beta_1}}} - \frac{Z_{I_\beta} e^2}{r_{I_{\beta_2}}}.$$

In order to get the total energy of formation of the molecule from individual atoms it is necessary to add to Equation (1) the coulombic repulsion energy between the atomic shells. This energy can be represented as

$$E_n = \sum_I \frac{Z_{I_\alpha} Z_{I_\beta} e^2}{r_{I_{\alpha\beta}}} + \frac{1}{2} \sum_{I,J,I+J} \frac{Z_{I_\alpha} Z_{J_\beta}}{r_{I_\alpha J_\beta}}. \tag{7}$$

Equation (7) is applicable to molecules with no rings, of the type examined below. In this case $Z_{I\alpha}$ and $Z_{I\beta}$ are the effective charges on the shells of atoms α and β forming the I-th bond, and $r_{I\alpha\beta}$ is the internuclear distance between these atoms; $Z_{I\alpha}$ and $Z_{J\beta}$ are the effective charges on the shells of atoms α involved in the I-th bond and atoms β in the J-th bond ($I \neq J$), and which atoms are not bound to each other, while $r_{I\alpha J\beta}$ are the internuclear distances between these atoms. Now the total energy of formation of a molecule from its component atoms will be

$$E = E_e + E_n = \sum_I R_I + \sum_{I,J,I+J} R_{IJ}, \tag{8}$$

where

$$R_I = I_I^0 + \frac{Z_{I_\alpha} Z_{I_\beta} e^2}{r_{I_{\alpha\beta}}}, \quad R_{IJ} = \frac{1}{2} \left(J_{IJ} - K_{IJ} + \frac{Z_{I_\alpha} Z_{J_\beta} e^2}{r_{I_\alpha J_\beta}} + 2\Delta_{IJ} \right). \tag{9}$$

For alkanes C_nH_{2n+2}, where we have only CC and CH bonds, Equation (8) can be written in the form

$$E_{C_nH_{2n+2}} = \sum_{CC} R_{CC} + \sum_{CH} R_{CH} + \sum_{CC,\,CC} R_{CC,\,CC} + \\ + \sum_{CC,\,CH} R_{CC,\,CH} + \sum_{CH,\,CH} R_{CH,\,CH}, \tag{10}$$

where the indices CC and CH in the first two sums denote summation over all the CC (or CH) bonds respectively. The indices CC, CC or CC, CH, or else CH, CH in the last three sums denote summation over all the CC and CC, CC and CH, or CH and CH bond-pairs respectively. One can readily see that the values of $R_{CC,\,CC}$ can be subdivided into two groups: 1) values of $R'_{CC,CC}$ referring to two adjacent CC bonds which share one C atom, and 2) values of $R''_{CC,CC}$ referring to two CC bonds separated by another CC bond. The values of $R_{CC,CH}$ and $R_{CH,CH}$ can be subdivided in a similar fashion. We will now get:

$$\sum_{CC,\,CC} R_{CC,\,CC} = \sum_{CC,\,CC} R'_{CC,\,CC} + \sum_{CC,\,CC} R''_{CC,\,CC} + \dots$$

$$\sum_{CC,\,CH} R_{CC,\,CH} = \sum_{CC,\,CH} R'_{CC,\,CH} + \sum_{CC,\,CH} R''_{CC,\,CH} + \dots \tag{11}$$

$$\sum_{CH,\,CH} R_{CH,\,CH} = \sum_{CH,\,CH} R'_{CH,\,CH} + \sum_{CH,\,CH} R''_{CH,\,CH} + \dots$$

We will limit the right hand side of these equations to the terms written out and neglect the remaining ones, since as a rule* they are known to be much smaller than the written ones. We will assume that the angles in an alkane molecule are strictly tetrahedral, that all the CC bonds are equal in length, and likewise for CH bonds. It will then turn out that all the terms in the sum $\Sigma R'_{CC,CC}$ are equal to each other, and likewise for terms in sums $\Sigma R'_{CC,CH}$ and $\Sigma R'_{CH,CH}$. Depending on whether the bond pairs are trans (t) or skew (g) with respect to each other the functions $R''_{CC,CC}$, $R''_{CC,CH}$, and $R''_{CH,CH}$ will each assume two different values $R^t_{CC,CC}$, $R^g_{CC,CC}$, $R^t_{CC,CH}$, $R^g_{CC,CH}$, $R^t_{CH,CH}$ $R^g_{CH,CH}$ respectively. We will then get from Eq. (10)

$$R_{C_nH_{2n+2}} = (n-1)R_{CC} + (2n+2)R_{CH} + y_{CC}R'_{CC,CC} + y_{CH}R'_{CC,CH} + \\ + y_{HH}R'_{CH,CH} + z^t_{CC}R''_{CC,CC} + z^g_{CC}R''_{CC,CC} + z^t_{CH}R''_{CC,CH} + z^g_{CH}R''_{CC,CH} + \\ + z^t_{HH}R''_{CH,CH} + z^g_{HH}R''_{CH,CH}, \tag{10a}$$

where $(n-1)$, $(2n+2)$, y_{CC}, y_{CH}, y_{HH}, z^t_{CC}, z^g_{CC}, z^t_{CH}, z^g_{CH}, z^t_{HH}, z^g_{HH}, are the numbers of the respective configurations. We have also assumed in this case that all the R_{CC} terms are equal and so are all R_{CH}, and that the number of CC bonds in a C_nH_{2n+2} alkane is $(n-1)$ while that of CH bonds $(2n+2)$.

We will denote the primary carbon atoms by C_1, secondary by C_2, tertiary by C_3, and quaternary by C_4. The number of C_i–C_j bonds in the alkane will be denoted by n_{ij}. The six atoms surrounding each bond of type C_2-C_2, C_2-C_3, C_3-C_3 can have two different stable (staggered) configurations. We will denote one of them by a superscript 1 and the other by 2. The numbers n_{23}, n_{33} will be split into the pairs $n^{(1)}_{22}$, $n^{(2)}_{22}$, $n^{(1)}_{23}$, $n^{(2)}_{23}$, $n^{(1)}_{33}$, $n^{(2)}_{33}$, while

$$\begin{aligned} n_{22} &= n^{(1)}_{22} + n^{(2)}_{22} = n_{22}\alpha_{22} + n_{22}(1-\alpha_{22}), \\ n_{23} &= n^{(1)}_{23} + n^{(2)}_{23} = n_{23}\alpha_{23} + n_{23}(1-\alpha_{23}), \\ n_{33} &= n^{(1)}_{33} + n^{(2)}_{33} = n_{33}\alpha_{33} + n_{33}(1-\alpha_{33}). \end{aligned} \tag{12}$$

It can readily demonstrated that $(n-1)$, $(2n+2)$, y_{CC}, y_{CH}, y_{HH}, z^t_{CC}, z^g_{CC}, z^t_{HH}, z^g_{HH} can all be expressed in terms of n_{ij}:

$$n-1 = \sum_{i,j=1,\, i\leqslant j}^{4} n_{ij}, \quad 2n+2 = \sum_{i,j=1,\, i\leqslant j}^{4} \left(\frac{4-i}{i} + \frac{4-j}{j}\right) n_{ij}; \tag{13}$$

$$y_{CC} = \sum_{i,j=1,\, i\leqslant j}^{4} \left(\frac{i-1}{2} + \frac{j-1}{2}\right) n_{ij}, \quad y_{CH} = \sum_{i,j=1,\, i\leqslant j}^{4} [(4-i)+(4-j)]\, n_{ij},$$

$$y_{HH} = \sum_{i,j=1,\, i\leqslant j}^{4} \left[\left(\frac{3-i}{2}\right)\left(\frac{4-i}{i}\right) + \left(\frac{3-j}{2}\right)\left(\frac{4-j}{j}\right)\right] n_{ij}; \tag{14}$$

$$z^t_{CC} = \frac{1}{3}\left[\sum_{i,j=1,\, i\leqslant j}^{4} n_{ij}(i-1)(j-1) + 2n^{(1)}_{22} - n^{(2)}_{22} - 2n^{(1)}_{23} + n^{(2)}_{23} + 2n^{(1)}_{33} - n^{(2)}_{33}\right],$$

$$z^g_{CC} = \frac{1}{3}\left[2\sum_{i,j=1,\, i\leqslant j}^{4} n_{ij}(i-1)(j-1) - 2n^{(1)}_{22} + n^{(2)}_{22} + \right.$$

$$\left. + 2n^{(1)}_{23} - n^{(2)}_{23} - 2n^{(1)}_{33} + n^{(2)}_{33}\right],$$

$$z^t_{CH} = \frac{1}{3}\left[\sum_{i,j=1,\, i\leqslant j}^{4} n_{ij}[(i-1)(4-j) + (j-1)(4-i)] - \right.$$

$$\left. - 4n^{(1)}_{22} + 2n^{(2)}_{22} + 4n^{(1)}_{23} - 2n^{(2)}_{23} - 4n^{(1)}_{33} + 2n^{(2)}_{33}\right], \tag{15}$$

* Yet not always, for with some reversibly isomeric forms of alkanes individual terms among those rejected in Eq. (11) may be equal to any of the preceding ones.

$$z^g_{CH} = \frac{1}{3}\Big[2 \sum_{i,\,j=1,\ i<j}^{4} n_{ij}\,[(i-1)(4-j)+(j-1)(4-i)] + 4n^{(1)}_{22} - 2n^{(2)}_{22} - 4n^{(1)}_{23} + 2n^{(2)}_{23} + 4n^{(1)}_{33} - 2n^{(2)}_{33}\Big],$$

$$z^t_{HH} = \frac{1}{3}\Big[\sum_{i,\,j=1,\ i<j}^{4} n_{ij}(4-i)(4-j) + 2n^{(1)}_{22} - n^{(2)}_{22} - 2n^{(1)}_{23} + n^{(2)}_{23} + 2n^{(1)}_{33} - n^{(2)}_{33}\Big],$$

$$z^g_{HH} = \frac{1}{3}\Big[2 \sum_{i,\,j=1,\,i<j}^{4} n_{ij}(4-i)(4-j) - 2n^{(1)}_{22} + n^{(2)}_{22} + 2n^{(13)}_{2} - n^{(2)}_{23} - 2n^{(1)}_{33} + n^{(2)}_{33}\Big].$$

Substituting Equations (13)-(15) into Eq. (10a) and making use of Eq. (12) we will get,

$$E_{C_nH_{2n+2}} = \sum_{i,\,j=1,\ i<j}^{4} n_{ij}\,B_{ij}, \tag{16}$$

where the constants B_{ij} have the form

$$\begin{aligned} B_{ij} = {} & R_{CC} + \left(\frac{4-i}{i} + \frac{4-j}{j}\right) R_{CH} + \left(\frac{i-1}{2} + \frac{j-1}{2}\right) R'_{CC,\,CC} + \\ & + [(4-i)+(4-j)]\,R'_{CC,\,CH} + \left[\left(\frac{3-i}{2}\right)\left(\frac{4-i}{i}\right) + \left(\frac{3-j}{2}\right)\left(\frac{4-j}{j}\right)\right] R'_{CH,\,CH} + \\ & + \frac{1}{3}\sum_{i,\,j=1,\ i<j}^{4} n_{ij}\,(i-1)(j-1)\,[R^t_{CC,\,CC} + 2R^g_{CC,\,CC}] + \\ & + \frac{1}{3}\sum_{i,\,j=1,\ i<j}^{4} n_{ij}\,[(i-1)(4-j)+(j-1)(4-i)]\,[R^t_{CC,\,CH} + 2R^g_{CH,\,CH}] + \\ & + \frac{1}{3}\sum_{i,\,j=1,\ i<j}^{4} n_{ij}\,(4-i)(4-j)\,[R^t_{CH,\,CH} + 2R^g_{CH,\,CH}] + f_{ij}, \end{aligned} \tag{17}$$

while the functions f_{ij} are equal to zero, except for f_{22}, f_{23}, and f_{33}:

$$\begin{aligned} f_{22} &= (\alpha_{22} - 1/3)\,[R^t_{CC,\,CC} - R^g_{CC,\,CC} - 2R^t_{CC,\,CH} + 2R^g_{CC,\,CH} + R^t_{CH,\,CH} - R^g_{CH,\,CH}], \\ f_{23} &= -(\alpha_{23} - 1/3)\,[R^t_{CC,\,CC} - R^g_{CC,\,CC} - 2R^t_{CC,\,CH} + 2R^g_{CC,\,CH} + \\ &\quad + R^t_{CH,\,CH} - R^g_{CH,\,CH}], \\ f_{33} &= (\alpha_{33} - 1/3)\,[R^t_{CC,\,CC} - R^g_{CC,\,CC} - 2R^t_{CC,\,CH} + 2R^g_{CC,\,CH} + R^t_{CH,\,CH} - R^g_{CH,\,CH}]. \end{aligned} \tag{18}$$

Thus by starting with simple concepts about the types and configurations of CC and CH bonds, we reduced the equation for the energy of formation of alkanes C_nH_{2n+2} to the form (16), which is completely identical to the one previously derived by us [2],

$$E_{C_nH_{2n+2}} = \sum_{i,\,j=1,\ i<j}^{4} n_{ij}\,A_{ij}.$$

Equation (16) was derived with some approximations which lead to certain relationships between the constants B_{ij}. These problems will be treated elsewhere.

LITERATURE CITED

[1] J. M. Parks, and R. G. Parr, J. Chem. Phys. 28, No. 2, 335 (1958).

[2] V. M. Tatevskii, Proc. Acad. Sci. USSR 75, No. 6, 819 (1950).

Received February 10, 1954

CHARGING CURVES FOR RHODIUM BLACK

Yu. M. Tyurin

M. V. Lomonosov State University, Moscow

(Presented by Academician A. N. Frumkin, February 24, 1959)

The electrochemical study of the surface properties of rhodium was begun by A. F. Lunev [1]. He recorded the charging curves for rhodium-covered platinum (in N H_2SO_4, HCl, HBr, KOH), and established the quantitative relationship between the adsorption of ions on the electrode and its potential in the range between the reversible hydrogen potential and the reversible oxygen potential in the given solution (N NaCl + 0.02 N or 0.05 N HCl; N Na_2SO_4 + 0.02 N and 0.05 N H_2SO_4) and showed the close similarity in structure of the electrode-solution boundaries for rhodium and platinum.

The present work is devoted to a study of the surface properties of rhodium black by the charging curve method.

The rhodium black charging curves were recorded using the method described in [2] (gauze method). The rhodium black was precipitated from alkaline $RhCl_3$ solution using formaldehyde, as described in [3]. The rhodium black precipitate was washed in a stream of twice-distilled water and then wrapped in fine platinum gauze, after which it was subjected to alternate anodic and cathodic polarization in frequently changed 0.1 N H_2SO_4 solutions and again given a prolonged washing in twice-distilled water. All the necessary solutions were prepared from twice-recrystallized salts and twice-distilled acids and water.

Figure 1* shows the anodic charging curves for rhodium black and rhodium-covered platinum [1]. For convenience the x-axis is the same for both (i.e. the results for rhodium-covered platinum were recalculated for the same quantities of electricity as were used for the rhodium black). When this is done the corresponding curves for rhodium black and rhodium-covered platinum coincide almost exactly. The surface properties of rhodium black and rhodium-covered platinum are evidently closely similar.

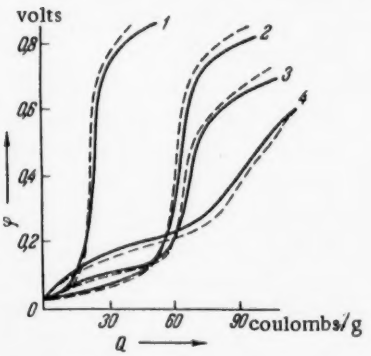

Fig. 1. Anodic charging curves for rhodium black (solid lines) and rhodium-covered platinum (broken lines), recorded in normal HBr (1), HCl (2), H_2SO_4 (3) and KOH (4).

On the other hand, the charging curves for dispersed rhodium are similar to the charging curves for platinized platinum [4]. In both cases the curves recorded in acid solutions consist of three parts—a hydrogen region, a two-layer region and an oxygen region—while the curves obtained in alkaline solution are characterized by a continuous change from the hydrogen region to the oxygen region. Within the limits of the hydrogen region the charging process is reversible (Fig. 2), which indicates that the states through which the rhodium black passes during the recording of the charging curves are approximately equilibrium states. In the region of surface oxidation the reversibility of the charging process is broken down and there is a hysteresis between the anodic and cathodic charging; the hysteresis is larger, the more positive the potential from which the cathodic charging starts. We shall show that in the case of rhodium black,

* All potential values are given relative to the reversible hydrogen potential in the same solution.

TABLE 1

Q_1	Q_2	Q_3	Q_1/Q_2	$\sum Q_3/Q_1$
3,0	66,5	50,1	0,12	6,4
6,6	66,5	36,3	0,10	5,5
11,3	66,5	58,0	0,17	5,6
7,8	66,5	51,5	0,12	6,6
		Mean	0,13	

unlike that of rhodium-covered platinum, the start of the oxygen halt on the charging curve recorded after prolonged anodic treatment with evolution of gaseous oxygen does not show the potential jump characteristic of the start of the process of phase oxide breakdown (Fig. 2) [1, 5, 6]. Finally, the energy of binding of the hydrogen adsorbed by the rhodium depends on the nature of the electrolyte and, as in the case of platinized platinum, decreases in the series KOH, H_2SO_4, HCl, HBr. This can be seen from Fig. 1, in which the hydrogen regions of the curves end at less positive potentials on going from left to right along the electrolyte series given.

In N H_2SO_4, the removal of hydrogen from the rhodium surface finishes at approximately +0.25 v, and the oxidation starts at 0.45-0.50 v (Fig. 1). The end of the hydrogen part of the platinum charging curve, recorded in N H_2SO_4, lies at +0.35 v, and the start of the oxygen part at 0.75-0.80 v [4]. The strength of the bond between hydrogen and the surface is therefore slightly less than in the case of platinum, while the oxidation of rhodium starts at less positive potentials. This is also confirmed by a comparison of the charging curves for disperse rhodium and platinized platinum obtained in other electrolytes (N HCl, HBr and KOH). A more detailed comparison of the surface properties of rhodium and platinum has been given by A. F. Lunev [1].

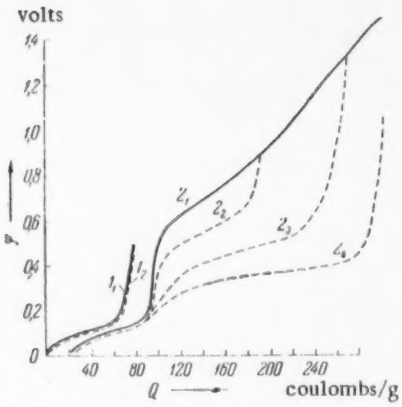

Fig. 2. Anodic (1_1, 2_1) and cathodic (1_2, 2_2, 2_3, 2_4) charging curves for rhodium black, recorded in N H_2SO_4. The start of Curve 2_1 is shifted 20 coulombs along the x-axis. The Curve 2_4 was recorded after anodic treatment of the rhodium black with oxygen evolution for 24 hours.

We give below data on the influence of solution pH and the presence of surface-active Cl^-, Br^- and I^- anions on the surface properties of rhodium black.

In the study of the influence of the iodide ion, the rhodium black was kept for 1 hour in acidified 0.1 N KI solution through which hydrogen was bubbled continuously, after which it was washed with twice-distilled water saturated with hydrogen, until no iodide could be detected in the wash water (with $AgNO_3$), then transferred to the gauze electrode [2] and its charging curve recorded in N H_2SO_4. When this curve had been recorded the potential of the rhodium black was brought to 1.0-1.3 v and the rhodium treated anodically for 2-3 hours to oxidize the adsorbed iodide ion. The quantity of iodate transferred to the solution was determined using sodium thiosulfate [7]. The charging curve of the rhodium black "cleaned" in this way was then recorded in N H_2SO_4, the anodic treatment repeated and the quantity of iodate transferred to the solution again determined; the charging curve was recorded again and the process repeated until no iodate could be detected in the solution.

The results of one series of experiments are given in Fig. 3. As in the case of platinized platinum [8], the "poisoning" of the rhodium black by the iodide ion is shown by a decrease in the length of the hydrogen region of its charging curve and in a shortening of its potential interval, while the successive "cleaning" operations produce a gradual restoration of the initial shape of the charging curve.

The results of the determination of the amount of adsorbed iodide ion, relative to 1 g of rhodium black, are given in Table 1 (Q_1 coulombs/g). Q_2 in the table denotes the length of the hydrogen halt for the unpoisoned rhodium black (in coulombs/g), i.e., a quantity proportional to the quantity of hydrogen adsorbed by the surface of the rhodium black free from iodide ion, in the interval between the reversible hydrogen region and the potentials of the two-layer region. Q_3 denotes the difference between the length of the hydrogen part of the curve for "unpoisoned" rhodium black and that for rhodium black "poisoned" with iodide ion (the difference between Curves 1 and 2 in Fig. 3), i.e., it is a quantity proportional to the amount of hydrogen desorbed from the rhodium black surface after "poisoning" in KI solution (in coulombs/g).

The mean value of the ratio Q_1/Q_2 is equal to 0.13. This indicates as an approximation that 13 iodide ions are adsorbed for every 100 hydrogen atoms adsorbed. According to [1], hydrogen covers a rhodium surface

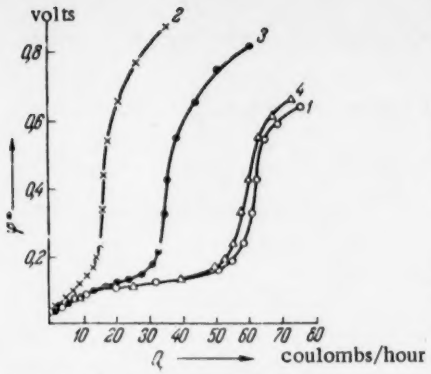

Fig. 3. The influence of iodide ion on the charging of rhodium black; 1) unpoisoned rhodium black, 2) poisoned rhodium black, 3) poisoned rhodium black after 1st cleaning, 4) poisoned rhodium black after 6th cleaning. Electrolyte N H_2SO_4.

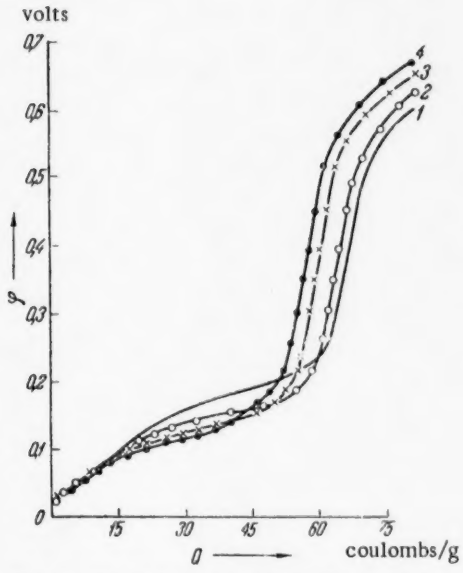

Fig. 4. The influence of electrolyte pH on the charging of rhodium black. 1) In $1 \cdot 10^{-3}$ N H_2SO_4 + 1 N Na_2SO_4; 2) in $2 \cdot 10^{-2}$ N H_2SO_4 + 1 N Na_2SO_4; 3) in 0.1 N H_2SO_4 + 0.9 N Na_2SO_4; 4) in 1 N H_2SO_4.

to a depth of only one layer, and the quantity of adsorbed iodine evidently is insufficient for one layer, which is in accordance with the data obtained for platinized platinum [8], iron [9] and lead [10].

The ratio Q_3/Q_1 is equal to 5-7, which means that 5-7 hydrogen atoms are desorbed for every iodide ion on the surface, i.e., the iodide ion exhibits a "long-range" action in the "poisoning" process, which has been detected earlier in the case of the poisoning of platinum by mercury and other poisons [11].

Figure 1 shows that the presence of chloride and bromide ions in the solution reduces the length of the hydrogen halt on the rhodium-black charging curve. Increase in the concentration of surface-active ion leads to an increase in this effect. The regular features observed are on the whole analogous to those observed earlier for platinized platinum [8].

The influence of pH was studied in $H_2SO_4 + Na_2SO_4$ solutions with constant sulfate ion concentration. Some typical data are given in Fig. 4.

Increase in the pH of the electrolyte leads to an increase in the energy of binding of the adsorbed hydrogen and to a slight increase in the length of the hydrogen region of the rhodium charging curve. The change in the energy of binding of hydrogen adsorbed on a metal electrode surface with change from acidic to alkaline solutions is a fairly general phenomenon [1, 4, 12, 13], but this is the first occasion upon which a clearly defined pH effect has been observed within the acid range in solutions (pH between 0.7 and 4.2). In the case of other metals (Pt, Ir) the question of the effect of pH on adsorptive properties requires further study.

LITERATURE CITED

[1] A. F. Lunev, Graduate Thesis, Inst. Fiz. Khim. Akad. Nauk. SSSR (Moscow, 1948).*

[2] Yu. A. Podvyazkin and A. I. Shlygin, Zhur. Fiz. Khim. 31, 1305 (1957).

[3] O. Loew, Ber. 23, 289 (1890).

[4] A. I. Shlygin and A. N. Frumkin, Acta Physicochim. URSS 3, 791 (1935); A. I. Shlygin, A. N. Frumkin, and V. Medvedovskii, Acta Physicochim. URSS 4, 911 (1936); A. N. Frumkin, and A. I. Shlygin, Izv. Akad. Nauk. SSSR, Otd. Khim. Nauk., No. 5, 773 (1936).

[5] A. N. Frumkin, Uspekhi Khim. 15, 4, 385 (1946); 18, 1, 9 (1949).

[6] A. D. Obrucheva, Zhur. Fiz. Khim. 26, 1742 (1952).

[7] I. M. Kolthoff and E. B. Sandell, Quantitative Analysis, M.-L., p. 635 (1948).**

[8] A. D. Obrucheva, Zhur. Fiz. Khim. 32, 2155 (1958).

[9] Z. A. Iofa and G. V. Rozhdestvenskaya, Dokl. Akad. Nauk. SSSR 91, 1159 (1953).

[10] A. A. Medvedeva and Ya. M. Kolotyrkin, Zhur. Fiz. Khim. 31, 2668 (1957).

* In Russian.

** Russian translation.

[11] A. I. Shlygin, E. Razumovskaya, and K. Rozental', Zhur. Fiz. Khim. 13, 1079 (1939); B. V. Ershler, Zhur. Fiz. Khim. 13, 1092 (1939).

[12] A. D. Obrucheva and I. A. Rubinshtein, Dokl. Akad. Nauk. SSSR 63, 403 (1948).

[13] V. É. Past, Graduate Thesis, (Moscow, 1956).*

Received February 9, 1959

* In Russian

THE SPECTRAL PROPERTIES OF OPTICALLY UNSENSITIZED PHOTOGRAPHIC EMULSIONS

B. G. Varshaver, Zh. L. Broun and Corresponding Member Acad. Sci. USSR K. V. Chibisov

All-Union Scientific Research Institute for Cinematography. Institute of Physics of the I. I. Mechnikov Odessa State University.

If the light sensitivity of an emulsion depended only on the optical properties of the silver halide, then its spectral region would be strictly limited to the absorption band of the halide. But it has been shown [1, 2] that AgBr, dispersed in gelatin , is not only sensitive to the rays which it absorbs itself, but, also has a long wave light sensitivity, rapidly decreasing toward the red end of the spectrum.

Investigation [3] of the effect of chemical ripening on spectral light sensitivity showed that the same times were required to reach general (S_Σ) and "blue" ($S_{\lambda 450}$) light sensitivity, and, that there was a considerable lag in the growth of long wave sensitivity. It was also found that S_Σ and $S_{\lambda 450}$ depended very much on the silver iodide content of the emulsion, but, that the latter had little effect on the long wave sensitivity.

These results are evidence of the important part played in emulsions by contaminating microcrystalline, local disturbances, formed by topochemical reactions. It would therefore, be reasonable to suppose that the change in light sensitivity of an emulsion was somewhat connected with changes in the spectral absorption of impurities, and this has actually been demonstrated experimentally [4]. It seemed important to investigate this phenomenon in more detail and to explain it theoretically.

To solve this problem, we measured the impurity spectra and the light sensitivity of emulsion layers after different times of ripening. Absorption measurements were carried out in parallel with an SF-4 spectrophotometer and with an E. A. Kirillov spectrophotometric apparatus with a photometric integrator [5]. For this purpose the emulsions were diluted and densitized with pinacriptol green, which does not affect the impurity centers [6].

A fine structure (Fig. 1) was observed in the impurity spectrum measured with the SF-4 spectrophotometer, and also with the E. A. Kirillov apparatus, but considerably more smoothed out.

Interrelation between the changes in impurity absorption and light sensitivity was investigated by comparing isochromatic curves, showing the relation between impurity absorption for different values of λ and ripening time, with kinetic curves for total light sensitivity (Figs. 2 and 3).

Crystallization of AgBr in the first ripening stage was accompanied by formation of silver impurity centers, as was shown by the fine structure of the absorption spectrum. The isochromatic curves also showed two special features: in the first place, they were more or less similar for different values of λ, and, in the second place, their maxima remained in the same position corresponding to the time required to reach S_{max}. In the first ripening stage, in the presence of similarity, the isochromatic curves had two maxima, which also corresponded to the light sensitivity maxima.

The similarity of the curves for different values of λ showed that the impurity spectrum remained qualitatively the same for different ripening times, and, consequently, that the primary centers, responsible for the fine structure of the absorption, were uniform. The existence of maxima in these curves indicated that there was a complex change in the concentration of these centers during ripening. The coincidence of the times for reaching

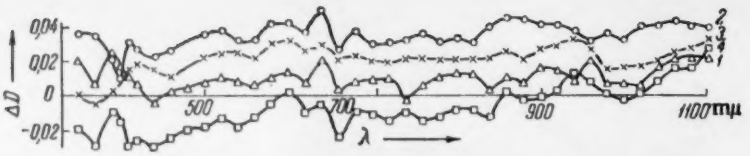

Fig. 1. Curves of spectral absorption by impurity centers of a silver bromide negative emulsion (obtained with a spectrophotometer SF-4): 1) time of secondary ripening t_2 = 90 minutes; 2) t_2 = 150 minutes; 3) t_2 = 180 minutes; 4) t_2 = 300 minutes.

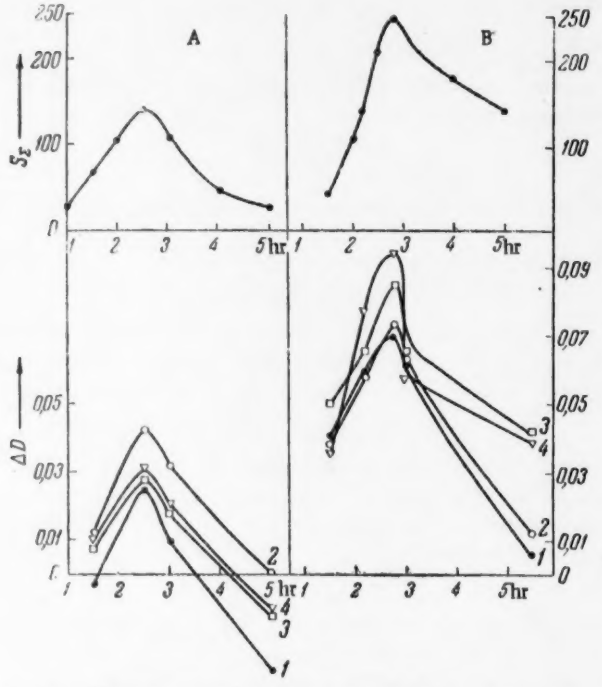

Fig. 2. Changes in total light sensitivity (S_Σ) and spectral absorption (ΔD) of impurity centers (measured with an SF-4 spectrophotometer) with the time of secondary ripening (t_2): A) silver bromide emulsion; B) silver iodide emulsion (5 mole % AgI); isochromatic curves (λ, ΔD): 1) λ 450 mμ; 2) λ 600 mμ; 3) λ 700 mμ; 4) λ 800 mμ.

maximum absorption and light sensitivity showed the direct influence of the silver primary centers on $S_{\lambda_{450}}$ and S_Σ. The lag in the rate of increase of long wave sensitivity showed, on the other hand, that S was produced by a different means in this region of the spectrum (λ ≥ 600 mμ). Another indication of this, was that the concentration of AgI did not affect the long wave light sensitivity, although it increased the concentration of primary centers and the total (and, therefore, also the "blue") light sensitivity (Fig. 2).

The complex change in the concentration of primary centers was, evidently, the result of their "coagulation" into coarser aggregates, caused by the migration of silver, as follows from the work of Mitchell [7]. At the beginning of the ripening process, the accumulation of primary centers exceeded their "coagulation"; subsequently, as the rate of the latter process speeded up, the concentration of primary particles fell, causing a reduction in the associated absorption. The concentration of the latter formed coarse aggregates, which were responsible for the

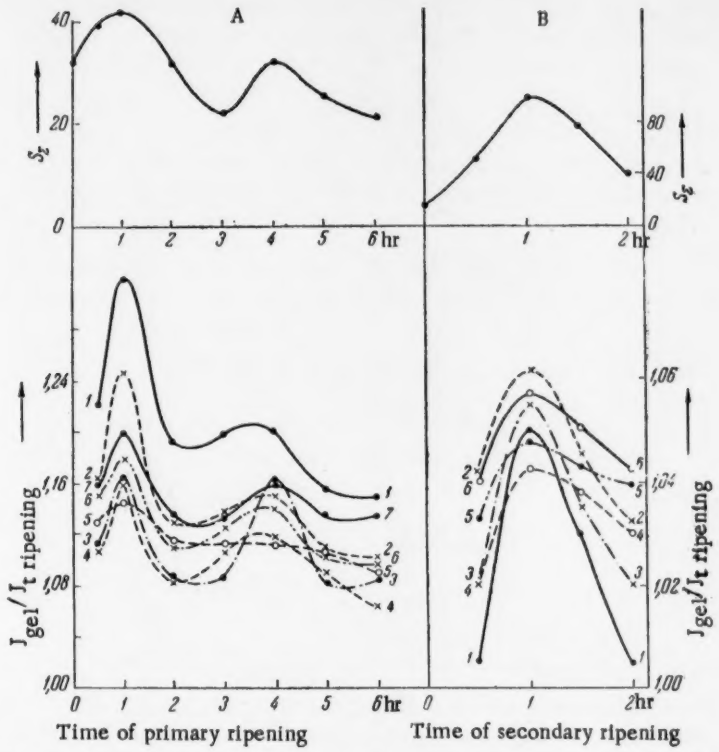

Fig. 3. The same as Fig. 2, except that measurements were made with the E.A. Kirillov spectrophotometric apparatus with photometric integrator: A) primary ripening; isochromatic curves (λ, J_{gel}/J_{t_1}): 1) λ 450 mμ; 2) λ 470 mμ; 3) λ 530 mμ; 4) λ 590 mμ; 5) λ 650 mμ; 6) λ 710 mμ; 7) λ 770 mμ; B) secondary ripening; isochromatic curves (λ, J_{gel}/J_{t_2}): 1) λ 420 mμ; 2) λ 450 mμ; 3),4),5) and 6) curves for the same λ as in the primary ripening.

long wave sensitivity, was very much less, as was shown by the fact that the long wave sensitivity was less by 4-6 orders of magnitude than the "blue" light sensitivity. Thus, since the spectrophotometry was carried out at the limit of sensitivity of the equipment used, it was not possible to reveal spectral absorption by secondary impurity centers. The difference from the picture of the primary ripening process was probably asosciated with the crystallization of AgBr, which caused renewal of the surface of the growing crystals and the formation of sites where reaction could occur. At this stage, center formation and crystal growth proceeded simultaneously, so that the impurity centers forming (primary and secondary) would remain inside internal local lattice defects.

In order to ascertain the dimensions and structure of the impurity centers, it was necessary to refer to the experiments of E. P. Kramalei [8]. These showed that Ag, in addition to its colloidal degree of dispersion, could occur in any state, including atomic molecules. It could therefore, be assumed that the primary silver centers also had the nature of atomic molecules. They occurred in equilibrium with silver bromide, i.e., adsorbed into the lattice defects of emulsified microcrystals, and were responsible for the constancy of the fine-structure absorption band of the different halides [9]. It should be noted that atomic-molecular particles were stable in the case of silver sols, and, on the other hand, are labile when occurring in equilibrium with AgBr.

Taking note of Mitchell's [10] findings about elementary silver particles it was reasonable to assume that the primary centers were, indeed, the same as his simple particles, mainly Ag_2. We could thus speak of three types of silver impurity centers: primary atomic-molecular centers, responsible for the levels of $S_{\lambda_{450}}$ and S_Σ, and characterized by the fine structure of their absorption spectrum; secondary centers in the form of aggregates,

responsible for long wave light sensitivity; and catalytically active development centers. Conversion of primary into secondary centers, and subsequent formation of development centers, occur during the ripening of emulsions and also under the influence of light. In the latter case, there is not only the simple conversion of Mott and Mitchell [11], but a direct sharing of impurity centers with formation of a latent image.

In this complex process, the primary centers clearly have the function of combining with "positive holes" (bromine atoms), for the following reason: although the fine-structure absorption spectrum of these centers is distributed over the whole visible region, yet their effect is restricted to only their own light sensitivity. It may therefore, be accepted that the equilibrium considered by Mott and Mitchell, $Ag_2 + Ag^+ \rightleftharpoons Ag_3^+$, is displaced to the side of neutral particles.

Secondary centers, in the first place make possible an increase in S_Σ at the expense of the electronic function [3], and, in the second place, finish up by changing into development centers. They are therefore sublatent centers.

Catalytically active centers, which initiate development, are amorphous silver particles [12] at the limit of thermodynamic instability [13], i.e., they are particles of high energy potential. They are formed by combination of photoelectrons with positively charged sublatent centers, almost in the state required for initiation of development. This can be represented, according to Mott and Mitchell, by the following scheme: $Ag_n + Ag^+ + \bar{e} \rightleftharpoons Ag_{n+1}^+ + \bar{e} \rightarrow Ag_{n+1}$

LITERATURE CITED

[1] J. Eggert and M. Biltz, Zs. wiss. Photogr. 39, 140 (1941); J. Eggert and F. G. Kleinschrod, Zs. wiss. Photogr. 39, 155, 165 (1941).

[2] H. Arens, J. Eggert and F. G. Kleinschrod, Zs. wiss. Photogr. 42, 33 (1943).

[3] B. G. Varshaver, L. Ya. Kraum, and K. V. Chibisov, J. Sci. and Appl. Photogr. and Cinematogr. 2, 413 (1957); K. V. Chibisov, L. Ya. Kraum, and S. R. Zhukovskii, Zs. wiss. Photogr. 52, 193 (1958).

[4] Zh. L. Broun, J. Sci. and Appl. Photogr. and Cinematogr. 3, 246 (1958).

[5] Zh. L. Broun, Optics and Spectroscopy 7 (1959).

[6] E. A. Nesterovskaya, Proc. Acad. Sci. USSR. 90, 587 (1953).

[7] J. M. Hedges and J. W. Mitchell, Phil. Mag. 44, 367 (1953).

[8] E. P. Kramalei, J. Sci. and Appl. Photogr. and Cinematogr. 3, 161 (1958).

[9] E. A. Kirillov, Zs. wiss. Photogr. 501, 253 (1955).

[10] J. W. Mitchell, Sci. et ind. photogr. 28, 457 (1952).

[11] K. F. Mott and J. W. Mitchell, Phil. Mag. 2, 1149 (1957).

[12] I. M. Ratner, K. V. Chibisov, and V. A. Kargin, J. Sci. and Appl. Photogr. and Cinematogr. 2, 7 (1957).

[13] K. V. Chibisov, J. Sci. and Appl. Photogr. and Cinematogr. 2, 3 (1957).

Received April 1, 1959

STRUCTURAL VISCOSITY OF AQUEOUS SOLUTIONS OF CARBOXYMETHYLCELLULOSE

K. F. Zhigach, M. Z. Finkel'shtein, and I. M. Timokhin

The I. M. Bubkin Institute for the Oil Chemistry and Gas Industries

(Presented by Academician A. V. Topchiev, February 28, 1959)

We showed in one of our previous papers [1] that different fractions of CMC possessed different colloid-chemical properties. It was noted, in particular, that aqueous solutions of CMC, as of other derivatives of cellulose, showed anomalous viscosity at concentrations above 0.1%.

There is some information in the literature (Höppler [2, 3]) on the relation between the viscosity of aqueous CMC solutions and rate of flow. The rheological properties of colloid systems and high polymers have been investigated in detail by Rebinder and his co-workers.

The object of our investigations was to elucidate the role of separate fractions in forming structures in solution, and to investigate the effect of addition of low molecular weight preparations on the viscosity of high molecular samples of CMC. Four samples of CMC, differing mainly in their degree of polymerization (Table 1), were selected for investigation.

The isolation of the gelatinous and sol-like fractions was carried out as previously described [1].

Viscosities were measured at different velocity gradients (G), using a Pinkevich viscometer, with application of an external pressure, at 25 ± 0.02°.

The results of the measurements, represented in Figs. 1 and 2 (Curves 1, 2 and 3), showed that the viscosity of the high molecular samples depended greatly on the velocity gradient. Anomalous viscosity was observed with solutions of sample No. 1 at CMC concentrations as low as 0.01% (Fig. 1, 1). The dependence of the viscosity on the velocity gradient increased markedly with increasing concentration of the solution. Thus, the viscosity of a 1% aqueous solution of sample No. 1 was 27.6 cp at G = 1750 seconds^{-1}, and 62.4 cp at G = 30 seconds^{-1}.

Of the three samples, Nos. 1, 2 and 3, the most marked anomalous viscosity was shown by the gelatinous fraction; solutions of the sol-like fraction showed the least variation of viscosity with velocity gradient (Fig. 2; 1, 2 and 3).

Solutions of the low viscosity sample, No. 4, showed very little variation of viscosity with velocity gradient (Table 2).

It follows from that data, given in Figs. 1 and 2, that solutions of high molecular preparations possessed considerable structural viscosity, which could be expressed quantitatively, by the method of Pasynskii and Rabinovich [4], as the tangent of the angle of slope (tan α) of the curve with coordinates η and log G.

The viscometric data was also used to calculate the dynamic pressure displacement, θ, which also characterizes the degree of structural viscosity of a solution. Values of tan α and θ for solutions of sample No. 1 are shown in Table 3.

A particularly high structural viscosity was possessed by solutions of the gelatinous fraction; solutions of the sol-like fraction were characterized by the lowest values of tan α and θ; sample No. 1, containing 19.3% of the gelatinous fraction, occupied an intermediate position (Table 4).

TABLE 1

Characteristics of CMC Samples

Sample No.	Description of sample	Degree of esterification	Degree of polymerization
1	High molecular	63.8	500
2	Gelatinous fraction of sample No. 1	58.9	635
3	Sol-like sample of fraction No. 1	66.3	276
4	Low molecular	66.2	70

TABLE 2

Viscosities of Solutions of Low Molecular Samples of CMC No. 4 in Centipoises

G, seconds^{-1}	Concentration of Solution, %					
	0.05	0.10	0.25	0.50	1.0	2.0
300	1.13	1.22	1.35	1.63	2.24	3.75
1000	1.01	1.08	1.24	1.49	2.07	3.50
2000	1.01	1.08	1.24	1.48	2.05	3.45

TABLE 3

Values of tan α and θ for Aqueous Solutions of CMC (Sample No. 1)

Function	CMC concentration, %					
	0.01	0.05	0.10	0.25	0.50	1.0
tan α	0.34	0.80	0.88	1.53	4.43	22.0
θ, dynes/cm^2	16	40	64	264	528	1702

TABLE 4

Values of tan α and θ for 0.25% Aqueous Solutions of CMC (Samples Nos. 1, 2 and 3)

Function	Sample No. 1	Sample No. 2	Sample No. 3
tan α	1.53	15.77	0.56
θ, dynes/cm^2	264	1678	32

Aqueous solutions of the low viscosity sample No. 4, containing practically none of the gelatinous fraction, possessed very low structural viscosity; for a 1% solution, the value of tan α did not exceed 0.58, and the dynamic pressure displacement was not above 5 dyne/cm^2.

TABLE 5

Changes in tan α and θ in 0.25% Solutions of High Viscosity CMC Samples, Nos. 1 and 2, on Addition of the Low Molecular Preparation No. 4

Sample No.	Index of structural viscosity	Addition of preparation No. 4, weight %							
		0	0.01	0.10	0.25	0.50	0.75	1.0	2.0
1	tan, α	1.5	–	1.2	1.0	0.9	0.8	1.1	1.4
	θ, dynes/cm^2	264	–	216	184	128	120	152	179
2	tan α	15.8	9.8	7.2	5.7	3.5	–	2.0	1.5
	θ, dynes/cm^2	1678	1518	799	424	344	–	296	256

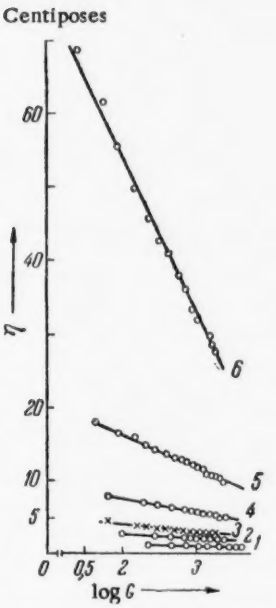

Fig. 1. Variation of the viscosity of solutions of high molecular sample No. 1 with the velocity gradient, for different CMC concentrations (%): 1) 0.01, 2) 0.05, 3) 0.1, 4) 0.25, 5) 0.5, 6) 1.0.

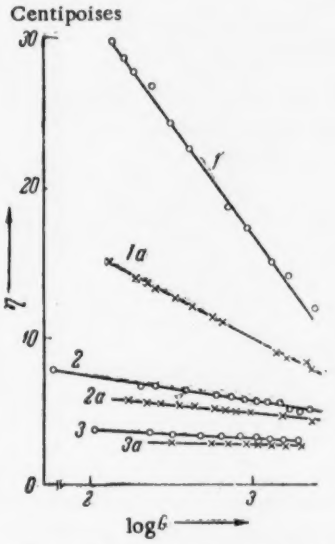

Fig. 2. Changes in the structural viscosity of 0.25% aqueous solutions of different CMC fractions as a function of the velocity gradient, with the addition of 0.25% of low molecular CMC No. 4. 1) Sample No. 2; 1a) Sample No. 2 + Sample No. 4; 2) Sample No. 1; 2a) Sample No. 1 + Sample No. 4; 3) Sample No. 3; 3a) Sample No. 3 + Sample No. 4.

These results support the view that structural viscosity in aqueous solutions of CMC is associated with the presence of the gelatinous fraction and the interaction of gel-forming particles with each other. Clearly, with a breakdown of the interaction between gel-forming particles, both the structural component of the viscosity and the total viscosity of CMC solutions will diminish.

Since the gelatinous particles possesses a surface of separation, it would be expected that their interaction might be affected by theaddition of sol or low viscosity preparations, which, when adsorbed on the gel particles,

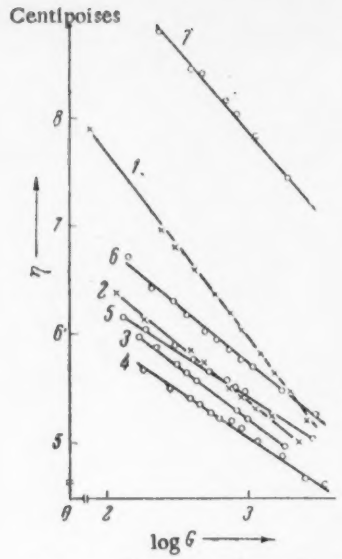

Fig. 3. Effects of adding different amounts (%) of low molecular CMC preparation No. 4 on the viscosity of a 0.25% solution of high molecular CMC Sample No. 1. 1) 0; 2) 0.1; 3) 0.25; 4) 0.5; 5) 0.75; 6) 1.0; 7) 2.0.

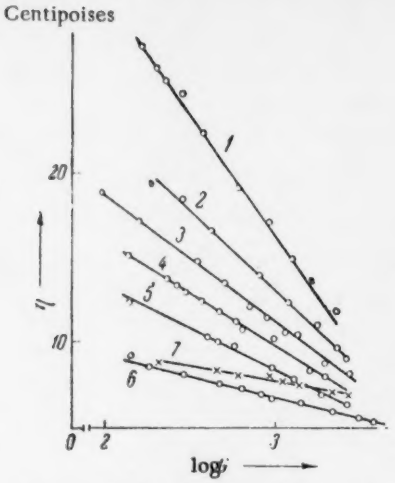

Fig. 4. Effect of adding different amounts (%) of low molecular CMC preparation No. 4 on the viscosity of a 0.25% solution of gelatinous CMC fraction (sample No. 2). 1) 0; 2) 0.01; 3) 0.10; 4) 0.25; 5) 0.5; 6) 1.0; 7) 2.0.

would change the structure of the solution. A similar phenomenon was observed and investigated by S. M. Lipatov and his co-workers [5, 6], for the interaction of soluble and insoluble fractions of gelatin and agar-agar.

To check this suggestion, we investigated the effect of the weakly polymerized preparation of CMC, No. 4, on the viscosity of 0.25% aqueous solutions of the highly polymerized samples Nos. 1 2 and 3. The results are given in Fig. 2, 3 and 4.

The results showed that addition of the low molecular to the high molecular fractions of CMC, in spite of an increase in the total CMC concentration, caused a decrease in both the total and structural viscosities of the aqueous solutions. The degree of reduction of viscosity was greater, the greater the content of gelatinous particles in the given preparation of CMC; it was greatest with the gelatinous fraction (Fig. 2; 1 and 1a) with sol-forming fraction (Fig. 2; 3 and 3a).

The greatest reduction in viscosity of a 0.25% solution of sample No. 1 was observed on the addition of 0.5% of the low viscosity preparation (Fig. 3; 4), while, with the gelatinous fraction, this was reached only after the addition of 1.0% of preparation No. 4 (Fig. 4; 6). Further increase in the concentration of the low viscosity preparation caused a rise in the total viscosity of the CMC solutions (Fig. 3; 5, 6, 7 and Fig. 4; 7), but the structural viscosity continued to fall, as was shown by the change in tan α and the dynamic pressure displacement. The structural viscosity increased only when the concentration of the low viscosity polymer was very great (Table 5).

These changes in the total and structural viscosities of solutions of high molecular CMC preparations could be explained in the following way.

When the low viscosity CMC preparation was added to the high viscosity samples, the value of the total viscosity of aqueous solutions of the mixture showed the influence of two factors: on the one hand, an increase in the concentration of CMC inevitably led to an increase in the viscosity of the solution, and, on the other hand, the increase in the concentration of the low viscosity preparation led to an increase in its adsorption on the gelatinous particles, and this produced a weakening in the interaction between the gelatinous particles and reductions in the total and structural viscosities.

The total factor began to take over control when the surface of the gelatinous particles was completely saturated with molecules of the weakly polymerized product, thus, accounting for the increase in viscosity.

It is clear that, the greater the concentration of gelatinous particles in the solution, the greater should be the requirement of low viscosity CMC preparation to reach the adsorption limit corresponding to the greatest reduction in structural viscosity. An increase in the total viscosity was observed a little before the minimum value of the structural viscosity was reached.

This fact can be explained as follows: when the amount of low molecular preparation adsorbed on the gelatinous particles approached its limiting value, and the progressive reduction in structural viscosity was becoming less marked, there began to be an increase in the total viscosity, as the result of the increase in concentration of the added weakly polymerized preparation.

This investigation has shown that the properties of solution of CMC preparations, having practically identical chemical composition, are greatly influenced by the interaction of fractions differing in their degree of polymerization. This means that it is possible to adjust the properties of CMC solutions to suit requirements.

LITERATURE CITED

[1] K. F. Zhigan, M. Z. Finkel'shtein, I. M. Timokhin, and A. I. Malinina, Proc. Acad. Sci. USSR 123, No. 2, 289 (1958).*

[2] F. Höppler, Koll. Zs. 98, 348 (1942).

[3] F. Höppler, Chemiker-Ztg 66, 132 (1942).

[4] A. G. Pasynskii and A. I. Rabinovich, J. Phys. Chem. 4, No. 5, 615 (1933).

[5] S. M. Lipatov and L. Lebedeva, Coll. J. 3, No. 8, 711.

[6] S. M. Lipatov and R. I. Fel'dman, Coll. J. 6, No. 9, 805 (1940).

Received February 25, 1959

* Original Russian pagination. See. C. B. translation.

INVESTIGATION OF UNSTABLE INTERMEDIATE PRODUCTS OF ELECTRODE REACTIONS BY MEANS OF A ROTATING DISC ELECTRODE

Yu. B. Ivanov and Corresponding Member Acad. Sci. USSR
V. G. Levich

Institute of Electrochemistry of the Academy of Sciences of the USSR

A. N. Frumkin [1] recently introduced the idea of investigating intermediate products (stable and especially unstable) of electrode reactions by making use of convective diffusion. Intermediate products, formed in the course of an electrochemical reaction at one electrode, are carried by the stream to the other electrode, separated in space from the first, where they are detected and recorded.

Appraisal showed that the best hydrodynamic properties were possessed by the ring-disc electrode system described in [1]. The theory of the action of such an electrode is given below.

The first electrode, designated below as zone 1, forms the inner surface of the disc. The electrode reaction $A \rightarrow B^*$ occurs in this zone. The particles of intermediate product, B^*, partly participate there in the second stage of the reaction and are transformed to the product, C, and are partly carried away be the stream of liquid. The particles of intermediate product carried away be the stream strike the second electrode, which consists of the ring zone (zone 3) of the outer part of the disc. Between the electrodes is an annular layer of insulator (zone 2).

We will suppose that B^* particles are electrically neutral, or that the solution contains sufficient supporting electrolyte so that transfer of B^* by ionic migration can be neglected.

The concentration of substance B^* must satisfy the equation of convective diffusion

$$v_r \frac{\partial C}{\partial r} + v_y \frac{\partial C}{\partial y} = D\left(\frac{\partial^2 C}{\partial y^2} + \frac{\partial^2 C}{\partial r^2} + \frac{1}{r}\frac{\partial C}{\partial r}\right), \tag{1}$$

where v_r and v_y are the radial and normal components of the velocity of the liquid, set in motion by the rotating disc. The concentration in our case (as opposed to an infinite uniform disc [2]) depends on the distance from the surface of the disc, y, and on the radius, r. Because of the symmetry of the system, the concentration does not depend on the angle φ.

The boundary conditions of the system have the following form:

In zone 1, the particles of substance B^* are formed at a constant rate uniformly over the surface. The number of B^* particles formed on 1 cm^2 of surface in 1 second is equal to the density, j_0 of the diffusion stream of particles of A to the surface of the disc. An expression has been derived [2] for the value of j_0. The disappearance of particles of the intermediate product, as the result of electrochemical reaction, is equal to $Q = kC|_{y=0}$, where $C|_{y=0}$ is the concentration of B^* at the surface, and k is a constant. The particles of intermediate product, which are not transformed at the surface of the disc, diffuse into the liquid. The balance of particles of intermediate product at the disc surface is expressed by:

$$j_0 = kC\Big|_{y=0} - D\frac{\partial C}{\partial y}\Big|_{y=0}, \quad r < r_1. \tag{2}$$

In zone 2, particles of intermediate product are neither formed nor destroyed, so that the flow of particles to the surface is here equal to zero:

$$\left.\frac{\partial C}{\partial y}\right|_{y=0} = 0, \quad r_1 < r < r_2. \tag{3}$$

In zone 3, the rate of the electrode reaction, in which the particles participate, may be reckoned as large compared with the rate of their arrival at the electrode surface. The concentration of particles of intermediate product at the surface of the disc may therefore, be put equal to zero:

$$C|_{y=0} = 0, \quad r_2 < r < r_3. \tag{4}$$

Anywhere far away from the surface of the disc, at $y \to \infty$, the concentration of intermediate product must be equal to zero:

$$\lim_{y\to\infty} C = 0, \quad 0 \leqslant r < r_3. \tag{5}$$

To solve the equation of convective diffusion for these boundary conditions, use is made of a general method [2] for transforming the convective diffusion equation into one of the heat transfer type.

We introduce the new variables

$$z = \frac{2}{3}\Psi^{3/4}, \quad \xi = \frac{D\gamma}{12} r^3,$$

where Ψ is a function of the field of flow of the rotating disc, and $\gamma = \sqrt{2 \cdot 0{,}51\,\omega}\sqrt[4]{\omega/\nu}$, and reckoning, as was shown in [2], that a change in concentration, with convective diffusion and $D \ll \nu$, proceeds near a solid surface, and simplifying the corresponding expression for Ψ

$$\Psi \simeq \frac{\gamma^2}{4} r^2 y^2,$$

we transform (1) into

$$\frac{\partial^2 C}{\partial z^2} + \frac{1}{3z}\frac{\partial C}{\partial z} = \frac{\partial C}{\partial \xi}. \tag{6}$$

With the new variables, the system of boundary conditions may be written in the form:

Zone 1:

$$\lim_{z\to 0}\left\{-z^{1/3}\frac{\partial C}{\partial z} + h(\xi)\,C(z,\xi)\right\} = g(\xi), \quad 0 \leqslant \xi < \xi_1, \tag{7}$$

where

$$h(\xi) = \frac{1}{\xi^{1/3}}\frac{k}{D\sqrt[3]{\gamma^2/D}}\sqrt[3]{4/9},$$

$$g(\xi) = \frac{1}{\xi^{1/3}}\frac{j_0}{D\sqrt[3]{\gamma^2/D}}\sqrt[3]{4/9}, \quad \xi_1 = \frac{D\gamma}{12} r_1^3.$$

Apart from the boundary condition (7), for the complete system it is necessary to define a boundary condition at infinity. We have, clearly,

$$\lim_{z\to\infty} C(z, \xi) = 0, \quad 0 \leqslant \xi < \xi_1. \tag{8}$$

In the plane (z, ξ), the point z = ξ = 0 is a special point for Equation (6). Writing $z \sim y^{3/2}\,\xi^{1/2}$, we see that the approach of ξ to 0, when $z \neq 0$, involves an unlimited increase in y. Accordingly

$$\lim_{\substack{\xi\to 0\\ z\neq 0}} C(z, \xi) = 0. \tag{9}$$

Zone 2:

$$\left.\begin{aligned} &\lim_{z\to 0}\left\{z^{1/3}\frac{\partial C}{\partial z}\right\} = 0,\\ &\lim_{z\to\infty} C(z, \xi) = 0,\\ &\lim_{\xi\to\xi_1} C(z, \xi) = C(z, \xi_1), \end{aligned}\right\} \quad \xi_1 < \xi < \xi_2. \tag{10}$$

The last condition expresses the continuity of the concentration of intermediate product at the transition from zone 1 to zone 2, not over the whole surface of the disc.

Zone 3:

$$\left.\begin{aligned} &\lim_{z\to 0} C(z, \xi) = 0,\\ &\lim_{z\to\infty} C(z, \xi) = 0,\\ &\lim_{\xi\to\xi_2} C(z, \xi) = C(z, \xi_2), \end{aligned}\right\} \quad \xi_2 < \xi < \xi_3. \tag{11}$$

We see that the solution for each inner zone leads to the solution for the outer zone in the form of a boundary condition.

Equations of type (6) were investigated by Sutton [3]. V. G. Levich and N. N. Meiman [4] used Sutton's method to calculate the convective flow of material to the surface of a plate with nonuniform boundary conditions, similar to the treatment in this paper.

A general solution of the boundary problem may be given in the form of the contour integral:

$$C(z, \xi) = \int (AX_1 + BX_2)\,[Pd\lambda + Qd\mu], \tag{12}$$

where X_1 and X_2 are fundamental solutions of Equation (6):

$$X_{1,2}(z, \lambda, \mu, \xi) = \frac{\lambda^{1/2} z^{1/3}}{2(\xi - \mu)} \exp\left[-\frac{z^3 + \lambda^3}{4(\xi - \mu)}\right] I_{\pm 1/3}\left[\frac{\lambda z}{2(\xi - \mu)}\right]. \tag{13}$$

Here λ and μ are parameters, and the + and − signs refer to X_1 and X_2 respectively. A, B, P and Q, in the integral (12), are some functions of λ and μ. These functions, and also the contour to be integrated in (12), must be selected so that the boundary conditions are fulfilled. $I_{\pm 1/3}$ is a Bessel function of imaginary argument.

The problem is completely solved, but requires cumbersome calculations. These were carried out in [5], but for geometrical conditions somewhat differing from those in [1].

Below is the final expression for the flow density of intermediate product to zone 3, obtained for a ring disc system with $(r_2-r_1) \ll r_2$, $(r_3 - r_2) \ll r_2$ (these are the experimental conditions considered in [1]):

$$j(r) = \frac{0{,}4 j_0}{1 + k\delta / D} \frac{r_1^2 r_2}{r^3} \frac{(1 - {}^3/_4 r_1^3 / r_2^3)^{1/6}}{(1 - r_2^3 / r^3)^{1/6} (1 - {}^3/_4 r_1^3 / r^3)}, \tag{14}$$

where j_0 is the flow density of the starting material to zone 1, and

$$\delta = 1{,}62 (D / \nu)^{1/3} \sqrt{\nu / \omega}.$$

In deriving Equation (14), an approximation function with a Whittaker exponent was used to achieve the quadrature. This gave a value for j(r) about 5% high.

The total flow of particles of intermediate product to zone 3 was obtained by integrating (14) for a ring of thickness (r_3-r_2):

$$J = \frac{0{,}8 [1 - {}^3/_4 r_1^3 / r_2^3]}{1 + k\delta / D} J_0 \int_1^{r_3/r_2} \frac{y^2 dy}{(y^3 - 1)^{1/6} (y^3 - {}^3/_4 r_1^3 / r_2^3)}, \tag{15}$$

where J_0 is the total flow of starting material to zone 1.

It was shown in [1] that Formulas (14) and (15) were in approximate quantitative agreement with experiment and could be used for determining conversion constants, k.

Considerable interest attaches to the more general case, where the particles of intermediate product, B*, undergo conversion in the volume of solution, for example, by interaction with water. We shall return to this in a future paper.

LITERATURE CITED

[1] A. N. Frumkin and L. I. Nekrasov, Proc. Acad. Sci. USSR, 126, No. 1 (1959).*

[2] V. G. Levich, Physicochemical Hydrodynamics (Acad. Sci. USSR Press, 1952).**

[3] W. Sutton, Proc. Roy. Soc. 182, 48 (1943).

[4] V. G. Levich and N. N. Meiman, Proc. Acad. Sci. USSR, 79, 97 (1951).

[5] Yu. B. Ivanov, Dissertation, Moscow Eng.-Phys. Inst. (1958).**

Received April 11, 1959

* See C. B. translation.

** In Russian.

CHEMICAL ENERGY OF SOLVATION OF IONS

I. A. Izmailov

The A. M. Gor'kii Khar'kov State University
(Presented by Academician A. N. Frumkin, February 28, 1959)

The chemical energies of hydration of ions (changes in isobaric potentials) are usually calculated from data on the heats and entropies of the process [1]. Chemical energies of solvation of ions (A_χ) in nonaqueous solvents have not yet been determined. Emf data is normally used to calculate the real energies of hydration of ions (A_r) [2]. $A_r = A_\chi + \varphi ze$, where ze is the charge on the ion. In this paper, consideration is given to calculation of the chemical energies of hydration and solvation of ions from the values for the emf of cells, with and without transport.

According to V. A. Pleskov [3], the emf of a cell with transport, $Pt(H_2) \mid H^+ \parallel Me^+ \mid Me$, is determined by the expression

$$E_0 = \frac{(1/2 D_{H_2} + I_H) - (S_{Me} + I_{Me})}{F} + \frac{A_{x_{H^+}} - A_{x_{Me^+}}}{F}.$$

I have shown that the emf of a cell without transport, reversible to cations and anions, depends on the sum of the chemical energies of solvation of both ions, for example, for the cell $Pt(H_2) \mid H^+ Hal^- \mid AgHal \backslash Ag$ is determined by the expression

$$E_0 = \frac{(1/2 D_{H_2} + I_H) - (S_{Ag} + I_{Ag}) - U_{0AgHal}}{F} + \frac{A_{x_{H^+}} + A_{x_{Hal}}}{F}.$$

Thus, the values of the emf of a cell, with and without transport, may be used to obtain the sum and the difference of the chemical energies of hydration or solvation of ions.

Using emf data for aqueous solutions collected by Bockris and Heringshaw [4], the emf data for cells with transport in nonaqueous solutions of Pleskov [2] and my own emf data for cells without transport in nonaqueous solutions [5], I have calculated the sum ($A_{xH^+} + A_{Hal^-}$) and the difference ($A_{xH^+} - A_{xMe^+}$) of the chemical energies of solvation of the ions, in water, ammonia, methanol, ethanol, and formic acid, and the total chemical energies of solvation of the ions of acid and salt

$$\sum A_{x_{MeHal}} (A_{x_{H^+}} + A_{x_{Hal}}) - (A_{x_{H^+}} - A_{x_{Me^+}}).$$

The values of ΣA_χ for the ions of HCl were also determined in a number of alcohols. For the calculations, use was made of the values for the energies of dissociation D_{H_2} and D_{Hal_2}, of ionization I_H and I_{Me} and of the electronic affinity ϵ_{Hal}, collected by K. P. Mishchenko and É. I. Kvyat [6], and also of the energies of the crystalline lattices U_{0AgHal}, calculated from data on heats and entropies [7]. The total chemical energies of solvation, found in this way for different solvents, were quite comparable with each other, as they were obtained by a single procedure and on the basis of the same type of data required for the calculation. They were also obtained directly from emf measurements, and, therefore, did not contain the errors associated with calculations

TABLE 1

Values of Hydration and Solvation Energies of Ions, Calculated From Emf Measurements, in kcal/g-ion at 25°

Ion	Solvent					
	NH_3	H_2O	H_2O, from [8]	CH_3OH	C_2H_5OH	HCOOH
H^+	281,0	258,0	258,0	253,0	252,0	246,0
Li^+	124,0	117,0	119,0	116,0	115,0	116,0
Na^+	99,0	96,0	95,0	93,0	90,0	99,5
K^+	79,4	78,0	78,0	76,0	73,2	73,9
Rb^+	73,3	74,4	72,0	—	—	73,2
Cs^+	65,6	64,0	64,0	60,4	—	65,0
Ag^+	132,0	112,0	112,0	108,0	108,0	120,8
Ca^{++}	360,0	372,4	373,0	—	—	309,2
Zn^{++}	536,0	492,0	478,0	481,0	473,5	488 3
Cd^{++}	546,0	430,4	423,0	417,0	413,0	410,4
Cl^-	65,5	74,0	80,0	71,0	71,3	78,3
Br^-	62,8	68,0	74,0	67,0	66,2	—
I^-	57,0	59,4	65,0	59,6	58,5	—

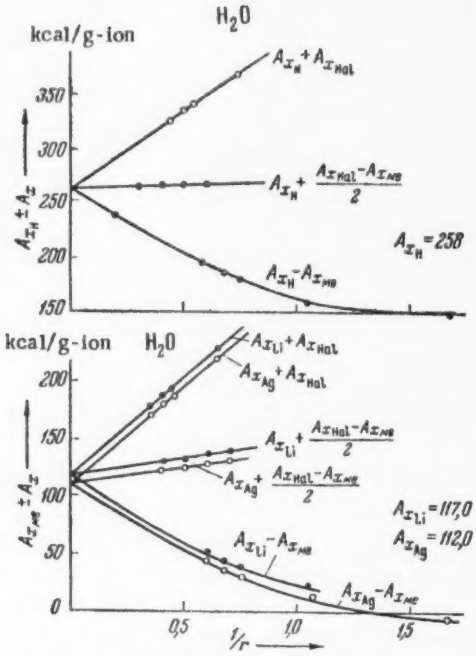

Fig. 1. Determination of the hydration energies of individual ions.

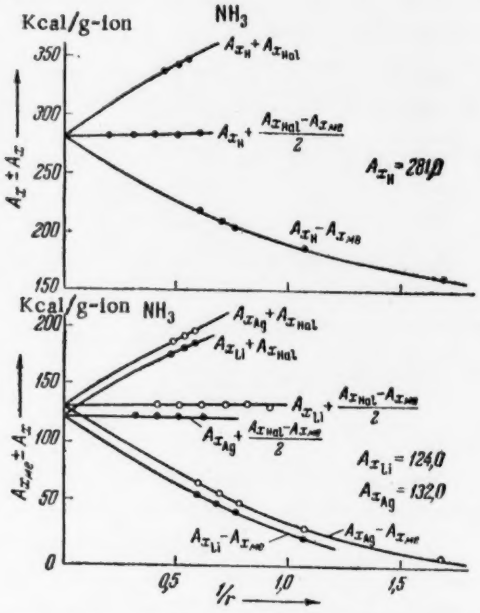

Fig. 2. Determination of the solvation energies of individual ions in ammonia.

based on heats and entropies. The calculated hydration energies were very close to those of Mishchenko [8] (see Table 1). The total energies of solvation of the ions of salts were close to the total hydration energies, falling slightly from water to methanol and ethanol (decrease in dielectric constant), increasing in formic acid and decreasing in ammonia. The greatest differences were observed for the solvation energies of the acid ions.

Special interest attached to determination of the solvation energies of the separate ions in nonaqueous solvents. For this purpose, it was necessary to devise a method of dividing up the total solvation energy, which

TABLE 2

Heats (−ΔH in kcal/g-ion), Energies (−ΔZ in kcal/g-ion) and Entropies (•ΔS in kcal/g-ion•degree) of Solvation of Ions at 25°

Ion	Water			Methanol*			Ethanol		
	ΔH	ΔZ	ΔS	ΔH	ΔZ	ΔS	ΔH	ΔZ	ΔS
Li^+	127,0	117,0	—33,6	127,0	114,0	—43,3	127,0	112,0	—50,0
Na^+	101,0	96,0	—16,8	100,0	90,7	—31,0	99,0	88,4	—35,3
K^+	81,0	78,0	—10,1	—	73,6	—	79,0	71,7	—24,3
Cl^-	84,0	74,0	—33,6	84,0	73,4	—52,0	90,0	72,2	—59,3
Br^-	76,0	68,0	—26,8	79,0	69,4	—32,0	78,0	86,1	—33,0
I^-	66,0	59,4	—22,1	70,0	61,8	—27,3	69,0	60,0	—30,3

*The total heats and energies of solvation in methanol and ethanol were split up according to the Mishchenko rule $\Delta H_{Cs} = \Delta H_I$ and $\Delta Z_{Cs} = \Delta Z_I$.

TABLE 3

Normal Electrode Potentials in Nonaqueous Solvents Referred to the Potential of the Normal Hydrogen Electrode in Water at 25°

Electrode	NH_3	H_2O	CH_3OH	C_2H_5OH	HCOOH
Li^+/Li	—3,24	—2,95	—2,90	—2,79	—2,96
Na^+/Na	—2,85	—2,71	—2,58	—2,43	—2,90
K^+/K	—2,98	—2,92	—2,72	—2,60	—2,85
Rb^+/Rb	—2,98	—2,93	—	—	—2,93
Cs^+/Cs	—2,95	—2,93	—2,95	—	—2,92
Ca^{++}/Ca	—2,64	—2,72	—	—	—2,68
Zn^{++}/Zn	—1,53	—0,76	—0,54	—0,39	—0,73
Cd^{++}/Cd	—1,20	—0,40	—0,23	—0,13	—0,23
H^+/H	—1,00	0	+0,20	+0,25	+0,52
Ag^+/Ag	—0,18	+0,80	+0,96	+1,00	+0,69
I^-/I_2	+0,45	+0,54	+0,56	+0,55	—
Br^-/Br_2	+0,83	+1,07	+1,04	+1,03	—
Cl^-/Cl_2	+1,03	+1,34	+1,32	+1,30	+1,51 (1,40)

would not depend on the conception of solvent structure, and which would be suitable for all the solvents investigated. A method was worked out, depending on extrapolation of the sums and differences of the chemical solvation energies for a given ion with a series of other ions of increasing radius, up to the value 1/r equal to zero (r is the crystallographic radius).

The value of $A_{x_{C^+}} + A_{x_{A^-}}$, at $1/r_{A^-} = 0$, would represent the total solvation energy of the ions of an electrolyte composed of a normal sized cation and an infinitely large anion with the same charge. Since the chemical solvation energy of such a hypothetical anion would be equal to zero ($A_{x_{A^-}} = 0$), the above energy represented the energy of solvation of the cation only. Similarly, $A_{x_{C^+}} - A_{x_{Me^+}}$ at $1/r_{Me^+} = 0$ was equal to the chemical energy of solvation of the cation. For example, if the sum $A_{x_{H^+}} + A_{x_{Hal^-}}$ was plotted as a function of 1/r for the corresponding halogen, and the difference $A_{x_{H^+}} - A_{x_{Me^+}}$ was plotted as a function of 1/r for the corresponding metal (Fig. 1), they both converged in the limit, at 1/r = 0, to the same value of $A_{x_{H^+}}$. Finding the value of $A_{x_{H^+}}$ was made possible by the fact that both functions converged to the same limit. Finding this limit was also facilitated by the construction of a line representing the mean of the sum and difference of energies. This mean line represented the expression $A_{x_{H^+}} + \frac{A_{x_{Hal}} - A_{x_{Me^+}}}{2}$ and approached the limit, i.e., $A_{x_{H^+}}$, considerably more rapidly. The method described could also be used to find the value of A_x for other ions with large solvation energies (Fig. 2). The process was carried out further as follows: $A_{x_{Hal^-}}$ was determined from the values found for A_{xH^+}, A_{xLi^+}, A_{xNa^+} and A_{xAg^+}. The mean of the values for A_{xHal^-} was then used to redetermine A_x for H^+ and the other ions.

The data in Table 1 shows that there were only small differences in the solvation energies of ions in different solvents, of the order of 2-3 kcal/g-ion, i.e., 2-3%. There was only a considerable difference in the case of the proton: this was 35 kcal/g-ion, i.e., about 15%, in changing from ammonia to formic acid (281 kcal/g-ion in ammonia and 246 kcal/g-ion in formic acid). This was due to the difference in basicity of the solvents. Solvent basicity also played an important role in the solvation of the other ions. The solvation energies of all cations were higher in ammonia than in water, and the solvation energies of all anions were less. In water,

and the alcohols, the solvation energies of both cations and anions diminished with decrease in dielectric constant. Differences in the solvation energy of ions, both in a single solvent and in different ones, decreased with increasing ionic radius [3], the smallest difference corresponding to the iodide ion. The marked increases in the solvation energies of the ions of silver, cadmium and zinc in ammonia was associated with complex formation.

The data presented above indicated that solvation energies of ions depend to a slight extent on the structures of the solvent and of their own molecules, and, are probably determined by more general causes than those at present assumed to influence the calculated hydration energies of ions [1, 3, 9].

The values found for the solvation energies of the individual ions in different solvents made it possible to throw light on a number of important problems:

1) Comparison of the energies of solvation ($-\Delta Z$) of ions in alcohols with the heats of solvation ($-\Delta H$), obtained by K. P. Mishchenko [8, 9], showed that these tended to change in opposite ways. The heats of solvation increased through the series water, methanol ethanol, while the energies decreased. Consequently, the entropies, ΔS, decreased more on solvation than on hydration. This was probably because the liquid alcohols have a less ordered structure than water, so that there was a greater difference between the structure of the alcohols in the solvation sheath and in the liquid (see Table 2).

2) The values of the solvation energies of ions in different solvents made it possible to establish a single scale of potentials in nonaqueous solvents, referred to the normal hydrogen electrode in aqueous solution as a single standard. These potentials are shown in Table 3, and it appears that the greatest change is obtained with the hydrogen electrode, whose potential alters by 1.52 v between ammonia and formic acid, while the potentials of the other electrodes do not alter by more than 0.5 v. It is interesting to note that the difference between the potentials of the most electropositive and electronegative electrodes, Li^+/Li and Cl^-/Cl_2, remains practically unchanged in the different solvents: 4.27 in ammonia, 4.296 in water, 4.226 in methanol, 4.1 in ethanol and 4.36 v in formic acid.

3) A knowledge of the solvation energies of ions in water and in nonaqueous solvents makes it possible to construct a single scale of acidity.

LITERATURE CITED

[1] V. E. Conway and J. Bockris, "Solvation of Ions," article in book, Some Problems of Modern Electrochemistry, Moscow (1958).*

[2] O. Klein, and E. Lange, Z. Electrochem, 43, 570 (1937).

[3] V. A. Pleskov, Prog. Chem. 16, 254 (1947).

[4] J. Bockris and J. Heringshaw, Prog. Chem., 20, 246 (1951).

[5] N. A. Izmailov, V. V. Aleksandrov, and E. F. Ivanova, Trans. Chem. and Sci. Research Inst. Chem. 18, 5 (1957).

[6] K. P. Mishchenko and E. I. Kvyat, J. Phys. Chem. 28, 1451 (1954).

[7] A. F. Kapustinskii, J. Gen. Chen. 13, 497 (1948); O. K. Rice, Electronic Structure and the Chemical Bond, IL, 235, 403 (1949).*

[8] K. P. Mishchenko and A. A. Ravdel', Short Handbook of Physicochemical Values, p. 39 (1957).**

[9] K. P. Mishchenko, Acta Physicochim. USSR 3, 693 (1935).

Received February 27, 1959

* Russian translation.

** In Russian.

CATHODIC POLARIZATION IN THE DEPOSITION OF VANADIUM FROM FUSED OXIDES

V. I. Musikhin, O. A. Esin, and B. M. Lepinskikh

Institute of Metallurgy of the Urals Branch of the Academy of Sciences of the USSR

(Presented by Academician A. N. Frumkin, March 4, 1959)

Sakharuk and Vainshtein [1] showed that it was possible to deposit vanadium electrically at a liquid iron cathode, from fused calcium containing V_2O_5. But the kinetics of the electrode processes occurring here have not, hitherto, been investigated. In order to find out the nature of the limiting stage and the charge on the discharging ions, we have investigated cathodic polarization in simple melts.

The method of measurement was similar to that previously described [2, 3]. The cathode was a fused alloy of iron (or copper) with up to 5% of V, and the anode was a platinum wire. The reference electrode was also a platinum wire, passing inside a corundum tube through which oxygen was led continuously. The potential of such an electrode in fused oxides is sufficiently stable and reproducible [4, 5]. The experiments were carried out in an oxidizing atmosphere at 1550-1570°. The cell was normally washed out with electrolyte, after fusion of the iron cathode, in order to remove iron oxide.

Figure 1 shows polarization curves obtained with an Fe, V cathode for two electrolytes: I) 42.5% CaO, 50.0% Al_2O_3 and 7.5% MgO (curves 1 and 2); II) 40.0% CaO, 25.0% Al_2O_3, 28.0% SiO_2 and 7.0% MgO (curves 3 and 4). To these were added 1.5, 3.0, 1.4 and 2.8% of V_2O_5 respectively. The limiting currents (i_l) observed were 0.12, 0.27, 0.16 and 0.27 amp/cm^2, proportional to the V_2O_5 contents of the melts. The first parts of the curves were compared with the equation for concentration polarization:

$$-\eta = -\frac{RT}{nF}\ln\left(1+\frac{i}{i_1'}\right)+\frac{RT}{nF}\ln\left(1-\frac{i}{i_1}\right) \qquad (1)$$

and it was reckoned that the diffusion coefficients in liquid iron were considerably greater than in fused oxides [6], so that $i_l' \gg i_l$, and

$$-\eta \cong \frac{RT}{nF}\ln\left(1-\frac{i}{i_1}\right). \qquad (2)$$

It was found that all the points on these parts of the curves, when plotted in terms of the coordinates η, $\log(1-i/i_l)$, lay on a straight line (Fig. 1, curve 5), with a coefficient of slope $n \cong 5$.

The proportionality of i_l to the V_2O_5 content, and the validity of Equation (2) with $n \cong 5$, showed that reduction of pentavalent vanadium to the metal took place at the cathode

$$V^{5+} + 5e = V. \qquad (3)$$

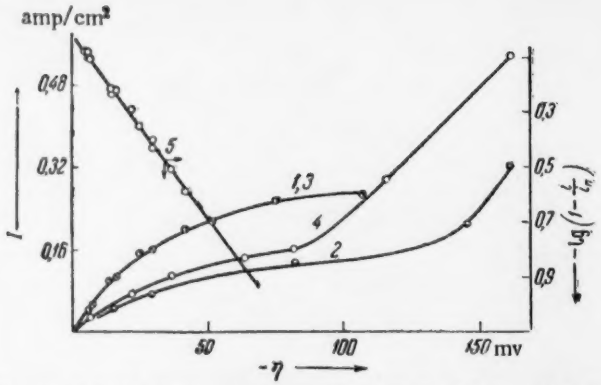

Fig. 1. Polarization curves for melts of $CaO - MgO - Al_2O_3 - SiO_2$ with addition of V_2O_5: 1) and 2) for melts without SiO_2 and with addition of 1.5 and 3.0% V_2O_5; 3) and 4) for melts with SiO_2 and with addition of 1.4 and 2.8% V_2O_5; 5) for the first parts of the curves with coordinates η and $\log (1 - i/i_l)$.

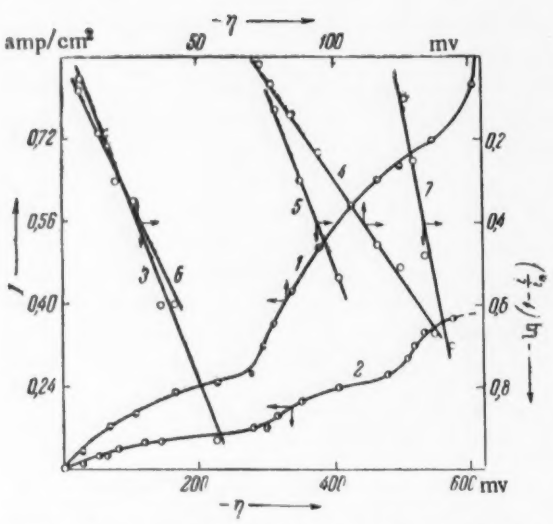

Fig. 2. Polarization curves for melts of $CaO - MgO - Al_2O_3$ with small addition of SiO_2 and V_2O_5. 1) With electrolytes containing no iron; 2) in the presence of FeO and Fe_2O_3; 3), 4), 5), 6) and 7) in terms of coordinates η and $\log (1 - i/i_l)$ for each step (up to the limiting current) for curves 1) and 2) respectively.

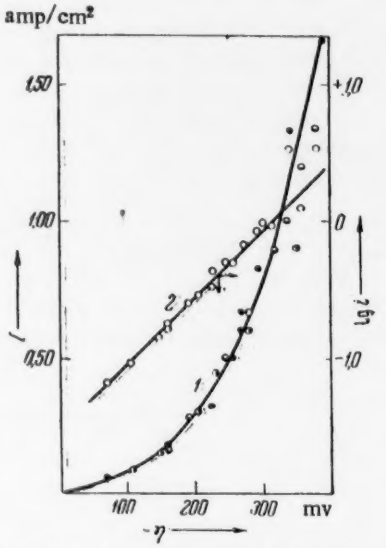

Fig. 3. Polarization curves. 1) For melts of $CaO - MgO - Al_2O_3 - SiO_2$ with large additions of V_2O_5; 2) straight line for the same points with coordinates η and $\log i$.

The rate of the process was accordingly limited by the diffusion of V^{5+} ions.

Judging by the values of the standard isobaric potentials of formation of oxides, from elements, the second step of curve 2 should represent the discharge of aluminum, and of curve 4, silicon. In other words, under our conditions it was possible to have separate deposition of vanadium and silicon. To confirm this, polarization was investigated in melts with small additions of SiO_2 and V_2O_5. Curve 1 of Fig. 2 was obtained at 1550°, with a Cu-V cathode, for a melt containing 40.0% CaO, 50.0% Al_2O_3, 6.0% MgO, 2.0% SiO_2 and 2.0% V_2O_5. This curve 1 had two steps (with i_l = 0.20 and 0.50 amp/cm², which, when plotted in terms of coordinates η and

$\log(1-i/i_l)$, gave the straight lines 3 and 4. The values of n calculated from the slope coefficients were close to five and four respectively. This indicated that the first step corresponded to the process (3), and the second to the discharge of silicon ions:

$$Si^{4+} + 4e = Si. \quad (4)$$

It should be noted that the values of i_l for silicon and vanadium differed by a factor of about 2.5 when their molar concentrations in the melt differed by a factor of 1.5. This indicated that silicon had a somewhat higher rate of diffusion than vanadium.

Previously, with electrolyte of similar composition but without any V_2O_5, limiting currents were not observed even with SiO_2 concentrations up to 10%. They were only observed when B_2O_3 was added. Evidently, in our case the effect of V_2O_5 was similar to that of B_2O_3, since it made it possible to detect the limiting current for the deposition of silicon.

Curve 2 of Fig. 2 was recorded for the same melt, but without washing out the cell with electrolyte after fusion of the iron cathode. This showed three steps, the first two of which were attributed to the presence of iron oxides in the melt. In fact, with coordinates η and $\log(1-i/i_l)$, the corresponding straight lines, 5, 6 and 7, gave coefficients n approximately equal to 1, 2 and 5. In other words, the first, second and third steps corresponded to the processes of reduction of Fe^{3+} to Fe^{2+}, of Fe^{2+} to Fe and of V^{5+} to V. These results are in agreement with previous findings on the behavior of iron oxides in melts of $CaO-MgO-Al_2O_3-SiO_2$ and $MnO-SiO_2$ with cathodes of fused Cu – Fe, Mn – Fe and Mn – Ag – Fe [7, 8].

It should be noted that, in our case, the polarization of iron ions at an Fe – V cathode was unstable and diminished rapidly, probably as the result of establishment of the equilibrium

$$Fe + 2Fe^{3+} = 3Fe^{2+} \quad (5)$$

It might be expected that, with a considerable rise in the V_2O_5 concentration, there would be a large increase in the value of the limiting current and a marked decrease in polarization. But experiments carried out with melts of composition 54% CaO, 23% SiO_2, 14% Al_2O_3 and 9% MgO, with the addition of 15, 19 and 35% of V_2O_5, at Fe – V cathodes, did not show this. It may be seen from Fig. 3 that there was a considerable polarization in this case, not in accordance with Equation (2). A similar phenomenon was observed, previously in the deposition of silicon from melts rich in SiO_2 [2]. In our case, this was probably due to the accumulation of ions of lower valence around the cathode, their diffusion into the electrolyte "surroundings" and oxidation by the gas phase to ions of higher valence. In this case $i_l \gg i$, and the change in the second term of Equation (1) could be neglected. Also, if the initial concentration of ions of lower valence was very small so that $i_l^* \ll i$, then

$$\eta \cong a - \frac{RT}{nF} \ln i. \quad (6)$$

In fact, the points of curve 1 of Fig. 3, when plotted in terms of the coordinates η and log i, gave the straight line 2, with a coefficient n close to two, which corresponded to the discharge process

$$V^{5+} + 2e = V^{3+}. \quad (7)$$

Thus, the deposition of metallic vanadium and the discharge of its ions were limited by the diffusion of the ions in oxide melts. This process took place at a higher positive potential than the liberation of silicon. But, the presence of iron oxides caused a reduction in the vanadium current, because the cathodic reduction of Fe^{3+} and Fe^{2+} occurred considerably more easily.

LITERATURE CITED

[1] S. A. Sakharuk and G. M. Vainshtein, Reports of the Leningrad Inst. Met., No. 15, 26 (1933).

[2] O. A. Esin and L. K. Gavrilov, J. Phys. Chem. 29, 566 (1955).

[3] V. I. Musikhin and O. A. Esin, J. Phys. Chem. 32, 2410 (1958).

[4] R. Didtschenko and E. Rochow, J. Am. Chem. Soc. 76, No. 12 (1954).

[5] L. N. Barmin, O. A. Esin, and S. K. Chuchmarev, Bull. Acad. Sci. USSR, Div. Tech. Sci., No. 9, 114 (1957).

[6] M. Paschke and A. Hartmann, Archiv Eisenhüttenwesen 9, 305 (1955).

[7] O. A. Esin and V. A. Chechulin, J. Phys. Chem. 32, 355 (1958).

[8] O. A. Esin and G. A. Toporishchev, J. Phys. Chem. 31, 474 (1957).

Received March 3, 1959

RELATIONS BETWEEN KINETIC ISOTOPE EFFECTS IN RUPTURE OF THE BONDS $C^{12} - C^{14}$ AND $C^{14} - C^{14}$

A. M. Brodskii, R. A. Kalinenko, and Corresponding Member Acad. Sci. USSR K. P. Lavrovskii

Institute of Oil-Chemical Synthesis of the Academy of Sciences of the USSR

In this paper we describe an investigation of the kinetic isotope effect in the high temperature cracking of a mixture of ethane $C^{12}H_3 - C^{12}H_3$ and doubly labelled with C^{14} ethane $C^{14}H_3 - C^{14}H_3$, and make a comparison with the corresponding effect in the cracking of $C^{14}H_3 - C^{12}H_3$, described in [1]. The reason for this investigation was that, in our previous paper [1] and in a number of other papers on the cracking of $C^{13}H_3 - C_2^{12}H_5$ [2] and $C^{14}H_3 - C_2^{12}H_5$ [3], values were found for the isotope effect exceeding those derived on the basis of present theoretical concepts. According to these concepts [4, 5], at high temperatures, when the relatively insignificant isotopic change in activation energy plays a secondary role, the "kinematic" influence of the change in mass makes the main contribution to the kinetic isotope effect in the case of a monomolecular dissociation reaction. This influence is determined only by the value of the reduced mass corresponding to the vibration frequency of the reacting bond, so that the ratio of the velocity constants $\underline{k}$ and $\underline{k'}$, for the rupture of the bonds $R_1 - R_2$ and $R_1' - R_2'$, with excitation of a single i-th vibration may be represented with good precision* by:

$$\frac{k}{k'} = \frac{k_0}{k_0'} \exp\left[\frac{-(E-E')}{RT}\right] = \sqrt{\frac{m'}{m}} \exp\left\{\frac{1}{RT}\left[\frac{h}{2}(\nu_i^0 - \nu_i^{0'}) - \Delta E_i^*\right]\right\} \cong$$

where

$$\cong 1 + \alpha\left(1 + \frac{C}{T}\right) \geqslant 1 + \alpha, \tag{1}$$

$$\alpha = \sqrt{\frac{m'}{m}} - 1 \ll 1,$$

$$\Delta E_i^* = E_i^* - E_i^{*'}; \quad C = \frac{1}{R}\left(\frac{h\nu_i^0}{2} - \frac{1+\alpha}{\alpha}\Delta E_i^*\right) \leqslant \frac{1}{R}\,\frac{h\nu_i^0}{2}; \tag{2}$$

ν_i^0 and $\nu_i^{0'}$ are the characteristic frequencies in the unexcited state; E^{*} and $E^{*'}$ are the energies of the excited (activated) states preceding rupture; $\underline{m}$ and m' are the reduced masses for normal vibrations corresponding to the bonds to be ruptured. The parenthesis mark after a symbol denotes the isotopically labelled molecule.

It is clear from Equation (1) that, at high temperatures, the main part of the kinetic isotope effect, as expressed by the difference $k/k' - 1$, is proportional to α. In particular, the relative change in frequency of rupture of the carbon-carbon bond should not amount to 8%, as found for the cracking of propane [2, 3], nor to 12%, as found for ethane [1], but, only to about 4% for rupture of the $C^{12} - C^{14}$ bond and 2% for rupture of the $C^{12} - C^{13}$ bond.

A possible explanation [1] of the anomaly of the large value of this effect and of the fact that it is approximately the same for rupture of the $C^{12} - C^{13}$ and $C^{12} - C^{14}$ bonds, is, as we reckon, that, in the case of a

*Equation (1) can be generalized without difficulty to the case of participation of several bonds in the reaction (normal vibrations).

TABLE*

Ethylene content of cracked gas in volume %	Activity	
	CH_4 as % of $\frac{1}{2}$ A	C_2H_4 as % of A
9.3	–	97 ± 1
12.7	94 ± 2.5	–
15.3	95 ± 1	97.9 ± 0.5
24.9	95 ± 1.5	97.8 ± 1

*The ethylene content of the cracked gas characterized the extent of conversion. A detailed composition of the cracking products is given in [7].

hydrocarbon molecule possessing a plane of symmetry perpendicular to the direction of the chain, or a rotational axis of symmetry corresponding to a mirror image [6], the introduction of a labelled carbon atom into the carbon skeleton disturbs the symmetry. This circumstance may have an essential effect on the rate of rupture of the bond, since the existence of an additional plane of symmetry, or of a mirror rotational axis, will cause a definite restriction on the possibility of transfer from the original to the final or activated state. On the other hand, the wave function of the $C^{12}H_3-C^{14}H_3$ molecule possesses no such uniformity (symmetrical properties) in the sense stated above, so that no such restrictions exist for this molecule*. In a similar way, a change in the isotopic composition of a hydrocarbon may lead to a considerable kinetic effect in the transition from a "symmetrical" to an "asymmetrical" molecule.

In this connection, a study of the kinetic isotope effect in the cracking of a mixture of the ethanes $C^{12}H_3-C^{12}H_3$ and $C^{14}H_3-C^{14}H_3$ should serve as an experimental check on the above hypothesis, since in this case, introduction of the isotope does not affect the symmetry. Also, the nuclei C^{12} and C^{14} both possess zero spin. Then, according to Equation (1), the isotope effect should be about half as great for the rupture of $C^{12}-C^{14}$ as for that of $C^{14}-C^{14}$. On the other hand, according to the hypothesis developed above, the effect should be greater for the cracking of $C^{12}H_3-C^{14}H_3$ than for $C^{14}H_3-C^{14}H_3$.

The investigation was carried out, at 850°, at a pressure of 94 ± 2 mm, by the method previously described [1, 7], in a reactor with practically complete mixing. The starting mixture of $C^{12}H_3-C^{12}H_3$ and $C^{14}H_3-C^{14}H_3$ had an activity A=1.1 × 10^4 counts/minute · cm^3**. The results obtained for the activities of the methane and ethylene formed are shown in Table 1.

Since the relative molar concentration of radioactive ethane in the starting gas was very small (~ 10^{-4}), the difference between the activity of the methane, A^{CH_4}, and $\frac{1}{2}$ A gave directly the value of the kinetic isotope for rupture of the C – C bond.

In a reactor with complete mixing, and with not too high a degree of conversion***

$$\frac{[C^{14}H_4]}{[C^{12}H_4]}=\alpha\frac{2k'}{2k}\frac{[C^{14}H_3C^{14}H_3]}{[C^{12}H_3C^{12}H_3]}=\frac{1}{2}\frac{\beta k'}{k}A, \qquad (3)$$

*It should be noted that the quantitative appraisal of this symmetry effect requires specialized consideration.

**The starting mixture was practically free from $C^{14}H_3-C^{12}H_3$.

***The same final equation as (3) held for the cracking of $C^{14}H_3-C^{12}H_3$, namely

$$\frac{[C^{14}H_4]}{[C^{12}H_4]}=\alpha\frac{k'[C^{12}H_3C^{12}H_3]}{2k[C^{12}H_3C^{12}H_3]+k'[C^{12}H_3C^{14}H_3]}\cong\beta\frac{1}{2}\frac{k'}{k}A.$$

where α and β are proportionality coefficients.

Hence

$$\frac{k'}{k} = \frac{\beta^{-1}\,[C^{14}H_4]}{{}^1/_2 A\,[C^{12}H_4]} = \frac{A^{CH_4}}{{}^1/_2 A}\,. \tag{4}$$

The experimental results given in Table 1 show that the kinetic isotope effect for methane, in the formation of methane from $C^{14}H_3 - C^{14}H_3$, was 5 ± 1%, considerably less than the value of 12 ± 2% found previously for the cracking of $C^{14}H_3 - C^{12}H_3$ [1]. It should be noted that, in both cases, the measurements were carried out under the same conditions and by the same method. Allowing for the fact that the natural $C^{12} - C^{12}$ ethane contained about 15% of $C^{12} - C^{13}$ ethane as an impurity, the value of the effect observed (5 ± 1%) agreed well with that calculated (~ 6.5%) from Equation (1), putting C = O. It should be noted that the relatively high isotope effect for ethylene (~ 2%) exceeded the corresponding value, obtained from Equation (1), for rupture of the C – H bond (~ 3%).

The experimental results obtained showed the existence of a linear proportionality between the kinetic isotope effect and the reduced mass, and confirmed the above hypothesis as to the effect of destruction of the symmetry of the molecule on the reaction rate.

The results of the experiments with $C^{14}H_3 - C^{14}H_3$ showed that

$$\frac{C}{T} \leqslant 0{,}01. \tag{5}$$

From the nonidentity (5) and Equation (2) it follows that

$$\frac{\nu^0_{C-C} - \dfrac{\Delta E^*\,(1+\alpha)}{\alpha}}{\nu^0_{C-C}} < \frac{2\cdot 10^{-2}\,RT}{h} \simeq 0{,}05.$$

This analysis shows that the isotopic shift of the vibration energy in the excited state is close to the value of the shift in the original state. It should be especially noted that the above results explain the possibility of an indirect effect of different nuclear states on the rates of the molecular reactions included in cracking.

In conclusion the authors wish to express their thanks to N. D. Sokolov for his valuable advice.

LITERATURE CITED

[1] A. M. Brodskii, R. A. Kalinenko, and K. P. Lavrovskii, Proc. Acad. Sci. USSR 124, No. 2 (1959).*

[2] D. P. Stevenson and C. D. Wagner, et al., J. Chem. Phys. 16, 993 (1948).

[3] H. M. Frey, C. J. Danby, and C. Hinshelwood, Proc. Roy. Soc. 234, No. 1198, 301 (1956).

[4] J. Bigeleisen and M. G. Mayer, J. Chem. Phys. 15, 261 (1947); J. Bigeleisen, J. Chem. Phys. 17, No. 3, 344 (1949).

[5] S. Z. Roginskii, Theoretical Basis of Isotopic Methods for Investigating Chemical Reactions (Acad. Sci. USSR Press (1956); V. N. Kondrat'ev, Kinetics of Gas Reactions, (Acad. Sci. USSR Press, 1958).* *

[6] L. Landau and E. Lifshits, Quantum Mechanics (1948).* *

[7] A. M. Brodskii, R. A. Kalinenko, K. P. Lavrovskii, and V. B. Titov, Proc. Acad. Sci. USSR 116, No. 5, 789 (1957).* * *

Received April 10, 1959

* See C. B. translation.

* * In Russian.

* * * Original Russian pagination. See C. B. translation.

ANODIC DISSOLUTION OF GERMANIUM

Yu. A. Vdovin, Corresponding Member Acad. Sci. USSR
V. G. Levich and V. A. Myamlin

Institute of Electrochemistry of the Academy of Sciences of the USSR

The electrochemical properties of semiconductors have been little investigated. Some investigations have been published on the properties of the contact between germanium and electrolyte [1-4]. These papers contain some inconsistencies, and the experimental results do not enable us to obtain a clear picture of the nature of the anodic dissolution of germanium. It has been established that a saturation current may be observed in the dissolution of n-type germanium, but, that there is no saturation current with p-type germanium.

In both cases, with currents considerably below the saturation current for n-type germanium, a linear relation is observed between the potential and the logarithm of the anode current density. It has also been established that holes are necessary for the primary electrochemical reaction at the electrode. In the present paper, we have attempted a quantitative analysis of the dissolution process.

We formulate basic equations describing the process in the body of the semiconductor. The equations for n-type germanium may be conveniently written in dimensionless form; they are

$$dz/dt = zy + \lambda_-; \tag{1}$$

$$dp/dt = -py - \frac{1}{K}(\lambda - \lambda_-); \tag{2}$$

$$d\lambda_-/dt = A(p - b); \tag{3}$$

$$dy/dt = z - p - 1, \tag{4}$$

where we have introduced the notation: $t = \varkappa x$; $\varkappa = \sqrt{\frac{4\pi e^2 N_-}{\varepsilon KT}}$; $y = \frac{e}{KT\varkappa}\frac{d\varphi}{dx} = \frac{d\psi}{dt}$;

$$z = \frac{n_-}{N_-}; \quad p = \frac{n_+}{N_-}; \quad \lambda_- = \frac{j_-}{u_- N_- KT\varkappa}; \quad \lambda = \frac{j_+ + j_-}{j_\lambda} = \frac{j}{KT\varkappa u_- N_-}; \quad K = \frac{u_+}{u_-};$$

$$b = \frac{n_i^2}{N_-^2}; \quad D_+ = \frac{KT}{e}u_+; \quad D_- = \frac{KT}{e}u_-; \quad A = \frac{D_+}{D_- L^2 \varkappa^2}.$$

Here D_- and D_+ denote the diffusion coefficients of electrons and holes; u_- and u_+ are the corresponding mobilites; n_- and n_+ are the concentrations of free electrons and holes; j_- and j_+ are the electric current densities of electrons and holes; φ is the potential of the electric field; N_- is the concentration of donor levels; e is the electronic charge; n_i is the concentration of electrons in the semiconductor itself; ϵ is the dielectric permeability of germanium; $n_+(\infty)$ is the concentration of holes at $x \to \infty$; L is the diffusion length of the minority carriers. Further details of these equations are considered in [5]. Equation (4) is the normal Poisson equation, in which it is assumed that the donor level is completely ionized.

To solve the problem of the anodic dissolution of germanium, we assume that the voltage gradient in the electrolyte can be neglected, except for that in the Helmholtz double layer. It is also assumed that the change in concentration of ions at the electrode surface is inconsiderable.

A number of authors consider [1, 6] that the reaction at the germanium surface is:

$$Ge + 2e^+ + 2OH^- \rightarrow Ge(OH)_2^{++} + 2e^-, \tag{5}$$

i.e., that two holes are absorbed, in the reaction and two electrons are freed. On the other hand, Flynn [4] considers the possibility of another reaction, which requires one hole and frees three electrons. For this series of calculations, we will suppose that r holes are absorbed and m electrons freed. In conformity with [7, 8], the boundary condition is written in the form

$$\lambda = -\lambda_0 \frac{p^r_k}{(p^0_k)^r} e^{\beta(\Delta\Psi - \Delta\Psi_0)}. \tag{6}$$

Here λ_0 is the exchange current for the given reaction; p_k and p°_k are the concentrations of holes at the surface of contact for the current λ and at equilibrium ($\lambda = 0$); $\Delta\Psi$ and $\Delta\Psi_0$ are the potential changes in the Helmholtz layer for current λ and at equilibrium ($\lambda = 0$). Since the reaction requires r holes, the concentration p_k must be raised to the r-th power.

The electron and hole currents at the interface are connected by the relation

$$\lambda_+(0)/\lambda_-(0) = r/m. \tag{7}$$

The plane $x = 0$ is taken as the interface. We further reckon that the electrolyte is located in the region $x < 0$ and the semiconductor where $x > 0$. Therefore, for the anode process, j is always < 0.

The relation (7) will be upset if there is any recombination on the surface of the semiconductor. If the recombination current is taken into account, the relation may be rewritten in the form:

$$\frac{\lambda_+(0) - \lambda_{+\text{rec}}}{\lambda_-(0) - \lambda_{-\text{rec}}} = \frac{r}{m}; \tag{8}$$

$$-\lambda_{+\text{rec}} = +\lambda_{-\text{rec}} = c_0(z_k p_k - b); \tag{9}$$

c_0 is the constant for surface recombination. At the boundary between Helmholtz double layer and the semiconductor we also require equality of the inductions

$$D_{2n} = D_{1n}. \tag{10}$$

In order to solve Equations (1) – (4) it is necessary to formulate boundary conditions at infinity. Reckoning that $b \ll 1$ ($b \sim 10^{-4}$), this condition may be written in the form

$$z(\infty) = 1; \quad p(\infty) = b; \quad \lambda_-(\infty) = \lambda(1 - kb); \quad y_\infty = -\lambda[1 + b(k+1)]. \tag{11}$$

The set of equations (1) – (4) cannot be solved exactly. We have solved the equations approximately, dividing the space into three regions. The first region, called the quasi-neutral, is located far enough from the interface for the effect of the latter to be neglected; the change in electron concentration is not large in this region. In the two other regions there is a space charge, dependent on the contact with the electrolyte. We will suppose, in conformity with [1, 6], that n-type germanium is enriched with holes in the equilibrium precontact region, and is consequently deficient in electrons. It is therefore, reasonable to suppose that, in the second region adjacent to the quasi-neutral one the conditions $z \ll 1$ and $p \ll 1$ are fulfilled; finally, in the third precontact region, $p \gg 1$ and $z \ll 1$.

Supposing that $z = 1 + \alpha$ for the quasi-neutral region, where $\alpha \ll 1$, the set of equations (1) – (4) may be rewritten in the form:

$$d\alpha/dt = y + \lambda_-; \tag{1'}$$

$$dp/dt = -\frac{1}{K}(\lambda - \lambda_-); \tag{2'}$$

$$d\lambda_-/dt = A(p - b); \tag{3'}$$

$$dy/dt = \alpha - p. \tag{4'}$$

In Equation (2') we omit the term py, since everywhere in this region it is of the order of magnitude, $b\lambda$; at the same time, as will be seen later $\frac{1}{K}(\lambda - \lambda_-)$ alters from $b\lambda$ to a value of the order λ.

Eliminating the variable t from the set of equations (1') – (4'), we can find the concentration of holes, p, as a function of λ_+:

$$p = b + \lambda_+/\sqrt{AK}. \tag{12}$$

Changes in z and y can be neglected in this region.

The second region is so narrow (in comparison with the diffusion length of the minority carriers) that recombination in it can be neglected. The same may be said of the third region. In the second region, equations corresponding to (3) and (4) will have the form:

$$d\lambda_-/dt = 0; \quad dy/dt = -1. \tag{13}$$

The solution of these equations can be written in the form

$$p = e^{y^2/2}\left[c_1 - \frac{1}{K}(\lambda - \lambda_-)\int_0^y e^{-y^2/2}dy\right], \quad z = e^{-y^2/2}\left[c_2 - \lambda_- \int_0^y e^{y^2/2}dy\right]. \tag{14}$$

The constants c_1 and c_2 are determined by combination with the solutions for the quasi-neutral region. For this, it is necessary to appreciate that, in virtue of (13), $\lambda_- = \lambda_-(0)$ at the boundary of the quasi-neutral region. Neglecting small terms, we obtain for the constants c_1 and c_2:

$$c_1 = b + \frac{1}{\sqrt{AK}}\lambda_+(0), \quad c_2 = 1. \tag{15}$$

In the third region, $\frac{1}{K}\lambda_+$ in Equation (2) can be neglected in comparison with py. In Equation (4), unity and the concentration of electrons, z, can be omitted in comparison with p. The solution has the form:

$$z = \frac{c_3 - \lambda_- y}{y^2/2 + c_4}, \quad p = y^2/2 + c^4. \tag{16}$$

The constants are determined by overlapping with the previous region at the plane p = 1:

$$c_3 = b\left(1 + \frac{\lambda_+(0)}{b\sqrt{KA}}\right) + \lambda_-(0)\sqrt{-2\ln\left(b + \frac{\lambda_+(0)}{\sqrt{KA}}\right)},$$
$$c_4 = -2\ln\left(b + \frac{\lambda_+(0)}{\sqrt{KA}}\right). \tag{17}$$

The potential drop in the semiconductor and the Helmholtz layer, ψ, is given by $\psi = \psi_1 + \psi_2 + \psi_3 + \Delta\psi$. Here, ψ_1, ψ_2, ψ_3 are the potential drops in the respective regions of the semiconductor, and $\Delta\psi$ is the potential drop in the Helmholtz layer. It follows from (10) that $\Delta\psi = y_k t_0$, where y_k is the value of y at the interface; $t_0 = d\kappa\epsilon/\epsilon_1$, where d is the thickness and ϵ_1 is the dielectric permeability of the Helmholtz layer. Thus, since we are not interested in the ohmic potential drop, and the field alters little in the quasi-neutral region the value of ψ_1 can be neglected. The other potentials are:

$$\Psi_2 = \int y\,dt = \int_{y'}^{y''} y\,\frac{dt}{dy}\,dy = -\ln\left[b + \frac{\lambda_+(0)}{\sqrt{KA}}\right]; \tag{18}$$

$$\Psi_3 = \int y\,dt = \int_{p_k}^{1} y\,\frac{dt}{dp}\,dp = \ln p_k. \tag{19}$$

We find the value of p_k by assuming that the original enrichment, p_k^0, of holes in the precontact region is so large that $p_k \gg 1$. Introducing the voltage-current characteristic, we write $y_k t_0 > 1$. Under these conditions, in Equation (6), the change in the preexponential factor can be neglected in comparison with the change in the exponent. Reckoning that $\Delta\Psi = y_k t_0$, we find from (6) that

$$y_k = y_k^0 + \frac{1}{\beta t_0}\ln\frac{-\lambda}{\lambda_0}. \tag{20}$$

The voltage-current characteristic can now be obtained:

$$\Psi = y_k^0 t_0 + \frac{1}{\beta}\ln\frac{-\lambda}{\lambda_0} + \ln\left[\frac{1}{2}\left(y_k^0 + \frac{1}{\beta t_0}\ln\frac{-\lambda}{\lambda_0}\right)^2\right] - \ln\left(b + \frac{\lambda_+(0)}{\sqrt{KA}}\right), \tag{21}$$

where, as follows from (8), (9), and (16), $\lambda_+(0)$ has the form

$$\lambda_+(0) = \lambda\,\frac{\frac{r}{m+r} + C_0 y_k}{1 + \frac{C_0}{\sqrt{KA}} + y_k C_0}. \tag{22}$$

It is obvious from (21) that the third and fourth terms alter very little up to currents close to the saturation current. There is thus, a logarithmic relation between potential and current.

The saturation current is given implicity by the equation

$$j_{sat} = -\frac{n_i^2 D_+ e^2 u_- \frac{\rho}{L}\left[1 + C_0'\frac{\varepsilon}{4\pi}\frac{|E_k^0|}{eD_-} + C_0'\frac{\varepsilon_1}{\beta 4\pi e u_-}\ln\frac{|j_{sat}|}{j_0}\right] + eC_0' n_i^2}{\frac{r}{r+m} + C_0'\frac{\varepsilon}{4\pi}\frac{|E_k^0|}{eD_-} + C_0'\frac{\varepsilon_1}{\beta 4\pi e u_-}\ln\frac{|j_{sat}|}{j_0}}. \tag{23}$$

Here C'_0 is the constant of surface recombination, which can be obtained from (9), if rewritten in dimensional form. If it is reckoned that the value of C'_0 is only of an order of magnitude less than in the system germanium – – gas [9], i.e., $C'_0 = 6 \cdot 10^{-13}$ cm^4/second, then, all the terms containing C'_0 in Equation (23) can be neglected. The saturation current then becomes

$$j_{sat} = -n_i^2 D_+ e^2 u_- \frac{\rho}{L}\left(1 + \frac{m}{r}\right) \tag{24}$$

where ρ is the specific resistance.

Comparing Equation (24) with the results of Flynn [4], who considered that surface recombination was unimportant in his experiments, we find the relation $m/r = 3$. This means that the reaction on the surface of the electrode consumes one hole and frees three electrons. It is possible that other values of the current amplification, obtained for example, in [2, 10], depend on the influence of surface effects. This means that it is not always permissible to ignore terms containing C'_0 and C'_0/E_k^0 in Equation (23).

A logarithmic relation between potential and current, at currents considerably below saturation, has been recorded in a number of papers [1, 3]. The experimental results are in agreement with those predicted by Equation (21) with the condition that $\beta = \frac{1}{2}$.

It is possible to derive the voltage-current characteristic for p-type germanium by similar means. The relation between voltage and current is again given by Equation (21), but, without the last term, leading to saturation in n-type germanium.

LITERATURE CITED

[1] D. Turner, J. Electrochem. 103, 252 (1956).

[2] W. Brattain and G. Garrett, Bell. Syst. Techn. J. 34, 129 (1955).

[3] E. A. Efimov and I. G. Erusalimchik, J. Phys. Chem. 32, 413, 1103 (1958).

[4] J. B. Flynn, J. Electrochem. 105, 715 (1958).

[5] K. V. Tolpygo and I. G. Zaslavskaya, J. Tech. Phys. 25, 995 (1955).

[6] K. Bohenkamf and H. J. Emgell, Zs. F. Electrochem. 61, 1184 (1957).

[7] Yu. A. Vdovin, V. G. Levich and V. A. Mamlin, Some Problems in Theoretical Physics, Moscow, (1958).*

[8] Yu. A. Vdovin, V. G. Levich, and V. A. Mamlin, Proc. Acad. Sci. USSR 124, 350 (1959).**

[9] W. H. Brattain and J. Bardeen, Bell. Syst. Techn. J. 32, 1 (1953).

[10] H. Gerischer and F. Beck, Zs. phys. Chem. 13, 389 (1957).

Received April 9, 1959

* In Russian.

** Original Russian Pagination. See C. B. translation.

THE ROLE OF SALT FORMATION IN ACID-CATALYZED PROCESSES
KINETICS OF THE HYDROLYSIS OF CYCLOHEXANONE OXIME

M. I. Vinnik, N. G. Zarakhani, I. M. Medvetskaya, and
N. M. Chirkov

(Presented by Academician V. N. Konrat'ev, February 26, 1959)

The hydrolysis of amides and oximes is accelerated by acids and bases. In the case of the acid hydrolysis of these substances, an anomalous relation has been observed between the reaction velocity and the acidity of the medium. For instance, in the hydrolysis of acetamide [1], thioacetamide [2], the amide of propionic acid [3] and acetoxime [4], the rate first rises with increasing concentration of the acid catalyst (HCl) to a definite value and then falls. To explain this phenomenon, it has been assumed [2] that the limiting stage of the hydrolysis is a bimolecular reaction between a protonized molecule of the reagent and water:

$$RCONH_2 + H^+ \rightleftarrows R\overset{+}{C}ONH_3; \tag{1}$$

$$R\overset{+}{C}ONH_3 + H_2O \rightleftarrows M^* \xrightarrow{k_{true}} \text{hydrolysis product} \tag{2}$$

According to this mechanism, the observed velocity constant, k_{ef}, will be:

$$(k_{ef})_{bim} = k_{true}\frac{k_B a_{H^+}}{1 + k_B h_0}\frac{f_B f_{H_3O}}{f_{M^*}} = k_{true}k_B\frac{C_{H_3O^+}}{1 + k_B h_0}\frac{f_B f_{H_3O^+}}{f_{M^*}}f_{H_2O}, \tag{3}$$

where h_0 is the acidity of the medium; f_B, f_{M^*} and $f_{H_3O^+}$ are the activity coefficients of the nonprotonized reagent, the active complex and the oxonium ion respectively.

According to the above mechanism, the observed fall in velocity constant at high acidity of the medium would be expected with considerable protonization of the reagent ($k_B h_0 \gg 1$), when h_0 increases more rapidly than the concentration of hydroxonium ions ($C_{H_3O^+}$), if the activity coefficient function, $f_B f_{H_3O^+} f_{H_2O}/f_{M^*}$ does not alter much. But, it is not possible to explain, by this mechanism, the regularity of the hydrolysis of amides and oximes over a wide range of concentration of the acid catalyst.

It appeared to us that the observed relation, between the velocity constants for the hydrolysis of amides and oximes and the acidity of the medium, could be explained quantitatively if it was assumed that the protonized form of the reagent was capable of forming an undissociated salt with the anion of the acid.

In order to elucidate the role of salt formation in acid processes, we investigated the hydrolysis of the oxime of cyclohexanone under the catalytic influence of hydrochloric acid. The kinetics of the process were studied spectrophotometrically by the decrease in optical density of a solution of cyclohexanone oxime in hydrochloric acid at 222 mμ.

The oxime concentration in the acid was from $2 \cdot 10^{-4}$ to $1 \cdot 10^{-3}$ mole/liter. The process was practically irreversible with HCl concentrations above 0.1 M; but, it was reversible in more dilute HCl solutions. Solutions of the reaction product, cyclohexanone, in HCl did not absorb at 222 mμ. It was therefore possible to determine

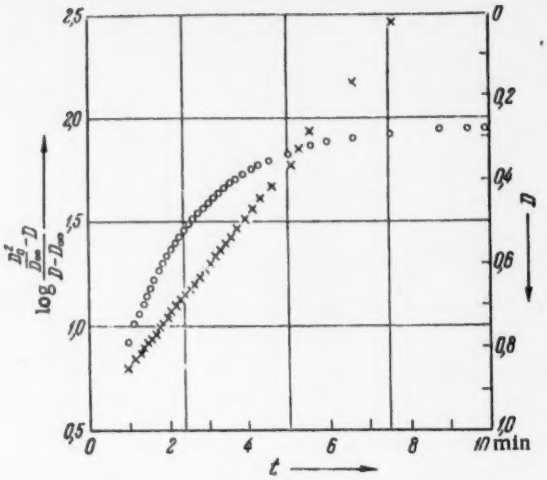

Fig. 1. Kinetic curve and its logarithmic anamorph for the hydrolysis of cyclohexanone oxime in a hydrochloric acid medium.

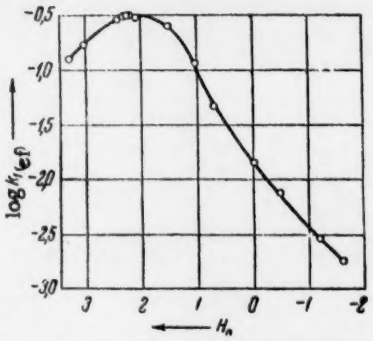

Fig. 2. Logarithm of velocity constant of hydrolysis of cyclohexanone oxime as function of acidity of medium.

the ratio of the equilibrium concentrations of oxime and cyclohexanone from the values of the initial optical density of the solution, D_0, and the optical density at the end of the process, D_∞. The reaction was monomolecular with respect to oxime. When the reaction was sufficiently reversible, the kinetic curves could be expressed by an equation which took into account the monomolecular hydrolysis of the oxime and a bimolecular process for the formation of oxime from cyclohexanone and hydroxylamine.

TABLE 1

Velocity Constants for the Hydrolysis of Cyclohexanone Oxime, k_{ef}, and the Reverse Reaction, k_2, for Different Concentrations of Hydrochloric Acid, at T = 25°

HCl molality	k_{ef}, min^{-1}	k_2, liters/mole · min	H_0	$\lg a_{HCl}$	$\log k_{ef} \times \frac{a_{HCl}}{h_0}$
$5 \cdot 10^{-4}$	0,125	925	3,30	−6,60	—
$9{,}3 \cdot 10^{-4}$	0,171	614	3,03	−6,06	—
$3{,}71 \cdot 10^{-3}$	0,291	246	2,43	−4,86	—
$4{,}65 \cdot 10^{-3}$	0,330	181	2,33	−4,66	—
$5{,}57 \cdot 10^{-3}$	0,330	190	2,25	−4,50	—
$6{,}52 \cdot 10^{-3}$	0,330	81	2,19	−4,38	—
$8{,}54 \cdot 10^{-3}$	0,307	—	2,10	−4,22	—
$4{,}64 \cdot 10^{-2}$	0,159	—	1,49	−2,81	−2,12
$9{,}3 \cdot 10^{-2}$	0,112	—	1,05	−2,23	−2,13
0,245	$4{,}57 \cdot 10^{-2}$	—	0,68	−1,43	−2,09
0,927	$1{,}41 \cdot 10^{-2}$	—	−0,03	−0,27	−2,15
1,940	$7{,}25 \cdot 10^{-3}$	—	−0,475	0,575	−2,02
4,63	$2{,}82 \cdot 10^{-3}$	—	−1,16	1,70	−2,01
5,43	$1{,}82 \cdot 10^{-3}$	—	−1,605	2,32	−2,02

Note. The values of a_{HCl} are taken from the book [5] and the values of H_0 from [6].

Fig. 1 shows a typical kinetic curve (relation between changing optical density, D, and time, t,) and its logarithmic anamorph (relation between $\log[(D_0^2/D_\infty - D)/(D_0 - D_\infty)]$ and t, where the process is considered to be reversible.

Table 1 and Fig. 2 show the experimental data obtained, from which it is evident that the hydrolysis velocity constant, k_{ef}, passed through a maximum with changing concentration of HCl. The relation

$$k_{ef}\frac{a_{HA}}{h_0} = \text{const.} \qquad (4)$$

was valid for HCl concentrations above 0.05 M.

If the ionized form of the oxime is in equilibrium with its salt:

$$\overset{+}{R}NOH_2 + A^- \rightleftarrows \overset{+}{R}NOH_2 \cdot A^-$$
(salt),

then, in the general case, the reacting substance will exist in solution in three forms: un-ionized RNOH, ionized $RNOH_2^+$ and salt. The relation between the concentrations of these forms is determined by the acidity of the medium, h_0, and the activity, a_{A^-}, of the anion of hydrochloric acid. Denoting the ionization constant by $k_B = a_{RNOH} a_{H^+}/a_{\overset{+}{R}NOH_2}$ and the constant for salt formation by $k_c = a^+_{RNOH_2} a_{A^-}/a_{salt}$, we can express the

concentration of the ionized form of the oxime as follows:

$$C_{RNOH_2^+} = \frac{C_0}{1 + k_B \frac{f_{RNOH_2^+}}{a_{H^+} f_{RNOH}} + a_{A^-} \frac{f_{RNOH_2^+}}{k_c f_{salt}}} = \frac{C_0}{1 + \frac{k_1}{h_0} + \frac{a_{HA}}{k_c h_0} \frac{f_{RNOH}}{f_{salt}}}, \quad (5)$$

where $a_{HA} = a_H + a_{A^-}$ is the thermodynamic activity of the acid and $C_0 = C_{RNOH} + C_{RNOH_2^+} + C_{salt}$.

The ratio of the activity coefficients of the two uncharged particles, oxime f_{RNOH} and salt f_{salt}, should clearly not alter with the concentration of acid. Putting $k_c f_{salt}/f_{RNOH} = k'_c$, we have

$$C_{BH^+} = \frac{C_0}{1 + \frac{k_B}{h_0} \frac{a_{HA}}{k'_c h_0}}. \quad (6)$$

Two variants – monomolecular and bimolecular – can be imagined for the limiting stage of the hydrolysis. If the limiting stage is assumed to be a monomolecular process of isomerization of the ion:

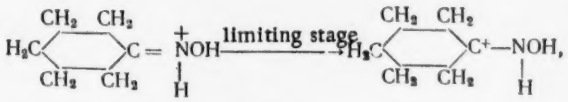

then the effective velocity constant will be given by the equation

$$k_{ef} = k_{true} \frac{1}{1 + \frac{k_B}{h_0} + \frac{a_{HA}}{k'_c h_0}} \frac{f_{BH^+}}{f_{M^*}}. \quad (7)$$

If the limiting stage is assumed to be a bimolecular reaction between the ion $RNOH_2^+$ and a molecule of water, then

$$k_{ef} = k_{true} \frac{1}{1 + \frac{k_B}{h_0} + \frac{a_{HA}}{k'_c h_0}} \frac{a_{H_2O} f_{BH^+}}{f_{M^*}}. \quad (8)$$

For the monomolecular mechanism, the activated complex does not differ in composition from the protonized form of the oxime, and their activity coefficients should be the same. Putting $f_{BH^+} = f_{M^*}$, we obtain

$$k_{ef} = \frac{k_{true}}{1 + \frac{k_B}{h_0} + \frac{a_{HA}}{k'_c h_0}}. \quad (9)$$

If $\left|1 + k_B/h_0 \ll a_{HA}/k'_c h_0\right|$, we obtain the relation:

$$k_{ef} \frac{a_{HA}}{h_0} = k_{true} k'_c. \quad (10)$$

TABLE 2

Velocity Constants for the Hydrolysis of Cyclohexanone Oxime in Mixtures of HCl with NaCl and LiCl

Molality of HCl	Molality of salt	k_{ef}, min^{-1}	HCl activity a_{HCl}	H_0	$\log k_{ef} \times \frac{a_{HCl}}{h_0}$
Mixture with NaCl					
1,0411	3,0274	$9{,}2 \cdot 10^{-3}$	1,89	−0,23	−1,99
1,0411	4,325	$7{,}24 \cdot 10^{-3}$	5,28	−0,47	−1,89
1,0411	3,089	$6{,}12 \cdot 10^{-3}$	8,61	−0,61	−1,89
1,0411	4,6136	$4{,}7 \cdot 10^{-3}$	22,61	−0,94	−1,91
0,1857	0,9943	$4{,}28 \cdot 10^{-3}$	0,124	0,50	−1,77
0,1888	3,0448	$2{,}48 \cdot 10^{-3}$	0,772	0,19	−1,53
Mixture with LiCl					
1,0411	2,9946	$4{,}44 \cdot 10^{-3}$	13,12	−0,74	−1,975

Note. The values of H_0 for solutions of HCl with NaCl and LiCl were determined by us. o-Nitroaniline was used as indicator. The activities, a_{HCl}, of these solution were calculated from Hückel's formula, using the data of Hawkins [7].

For the bimolecular mechanism the activated complex consists of a protonized molecule of oxime and a molecule of water. Since, the activated complex has the same charge as the ionized form, it is reasonable to suppose that f_{BH^+} and f_{M^*} will alter in the same way with changing acidity of the medium. In this case, if $|1 + k_B/h_0 \ll a_{HA}/k_c^* h_0|$, it follows that $a_{HA}\, k_{ef}/h_0\, a_{H_2O} = k_c^*\, k_{true}$.

It can be seen from Table 1, that the experimental results were in good agreement with Equation (10), which presupposes a monomolecular limiting stage. It follows from Equation (9) that the maximum value of k_{ef}, should be observed at an acidity of the medium h_0, such that

$$\frac{k_B}{h_0^2} - \frac{1}{k_c'} \frac{da_{HA}}{dh_0} + \frac{a_{HA}}{k_c' h_0^2} = 0. \qquad (11)$$

The maximum value of the velocity constant for hydrolysis of the oxime was observed over the range of HCl molality $\sim 4.6 \cdot 10^{-3} - 6.5 \cdot 10^{-3}$, where $a_{HA} = h_0^2$. This enabled us to simplify Equation (11), so that, combining k_B and k_c^*, $k_B\, k_c^* = (h_0)^2_{max}$.

Putting the value of k_B in Equation (9), we obtained

$$(k_{ef})_{max} = \frac{k_{true}}{1 + 2\, h_0/k_c^*} = 0.33 \text{ minutes}^{-1} \qquad (12)$$

Since the maximum was diffuse in this case, the value taken for $(h_0)_{max}$ was $5.5 \cdot 10^{-3}$.

From $k_c^*\, k_{true} = 1 \cdot 10^{-2}$ and (12), we calculated the values $k_c^* = 1.9 \cdot 10^{-2}$, $k_{true} = 0.53$ minutes^{-1} and $k_B = 1.6 \cdot 10$ ($pk_B = 2.8$).

If the hydrolysis of the oxime proceeds by a bimolecular mechanism, then the relation, $a_{H_2O}\, f_{RNOH}/f_{M^*} =$ = constant, must be obeyed, and this is obviously improbable.

In order to confirm the hypothesis of the possibility of conversion of the protonized form of the oxime into an undissociated salt, experiments were carried out on the hydrolysis of $C_6H_{10}NOH$ in HCl solutions with addition of NaCl and Li Cl. The results are shown in Table 2.

As would be expected, addition of NaCl and LiCl to the HCl by increasing the activity of the anion reduced the rate of hydrolysis. In this case also, $k_{ef}\, a_{HA}/h_0$ was found to be constant.

It may be concluded that, on the basis of these results, that salt formation retards acid catalyzed processes, since, it leads to a decrease in the concentration of the reactive form of the reagent. The limiting stage in the hydrolysis of cyclohexanone oxime is isomerization of the protonized form.

LITERATURE CITED

[1] H. Euler and A. Olander, Zs. phys. Chem. 131, 107 (1928); T. W. J. Taylor, J. Chem. Soc., 1930, 2741.

[2] D. Rosental and J. Taylor, J. Am. Chem. Soc. 79, 2684 (1957).

[3] B. S. Rabinovich and C. A. Winkler, Canad. J. Res. 20, No. 5, 73 (1942).

[4] A. Olander, Zs. phys. Chem. 129, 1 (1927).

[5] G. N. Lewis and M. Randall, Chemical Thermodynamics, Leningrad (1936) [Russian translation].

[6] M. I. Vinnik, R. N. Kruglov, and N. M. Chirkov, J. Phys. Chem. 30, 827 (1956).

[7] J. E. Hawkins, J. Am. Chem. Soc. 54, 4480 (1932).

Received February 20, 1959

BRITTLE FRACTURE OF PURE AND ALLOYED MONOCRYSTALS OF ZINC

L. A. Kochanova, I. A. Andreeva, and E. D. Shchukin

(Presented by Academician P. A. Rebinder, February 17, 1959)

Institute of Physical Chemistry of the Academy of Sciences of the USSR

We have previously described [1-4] the rules governing the fracture of pure zinc monocrystals along the cleavage plane (0001) and formulated conditions for the constancy of production of normal and shearing stresses in brittle fracture:

$$p_c \tau_c = \text{const} = K^2; \quad K = \gamma (G\sigma/L)^{1/6}; \quad P_c = K (\sin^3 \chi_1 \cos \chi_1)^{-1/6},$$

where G is the shear modulus, σ is the specific free surface energy, L is the maximum size of the region of localization of incomplete dislocations (of the order of the diameter of a monocrystal), P_c is the true tensile stress, χ_1 is the angle between the axis of the sample and the (0001) plane at fracture. The dimensionless constant, γ, for zinc monocrystals at −196°, is about 0.4; the same value for γ was obtained using the data of [5, 6]. This coefficient evidently retains about the same value at room temperature.

Zinc monocrystals covered with a film of mercury, because of the considerable reduction in σ, become brittle even at room temperature [1-4, 7-11]; K falls by a factor of more than two, which corresponds to a decrease in σ of up to 200 erg/cm^2.

Impurities greatly affect the plasticity and strength of the crystals; there was therefore, a definite interest in a comparison of the conditions for brittle fracture for monocrystals of different purity. In the present investigation, we used pure zinc of 99.999 and 99.99% purity, technical zinc and zinc alloyed with cadmium. The alloys contained 0.2 and 0.5% by weight of cadmium, and were prepared from 99.99% pure zinc. Polarographic analysis was used to measure the precise cadmium contents, which were found to be 0.20 and 0.45% by weight respectively. Monocrystals of different orientation were grown by the method of zone crystallization [12, 13]; rupture of the samples was carried out with a Polyani apparatus at a stretching rate of 10-15% per minute.

Highly reproducible results were obtained for the brittle fracture of monocrystals of the 99.99% and purer zinc, and also, for the alloy crystals if nonamalgamated at −196° or covered with mercury at 20°. K values for all the samples investigated are shown in Table 1. Fig. 1 shows, as an example, the complete coincidence of the results for 99.999 and 99.99% Zn (these are subsequently denoted by the general term pure zinc); the curves were obtained to correspond to the condition $p_c \tau_c$ = constant, i.e., they show the function $K(\sin^3 \chi_1, \cos \chi_1)^{-\frac{1}{2}}$ for K = 209 kg/mm^2 (curve a) and K = 95 kg/mm^2 (curve b).

When the sample was amalgamated, the value of K decreased on the average by a factor of more than two, which corresponded approximately to a reduction in σ by a factor of 4 (or slightly more). Reckoning $G = 3 \cdot 10^{11}$ dynes/cm^2 and $\sigma = 10^3$ ergs/cm^2 for pure zinc monocrystals, of diameter 0.9 mm, ruptured in liquid nitrogen, we found $\gamma = 0.36$.

It is clear from Table 1, that K increased with increasing concentration of impurities. Since the condition $p_c \tau_c = K^2$ is associated with the conception of the formation of incomplete localized displacements in the process of plastic flow, differences in the value of K for samples of pure and alloyed zinc should agree with differences

TABLE

Zinc purity	Diameter of sample, L_0, mm	$K = (P_c\sqrt{\sin^3\chi_1 \cos\chi_1})_{av}$, kg/mm²		a_0, %	$\frac{a_0}{a_0'}$	$f = \frac{K'^2 L_0'}{K^2 L_0}$ at −196°C
		nonamalgamated at 196°C	amalgamated at 20°C			
Zn—99,999%	0,9=L'_0	209=K'	92	6—7=a'_0	1	1
Zn—99,99%			97			
Zn+0,2% Cd	0,54	316	153	3	~0,5	0,72
Zn—Tech.	0,9	263	124	2—3	~0,4	0,63
Zn+0,5% Cd	0,54	381	230	2	~0,3	0,50

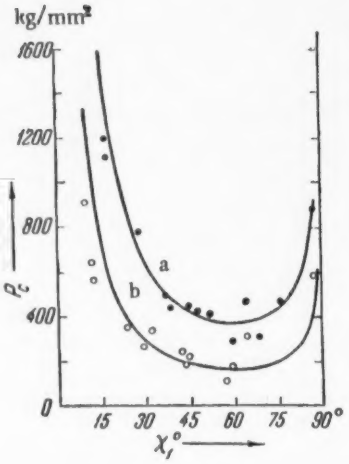

Fig. 1. True values for the tensile strengths, P_c, of pure zinc monocrystals for different orientations, χ_1, at the moment of rupture: a) nonamalgamated samples at −196°; b) amalgamated samples at 20°.

in their deformation curves. Fig. 2 shows the values of the shearing stresses, τ, for samples of pure zinc; the points labelled with arrows correspond to the moment of rupture, i.e., to the points shown in Fig. 1 (the large values of slip, a_c, correspond to crystals of small angle χ_1 [1]); the continuous lines correspond to the mean shapes of the curves of τ as a function of a.

Figure 2 shows that a characteristic break in the deformation curves ("yield point"), for pure zinc crystals under the given conditions, occurred at displacement $a_0 \sim 0.06$-0.07; the points for rupture of the crystals, labelled with arrows, occurred at larger values of a. It may be presumed that the break in the $\tau - a$ curve was due to a change in the character of the shearing process [4, 11]; the high toughness coefficient for $a < a_0$ was associated with the formation and growth of incomplete displacements (accumulated dislocations); in this process the parameter, L, increased rapidly to some value of the order of the crystal diameter, which was greater, the greater the displacement a_0; after a definite value of τ was reached, the obstacles to shearing became surmountable, the increase in the number of incomplete displacements ceased, and the value of L altered slowly, thus, explaining the constancy of K for the rupture of monocrystals over a wide range of orientations.

Values of the slip, a_0, for pure and alloyed zinc samples, are shown in Table 1 (the values of a_0 were approximately the same for amalgamated and nonamalgamated samples of the same purity). With increasing extent of alloying (and increasing toughness), a_0 decreased. It should be stated that the effective value of L, characterizing the degree of heterogeneity of slip, was directly related to the value of a_0; we supposed, as before, that L for pure zinc monocrystals was the same as the diameter of the sample, L_0; then, introducing an index stroke, ', to denote samples of pure zinc, we wrote the relation between L and a_0 in the form of $L = f(a_0/a'_0)L_0$, so that $f(1) = 1$. Comparing the expressions $K' = \gamma[G\sigma/L_0']^{1/2}$ and $K = \gamma[G\sigma/f\,(a_0/a_0')\,L_0]^{1/2}$, we had that the dimensionless function, f, comprised only experimental data: $f = (K'/K)^2 L_0'/L_0$. The values of f are shown in Table 1; the relation between f and a_0/a'_0 was given by function $f \sim (a_0/a'_0)^{1/2}$, but, because of the limited number of approximately determined points in the table, the above form of the relation cannot be considered as finally established.

In view of the above, it was of considerable interest to present an analysis of the data of Deruyttere and Greenough (Fig. 3). Curve b of Fig. 3 was drawn by us on the basis that $P_c\tau_c = K^2$, where K was taken as 104 kg/mm², the mean value of $P_c(\sin^3\chi_1 \cos\chi_1)^{1/2}$ for all the 25 experimental points. On the whole, this curve agreed satisfactorily with the distribution of experimental points (for comparison, curve a was drawn in accordance

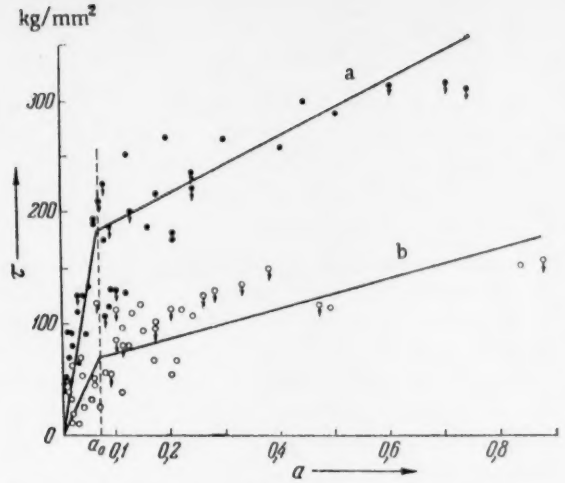

Fig. 2. Relation between shear stress, τ, and crystalline slip, a, for pure zinc monocrystals: a) nonamalgamated samples at −196°; b) amalgamated samples at 20°.

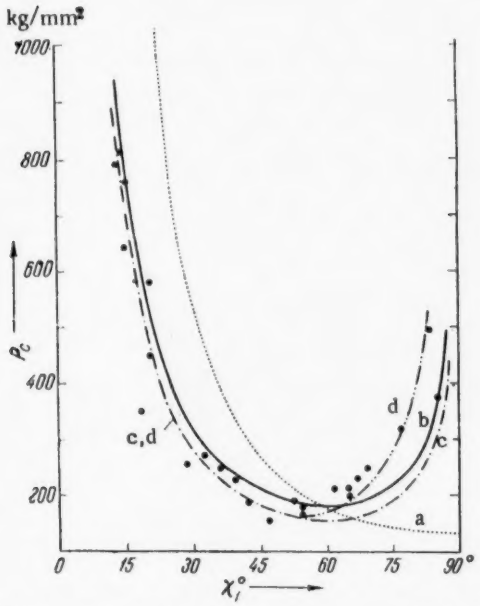

Fig. 3. Values of the true tensions, P_c, at rupture in liquid nitrogen, for 6 mm diameter zinc monocrystals with different orientations of the base plane, under the action of a uniform shearing tension, according to the data of [5].

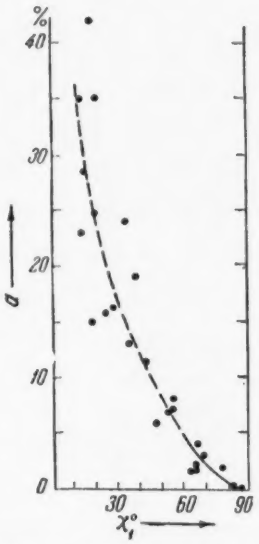

Fig. 4. Experimental values for the limiting deformations at rupture, a_c, for zinc monocrystals with different orientations, according to the data of [5]; the mean curve was drawn by us.

with Zonke's law, p_c = constant, i.e., P_c = constant/$\sin^2 \chi_1$, where the constants 135 kg/mm², was taken as the mean of all the experimental values of $P_c \sin^2\chi_1$); but, for $\chi_1 > 60°$, the experimental points lay considerably above curve b. An explanation of this anomaly was found by analyzing the data [5] for limiting displacement a_c, preceding rupture for the same 25 crystals (Fig. 4); for the 8 crystals with large values of χ_1, the limiting

displacements, a_c, were very small under the given experimental conditions, less than the value 0.05-0.06 $\sim a'_0$, and in this region of values of a_c, it was natural to expect an increase of K with decreasing a_c.

Curve c of Fig. 3, like curve b, was based on the condition $p_c\tau_c = K^2$, but with K taken as $K' = 91$ kg m^2, the mean value for the 17 left hand points with $\chi_1 < 60°$. Finally, curve d, for $a_c > a'_0$, agreed with curve c (i.e., $K = K'$), but, since $a_c < a'_0$, then $K = K'/f^{1/2}$, where, by analogy with Table 1, it was assumed that $f = (a_c/a'_0)^{1/2}$; the values of a_c as a function of χ_1 were taken from the mean curve shown in Fig. 4. Curve d of Fig. 3 agreed well with the experimental points over the whole range of orientations investigated.

Thus, in the fracture of zinc monocrystals along the cleavage plane, a very large effect was produced by previous plastic deformation, for, in the course of this, heterogeneities in slip formation and the associated concentrations of stress produced the germ of fracture, in the form of microcracks. If the plastic deformation was not too small for the formation of heterogeneities to be included in the fundamental law, then there was good fulfillment of the condition $p_c\tau_c$ = constant = K^2, where K was greater the smaller the region of localization of these heterogeneities, i.e., the more uniform was the slip formation (in alloys). K also increased if the shear preceding rupture was very small (the process of forming heterogeneities was incomplete); this could happen at high values of χ_1.

The condition $p_c\tau_c = K^2$ was also valid for the fracture of nonamalgamated zinc monocrystals of different purity at low temperatures, and for the fracture of amalgamated samples at room temperature; in the latter case, because of the large fall in σ, the value of K fell by a factor of two or more.

The authors would like to thank V. I. Likhtman for his advice and continuous interest in this work.

LITERATURE CITED

[1] V. I. Likhtman, L. A. Kochanova, and L. S. Bryukhanova, Proc. Acad. Sci. USSR 120, 757 (1958).*

[2] V. N. Rozhanskii, N. V. Pertsov, E. D. Shchukin, and P. A. Rebinder, Proc. Acad. Sci. USSR 116, 769 (1957).*

[3] E. D. Shchukin and V. I. Likhtman, Proc. Acad. Sci. USSR 124, 307 (1959).*

[4] V. I. Likhtman and E. D. Shchukin, Prog. Phys. Sci. 66, 213 (1958).

[5] A. Deruyttere and G. B. Greenough, J. Inst. Metals 84, No. 9, 337 (1955-56).

[6] E. Shmid and V. Boas, Plasticity of Crystals, Moscow (1938).**

[7] P. A. Rebinder, V. I. Likhtman, and L. A. Kochanova, Proc. Acad. Sci. USSR 111, 1278 (1956).

[8] P. A. Rebinder, "New Problems in Physicochemical Mechanics," paper to a Foreign Colloquium on Solid Phases of Variable Composition,** and also, to the Moscow Colloid Colloquium, Jan. 26, 1956;** P. A. Rebinder, Bull. Acad Sci. USSR, Div. Chem. Sci., 11, 1284 (1957).*

[9] E. D. Shchukin and P. A. Rebinder, Coll. J. 20, 645 (1958).*

[10] N. V. Pertsov and P. A. Rebinder, Proc. Acad. Sci. USSR 123, 1068 (1958).*

[11] E. D. Shchukin, Proc. Acad. Sci. USSR 118, 1105 (1958).*

[12] V. I. Likhtman and B. M. Maslennikov, Proc. Acad. Sci. USSR 67, 93 (1949).

[13] V. N. Rozhanskii, N. V. Dekartova, and I. A. Bakeeva, Phys. Met. and Metallography 4, No. 3 (1957).

Received February 10, 1959

* Original Russian pagination. See C. B. pagination.

** In Russian.

THE EFFECTS OF ABSORBED ANIONS ON HYDROGEN OVERVOLTAGE

Tza Chyuan-Sin and Z. A. Iofa

(Presented by Academician A. N. Frumkin, March 20, 1959)

The M. V. Lomonosov Moscow State University

According to the theory of retarded discharge [1], the equation for the overvoltage for the liberation of hydrogen from acid solutions has the form:

$$\eta = \frac{RT}{\alpha F} \ln i - \frac{1-\alpha}{\alpha} \frac{RT}{F} \ln [H_3O^+] + \frac{1-\alpha}{\alpha} \psi_{10} + \text{const}, \quad (1)$$

where ψ_{10} is the mean value of the potential at a distance of one ionic radius from the surface of the electrode (the potential of "the external Helmholtz layer").

In [2] an experimental comparison was made of the overvoltage curves with the electrocapillary curves for the same solution. It was found that, in qualitative agreement with the above equation (1), the halide ions Cl^-, Br^- and I^- reduced the hydrogen overvoltage at mercury in the low polarization regions, and that, in approximately the same potential regions, they lowered the interfacial tension at the mercury-solution boundary. But, deviations from linearity in the η - log i curve, and an initial reduction in overvoltage, were observed at considerably more negative potentials than those corresponding to the beginning of divergences between the electrocapillary curves for the given soltuion and for solutions not containing surface active anions. It was therefore, considered that the lack of agreement between the desorption potentials of these anions, as determined by the two methods, might be explained on the assumption that small amounts of adsorbed material did not affect the electrocapillary curve, but, had a considerable influence on the overvoltage.

As the result of improvements in the technique of measurement, we now have available a more sensitive method of investigating the structure of the double layer, namely, the differential capacity method. It was therefore, of interest to carry out more precise measurements on the effects of adsorbed anions on the hydrogen overvoltage, using this method.

Figure 1 shows curves for the hydrogen overvoltage in acid solutions containing KCl, KBr and KI. These curves were obtained, using a dropping electrode at 20°, by the method described in [3]. Fig. 2 shows differential capacity curves, obtained with the same solutions at a dropping mercury electrode, by the method of [4]. Since, at sufficiently negative potentials, hydrogen evolution began in these acid solutions, and the system showed conductivity with alternating current, the true value of the capacity of the double layer, in these regions of potential, was calculated from the formula

$$C_{\text{true}} = \frac{C_M}{1 + 4\pi^2 f^2 C_M^2 (R_M - R_p)^2},$$

where C_M and R_M were the values of capacity and resistance, obtained directly by means of a bridge, in which the standard resistance and capacitor boxes were connected in series; f was the frequency of the alternating current used; R_p was the total resistance of capillary and solution.

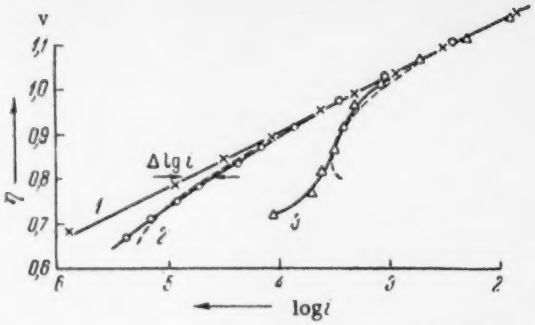

Fig. 1. Overvoltage curves in solutions: 1) N HCl + + 2N KCl, 2) N HCl + 2N KBr, 3) NHCl + 2N KI.

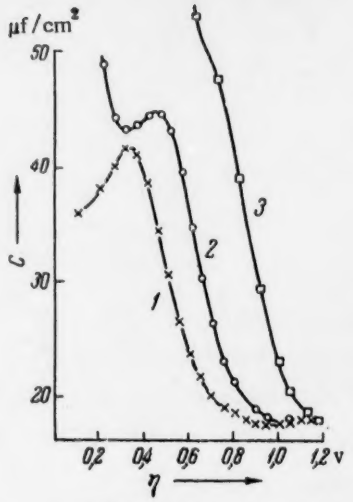

Fig. 2. Differential capacity curves, for the same solutions as in Fig. 1, at a frequency of 5000 cps.

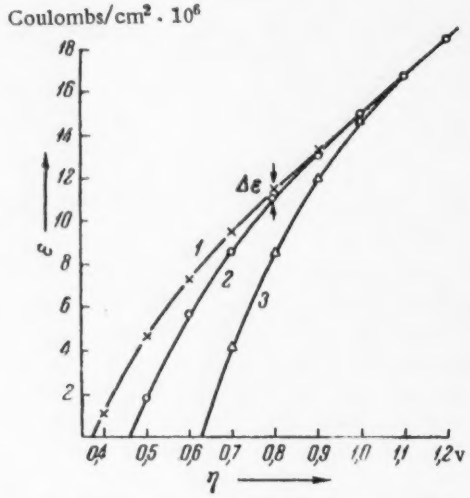

Fig. 3. Relation between discharge density, ϵ, and potential for the same solutions.

Comparison of the overvoltage and capacity curves showed that the differential capacity was more sensitive to the absorption of anions than were the interfacial tension or the overvoltage. Divergences between the differential capacity curves were observed at considerably more negative potentials than divergences between the overvoltage curves. As will be shown below, in order to elucidate the effect of the double layer structure on the kinetics of electrochemical processes, it is convenient to use the value of the discharge density, ϵ, rather than the interfacial tension or the differential capacity.

To calculate ϵ, we first used the values of $\varphi_{\epsilon=0}$ found from the electrocapillary curves for the same solutions. But the values of ϵ, obtained in this way, for the three solutions differed from each other by about 1-2% at η = 1.2 v, where the capacity curves converged. This difference showed a lack of precision in the determination of $\varphi_{\epsilon=0}$ by the electrocapillary curve method, so we took the mean value of ϵ at η = = 1.2 v as an integration constant for all three solutions, and integrated in the reverse order, starting with η = = 1.2 v. The relation between ϵ and potential is shown in Fig. 3.

There was satisfactory agreement between the curves for ϵ, η and η -log i. In the potential regions where the ϵ-η curves were practically straight lines, the η -log i curves were also straight. With KCl solutions, the curve remained a straight line over the range of potential investigated. The potentials at which deviations from linearity began for KBr and KI were of the same order (−0.95 v for KBr and −1.05 v for KI).

For the range of potential in which the absorption of anions was still not very great, the following empirical relation was found:

$$\left(\frac{\Delta \lg i}{\Delta \varepsilon}\right)_{\eta} \approx 0{,}5, \qquad (2)$$

where Δ log i and $\Delta\epsilon$ were the deviations of log i and ϵ from the corresponding values determined for KCl solutions at the same potential, and ϵ was expressed in μ coulombs/cm^2 (see Fig. 1 and 3). Fig. 1 shows both the experimental points (continuous curves) and the values of log i calculated from the relation Δ log i = $0.5\Delta\epsilon$ (dotted curves). It is clear that the calculated and experimental curves agreed satisfactorily up to $\eta < 0.70$ v for KBr and $\eta < 0.65$ v for KI.

It is not difficult to derive Relation(2) from Equation (1) and some elementary considerations on the structure of the double layer.

From Equation (1) we obtain:

$$\left(\frac{\partial \lg i}{\partial \psi_{10}}\right)_\eta = -\frac{(1-\alpha)F}{2{,}3\,RT}. \tag{3}$$

So long as the adsorption of anions is small, we can reckon, without serious error, that the electric field in the close part of the double layer is determined only by the value of ϵ at the electrode surface, and we obtain:

$$\varepsilon = C_r\,(\varphi - \psi_{10}), \tag{4}$$

where C_r is the capacity of the outer Helmholtz layer in the presence of adsorbed anions. It follows from (4) that:

$$\left(\frac{\partial \psi_{10}}{\partial \varepsilon}\right)_\eta = -\frac{1}{C_r}. \tag{5}$$

Since, in the presence of adsorbed anions, the capacity alters little with potential over the range of potential considered, the value of C_r can be put equal to the differential capacity of the outer Helmholtz layer. The latter, with solutions of the concentration considered, hardly differs from the capacity of the double layer as a whole. From (3) and (5) it follows that:

$$\left(\frac{\partial \lg i}{\partial \varepsilon}\right)_\eta = \left(\frac{\partial \lg i}{\partial \psi_{10}}\right)_\eta \left(\frac{\partial \psi_{10}}{\partial \varepsilon}\right)_\eta = \frac{(1-\alpha)F}{2{,}3RTC_r}. \tag{6}$$

Putting C_r = 18 μf/cm^2 and α = 0.5 in (6), we obtain:

$$\left(\frac{\partial \lg i}{\partial \varepsilon}\right)_\eta \approx 0{,}5. \tag{7}$$

When the adsorption of anions became greater, ψ_{10} was determined, not only by the value of ϵ at the electrode surface, but, also by the charge of the adsorbed anions, so that Equation (3) was no longer correct. But, according to Grahame's latest data for KI [5], when $|\epsilon| > 10$ μcoulombs/cm^2 ($\eta > 0.85$ v), the adsorbed ions were still at some distance from the electrode surface, so that our assumption was evidently still applicable as a first approximation.

It is clear from the above that the effect of adsorption of halide anions on the hydrogen overvoltage can be related quantitatively to the change in surface charge, ϵ. Measurements of overvoltage should therefore, be compared with the values of ϵ, and not with the interfacial tension or differential capacity. The interfacial tension – the result of integrating the charge density $\left(\sigma = \int \varepsilon\, d\varphi\right)$, – is not sensitive enough to small changes in the structure of the double layer. The differential capacity, which is a derivative of ϵ, is too sensitive to small changes in structure which are not reflected in the polarization curves.

Using the same solutions, $\eta - \log i$ curves were recorded at a large stationary mercury cathode. The absence of hysteresis loops in the curves for direct and reverse polarization indicated that the adsorption of I^- ions proceeded rapidly. The hysteresis loops observed previously [2] were possibly due to traces of iodine or of mercury ions in the solution.

We would like to thank Academician A. N. Frumkin for his interest and advice during the progress of the work and the interpretation of the results.

LITERATURE CITED

[1] A. Frumkin, Zs. phys. Chem. A164, 121 (1933).

[2] Z. Iofa, B. Kabanov, E. Kuchinskii, and F. Chistyakov, J. Phys. Chem. 13, 1105 (1939).

[3] Z. A. Iofa and A. I. Kolychev, J. Phys. Chem. 14, 58 (1940); Tza Chyuan-Sin and Z. A. Iofa, Proc. Acad. Sci. USSR, 125, No. 5, (1959).*

[4] D. C. Grahame, J. Am. Chem. Soc. 68, 301 (1946); 71, 2975 (1949); V. I. Melik-Gaikazyan, J. Phys. Chem. 26, 560 (1952); B. B. Damaskin, J. Phys. Chem. 32, 2199 (1958).

[5] D. C. Grahame, J. Am. Chem. Soc. 80, 4201 (1958).

Received March 12, 1959

* Original Russian pagination. See C. B. translation.